ACCSCIENCE PUBLISHING

Tumor Discovery

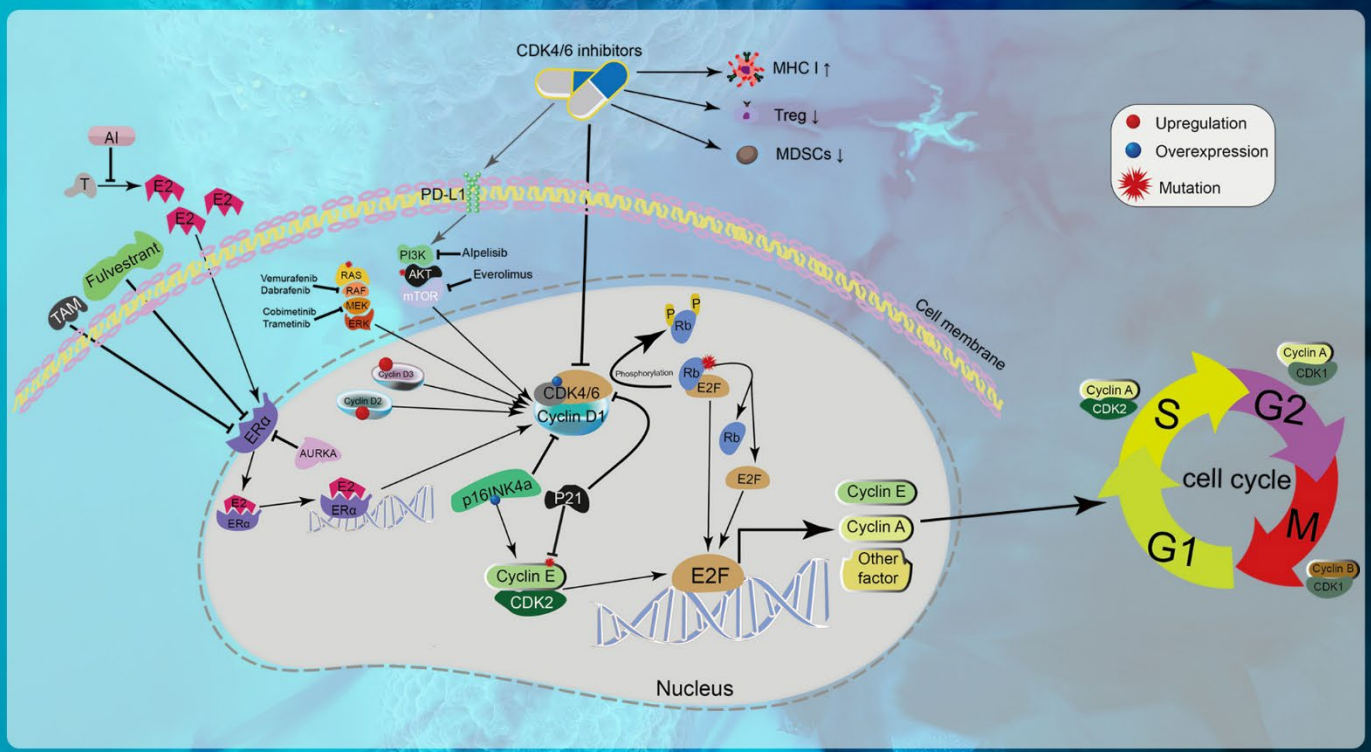

Cyclin-dependent kinase 4/6 inhibitor resistance mechanisms and strategies for subsequent treatment in breast cancer

ISSN: 3060-8597 (Print)
ISSN: 2810-9775 (Online)
Volume 4 • Issue 1
March 2025

ACCSCIENCE PUBLISHING

Tumor Discovery

Print ISSN: 3060-8597
Online ISSN: 2810-9775

Tumor Discovery is a peer-reviewed and open-access journal that aims to present new cancer research with strong emphasis on fundamental and translational studies. *Tumor Discovery* covers topics such as etiology and pathogenesis of cancer, mechanisms and molecular pathways underlying cancer initiation and progression, tumor metastasis, etc.

Scan to access website:

Scan to submit papers:

About the Publisher

AccScience Publishing is a publishing company based in Singapore. We publish a range of high-quality, open-access, peer-reviewed journals and books from a broad spectrum of disciplines.

Contact Us

Managing Editor
td.office@accscience.sg

AccScience Publishing
8 Burn Road, #15-03 Trivex, Singapore 369977.

Volume 4 • Issue 1 • March 2025
ISSN 3060-8597 (print) ISSN 2810-9775 (online)

TUMOR DISCOVERY

ACCSCIENCE PUBLISHING

Access Science Without Barriers

TUMOR DISCOVERY

ISSN: 3060-8597 (print)
ISSN: 2810-9775 (online)

Editorial and Production Credits

Publisher: AccScience Publishing
Managing Editor: Daisy Zhao
Production Editor: Sharmila Velapasamy
Article Layout and Typeset: Sinjore Technologies (India)

For all advertising queries, contact td.office@accscience.sg.

Supplementary file

Supplementary files of articles can be obtained at https://accscience.com/journal/TD/4/1.

Disclaimer

AccScience Publishing is not liable to the statements, perspectives, and opinions contained in the publications. The appearance of advertisements in the journal shall not be construed as a warranty, endorsement, or approval of the products or services advertised and/or the safety thereof. AccScience Publishing disclaims responsibility for any injury to persons or property resulting from any ideas or products referred to in the publications or advertisements. AccScience Publishing remains neutral with regard to jurisdictional claims in published maps and institutional affiliations.

Tumor Discovery

Editorial Board

Youth Editorial Board Members

*Editorial Board Members as of March 17, 2025

ACCSCIENCE PUBLISHING

Volume 4 | Issue 1 | March 2025 | Page 1 – 131 |

Tumor Discovery

https://accscience.com/journal/TD

CONTENTS

ACCSCIENCE PUBLISHING

Tumor Discovery

REVIEW ARTICLE

EpCAM-targeting cancer immunotherapies: Evidence from clinical studies and the way forward

Dennis Makafui Dogbey[1], Ursula-Claire Andong-Koung-Edzidzi[1], Gomolemo Atlegang Molope[1], Jesmika Singh[1], Tatenda Lovemore Bvudzijena[1], Krupa Naran[1], and Stefan Barth[1,2*]

[1]Medical Biotechnology and Immunotherapy Research Unit, Institute of Infectious Diseases and Molecular Medicine, Faculty of Health Sciences, University of Cape Town, Cape Town, South Africa

[2]Department of Integrative Biomedical Sciences, South African Research Chair in Cancer Biotechnology, Division of Chemical and Systems Biology, University of Cape Town, Cape Town, South Africa

Abstract

Overexpressed cell-surface receptors play a crucial role as biomarkers in immunodiagnostics and immunotherapy. Epithelial cell adhesion molecule (EpCAM) is a 40 kDa cell-membrane glycoprotein associated with cell differentiation, survival, migration, and proliferation. The structure, biological functions, and role of EpCAM in tumorigenesis have been extensively studied, including its involvement in metastasis, tumor cellular signaling, and pro-proliferating pathways. It is differentially overexpressed on the surface of several tumor types, with substantial evidence suggesting a positive correlation with poor disease prognosis and overall survival. Consequently, it has emerged as a significant target for immunotherapy development, with some of them already entering clinical evaluation and one having been approved by the U.S. Food and Drug Administration to date. Pre-clinical and clinical studies evaluating anti-EpCAM immunotherapies have reported diverse outcomes necessitating critical assessment in considering future therapy development. EpCAM-targeting immunotherapies including monoclonal antibodies, adoptive cell transfer therapy, immunocytokines, recombinant immunotoxin, and bispecific T-cell engagers have been studied as monotherapy or in combination with other treatments resulting in improved outcomes. Depending on disease status, EpCAM-targeting therapies are studied in adjuvant and neoadjuvant settings by integrating the clinical features of patients and treatment intent. However, the wide range of adverse events reported in various unsuccessful clinical studies has implications for future clinical trial designs, patient stratification, and endpoint criteria measures. This review examines the efficacy and toxicity profiles of anti-EpCAM immunotherapeutic approaches that have undergone clinical investigations for the treatment of antigen-positive malignancies and provides perspectives to guide future research and development strategies toward precision medicine.

Keywords: Epithelial cell adhesion molecule; Immunotherapy; Clinical research; Solid tumors; Clinical trial

***Corresponding author:**
Stefan Barth
(stefan.barth@uct.ac.za)

Citation: Dogbey DM, Andong-Koung-Edzidzi U, Molope GA, *et al*. EpCAM-targeting cancer immunotherapies: Evidence from clinical studies and the way forward. *Tumor Discov*. 2025;4(1):1-13.
doi: 10.36922/td.4926

Received: September 24, 2024

Revised: November 5, 2024

Accepted: November 11, 2024

Published online: December 13, 2024

1. Introduction

Tumor cell-surface receptors (CSR) play a vital role as overexpressed biomarkers and are regarded as pivotal targets for cancer immuno-diagnosis and -therapy. A significant example is the epithelial cell adhesion molecule (EpCAM) or CD326. Interestingly, the structural similarities between the human EpCAM antigen and those found in mice or other surface markers in the GA733 family present challenges in developing fully humanized, high-affinity targeting agents against this antigen.[1] Numerous clinical studies on anti-EpCAM immunotherapeutics have yielded inconclusive outcomes, creating uncertainties for future therapy developments aimed at targeting this differentially overexpressed CSR.

1.1. Brief biology and function of EpCAM

EpCAM is a cell surface type 1 transmembrane glycoprotein belonging to the unique GA733 protein family. It is encoded by the *TACSTD1* gene and functionally mediates cell-to-cell adhesion, resulting in intracellular dimerization cascades of major pro-proliferative signaling pathways.[2,3] EpCAM is expressed on epithelial cells and during the embryonic states in vertebrates, where it is located at tight junctions. In addition, it is responsible for the differentiation and survival of parietal trophoblast giant cells, the normal development of the placental labyrinth, and the establishment of competent maternal-fetal circulation *in vivo*. Gene-knockout mice, which died *in utero*, were significantly small-for-age and displayed extensive placental abnormalities, highlighting its involvement in the embryogenesis of vital organs and body structures, such as ear, upper and lower extremities, and abdominal organs of vertebrates, signifying the cardinal role of the molecule in the physiological processes of fetal development.[4] Structurally, EpCAM (38 kDa) consists of an extracellular cell surface-exposed part (EpEX, 27 kDa), transmembrane and intracellular components. The intracellular domain, known as the EpIC (3 kDa), is involved in ligand-dependent dimerization. The polypeptide chains of the EpEX are structurally arranged into three distinctive domains: N-domains, thyroglobulin type 1A, and C-domains, known for mediating signal transductions.[5] EpCAM is cleaved mainly at residues Arg80 – Arg81 by proteolytic substrates.[6] However, detailed structural analysis showed that its exposed basolateral positions are covered with glycan side chains, which are involved in N-linked glycosylation at three sites and harbor epitopes that serve as the binding pockets for an affinity ligand.[7] Recent functional studies have implicated it as a crucial mediator of immune homeostasis of the intestinal tract by upregulating the polymeric immunoglobulin receptor within the intestinal epithelium.[8] In addition, there is a positive correlation between EpCAM co-expression and pro-neovascularization growth factors.[9]

2. Approved and clinical studies of anti-EpCAM immunotherapies

Almost all types of EpCAM-targeting immunotherapies have demonstrated remarkable pre-clinical efficacy, and a significant number of these treatments have transitioned to clinical trials. Figure 1 shows the mechanism of action of common EpCAM-specific antibody-based immunotherapies that have entered clinical evaluation. Regarding armed recombinant antibodies, the toxic (cytolytic) domain fused to the EpCAM-targeting ligands can be derived from bacterial, human, or plant origin. The selection of these sources depends on various factors, including immunogenicity, potency, and host of expression. Upon release through endosomal escape, the effector domains cleave their specific substrates, resulting in the intracellular induction of cell death.

3. Monoclonal antibodies

This type of monoclonal antibody induces cancer cell death by direct immune-related toxicity and disruptions of pathophysiological pathways of malignant cells resulting in antibody-dependent cellular cytotoxicity. Thus, the EpCAM-specific antibody (IgG1) interacts with the

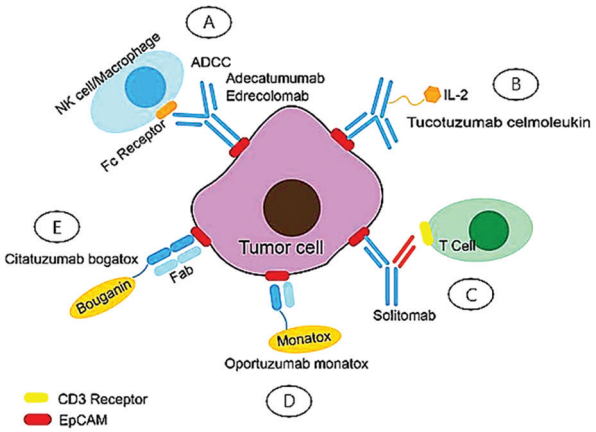

Figure 1. Mechanism of action of selected EpCAM-specific antibody-based immunotherapies. The anti-EpCAM immunotherapy types consist of a full antibody or antibody fragment at one end that is specific to the EpCAM antigen on cancer cells (red) and binds through the Fc receptor and recruits immune effector cells (A), immunomodulatory cytokine (B), secondary antibody fragment that binds to T cells through CD3 receptor (C), bacterial (D) or plant toxin as the cytolytic domain (E). Adapted from Creative Biolabs available at https://www.creativebiolabs.net/adecatumumab-overview.htm.

Abbreviations: ADCC: Antibody-dependent cellular cytotoxicity; EpCAM: Epithelial cell adhesion molecule; IL: Interleukin; NK cell: Natural killer cell.

antigen, leading to the disruption of the EpCAM-signaling pathways and the recruitment of immune effector cells to close proximity to tumor cells. Over the years, there have been numerous clinical trials using antibodies targeting EpCAM; some trials have shown excellent results and were approved, whereas others require further improvements to achieve success.

One of the very first clinical studies involved an EpCAM-specific monoclonal antibody called 17-A or edrecolomab to treat patients with colorectal cancer in Dukes' stage C (stage III), who had undergone curative surgery without residual disease.[10] While this mouse-derived monoclonal antibody extended survival and delayed disease remission with adjuvant treatment, it also caused several toxicities in patients. To enhance its effectiveness, combination therapy including edrecolomab with established anticancer treatment options was explored in a multicenter randomized trial, involving 27 countries, led by Punt *et al.*[11] The study included 2761 stage III colon cancer patients administered with edrecolomab as neoadjuvant therapy in combination with fluorouracil and folinic acid. Patients were randomly assigned to receive combination therapy (n = 912), chemotherapy plus folinic acid (n = 927), or edrecolomab alone (n = 922). Besides aiming for successful treatment, the study also assessed the efficacy of combined treatments on overall survival compared to other options. In addition, it compared edrecolomab's effectiveness alone versus chemotherapy on disease-free survival. With a median follow-up of 26 months, the study found no significant difference in 3-year overall survival between patients receiving combination therapy (74.7%) and those on chemotherapy plus folinic acid (76.1%). However, disease-free survival was notably lower for patients on edrecolomab alone compared to those on chemotherapy (53.0% vs. 65.5%). Due to hypersensitivity reactions experienced by some patients (25%), 4% chose to discontinue treatment. The combination therapy did not worsen the adverse events compared to previous trials. Thus, edrecolomab monotherapy was associated with significantly shorter overall and disease-free survival compared to treatment with fluorouracil and folinic acid, indicating it as a less effective option.[11]

With the limited success of edrecolomab therapy, adecatumumab (MT201) – a human recombinant IgG1 monoclonal antibody – was approved for clinical trial studies. This antibody was known to bind with a low affinity to EpCAM compared to edrecolomab, so its pharmacokinetics (PK) requires to be closely assessed. In phase I trial evaluation of adecatumumab led by Oberneder *et al.*,[12] 20 patients were treated with two intravenous (IV) infusions on days 0 and 14 up to a maximum dose of 262 mg/m^2. This dose escalation study was observed to have induced an increase in serum level of tumor necrosis factor-alpha (TNFα).[12] In a subsequent open-label phase II clinical trial, 109 patients were categorized into two groups: EpCAM^{high} and EpCAM^{low} metastatic breast cancer. The patients were randomly subjected to either 6 mg/kg or 2 mg/kg monotherapy every 2 weeks. Notable findings after study completion included reduced tumor progression in EpCAM^{high} subset of patients. In addition, only three out of 18 patients with high expression levels of EpCAM (14 out of 29) developed new metastases within 6 weeks post-treatment. Significant similar side effects that were observed in both groups were primarily mild to moderate such as chills, nausea, diarrhea, and fatigue. Interestingly, this study found that adecatumumab reduced peripheral natural killer (NK) cells, increased serum levels of TNFα at the highest dose, and induced no detectable antidrug immune response.[12]

4. Antibody-drug conjugates (ADCs)

Information on EpCAM-specific ADCs under clinical evaluation is limited. However, at the 2023 World ADC Conference, CytomX Therapeutics announced the pre-clinical data for CX-2051, which is developed based on the Probody therapeutics technology consisting of topoisomerase-1 inhibitor payload and CX-801 (a conditionally activated interferon [IFN] alpha-2b). The adoption of probody technology is to deliver a proteolytically activated antibody prodrug and to localize the antitumor activities of the ADC to the tumor microenvironment.[13] These compelling pre-clinical data revealed a satisfactory therapeutic index of CX-2051 against many EpCAM-positive carcinomas, becoming the first publicly announced EpCAM-specific ADC (having received investigational new drug approval) transitioning to clinical evaluation. CX-2051 received U.S. Food and Drug Administration clearance to commence phase I dose-escalation clinical studies scheduled to begin in the first quarter of 2024 in patients with solid tumors including colorectal, melanoma, and head and neck squamous cell carcinomas.

Earlier in 2024, ClinicalTrials.gov (through the study identifier NCT06265688) announced the initiation of the clinical evaluation of CX-2051 as a monotherapy. The ongoing recruitment process, which began in March 2024, included the following eligibility criteria: adults (≥18 years) with advanced-stage solid malignancies as determined by Response evaluation criteria in solid tumours (RECIST) criteria, and an Eastern Cooperative Oncology Group (ECOG) performance status of 0 – 1. The study aimed to evaluate the safety and tolerability profiles of the ADC within 44 months from the date of administration with an expected enrollment duration of 5 years.

5. Immunocytokines

Immunocytokines are antibody-cytokine recombinant fusion proteins, with the potential to selectively localize at tumor sites and to stimulate localized and systemic anticancer immunity.[14,15] To date, one anti-EpCAM immunocytokine has undergone clinical evaluation. Tucotuzumab celmoleukin-interleukin-2 (huKS-IL2) is an anti-EpCAM fusion protein consisting of a humanized antibody specific for EpCAM linked at its Fc end to two molecules of IL2.[16,17] A phase 1b clinical study assessed the safety and unraveled the maximum tolerated dose (MTD) of huKS-IL2 following a single low-dose of cyclophosphamide in patients with EpCAM-expressing advanced solid cancers.[17] The investigators evaluated the immunogenicity, antitumor, biological activity, and PK profiles of the fusion protein. The study recruited 22 patients aged >18 years, who had advanced or recurrent EpCAM-positive (25% or higher) solid tumors. The patients underwent up to six cycles of treatment. The treatment was 300 mg/m^2 cyclophosphamide on day 1 and then increasing doses of 0.5 – 4.0 mg/m^2 intravenous continuous infusion of huKS-IL2 over 4 h the following day and for 3 days within the 21-day cycle. The most common adverse reaction was transient lymphopenia (which is considered grade 3 and 4 adverse reactions),[18] whereas nausea, pyrexia, rash, chills, diarrhea, fatigue, headache, vomiting, hypophosphatemia, increased serum creatinine, and hypotension were the frequently observed minor adverse effects. In addition, 88.5% of patients had a transient immune response to huKS-IL2. The authors established that the MTD was 3.0 mg/m^2 for huKS-IL2 when combined with 300 mg/m^2 cyclophosphamide, with dose-limiting myelosuppression noted at higher dose concentrations. The dose-limiting toxicity was attributed to non-specific activities of the cyclophosphamide because the huKS-IL2 exposure was not dose-proportional but dose-dependent with negligible off-target accumulation. A transient immune response to huKS-IL2 was noted for most patients (mainly anti-idiotype or antilinker antibody induction) without an established association of these responses to the neutralizing effect of the immunocytokine. The best response was stable disease which lasted for more than four cycles in three out of 22 patients. The combination of huKS-IL2 and cyclophosphamide was well-tolerated without beneficial clinical endpoints. This study showed that there is a potential for huKS-IL2 as an immunotherapeutic in combination with low-dose cyclophosphamide. The combination of these drugs in patients with advanced tumors was deemed to be a feasible and safe treatment strategy.

6. Recombinant immunotoxins (rITs)

rITs are an emerging class of anticancer therapeutics involving the genetic fusion of antigen-specific antibodies or cytokines to plant or bacterial toxins.[19] As a subclass of anticancer protein therapeutics, rITs specifically target and cleave a designated substrate, ultimately inducing apoptosis. The development of EpCAM-targeting rITs has reached various degrees of clinical success. An example is opportuzumab monatox (VB4-845), which was evaluated in patients with non-muscle-invasive bladder cancer (NMIBC) refractory to or intolerant of Bacillus Calmette–Guerin (BCG). VB4-845 is a recombinant fusion protein that targets EpCAM-positive cancer cells. It is made up of an anti-EpCAM humanized single-chain variable fragment (scFv) linked to a truncated form of *Pseudomonas* exotoxin A (ETA252 – 608) that lacks the cell-binding domain.[20] Regarding bacterial-based rITs, the mode of action of VB4-845 is through antigen-specific binding and endocytosis into the cytosol, followed by the release of the toxin through escape from endosomal cleavage, leading to inhibition of EF1 protein synthesis and cell death.[21] A phase I dose-escalation clinical study was conducted to investigate the MTD of VB4-845. As a secondary aim of the clinical study, the authors investigated the immunogenicity, safety, efficacy, tolerability, and PKs profile of VB4-845.[22,23] The study recruited 64 participants (>18 years old), with early-stage transitional cell carcinoma or *in situ* carcinoma, grade 2/3, who were refractory and intolerant to BCG therapy. Other inclusion criteria of the study were patients with adequate renal, hepatic, and hematological function. Second, the recruitment of patients of childbearing age was expected to undergo contraceptives before and during the study. The rIT was administered intravesically for 6 consecutive weeks, in increasing weekly doses (from 0.1 to 30.16 mg) through an indwelling urinary catheter. The study participants were tracked for 4 – 6 weeks following treatment and assessed at the 12th week. After the study, 64% of patients had adverse reactions, with 33% facing pharyngolaryngeal pain, bladder spasm, urinary tract infection, incontinence, and nocturia. These reactions were believed to have resulted from concomitant medications. In addition, a third of patients experienced mild-to-moderate adverse reactions that were believed to be caused directly by rIT including dysuria and hematuria, fatigue, loss of appetite, fever and chills, myalgia, nausea, and dizziness. However, these reactions did not increase in frequency with dose. Following the last dose of VB4-845, one patient died from cardiac failure, and his demise was unrelated to the effects of the rIT. Overall, the adverse reactions were mild and adequately managed. The authors were unable to determine an MTD for VB4-845, and the apparent lack of relationship between the adverse reactions and the

dose indicated a satisfactory safety profile. VB4-845 was shown to not be systemically absorbed but remained in the bladder until elimination, probably due to the molecular size of the drug and cellular integrity of the bladder. In addition, VB4-845 was found to be specific to antigen-positive tumors. Although it induced an immunogenic response, this expected outcome was attributed to the origin of the antibody fragment and the bacterial toxin. The authors proposed that tumor response may be saturated at higher doses due to the dose range of administered VB4-845 exceeding the drug concentration required to kill more than 99% of cells in EpCAM-positive bladder tumor cell lines. Thus, VB4-845 can safely inhibit the growth of tumors in high-grade EpCAM-positive NMIBC patients in a dose-dependent manner.

Another rIT evaluated against EpCAM-positive cancers is MOC31PE consisting of the full murine MOC31 IgG1 monoclonal anti-EpCAM antibody covalently linked to the complete *Pseudomonas* exotoxin A (PE) was investigated in metastatic colorectal cancer patients in a phase I clinical study.[24] Because the main limitation of rITs is immunogenicity, MOC31PE was administered intravenously with and without the immunosuppressant cyclosporine. The aim was to minimize the generation of systemic antidrug immunogenic responses. The administration of MOC31 as monotherapy demonstrated improved overall survival (12.7 versus 6.2 months) in a cohort of colorectal cancer patients compared to combination therapy with immunosuppressant.[25] Second, another study investigated the safety and maximum tolerable doses in patients diagnosed with EpCAM-positive tumors in combination with immunosuppression.[24] The study included 63 patients divided into three groups: 34 received MOC31PE alone, 23 received MOC31PE in conjunction with IV cyclosporine, and the remaining six were administered MOC31PE and cyclosporine orally. Inclusion criteria include adults 18 years or older, ECOG performance status of 0 – 2, and evidence of at least 10% EpCAM-positive metastatic carcinoma. In addition, conventional treatments were discontinued 4 weeks before and during the study. MOC31PE was administered up to 4 times every 2 weeks, while cyclosporine was given 1 day before MOC31PE and continued for four days post-initial administration. At the end of the study, the authors observed that patients undergoing monotherapy had better therapeutic outcomes compared to those receiving combination therapy. Conceivably, the efficacy of the rIT was compromised by the coadministration of the immunosuppressant in the combination therapy group, as in previous studies.[25,26] indicated that MOC31PE can induce an unexplained antitumor immune response that can provide additional antitumor activities. These findings challenge the notion that existing neutralizing antibodies are a primary cause of immunogenicity to bacteria-based rITs in humans.[27] Furthermore, a clinical study of MOC31PE was conducted with the aim of establishing the efficacy of the rIT in the context of intraperitoneal administration in late-stage colorectal cancer patients with confirmed peritoneal metastasis.[28] The study was conducted to analyze the local and systemic cytokine response in these patient populations undergoing cytoreductive surgery and hyperthermic intraperitoneal chemotherapy with or without intraperitoneal treatment with MOC31PE. The rIT activated local and systemic cytokines, an added advantage that can potentiate its antitumor activities. The investigators enrolled 21 and 26 adult patients who were administered with or without MOC31PE, respectively. A tumor debulking cytoreductive surgery baseline treatment was performed on all patients before receiving the rIT as a single rapid intraperitoneal instillation through two abdominal drainage catheters. To assess cytokine responses, the authors analyzed 27 growth factors, chemokines, IFN, and pro- and anti-inflammatory interleukins in serum and intraperitoneal fluids. Higher levels of pro-inflammatory cytokines were observed in the MOC31PE group compared to patients who did not receive the rIT, with time-dependent variability. In addition, elevated levels of innate proinflammatory cytokines, TNF, and a time-response curve for the strong T-cell stimulator IFN and its associated chemokine IFNγ-induced protein/chemokine (C-X-C motif) ligand 10 (IP-10) were noted in the serum of patient who received the rITs. Inferentially, elevated pro-inflammatory cytokines are associated with the induction of immunogenic cell death and have the potential to overturn "cold" tumors into immunologically "hot."[29] The study concluded that the overall survival in approximately 78% of patients was 3 years, with 53% achieving an overall survival rate of up to 5 years. In contrast, an intensified local inflammatory response was not found to adversely affect long-term outcomes. The authors reported a compartmentalized inflammatory response in the peritoneal cavity that correlates with the localized response, which was further enhanced by the peritoneal infusion of MOC31PE.

7. Bi-specific T-cell engagers (BiTEs)

BiTEs are a relatively new class of monoclonal antibodies that drive T-cells to cancer cells by binding to T-cells specific antigen (usually CD3) and tumor-specific surface antigens simultaneously.[30] For EpCAM-specific BiTEs, one arm of the antibody binds to T-cells, whereas the others recognize and bind to EpCAM. Catumaxomab is a chimeric (rat-murine) bispecific and trifunctional antibody that combines the qualities of bispecific molecules and traditional

monoclonal antibodies. Specifically, the antibody binds to three different cell types: dendritic cells, macrophages, and NK cells – the immune system's accessory cells which are activated when the Fc region binds to type I, IIa, and III Fcγ receptors on these cells. In 2010, a pivotal clinical study led by Heiss *et al.*[31] was conducted to investigate the efficacy of catumaxomab in treating malignant ascites, a common occurrence in aggressive cancers. A randomized phase II/III clinical trial was conducted in patients with EpCAM-positive tumors.[31] In the trial, cancer patients (n = 258) with recurrent symptomatic malignant ascites resistant to conventional treatment were randomly assigned to receive either paracentesis abdominis plus catumaxomab (experimental group) or to undergo paracentesis alone (control group). The catumaxomab treatment involved intraperitoneal administration on days 0, 3, 7, and 10 at doses of 10, 20, 50, and 150 μg, respectively. The results demonstrated that patients in the experimental group had significantly increased puncture-free survival time following paracentesis compared to the control group, with durations of 46 days versus 11 days and 77 days versus 13 days, respectively. In addition, patients treated with catumaxomab exhibited fewer signs and symptoms of ascites compared to the control group, with an overall survival of 77 days versus 44 days. The reported side effects were generally reversible and primarily associated with the immunologic mode of action. Overall, catumaxomab demonstrated a clear therapeutic benefit with an acceptable safety profile in patients with malignant ascites caused by epithelial malignancies, particularly in gastric cancer. This finding contradicts the results of a similar study in which a subset of patients with malignant pleural effusion who were administered with catumaxomab developed severe dose-limiting toxicities, including fatal sepsis, grade 3 erythema, and hepatobiliary tract disorders.[32] This further raises concerns regarding patient selection and the mechanism of action of catumaxomab. In this context, successive evaluations of catumaxomab have concentrated on its use for palliative intents for patients with late-stage diseases characterized by significant tumor burden associated with malignant ascites.[33,34] Further evaluation of catumaxomab was conducted to compare intravenous to intraperitoneal routes of administration. This is based on the premise that there is a positive correlation in the increased accumulation of fluid in the peritoneal cavity of patients with EpCAM-positive tumors.[35]

A multicenter, prospective, randomized, open-label phase II study consisting of 31 patients (≥18 years), with 15 patients receiving catumaxomab and chemotherapy with 5-fluorouracil, leucovorin, oxaliplatin, and docetaxel (FLOT), and 16 patients receiving only FLOT, was conducted.[36] A full set of catumaxomab consisted of four doses, and 12 patients in the study received the full dose. All patients had a histologically confirmed diagnosis of gastric cancer, including metastatic esophagogastric junction cancer types II and III, macroscopic peritoneal carcinomatosis (stages P1–4 according to Gilly's classification), and an ECOG performance status of 0 or 1. Patients were also required to have a life expectancy of at least 12 weeks, be medically fit to undergo gastrectomy after primary systemic and intraperitoneal treatment and have adequate organ function. Regarding exclusion criteria, patients with clinically significant cardiovascular disease within the past year, a history of human immunodeficiency virus infection, chronic hepatitis B or C, active and clinically serious infection, pre-existing neuropathy higher than grade 1, or distant metastasis other than peritoneal carcinomatosis were deemed ineligible for enrolment. In this study design, catumaxomab was administered every 3 days over a 10-day cycle using a constant infusion pump system to control the delivery of the drug over a period of 3 h. Dosage escalation from 10 to 150 μg was initiated before the administration of catumaxomab and the intravenous injection of 1 g of paracetamol as prophylaxis for cytokine-release-associated symptoms. After 7 days and the final infusion of catumaxomab, six cycles of FLOT chemotherapy were administered. The regimen consisted of 5-fluorouracil (2600 mg/m² as a 24-h infusion on day 1), leucovorin (200 mg/m² on day 1), oxaliplatin (85 mg/m² on day 1), and docetaxel (50 mg/m² on day 1), delivered every 2 weeks. The median follow-up period for patients was 52 months. Observed side effects (grade 3 – 4) associated with catumaxomab included nausea, elevated levels of liver enzymes and bilirubin, and abdominal pain. The authors did not observe any significant differences in median progression-free survival and overall survival between the various treatment strategies. The addition of catumaxomab to chemotherapy was well tolerated and feasible for advanced gastric cancer. Although the study did not demonstrate an improvement in the macroscopic complete remission rate of peritoneal carcinomatosis, catumaxomab exhibited an acceptable safety profile, and the addition of chemotherapy did not result in unexpected adverse reactions.[38] Another anti-EpCAM BiTE, known as solitomab, MT110, or AMG 110, was developed by Amgen. In a recent clinical trial, the bispecific single-chain antibody (scFv) construct/bispecific T-cell-engaging solitomab demonstrated efficacy in patients with refractory solid tumors.[37,38] This multicenter phase I study enrolled 65 patients who received varying doses (ranging between 1 and 96 μg/day) of solitomab via continuous intravenous infusion over a period of approximately 28 days. Following treatment, 15 patients experienced dose-limiting toxicities, whereas eight patients exhibited transient abnormal

liver parameters shortly after infusion initiation or dose escalation (grade 3, $n = 4$; grade 4, $n = 4$). In addition, one patient experienced grade 3 supraventricular tachycardia resulting in treatment discontinuation in all affected patients. Furthermore, six patients experienced dose-limiting toxicity in the form of diarrhea. Among these six patients, four (grade 3, $n = 3$; grade 4, $n = 1$) experienced resolution, one (grade 3) still experienced symptoms at the time of treatment-unrelated death, and one (grade 3) progressed to grade 5 after cessation of therapy. The MTD was determined to be 24 μg/day. Diarrhea, elevated liver parameters, and high lipase levels were the most frequently observed grade ≥3 treatment-related adverse events, occurring in 95% of patients. However, solitomab exhibited a half-life of 4.5 h, and serum levels reached a plateau within 1 day. The treatment of relapsed/refractory EpCAM-positive solid tumors with solitomab, a BiTE® antibody construct targeting solid tumors, resulted in dose-limiting toxicities, including severe diarrhea and elevated liver enzymes, thereby impeding dose escalation to potential therapeutic levels. Despite achieving the key endpoints of assessing the frequency and severity of adverse events, as well as understanding its PKs and antitumor activity, further investigation and exploration are required.[37] Table 1 presents a general overview of antibody-based targeted immunotherapies, which have either received approval or are currently in various stages of clinical evaluation.

8. Adoptive cell therapy (ACT)

Clinical trials of ACT-based immunotherapy against EpCAM-positive cancers have expanded within the last 5 years based on promising pre-clinical data. For example, an anti-EpCAM nanobody Chimeric antigen receptor T-cells (CAR T) with dectin-1 costimulatory domain demonstrated higher T-cell activation and less exhaustive phenotypes in xenograph mouse models, a finding that led to the initiation of clinical evaluation.[39] In the study, the authors conducted a phase I clinical investigation by enrolling 12 patients who were diagnosed with EpCAM-positive epithelial tumors (NCT02915445). During the study, 50% of patients experienced grade 1/2 toxicities. A total of 384 enrolled patients with multiple advanced-stage cancer types have been administered with anti-EpCAM CAR T.[42] In addition, an anti-EpCAM (scFv) CAR T therapy, indicated for antigen-positive colon, esophagus, pancreas, and prostate tumors, concluded its Phase I/II recruiting 60 patients (NCT03013712) concluded in 2020 without further information on study outcome (https://clinicaltrials.gov/study/NCT03013712). In the study, a novel CAR consisting of an anti-EpCAM(scFv) fused to two intracellular co-stimulatory signaling domains derived from CD3-zeta and CD28 was administered at the infusion dose of $1 - 10 \times 10^6$ modified T cells/kg.[40] Table 2 provides a list of the ongoing and completed anti-EpCAM CAR T clinical studies, with the majority still in early phases. Out of the 10 ongoing clinical trials, five are clinical

Table 1. Selected anti-EpCAM antibody-based immunotherapies that have been approved or currently undergoing clinical evaluation

Product name/Clinical trial #	Status	Indications	Reported adverse effects
Catumaxomab	Approved	• EpCAM-positive tumors • Malignant Ascites	Fever, nausea, vomiting, abdominal pain, and elevated liver enzymes
Edrecolomab (17-1A)	Phase III	• Mucinous adenocarcinoma of the colon • Adenocarcinoma of colon • Stage IIA – IIC colon cancer	High immunogenicity, short serum half-life
Adecatumumab (MT201)	Phase II	• Metastatic breast cancer	Chills, nausea, fatigue, and diarrhea
M701	Phase I	• Malignant ascites • Advanced solid tumors	Grade 1 adverse drug events
EMD 273066	Phase I	• EpCAM-positive ovarian and colorectal carcinomas • Non-small-cell lung cancer • Prostate cancer	Unknown
ING-1	Phase I	• Advanced adenocarcinomas	Acute pancreatitis, asthenia
Citatuzumab bogatox	Phase I	• Advanced epithelial tumors	Fever, hypotension, and hypoalbuminemia
Opportuzumab monatox	Phase I and II	• Squamous cell carcinoma of the head and neck • Non-muscle invasive bladder cancer • *In situ* urothelial carcinoma of the bladder	Pain at the site of injection, mild-to-moderate adverse effects
MOC31PE	Phase I	• Advanced adenocarcinomas	Reversible liver toxicity
Solitomab (MT110)	Phase 1	• Relapse/refractory tumors	Elevated hepatic enzymes, and diarrhea

Abbreviation: EpCAM: Epithelial cell adhesion molecule.

Table 2. Selected ongoing and clinically approved anti-EpCAM ACTs clinical trials (Clinicaltrial.gov)

Trial identifier	Phases	Year	Indications	No. of enrolments	Study location
NCT02729493	NA	2019	Hepatocellular carcinoma	25	China
NCT02725125	NA	2015 – 2019	Stomach neoplasms	19	China
NCT02915445	Phase I	2016 – 2023	Malignant neoplasms of nasopharynx, breast, and stomach cancer with metastasis	30	China
NCT03563326	Phase I	2018 – 2022	Advanced-stage gastric cancer with peritoneal metastasis	40	China
NCT03013712	Phase I and II	2017 – 2020	Multiple cancer types	60	China
NCT04151186	NA	2019 – 2021	Advanced solid tumor	72	China
NCT05703815	NA	2023 – ongoing	Invasive breast cancer with EpCAM and p53 expressions	40	Egypt
NCT05576519	NA	2017 – 2022	Ovarian carcinoma	50	Egypt
NCT05028933	Phase I	2021 – 2024	Advanced-stage hepatocellular carcinoma, as well as colorectal, gastric and pancreatic cancers	48	China

Abbreviations: ACT: Adoptive cell therapy; EpCAM: Epithelial cell adhesion molecule.

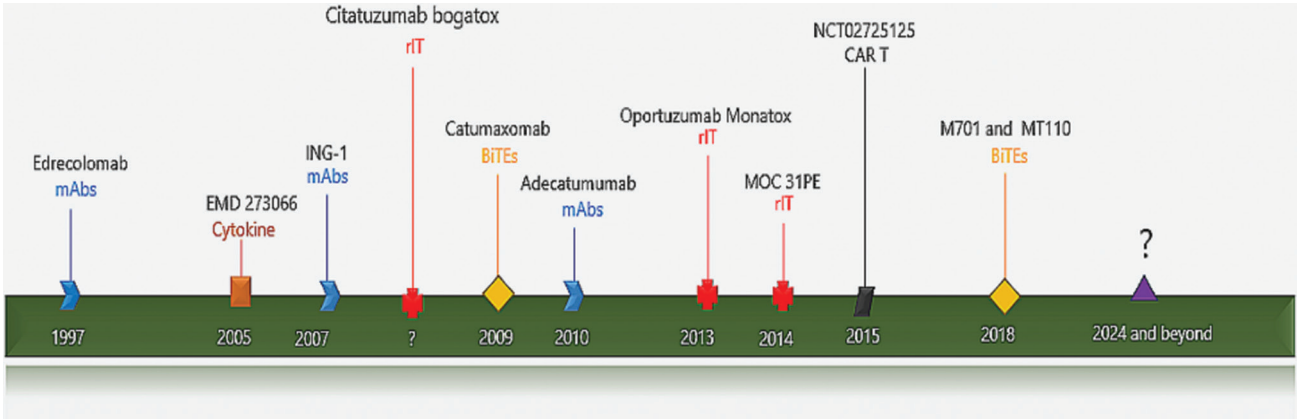

Figure 2. Timelines for the initial clinical evaluation of selected anti-EpCAM immunotherapies. The schematic is derived from pooled study evidence pertaining to the initial year in which the clinical studies were conducted (https://clinicaltrials.gov).
Abbreviation: CAR T: Chimeric antigen receptor T-cells.

observational studies. Taken together, it appears that CAR T therapy targeting EpCAM-overexpressing cancers is primarily indicated for advanced-stage solid malignancies.

The anti-EpCAM therapy landscape has expanded to cover almost all aspects of cancer immunotherapy. Figure 2 represents the timelines for the initial clinical evaluation of selected anti-EpCAM immunotherapies (https://clinicaltrials.gov). The estimated year of the evaluation was based on the reported year of publication of the first clinical study results.

9. Concluding remarks and perspectives

Precision medicine seeks to provide customized solutions for disease management by stratifying patients into subpopulations based on disease-specific profiles,[41] allowing for the identification of patients with the highest probabilities of responding positively to targeted therapies. However, tumor classification based on routine diagnostic assays undermines the precision medicine paradigm due to its limitations: (i) variability in therapeutic response and clinical outcomes, even among tumors with similar clinicopathological features; and (ii) neglect of the biological significance and molecular pathways that differentiate tumors into distinct subtypes and stages.

In breast cancer, for example, variability in tumor responses and drug-induced adverse events is associated with the transcriptional profiles of CSRs in breast tumors and normal tissues. Clinical trials designed to evaluate the efficacy of CSR-targeting treatments often fail due to dose-limiting toxicity and other undesirable side effects.[42,43] The toxicity and side effects of CSR-targeting drugs are at least partially attributable to the expression of the targeted CSR in healthy tissues.[44,45] Therefore,

treatment success rates could be improved, and associated off-target toxicity limited, by targeting CSRs that are both overexpressed in cancer cells and under-expressed in proximal and distal healthy tissues. In light of this, statistical methods, machine learning, and predictive modeling have been applied to determine which CSRs in breast cancer subtypes, if targeted by therapeutics, would have the lowest likelihood of off-target toxicity.[46] However, the varied outcomes in pre-/clinical settings when targeting EpCAM can be attributed to the substantial heterogeneity of EpCAM expression, both within tumor subtypes and between diseased and healthy tissues suggesting that EpCAM may not be an "easy" therapeutic target.[42,43] Although monoclonal antibody-based immunotherapy was the first to undergo clinical testing against EpCAM-positive cancers, an increasing focus on armed antibody-based targeted therapies, specifically rIT, has been subjected to clinical evaluation in recent decades. This trend may be attributed to the marginal successes achieved by relying on monoclonal antibodies as monotherapy. Researchers have recognized the importance of actively inducing cytotoxicity in EpCAM-positive tumor cells by arming antibodies with bacterial or plant-derived toxins. Nevertheless, adverse effects associated with earlier generations of rITs have primarily emerged from dose-limiting antidrug immune responses and vascular leak syndromes, which have led to severe clinical complications.[47,48] Furthermore, immunotherapy strategies such as BiTEs, cytokines, ACTs targeting EpCAM overexpression, and recruitment of cytotoxic T cells to tumor sites have made significant strides in clinical studies, despite some minor limitations. For instance, the favorable clinical outcomes of anti-EpCAM BiTEs were only observed in combination with chemotherapy. This is similar to the limited clinical trial reports on ACTs (which mainly rely on T-cell mediated cytotoxicity) and therefore may require active immunotherapy or chemoradiation combination for improved efficacy against EpCAM-positive solid cancers.[49] Because clinical endpoints of early-phase clinical testing are measured with the toxicity and efficacy profiles, there is a need to strike a balance in designing future EpCAM-specific clinical trials. In this regard, EpCAM-specific immunotherapy may be enhanced by adopting a more recent innovative approach such as the delivery of therapeutic payloads by envelope-targeted vectors.[50]

Furthermore, EpCAM overexpression mediates the development of resistance to several anticancer therapies in different tumor types.[51-53] This induced tumor plasticity post-therapy observed in pre-clinical models partly contributes to the challenges affecting the smooth translation of anti-EpCAM therapies into clinical practice. This concept may be considered in future therapy development and clinical trial designs, including patient selection and measurement of baseline characteristics. In addition, the development of new therapies may require an improved understanding of the biology and signaling pathways associated with EpCAM such that their selective efficacy is dependent on the affinity of the receptor-targeting domain, which drives the toxic domains to the target in the case of armed antibody therapies. Importantly, the high specificity of the EpCAM-targeting ligands can contribute to limiting off-target toxicities and interference with signaling pathways involving similar surface receptors through crosstalk signaling. However, it is important to strike the balance between the binding affinity of anti-EpCAM ligands and on- and off-target toxicities. In this context, our group and others have demonstrated the potential of recombinant antibodies fused to the N-terminus of bacteria and human-based toxins for the generation of rITs and cytolytic fusion proteins targeting multiple cancers.[54,55] In addition to these advances, other immunotherapeutics such as CAR T, cytokines, therapeutic nucleic acids, and oncolytic viruses for the therapy of EpCAM-positive cancers are under development, harboring the potential to transition into clinical evaluations.[55-58] Furthermore, arming EpCAM-targeting antibodies with humanized toxin moieties is a promising approach for reducing antitoxin immune responses. In this regard, supercomputing and protein engineering techniques aimed at identifying and ablating reactive epitopes while retaining the cytolytic properties of the attached toxin remain the gold standard that needs to be explored.[59] These approaches, together with the development of less immunogenic and humanized toxin domains and the activation of antitumor immune effectors, are the desired anti-EpCAM-targeted therapeutic strategies awaiting future applications. Finally, high-throughput analysis of spatiotemporal distribution, identification, and capitalization on significant tumor vulnerabilities, as well as the density of EpCAM overexpression in heterogeneous tumor lesions remain important factors to be explored.[60-62] Taken together, these suggestions may guide the design of future clinical trials allowing for the potential approval of EpCAM-specific immunotherapies.

Acknowledgments

D.M.D. acknowledges the award of the Google PhD Fellowship by Google LLC.

Funding

This work is based on the research supported by the South African Research Chairs Initiative of the Department

of Science and Technology administered through the National Research Foundation of South Africa (Grant Number 47904).

Conflict of interest

The authors declare no conflicts of interest.

Author contributions

Conceptualization: Dennis Makafui Dogbey, Stefan Barth
Writing–original draft: Dennis Makafui Dogbey, Ursula-Claire Andong-Koung-Edzidzi, Gomolemo Atlegang Molope, Jesmika Singh, Tatenda Lovemore Bvudzijena
Writing–review & editing: Krupa Naran, Stefan Barth

Ethics approval and consent to participate

Not applicable.

Consent for publication

Not applicable.

Availability of data

Not applicable.

References

1. Satofuka H, Wang Y, Yamazaki K, *et al*. Characterization of human anti - EpCAM antibodies for developing an antibody - drug conjugate. *Sci Rep.* 2023;13:4225.

   doi: 10.1038/s41598-023-31263-x

2. Pavšič M, Gunčar G, Djinovi-Carugo K, Lenarčič B. Crystal structure and its bearing towards an understanding of key biological functions of EpCAM. *Nat Commun.* 2014;5:4764.

   doi: 10.1038/ncomms5764

3. Mitra M, Kandalam M, Verma RS, Umamaheswari K. Genome-wide changes accompanying the knockdown of Ep-CAM in retinoblastoma. *Mol Vis*. 2010;16:828-842.

4. Nagao K, Zhu J, Heneghan MB, *et al*. Abnormal placental development and early embryonic lethality in EpCAM-Null mice. *PLoS One*. 2009;4:e8543.

   doi: 10.1371/journal.pone.0008543

5. Imrich S, Hachmeister M, Gires O. EpCAM and its potential role in tumor-initiating cells. *Cell Adh Migr*. 2012;6:30-38.

   doi: 10.4161/cam.18953

6. Schnell U, Kuipers J, Giepmans BN. EpCAM proteolysis: New fragments with distinct functions? *Biosci Rep.* 2013;33:321-332.

   doi: 10.1042/BSR20120128

7. Keller L, Werner S, Pantel K. Biology and clinical relevance of EpCAM. *Cell Stress*. 2019;3:165-180.

   doi: 10.15698/cst2019.06.188

8. Lei Z, Liu W, Nie Y, Yang Y, Chen G, Huang L. EpCAM is essential to maintaining the immune homeostasis of intestines via keeping the expression of pIgR in the intestinal epithelium of mice. *Front Immunol*. 2022;13:1-15.

   doi: 10.3389/fimmu.2022.843378

9. Siddiqui H, Rawal P, Bihari C, Arora N, Kaur S. Vascular endothelial growth factor promotes proliferation of epithelial cell adhesion molecule-positive cells in nonalcoholic steatohepatitis. *J Clin Exp Hepatol*. 2020;10:275-283.

   doi: 10.1016/j.jceh.2019.11.011

10. Schwartzberg LS. Clinical experience with edrecolomab: A monoclonal antibody therapy for colorectal carcinoma. *Crit Rev Oncol Hematol*. 2001;40:17-24.

    doi: 10.1016/S1040-8428(01)00131-7

11. Punt CJ, Nagy A, Douillard JY, *et al*. Edrecolomab alone or in combination with fluorouracil and folinic acid in the adjuvant treatment of stage III colon cancer: A randomised study. *Lancet*. 2002;360:671-677.

    doi: 10.1016/S0140-6736(02)09836-7

12. Oberneder R, Weckermann D, Ebner B, *et al*. A phase I study with adecatumumab, a human antibody directed against epithelial cell adhesion molecule, in hormone refractory prostate cancer patients. *Eur J Cancer*. 2006;42:2530-2538.

    doi: 10.1016/j.ejca.2006.05.029

13. Autio KA, Boni V, Humphrey RW, Naing A. Probody therapeutics: An emerging class of therapies designed to enhance on-target effects with reduced off-tumor toxicity for use in immuno-oncology. *Clin Cancer Res.* 2020;26:984-989.

    doi: 10.1158/1078-0432.CCR-19-1457

14. Zheng X, Wu Y, Bi J, *et al*. The use of supercytokines, immunocytokines, engager cytokines, and other synthetic cytokines in immunotherapy. *Cell Mol Immunol*. 2022;19:192-209.

    doi: 10.1038/s41423-021-00786-6

15. Neri D, Sondel PM. Immunocytokines for cancer treatment: Past, present and future immunocytokine formats Europe PMC Funders Group. *Curr Opin Immunol*. 2016;40:96-102.

    doi: 10.1016/j.coi.2016.03.006.Immunocytokines

16. Ko YJ, Bubley GJ, Weber R, *et al*. Safety, pharmacokinetics, and biological pharmacodynamics of the immunocytokine EMD 273066 (huKS-IL2). *J Immunother*. 2004;27:232-239.

    doi: 10.1097/00002371-200405000-00008

17. Connor JP, Lewis NL. A phase 1b study of humanized KS-interleukin-2 (huKS-IL2) immunocytokine with cyclophosphamide in patients with EpCAM-positive advanced solid tumors. *BMC Cancer.* 2013;13:20.

doi: 10.1186/1471-2407-13-20

18. Nambiar I. Analysis of serious adverse event: Writing a narrative. *Perspect Clin Res*. 2018;9:103-106.

doi: 10.4103/picr.PICR-52-18

19. Alewine C, Hassan R, Pastan I. Advances in anticancer immunotoxin therapy. *Oncologist*. 2015;20:176-185.

doi: 10.1634/theoncologist.2014-0358

20. Di Paolo C, Willuda J, Kubetzko S, *et al*. A recombinant immunotoxin derived from a humanized epithelial cell adhesion molecule-specific single-chain antibody fragment has potent and selective antitumor activity. *Clin Cancer Res*. 2003;9:2837-2848.

21. Pastan I, Hassan R, FitzGerald DJ, Kreitman RJ. Immunotoxin therapy of cancer. *Nat Rev Cancer*. 2006;6:559-565.

doi: 10.1038/nrc1891

22. Kowalski M, Entwistle J, Cizeau J, *et al*. A phase i study of an intravesically administered immunotoxin targeting EpCAM for the treatment of nonmuscle-invasive bladder cancer in BCG-refractory and BCG-intolerant patients. *Drug Des Devel Ther*. 2010;4:313-320.

doi: 10.2147/DDDT.S14071

23. MacDonald GC, Rasamoelisolo M, Entwistle J, *et al*. A phase I clinical study of VB4-845: Weekly intratumoral administration of an anti-EpCAM recombinant fusion protein in patients with squamous cell carcinoma of the head and neck. *Drug Des Devel Ther*. 2009;2:105-114.

doi: 10.2147/dddt.s3442

24. Andersson Y, Engebraaten O, Juell S, *et al*. Phase I trial of EpCAM-targeting immunotoxin MOC31PE, alone and in combination with cyclosporin. *Br J Cancer*. 2015;113:1548-1555.

doi: 10.1038/bjc.2015.380

25. Andersson Y, Inderberg EM, Kvalheim G, *et al*. Immune stimulatory effect of anti-EpCAM immunotoxin-improved overall survival of metastatic colorectal cancer patients. *Acta Oncol (Madr)*. 2020;59:404-409.

doi: 10.1080/0284186X.2019.1704864

26. Billmann Thorgersen E, Asvall J, Storhaug Frøysnes I, *et al*. Increased local inflammatory response to MOC31PE immunotoxin after cytoreductive surgery and hyperthermic intraperitoneal chemotherapy. *Ann Surg Oncol*. 2021;28:5252-5262.

doi: 10.1245/s10434-021-10022-0

27. Hassan R, Alewine C, Pastan I. New life for immunotoxin cancer therapy. *Clin Cancer Res*. 2016;22:1055-1058.

doi: 10.1158/1078-0432.CCR-15-1623

28. Thorgersen EB, Asvall J, Frøysnes IS, *et al*. Increased local inflammatory response to MOC31PE immunotoxin after cytoreductive surgery and hyperthermic intraperitoneal chemotherapy. *Ann Surg Oncol*. 2021;28:5252-5262.

doi: 10.1245/s10434-021-10022-0

29. Showalter A, Limaye A, Oyer JL, *et al*. Cytokines in immunogenic cell death: Applications for cancer immunotherapy. *Cytokine*. 2017;97:123-132.

doi: 10.1016/j.cyto.2017.05.024

30. Simão DC, Zarrabi KK, Mendes JL, *et al*. Bispecific T-Cell engagers therapies in solid tumors: Focusing on prostate cancer. *Cancers (Basel)*. 2023;15:1412.

doi: 10.3390/cancers15051412

31. Heiss MM, Murawa P, Koralewski P, *et al*. The trifunctional antibody catumaxomab for the treatment of malignant ascites due to epithelial cancer: Results of a prospective randomized phase II/III trial. *Int J Cancer*. 2010;127:2209-2221.

doi: 10.1002/ijc.25423

32. Sebastian M, Kiewe P, Schuette W, *et al*. Treatment of malignant pleural effusion with the trifunctional antibody catumaxomab (removab) (anti-EpCAM Â anti-CD3) results of a phase 1/2 study. *J Immunother*. 2009;32:195-202.

doi: 10.1097/CJI.0b013e318195b5bb

33. Jäger M, Schoberth A, Ruf P, *et al*. Immunomonitoring results of a phase II/III study of malignant ascites patients treated with the trifunctional antibody catumaxomab (Anti-EpCAM x anti-CD3). *Cancer Res*. 2012;72:24-32.

doi: 10.1158/0008-5472.CAN-11-2235

34. Burges A, Wimberger P, Kümper C, *et al*. Effective relief of malignant ascites in patients with advanced ovarian cancer by a trifunctional anti-EpCAM x anti-CD3 antibody: A phase I/II study. *Clin Cancer Res*. 2007;13:3899-3905.

doi: 10.1158/1078-0432.CCR-06-2769

35. Seeber A, Martowicz A, Spizzo G, *et al*. Soluble EpCAM levels in ascites correlate with positive cytology and neutralize catumaxomab activity *in vitro*. *BMC Cancer*. 2015;15:372.

doi: 10.1186/s12885-015-1371-1.

36. Knödler M, Körfer J, Kunzmann V, *et al*. Randomised phase II trial to investigate catumaxomab (anti-EpCAM × anti-CD3) for treatment of peritoneal carcinomatosis in patients with gastric cancer. *Br J Cancer*. 2018;119:296-302.

doi: 10.1038/s41416-018-0150-6

37. Kebenko M, Goebeler ME, Wolf M, *et al*. A multicenter phase 1 study of solitomab (MT110, AMG 110), a bispecific EpCAM/CD3 T-cell engager (BiTE®) antibody construct, in patients with refractory solid tumors. *Oncoimmunology*. 2018;7:e1450710.

doi: 10.1080/2162402X.2018.1450710

38. Bellone S, Black J, English DP, *et al*. Solitomab, an EpCAM/CD3 bispecific antibody construct (BiTE), is highly active against primary uterine serous papillary carcinoma cell lines *in vitro*. *Am J Obstet Gynecol*. 2016;214:99.e1-99.e8.

doi: 10.1016/j.ajog.2015.08.011

39. Li D, Guo X, Yang K, *et al*. EpCAM-targeting CAR-T cell immunotherapy is safe and efficacious for epithelial tumors. *Sci Adv*. 2023;9:eadg9721.

doi: 10.1126/sciadv.adg9721

40. Yu YD, Kim TJ. Chimeric antigen receptor-engineered T cell therapy for the management of patients with metastatic prostate cancer: A comprehensive review. *Int J Mol Sci*. 2021;22:640.

doi: 10.3390/ijms22020640

41. Ashley EA. Towards precision medicine. *Nat Rev Genet*. 2016;17:507-522.

doi: 10.1038/nrg.2016.86

42. Arrowsmith J, Miller P. Trial watch: Phase II and phase III attrition rates 2011-2012. *Nat Rev Drug Discov*. 2013;12:569.

doi: 10.1038/nrd4090

43. Mak IW, Evaniew N, Ghert M. Lost in translation: Animal models and clinical trials in cancer treatment. *Am J Transl Res*. 2014;6(2):114-118.

44. Ryaboshapkina M, Hammar M. Tissue-specific genes as an underutilized resource in drug discovery. *Sci Rep*. 2019;9:7233.

doi: 10.1038/s41598-019-43829-9

45. Nguyen PA, Born DA, Deaton AM, Nioi P, Ward LD. Phenotypes associated with genes encoding drug targets are predictive of clinical trial side effects. *Nat Commun*. 2019;10:1579.

doi: 10.1038/s41467-019-09407-3

46. Sinkala M, Naran K, Ramamurthy D, *et al*. Machine learning and bioinformatic analyses link the cell surface receptor transcript levels to the drug response of breast cancer cells and drug off-target effects. *PLoS One*. 2024;19:e0296511.

doi: 10.1371/journal.pone.0296511

47. Wayne AS, Fitzgerald DJ, Kreitman RJ, Pastan I. Immunotoxins for leukemia. *Blood*. 2015;123:2470-2478.

doi: 10.1182/blood-2014-01-492256.2470

48. Morgan RN, Saleh ES, Farrag AH, Aboshanab MK. New insights on Pseudomonas aeruginosa exotoxin A-based immunotoxins in targeted cancer therapeutic delivery. *Ther Deliv*. 2023;14:31-60.

doi: 10.4155/tde-2022-0055

49. Papaioannou NE, Beniata OV, Vitsos P, Tsitsilonis O, Samara P. Harnessing the immune system to improve cancer therapy. *Ann Transl Med*. 2016;4:261.

doi: 10.21037/atm.2016.04.01

50. Lv Y, Zhang H, Cui Z, *et al*. Gene delivery to breast cancer by incorporated EpCAM targeted DARPins into AAV2. *BMC Cancer*. 2023;23:1220.

doi: 10.1186/s12885-023-11705-5

51. Tavsan Z, Ayar Kayalı H. EpCAM-claudin-tetraspanin-modulated ovarian cancer progression and drug resistance. *Cell Adh Migr*. 2020;14:57-68.

doi: 10.1080/19336918.2020.1732761

52. Ni J, Cozzi P, Beretov J, *et al*. Epithelial cell adhesion molecule (EpCAM) is associated with prostate cancer progression and chemo-/radio-resistance *in vitro* and *in vivo*. *BMC Cancer*. 2017;18:2833-2833.

doi: 10.1158/1538-7445.am2017-2833

53. Mal A, Bukhari AB, Singh RK, *et al*. EpCAM-mediated cellular plasticity promotes radiation resistance and metastasis in breast cancer. *Front Cell Dev Biol*. 2021;8:597673.

doi: 10.3389/fcell.2020.597673

54. Hristodorov D, Amoury M, Mladenov R, *et al*. EpCAM-selective elimination of carcinoma cells by a novel MAP-based cytolytic fusion protein. *Mol Cancer Ther*. 2014;13:2194-2202.

doi: 10.1158/1535-7163.MCT-13-0781

55. Qu W, Meng B, Yu Y, Wang S. EpCAM antibody-conjugated mesoporous silica nanoparticles to enhance the anticancer efficacy of carboplatin in retinoblastoma. *Mater Sci Eng C*. 2017;76:646-651.

doi: 10.1016/j.msec.2017.03.036

56. Kapka-Skrzypczak L, Popek S, Sawicki K, *et al*. IL-6 prevents CXCL8-induced stimulation of EpCAM expression in ovarian cancer cells. *Mol Med Rep*. 2019;19:2317-2322.

doi: 10.3892/mmr.2019.9890

57. Zhang BL, Li D, Gong YL, *et al*. Preclinical evaluation of chimeric antigen receptor-modified T cells specific to epithelial cell adhesion molecule for treating colorectal cancer. *Hum Gene Ther*. 2019;30:402-412.

doi: 10.1089/hum.2018.229

58. Zhang Y, Xie X, Yeganeh PN, *et al*. Immunotherapy for breast cancer using EpCAM aptamer tumor-targeted gene knockdown. *Proc Natl Acad Sci U S A*. 2021;118: e2022830118.

doi: 10.1073/pnas.2022830118

59. Kouba P, Kohout P, Haddadi F, *et al*. Machine learning-guided protein engineering. *ACS Catal*. 2023;13:13863-13895.

doi: 10.1021/acscatal.3c02743

60. Guo L, Kong D, Liu J, *et al*. Breast cancer heterogeneity and its implication in personalized precision therapy. *Exp Hematol Oncol.* 2023;12:1-27.

doi: 10.1186/s40164-022-00363-1

61. Patkulkar PA, Subbalakshmi AR, Jolly MK, Sinharay S. Mapping spatiotemporal heterogeneity in tumor profiles by integrating high-throughput imaging and omics analysis. *ACS Omega.* 2023;8:6126-6138.

doi: 10.1021/acsomega.2c06659

62. Shieh GS. Harnessing synthetic lethal interactions for personalized medicine. *J Pers Med*. 2022;12:98.

doi: 10.3390/jpm12010098

ACCSCIENCE PUBLISHING

Tumor Discovery

REVIEW ARTICLE

Immunocytochemistry profiling of ovarian cysts: A review of its clinical utility, future direction, and challenges

Owajioniro Godstime Mordecai[1†], Yibala Ibor Oboma[2*], and Raphael Teme[3†]

[1]Department of Histopathology and Cytology, Faculty of Medical Laboratory Science, Federal University, Otuoke, Bayelsa State, Nigeria

[2]Department of Medical Laboratory Science, School of Allied Health Sciences, Kampala International University Western Campus, Kampala, Uganda

[3]Department of Histopathology/Cytopathology, Faculty of Medical Laboratory Science, Rivers State University, Port Harcourt, Rivers State, Nigeria

Abstract

Ovarian cysts are fluid-filled sacs located in or on the surface of the ovaries. They can affect women of all ages but are most commonly seen in those of reproductive age and postmenopausal women. The two primary types of ovarian cysts are functional and pathological. Due to their asymptomatic nature, ovarian cysts are frequently diagnosed at later stages, potentially limiting therapeutic options and negatively affecting patient outcomes. Early detection requires diagnostic modalities that can differentiate between benign and malignant ovarian lesions. One promising approach is the use of immunocytochemistry (ICC) in the diagnosis of ovarian cysts, a rapidly evolving method in ovarian pathology. ICC utilizes antibodies to detect and visualize specific cellular antigens (proteins) in cytology specimens, serving as an ancillary diagnostic technique for establishing empirical diagnoses, predicting biomarkers, and assessing prognosis. A standard ICC protocol entails sample preparation, fixation, permeabilization, blocking, immunolabeling, counter-staining, and microscopic imaging of stained cells. Specific biomarkers play a significant role in distinguishing between benign and malignant ovarian cysts. Commonly used biomarkers include Cancer antigen 125, Ki-67, p53, HE4, and WT1. Future directions in this field are likely to focus on multiplex ICC, the discovery of novel biomarkers, the integration of artificial intelligence with other diagnostic modalities, and improving the standardization of ICC practice. Integrating these biomarkers into ovarian pathology will enable accurate diagnosis with reduced turnaround times, overcoming the limitations of hematoxylin and eosin staining methods.

Keywords: Immunocytochemistry; Profiling; Ovarian cyst; Review

†These authors contributed equally to this work.

***Corresponding author:**
Yibala Ibor Oboma
(yibalaoboma@kiu.ac.ug)

Citation: Mordecai OG, Oboma YI, Teme R. Immunocytochemistry profiling of ovarian cysts: A review of its clinical utility, future direction, and challenges. *Tumor Discov*. 2025;4(1):14-26.
doi: 10.36922/td.5369

Received: October 21, 2024

1st revised: December 9, 2024

2nd revised: December 16, 2024

Accepted: December 16, 2024

Published online: January 9, 2025

1. Introduction

Ovarian cysts, also known as adnexal cysts, are among the plethora of gynecological challenges faced by clinicians every day. These cysts are best described as fluid-filled sacs located inside or on the epithelial surface of the ovaries. While ovarian cysts can occur in females of all ages, they are more prevalent in those of reproductive age, particularly

around menarche, due to increased endogenous hormone production.[1-3] Their asymptomatic nature complicates early detection, which could have enhanced clinical management and improved patient outcomes. Consequently, ovarian cysts are often diagnosed at a later stage, negatively impacting therapeutic options and patient outcomes. These ovarian masses can significantly affect the reproductive vibrancy of women, survival, and overall health status.[4,5] Ovarian cysts are broadly grouped into functional (physiological) and non-functional (pathological) cysts. Functional cysts include follicular and luteal cysts, while pathological cysts are further classified into benign and malignant cysts.[6] Benign cysts often resolve spontaneously and require minimal intervention, whereas malignant cysts engender prompt and aggressive treatment.[7] An accurate diagnostic distinction between benign and malignant ovarian cysts is significant for definitive patient treatment and outcomes. Immunocytochemistry (ICC) plays a key role in distinguishing between benign and malignant ovarian lesions. This diagnostic technique uses antibodies to detect and visualize specific cellular antigens (proteins) in cytology specimens, offering detailed and distinct cellular and molecular insights on tissues.[8] Clinical manifestations of ovarian cysts may include pelvic and abdominal pain, bloating, and menstrual irregularities. Complications such as ovarian torsion (twisting of the ovaries) and rupture can arise, underscoring the need for timely diagnosis and management.[9] This review explores the diagnostic role of ICC in distinguishing between benign and malignant ovarian lesions.

2. Scope and methodology of the review

The research strategy for this review involved a systematic and integrative approach encompassing literature collection, data extraction, synthesis, and analysis. This strategy ensured a thorough exploration of the topic across multiple perspectives. Key biomedical, public health, and imaging databases such as PubMed, Scopus, Web of Science, and EMBASE were used. The search strategy incorporated specific keywords and Medical Subject Headings terms related to ovarian cancer and tumor markers.

3. Pathogenesis of ovarian cysts

The pathogenesis of ovarian cysts remains poorly understood, though several established hypotheses suggest a complex interplay of hormonal, molecular, immunological, and environmental factors (Figure 1). One of the most common hypotheses involves alterations in the regulation of hormones associated with ovulation,[10] particularly disruptions in the hypothalamus-pituitary axis that impair the adequate release of luteinizing hormone. This deficiency can prevent ovulation, leading to the formation of follicular cysts. Another molecular hypothesis suggests that mutations in oncogenes, such as *KRAS* and *BRAF*, activate the MAPK signaling pathway,[11] contributing to cyst development. In addition, ovarian cysts may also arise from the exposure of ovarian surface epithelial cells to inflammatory cytokines, such as interleukin-6, and reactive oxygen species linked to ovulation or physical trauma, resulting in DNA damage.[12]

4. Classification of ovarian cysts

Ovarian cysts are classified into functional (physiological) and non-functional (pathological) cysts. The World Health Organization's histological classification includes benign, malignant, and metastatic cysts based on their histogenesis.[10] Functional cysts include follicular and luteal cysts, which are typically self-limiting and may require less therapeutic intervention. In contrast, pathological cysts, further classified into benign and malignant cysts, require prompt and aggressive therapeutic interventions due to their life-threatening potential.[7]

4.1. Physiological cysts

Functional cysts: These cysts are non-neoplastic masses or enlargements (<3 mm) in women of reproductive years. They are the most common type of cysts during the menstrual cycle and arise due to either ovulation failure or corpus luteum formation. In cases of ovulation failure, cysts that form are lined by granulosa cells, persisting for a few days to a few weeks. The corpus luteum is formed from follicular remnants after ovulation and can develop into a cyst if it fails to dissolve within 14 days. Hyper-physiological ovarian response induces the development of functional cysts, such as the follicular, corpus luteum, and theca-lutein cysts.[14,15]

Follicular cysts: These are ovarian cysts that are formed when ovulation fails to occur, causing the follicles to grow without releasing a matured ovum. Histopathologically, follicular cysts are characterized by thin walls and pale acidophilic remnants. They often contain pigmented macrophages, degenerated oocytes, and cellular debris. Follicular cysts are lined by one to four layers of cuboidal granulosa cells without luteinization[15,16] (Figure 2).

Corpus luteum cysts: These are ovarian cysts that occur after successful ovulation, when the follicle releases the ovum, leading to the formation of corpus luteum from the follicular remnants (Figure 3). The corpus luteum is responsible for secreting progesterone. If fluid accumulates inside the corpus luteum and it fails to dissolve within 14 days of no pregnancy or 14 weeks after pregnancy, it enlarges into a cyst. These cysts are characterized by thick walls and are lined by many layers of luteinized granulosa

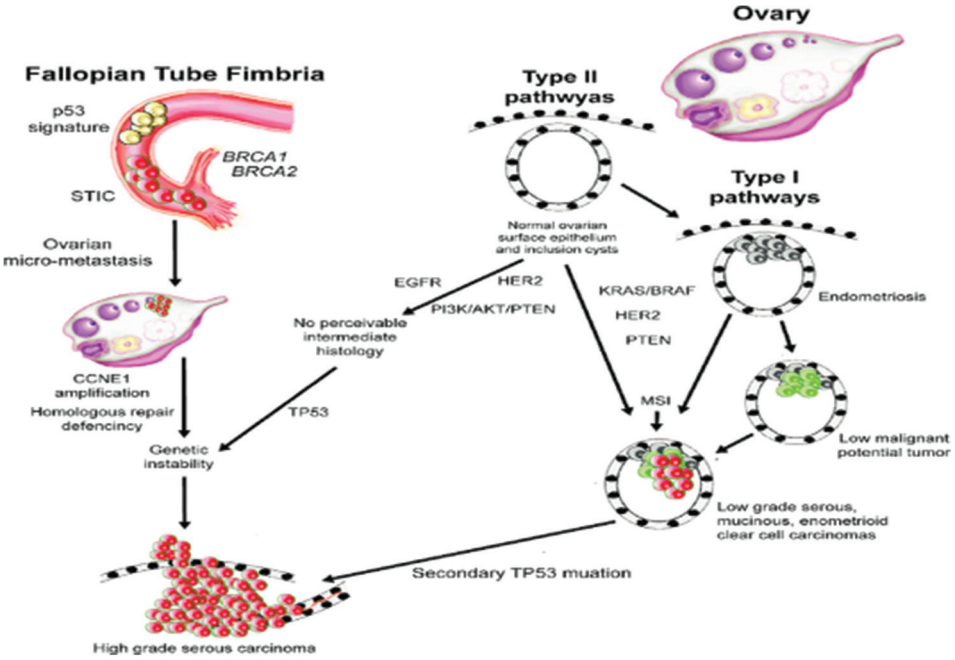

Figure 1. Pathogenesis of ovarian lesions[13]

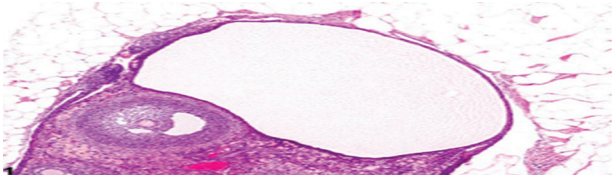

Figure 2. Follicular cysts.[23] Magnification ×100.

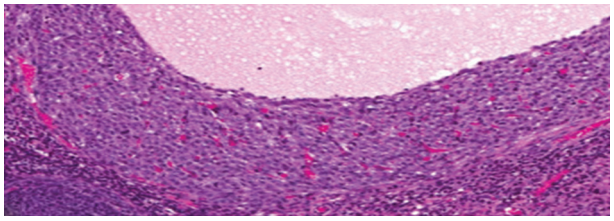

Figure 3. Corpus luteum cyst.[23] Magnification ×100.

cells (polygonal cells), containing abundant eosinophilic luteal cells with fine vacuoles.[3,16]

Theca-lutein cysts: These are ovarian cysts or luteinized follicle cysts that arise from hyperstimulation, leading to increased production of human chorionic gonadotropin hormone. Theca-lutein cysts usually occur during pregnancy, in women with gestational trophoblastic disease, multiple gestation, or ovarian hyperstimulation. These cysts are multilocular, thin-walled, and lined by luteinized theca cells exhibiting abundant stroma and hyperplasia.[16,17]

4.2. Pathological cysts

Benign ovarian cysts: These cysts are non-functional and can be self-limiting. Common types of benign ovarian cysts include serous and mucinous cystadenomas, dermoid cysts, polycystic ovarian syndrome, endometriotic cysts, and paraovarian cysts.[14,18] Histologically, serous cysts are lined by a monolayer of ciliated columnar epithelial cells, while the mucinous cysts are lined by epithelial cells that produce mucin.[19]

Mucinous cystadenoma: These cysts are benign ovarian cysts primarily resulting from the metaplasia of germinal epithelial cells. Occasionally, they can originate from a Brenner tumor or teratoma, typically preceded by mucinous transformation of the epithelium. Mucinous cystadenomas appear as translucent, ovoid masses with smooth capsules. Microscopically, they are lined by tall, secretory epithelium coupled with goblet cells and are characterized by thick walls and multiloculated structures.[14,19]

Serous cystadenoma: These cysts are notably more common compared to mucinous cystadenomas. The cystic fluid is characterized as thin, watery, and yellow-tinged with a smooth surface. Microscopically, distinguishing features of these cysts include psammoma bodies, which are calcified granules resulting from the degeneration of papillary implants. Serous cystadenomas are lined by a monolayer of ciliated columnar epithelial cells.[19]

Dermoid cyst: These cysts are a type of neoplastic cyst that originates from young ova, hypothesized to be

triggered by parthenogenetic processes in younger women. Gross examination indicates that they are thick-walled, opaque, and whitish (Figure 4). The contents of dermoid cysts include hair, cartilage, bone, and a significant amount of sebaceous greasy fluid. Histomorphologically, these cysts present with thick walls composed of ectodermal, mesodermal, and endodermal tissues.[7,14]

5. Malignant ovarian cysts

Malignant ovarian cysts are less common and primarily of histological origin, with various subtypes, as shown in Figure 5. Epithelial malignant ovarian cysts are the most prevalent, accounting for 90% of total cases. The incidence of these cysts is particularly high among postmenopausal women, especially those aged 60 – 70 years.[14] Malignant ovarian cysts include epithelial ovarian cancer, stromal tumors, and germ cell tumors.[13,20] Epithelial ovarian malignant lesions are subdivided into serous carcinoma, mucinous carcinoma, endometrioid, and clear cell carcinoma. Malignant germ cell tumors encompass embryonal carcinoma, immature teratoma, polyembryoma, and endodermal sinus tumors. Risk factors for malignancy include age, family history, genetic predispositions (such as *BRCA* mutations), and certain reproductive histories.[20,21] Histopathologically, malignant ovarian cysts exhibit complex papillae, necrotic foci, cystic spaces, neuroepithelial cells in solid sheets, and Call-Exner bodies.[22]

6. ICC

ICC is a diagnostic technique that involves applying antibodies to detect and visualize cellular antigens (proteins) of interest in cytology specimens, offering detailed cellular and molecular information on tissues.[8] This technique is particularly relevant in diagnostic cytopathology, offering improved sensitivity and specificity for detecting benign and malignant lesions compared to traditional hematoxylin and eosin staining. ICC can be performed using either direct or indirect methods, with the latter requiring a secondary antibody coupling. According to Kirbiš *et al*.,[24] ICC is considered an invaluable diagnostic technique for establishing empirical diagnosis, predicting biomarkers and prognosis, and determining the origin of tumors.[8,24] It can be applied to various cytology preparations, including direct smears, liquid-based preparations, cell blocks, cytospins, and cell cultures. Many institutions prefer using cell blocks due to their advantage of producing several identical sections for cases requiring a panel of ICC stains. In addition, most biomarkers have been validated on formalin-fixed paraffin-embedded (FFPE) tissue, eliminating the need for separate validation.[25-27] With the discovery of specific biomarkers, ICC has demonstrated the capability to distinguish between benign and malignant ovarian cysts.[28]

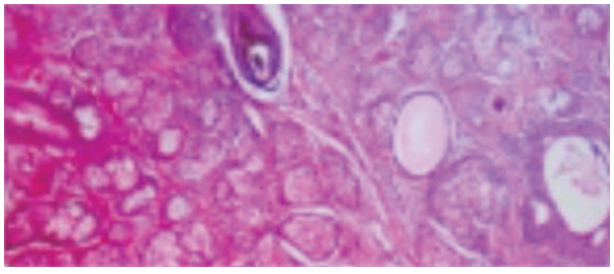

Figure 4. Dermoid cyst.[13] Magnification ×100.

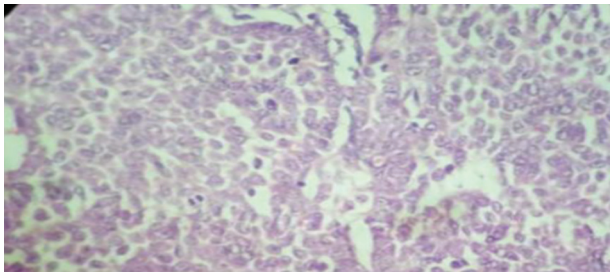

Figure 5. Malignant ovarian cancer.[13] Magnification ×100.

7. Principles and application of ICC

ICC relies on the complementary binding of antibodies to target proteins, known as antigens, in cells from pathological specimens. This technique involves labeling antibodies with enzymes, optionally counterstained with hematoxylin and eosin, and visualizing the results using a light microscope. ICC merges principles from immunology, cytochemistry, and histology to identify specific cellular structures. The fundamental principle of ICC is the identification, visualization, and localization of specific antigens based on a satisfactory signal-to-noise ratio. Signal amplification and the reduction of non-specific background staining are crucial strategies for achieving reliable results, which are invaluable for routine practices. The reaction involves primary and, in some cases, secondary antibodies, blockers, enzymes, and enzyme or fluorescent labels.[29] An antibody is an immunoglobulin molecule produced in response to the presence of an antigen. The choice of antibody for ICC is dependent on the specificity and sensitivity of the antibody-antigen binding reaction. Since antibodies are not visible under light or electron microscope, they must be labeled for visualization. This technique has widespread applications in diagnostic cytopathology, research, and therapeutic monitoring. In the context of ovarian cysts, ICC can identify specific biomarkers associated with benign and malignant lesions, offering critical information for diagnosis and clinical management. Profiling ovarian cysts involves using an antibody panel that targets specific biomarkers associated with benign and malignant cells, such as Cancer

antigen 125 (CA125), Ki-67, and p53. The expression of these biomarkers is analyzed using imaging techniques to distinguish between benign and malignant lesions.[29,30]

8. ICC versus traditional diagnostic methods

A standard ICC protocol entails several key steps: sample preparation, fixation, permeabilization, blocking, immunolabeling, counterstaining, and microscopic imaging of stained cells. Each step requires optimization, as experimental variables can significantly impact the overall staining outcome.[31-33] Traditional diagnostic methods for ovarian cysts include ultrasound, computed tomography (CT) scans, and magnetic resonance imaging (MRI). While these techniques provide essential cytomorphological information about the cyst's appearance and size, they are ineffective in distinguishing between benign and malignant cysts. Studies indicate that the sensitivity and specificity of these traditional diagnostic techniques range between 60% and 70%.[34] In contrast, ICC has shown improved sensitivity and specificity for differentiating benign from malignant cysts. A study by Li *et al*.[35] showed that a panel of antibodies targeting CA125, p53, and Ki-67 yielded a sensitivity of 93% and a specificity of 95% in distinguishing between benign and malignant cysts. Similarly, Lee *et al*.[36] demonstrated that ICC yielded a sensitivity of 91% and a specificity of 94% for detecting malignant ovarian cysts.

9. Advantages and limitations of ICC

The use of ICC in ovarian cyst profiling offers several advantages over traditional diagnostic techniques. It is a non-invasive, time-saving, and cost-effective technique.[37] ICC allows for accurate antigen localization and offers improved specificity and sensitivity in distinguishing between benign and malignant cysts, thereby reducing the likelihood of unnecessary surgical interventions. In addition, it facilitates the detection of specific biomarkers associated with benign and malignant lesions, which is crucial for therapeutic planning. It is often applied in both clinical and basic research.[38] However, ICC has limitations. One of the biggest limitations of ICC is the difficulty in standardizing the procedure due to the variations in specimen preparations, unlike ICC, which uses FFPE tissue sections. This variability can affect the interpretation of results, leading to diagnostic variability across different laboratories. Moreover, the choice of antibody panels in immunocytochemical profiling may differ among laboratories, contributing to diagnostic variability. A false negative result may occur due to inadequate samples or low cellularity.[39]

10. Markers in ovarian pathology

Tumor markers have emerged as critical diagnostic tools for characterizing and differentiating between tumor types. Biomarkers are biological substances or structures (antigens) produced by tumors and can be measured to detect the presence and stages of suspected tumors.[40] Various markers play significant roles in understanding ovarian pathology.

CA125: CA125 is encoded by the *MUC16* gene. It is one of the earliest known biomarkers of ovarian pathology. In healthy women, CA125 levels are typically below 36 units/mL.[40-42] Elevated serum levels of CA125 can indicate the presence of ovarian masses and other pathologies, such as uterine fibroid, endometriosis, pelvic inflammatory disease, and liver cirrhosis.[43] While approximately 80% of women with advanced epithelial ovarian cancer exhibit elevated levels of CA125, about 50% of cases with early-stage ovarian cancer also showed increased levels of CA125. This drawback disqualifies CA125 as a marker for ovarian cancer screening.[44] When used independently, CA125 has a sensitivity of 60% and specificity of 90%, with higher sensitivity and specificity observed in postmenopausal women as compared to premenopausal women. Integrating CA125 into the risk malignancy index algorithm (a risk assessment of ovarian cancer in clinical settings) enhanced its sensitivity to 87% and specificity to 97% for the detection of ovarian cancer.[45] However, CA125 is not suitable for early-stage detection of ovarian cancer. It offers a good diagnostic value for epithelial ovarian cancer, although its level is also elevated in benign ovarian cysts.[45]

Kallikreins (KLKs): KLKs are part of a 15-member *KLK* human gene family located on chromosome 19q. Their diagnostic and prognostic utility in cancer has been demonstrated in many studies. Twelve out of 15 members are upregulated in ovarian cancer, and these biomarkers are expressed in the endocrine epithelium. They are regulated by cancer hormones and are released and detected in various body fluids.[46,47] A study measuring the pre-operative serum levels of human KLK10 in 318 participants found significantly elevated results in 146 patients with ovarian cancer. The specificity and sensitivity of KLKs were reported to be 75% and 77%, respectively.[48]

Osteopontin (OPN): OPN is a glycophosphoprotein expressed in ovarian cancer, as well as in cervical, gastric, endometrial, hepatocellular, prostate, and breast cancers. Its secretion is primarily attributed to activated T-lymphocytes, leukocytes, and macrophages found at sites of inflammation and within the extracellular matrix. OPN, first discovered in 2001 from RNA isolated from ovarian cancer cell lines,[49] is associated with tumor progression, invasion, and metastasis. A study showed that OPN levels are more elevated in epithelial ovarian cancer compared to ovarian cyst.[50] Moreover, the study also revealed that

OPN plays a prognostic role by predicting the progression of disease in late-stage epithelial ovarian cancer with a specificity of 34% and sensitivity of 81%. The possibility of measuring OPN in urine samples of patients with high-grade ovarian cancer presents an opportunity for early diagnosis of ovarian cancer.[50]

Bikunin: Bikunin is a glycoprotein with several functions, known to mediate the suppression of invasion and metastasis of cancer cells. It can be measured in the tissue and plasma of patients with malignant conditions and serves as a prognostic marker for benign and malignant ovarian pathologies. A study reported that high levels of pre-operative bikunin are indicative of ovarian cancer prognosis.[51] This finding was consolidated by Tanaka *et al*.,[52] who analyzed bikunin protein levels in the plasma of ovarian cancer patients (n = 327), benign ovarian cyst patients (n = 200), and healthy controls (n = 200). The study concluded that bikunin is a useful prognostic marker of ovarian pathology, demonstrating 70% specificity and 75% sensitivity.

Vascular endothelial growth factor (VEGF): VEGF is a protein that enhances vascular permeability and plays a role in regulating physiological and pathological angiogenesis, as well as tumorigenesis. Elevated levels of VEGF levels have been observed in ovarian cancer patients. In a study by Matsuzaki *et al*.,[53] 12 out of 18 tumor samples from late-stage serous epithelial ovarian cancer patients showed strong positivity for VEGF, while six revealed low to negative expression of VEGF. The study reported that the levels of VEGF sensitivity and specificity were 79% and 74%, respectively.[53]

Human epididymis protein 4 (HE4): HE4 was first discovered as a biomarker of ovarian cancer in 1999. It is a peptide protease inhibitor that plays a critical role in the innate immune response of epithelial tissues and belongs to the whey acidic four-disulfide core (WFDC) protein family. HE4 was identified in the epithelium of the distal epididymis.[54] Since its discovery, HE4 has been observed to be significantly elevated in ovarian cancer and endometrial cancer, with a specificity of 95% and a sensitivity of 73%. Interestingly, studies indicated that HE4 protein is not expressed on the surface epithelium of the ovaries; however, its expression is found in 100% of human endometrioid epithelial ovarian cancer cases and slightly less in serous ovarian carcinoma.[55]

Creatine kinase B (CKB): CKB is known for its function in the metabolism of vertebral cells and exhibits unregulated expression in some cancers. CKB is a cytosolic form of creatine kinase. Studies have documented elevated expression of CKB in ovarian cancer. Research indicates that CKB activity is significantly higher in pre-operative serum in women with ovarian cancer compared to women with benign ovarian cysts. Notably, CKB expression is high in early-stage ovarian tumors, making it a potential biomarker for early detection of ovarian cancer.[56,57]

Human prostasin (PSN): PSN is located on chromosome 16p11.2 and is a 40 kDa, trypsin-like proteinase responsible for activating epithelial sodium channels. PSN has been designated as a novel biomarker for ovarian cancer, demonstrating a sensitivity of 51% and specificity of 94%.[58] However, a study by Tamir *et al*.[59] reported a sensitivity of 92% and specificity of 94% for detecting ovarian cancer when PSN was combined with CA125. Clinically, PSN serves as a differential diagnostic biomarker for ovarian cancer.

Mesothelin: Mesothelin was discovered at the National Cancer Institute, United States, in 1996. It is found in the mesothelial cells lining the peritoneum, pleura, and pericardium. It is an antigen with tumor differentiation properties, exhibiting a widespread expression in tumors, particularly in 70% of ovarian cancers. Tumor cells expressing mesothelin showed a greater tendency to migrate and metastasize.[60] As a potential novel biomarker for ovarian cancer, higher levels of mesothelin are associated with poor overall survival rates in patients. McIntosh *et al*.[61] demonstrated that a panel combining mesothelin and CA125 biomarkers yielded enhanced sensitivity for early detection of ovarian cancer.[62,63]

Transthyretin (TTR): TTR, a natural serum protein, is synthesized in the liver, retina, and choroid plexus. As a major carrier for serum thyroxine and retinal complex, it is responsible for transporting thyroid hormone and retinol-binding proteins. TTR has been identified as a potential diagnostic biomarker for early-stage ovarian cancer (I-II), with reduced levels correlating with the disease. It is found to negatively regulate epithelial ovarian cancer, and further reductions in TTR levels are associated with the progression of ovarian cancer. TTR has a sensitivity of 47% and specificity of 95%, respectively, in detecting ovarian cancer. However, when combined with HE4, TTR demonstrated improved sensitivity and specificity as compared with CA125, independently.[63,64]

Transferrin: Transferrin is a protein synthesized in hepatocytes that plays a crucial role in transporting plasma iron to the cells. It has been implicated in promoting tumor development and survival through its anti-apoptotic effects. While transferring has clinical applications in ovarian cancer detection, it exhibits low sensitivity (73%) and specificity (74%). However, its diagnostic performance can be improved when used in combination with other biomarkers.[65] A study reported that transferrin levels are negatively regulated in the sera of patients with ovarian

cancer. A combination of transferrin, CA-125, TTR, and ApoA1 using a proteomic analytical method, the panel achieved a sensitivity of 89% and specificity of 92% for early detection of ovarian cancer.[66,67]

Apolipoprotein A-I *(ApoA-I):* ApoA-I is a primary component of high-density lipoprotein and has been shown to have reduced levels in the serum of patients with ovarian cancer. The mechanism linking ApoA-I to cancer remains unclear, but it has been proposed that it may be associated with free radical-mediated damage to cell membranes, leading to lipid peroxidation. A panel of ApoA-1, CA125, and β2-M biomarkers has been identified as critical for the early detection of ovarian cancer, enhancing higher specificity of 98% and higher sensitivity of 94%.[67,68]

Tumor antigen-associated auto-antibody (TAAbs): TAAbs are produced by an over-expression of proteins or mutations in cancer patients, with different types corresponding with specific tumor types. They represent a novel serum biomarker for the early detection and diagnosis of high-grade serous epithelial ovarian cancer, among other cancers. One of the most studied TAAbs in ovarian cancer is serum antibodies against p53. Different panels (p53, PTPRA, and PTGFR) have been designed for early detection and differential diagnosis of ovarian tumors.[69] The study by Gadomska *et al.*[69] identified 11 TAAbs: ICAM3, CTAG2, p53, STYXL1, PVR, POMC, NUDT11, TRIM39, UHMK1, KSR1, and NXF3. These TAAbs helped to distinguish high-grade serous ovarian cancers from healthy controls with 45% sensitivity and 98% specificity.

B7-H4: B7-H4 is a surface protein composed of 282 amino acids, primarily found in cells of the immune system. It is a negative regulator of T-cell response and plays a role in the development of various malignancies. B7-H4 is expressed in tissue from endometrial, serous, and clear cell carcinoma. When combined with CA125, B7-H4 has been shown to detect a higher percentage of early-stage ovarian cancer (65%).[70] A study conducted by Simon *et al.*[71] analyzed B7-H4 protein levels in more than 2500 serum samples, tissue lysates, and ascites fluids. The study revealed high levels of B7-H4 protein in ovarian cancer tissue lysates. Meanwhile, there was a significant elevation of B7-H4 in patients with benign pathology.[71]

Methylated DNA: Methylated DNA is a versatile potential biomarker for several oncological pathologies. It can serve as a diagnostic, predictive, prognostic, and staging biomarker. Methylated DNA biomarkers are preferred over types due to their stability, region restriction, and amplification potentials.[64] Commonly downregulated and hypermethylated genes in ovarian cancer include but are not limited to *DAPK, TMS1/ASC, BRCA1, p16, ICAM-1, CDH1,* and *PAR-4.*[72] The use of methylation-specific PCR recorded 82% sensitivity and 100% specificity of a panel of tumor-specific methylated DNA (*BRCA1, RASSF1A, APC, p14ARF, p16INK4a*, and *DAPK*) in the serum of ovarian cancer patients.[64]

MicroRNAs (MiRNAs): MiRNAs have garnered attention as potential epigenetic biomarkers of ovarian cancer. They are a family of non-protein-coding single-stranded RNA molecules (18 – 24 nucleotides) that serve as downregulators of gene expression. They specifically bind to messenger RNAs. MiRNAs are involved in regulating over 60% of the total human genes and play key roles in the cell cycle, differentiation, development, metabolism, inflammation, proliferation, and immune response. Studies have noted distinct miRNA expression profiles in different ovarian cancers,[73] suggesting their potential use as diagnostic and prognostic biomarkers of ovarian cancer as well as other cancer types.[74] Previous study[75] on the role of miRNA in ovarian cancer has revealed that miR-21, miR-200a, miR-200b, miR-200c, miR-141, miR-214, miR-203, and miR-205 are potential biomarkers for ovarian cancer diagnosis.

Aldehyde dehydrogenase-1 (ALDH-1): ALDH-1 is a protein belonging to the ALDH family, encoded by the gene *ALDH1A1* gene located on chromosome 9q21. It plays a role in the oxidation of aldehydes through a pyridine-dependent mechanism. Studies have confirmed ALDH1's role in ovarian cancer stem cell differentiation and expression of ALDH1 in epithelial ovarian cancer stem cell clones, making it a potential biomarker for tumorigenic stem cells.[76,77] It has been suggested that increased expression of *ALDH1A1* in ovarian cancers supports its potential as a potential biomarker for early detection of ovarian cancer.[77]

Folate receptor alpha 1 (FOLR1): FOLR1 is a membrane protein and is responsible for the transport of folate into cells, essential for cellular processes, particularly in rapidly dividing cancer cells that have an increased demand for folate to sustain DNA synthesis. Folate concentration plays a critical role in tumor etiology and progression. Studies have reported overexpression of FOLR1 in various tumors of epithelial origin, including ovarian cancer, with specific detection in serous ovarian cancer. These findings suggest that FOLR1 is a potential biomarker for the detection of ovarian cancer, as well as for prognosis and assessment of chemotherapy responses.[78] Quantitative PCR and flow cytometry were used to study the diagnostic and prognostic utility of FOLR1 and FOLR3 in effusion cytology from ovarian cancer, breast cancer, and malignant mesothelioma. The result revealed significantly higher concentrations of FOLR1 and FOLR3 in ovarian cancer samples compared to other samples.[79]

AXL receptor: AXL receptor is a member of the tyrosine kinases family of receptors, known to promote cell survival and inhibit apoptosis, thereby playing a significant role in ovarian cancer progression. AXL is often overexpressed in ovarian cancer cells, making it a biomarker of interest. Its positive regulation is associated with tumor metastasis, aggressiveness, and resistance to conventional therapies. Activation of AXL signaling pathways can lead to epithelial-to-mesenchymal transition, facilitating cancer cell invasion. In addition, AXL can evade antitumor immune response, contributing to its role in cancer progression.[80,81]

CA72-4: CA72-4 is a tumor-related glycoprotein and a specific epitope on MUC1. An unusual increment of CA72-4 has been reported in ovarian cancer, although the levels are not affected by menstrual cycle, pregnancy, and endometriosis, but are slightly affected by inflammatory conditions. This stability suggests that CA720-4 could serve as a potential diagnostic marker for ovarian cancer. Moreover, a study detected overexpression of CA72-4 in mucinous tumors and clear ovarian cell carcinomas, while CA125 and HE4 levels were not elevated in those two histotypes.[82]

The 21st century is witnessing emerging ICC biomarkers for ovarian cysts. They include Ki-67, p53, and WT1.[83] Studies have shown that ICC biomarkers, such as CA-125 and Ki-67, are frequently used to detect benign ovarian lesions. CA-125 is said to be elevated in benign ovarian cysts such as endometriosis and cystadenomas. Ki-67 is associated with cellular proliferation.[84] Benign cystic lesions typically show low expression of malignant biomarkers.[85] Malignant ovarian lesions often express p53, HE4, and WT1. p53 mutations are particularly associated with high-grade serous carcinomas, while HE4 and WTI are specific to ovarian malignancies.[86] A study has demonstrated that a combination of CA-125 and HE4 enhanced diagnostic accuracy for ovarian cancer.[87]

11. Current state of research and future directions

The application of ICC in ovarian cyst diagnosis is a rapidly evolving method, with ongoing research aimed at improving diagnostic accuracy and consistency. A critical area of concern is the development of standardized antibody panels for use across laboratories. Artificial intelligence (AI) and machine learning (ML) algorithms are emerging fields of research that aim to improve the interpretation of results and enhance objectivity and consistency. AI algorithms can analyze complex signaling and imaging data, enabling early detection and characterization of ovarian cysts, by recognizing unique patterns and identifying easily missed features, allowing for definitive diagnosis. AI and ML offer the advantage of reducing false-positive and false-negative results. Integrating ICC with molecular diagnostics and AI could enhance diagnostic precision.[88] Further studies have explored the combination of the ICC method with other diagnostic techniques such as CT, ultrasound, and MRI. A conducted by van den Brule *et al*.[89] revealed that the combination of ICC and ultrasound yielded a sensitivity of 98% and specificity of 96% in diagnosing malignant ovarian cysts. Similarly, Lee *et al*.[36] discovered that the combination of ICC and MRI yielded a sensitivity of 97% and specificity of 95% in the diagnosis of malignant ovarian cysts.

Future directions focus on multiplex ICC for simultaneous detection of multiple markers and digital pathology for enhanced accurate results and consistent interpretations,[90,91] Novel biomarkers, such as YKL-40 and mesothelin, are being investigated for their potential to improve ovarian cancer diagnosis and prognosis. Researchers are also working towards improving the standardization of ICC practice and existing techniques.[92,93]

12. Conclusion

ICC has emerged as a critical diagnostic tool for distinguishing between benign and malignant ovarian lesions. The use of a panel of antibodies targeting specific biomarkers (antigens) associated with benign and malignant ovarian cysts provides a high level of sensitivity and specificity compared to traditional diagnostic techniques. ICC significantly enhances the diagnostic accuracy of ovarian cysts, providing a distinction between benign from malignant lesions with greater precision than traditional methods. Key biomarkers such as CA-125, HE4, p53, and Ki-67 play critical roles in this distinction. Despite its strength, ICC poses several limitations. However, the combination of ICC with other advanced diagnostic methods holds the potential to enhance the diagnosis and management of ovarian cysts, leading to improvement in patient outcomes. Ongoing research is aimed at improving protocol standardization, discovering novel markers, exploring multiplex marker panels, and integrating ICC with other diagnostic methods.

Acknowledgments

None.

Funding

None.

Conflict of interest

The authors declare that they have no competing interests.

Author contributions

Conceptualization: All authors
Writing-original draft: All authors
Writing-review & editing: All authors

Ethics approval and consent to participant

Not applicable.

Consent for publication

Not applicable.

Availability of data

Not applicable.

References

1. Zina AA. Causes and management of ovarian cysts. *Egypt J Hosp Med*. 2018;70(10):1818-1822.

   doi: 10.12816/0044759

2. Rana M, Nasa P. An overview of ovarian cysts. *Int J Pharm Sci Res*. 2020;11(11):5434-5440.

   doi: 10.13040/IJPSR.0975-823

3. Hemavathy V, Sathiyalathasarathi Gayathri M. Ovarian cyst: A literature review. *Int J Novel Res Dev.* 2023;8(9):663-666.

4. Sahu SA, Shrivastava D. A comprehensive review of screening methods for ovarian masses: Towards earlier detection. *Cureus*. 2023;15(11):e49063.

   doi: 10.7759/cureus.49063

5. Ding Y, Huang X, Ji T, Qi C, Gao X, Wei R. The emerging roles of miRNA-mediated autophagy in ovarian cancer. *Cell Death Dis.* 2024;15(4):314.

   doi: 10.1038/s41419-024-06630-3

6. Sharma D, Vinocha A. Benign ovarian cysts with raised CA-125 levels: Do we need to evaluate the fallopian tubes? *J Lab Physicians*. 2020;12(4):276-280.

   doi: 10.1055/s-0040-1716394

7. Chanu SM, Dey B, Raphael V, Panda S, Khonglah Y. Clinico-pathological profile of ovarian cysts in a tertiary care hospital. *Int J Reprod Contracept Obstet Gynecol.* 2017;6(10):4642-4645.

   doi: 10.18203/2320-1770.ijrcog20174376

8. Kanber Y, Pusztaszeri M, Auger M. Immunocytochemistry for diagnostic cytopathology-a practical guide. *Cytopathology.* 2021;32(2):562-587.

   doi: 10.1111/cyt.13008

9. Smith LH, Chen Y. Clinical features and diagnosis of ovarian cysts. *Am J Obstet Gynecol.* 2019;221(6):642-653.

   doi: 10.1016/j.ajog.2019.06.023

10. Mimoune N, Baazizi R, Azzouz MY, Benaissa MH, Kaidi R. Basic and new concepts in ovarian cysts pathogenesis in cattle. *Veterinaria.* 2019;68(2):73-80.

    doi: 10.2478/vet-2019-0028

11. Karst AM, Drapkin, R. Ovarian cancer pathogenesis: A model in evolution. *J Oncol.* 2010;2010:932371.

    doi: 10.1155/2010/980203

12. Davis BJ, Dixon D, Herbert RA. Ovary, oviduct, uterus, cervix and vagina. In: Maronpot, RR, Boorman GA, Gaul BW, editors. *Pathology of the Mouse: Reference and Atlas*. Vienna, IL: Cache River Press; 1999. p. 409-444.

    doi: 10.1007/978-3-662-07973-7

13. Hirst J, Crow J, Godwin A. *Ovarian Cancer Genetics: Subtypes and Risk Factors*. London: IntechOpen; 2018.

    doi: 10.5772/intechopen.72705

14. Kashyap P. Ovarian tumor: A review. *Int J Reprod Contracept Obstet Gynecol*. 2021;10(9):3657-3667.

    doi: 10.18203/2320-1770.ijrcog20213626

15. Levine D, Brown DL, Andreotti RF. Imaging of ovarian masses. *Radiology*. 2020;296(2):365-381.

    doi: 10.1148/radiol.2020191645

16. Kant RH, Rather S, Rashid S. *Clinical and Histopathological Profile of Patients with Ovarian Cyst Presenting in a Tertiary Care Hospital of Kashmir, India.* Available from: https://core.ac.uk/download/pdf/539900619.pdf [Last accessed on 2024 Jul 04].

17. Mobeen S, Apostol R. Ovarian cyst. In: *StatPearls*. Treasure Island, FL: StatPearls Publishing; 2024. Available from: https://www.ncbi.nlm.nih.gov/books/NBK560541 Accessed 2024 Jul 10].

18. Reid BM, Permuth JB, Sellers TA. Epidemiology of ovarian cancer: A review. *Cancer Biol Med.* 2017;14(1):9-32.

    doi: 10.20892/j.issn.2095-3941.2016.0046

19. Parmar RA, Patel KA. Fine needle aspiration cytology's role in the diagnosis of ovarian tumor. *J Midlife Health.* 2023;14(2):159-164.

    doi: 10.4103/jmh.jmh_32_23

20. Matsas A, Stefanoudakis D, Troupis T, *et al*. Tumor markers and their diagnostic significance in ovarian cancer. *Life* (*Basel*). 2023;13(8):1689.

    doi: 10.3390/life13081689

21. Shaaban AM, Rezvani M, Elsayes KM, Baskin H. Ovarian malignant germ cell tumors: Cellular classification and clinical and imaging features. *Radiographics*. 2014;34(3):777-801.

    doi: 10.1148/rg.343130050

22. Ezejiofor IF, Ozor NS, Ogbu CC, Olaofe OO, Menkiti FE.

Histopathological profile of primary ovarian lesions in Nnewi, Nigeria: A 5 year retrospective study. *Orient J Med*. 2021;33(1-2):13-21.

doi: 10.4314/ojm.v33i1-2.2

23. Kanasagara A, Sarvaiya A, Sakariya D. Histomorphologic spectrum of ovarian cystic lesions at a tertiary care centre. *Trop J Pathol Microbiol*. 2018;4(3):270-275.

doi: 10.17511/jopm.2018.i3.08

24. Kirbiš IS, Roque RR, Bongiovanni M, Fležar MS, Cochand-Priollet B. Immunocytochemistry practices in European cytopathology laboratories-review of european federation of cytology societies (EFCS) online survey results with best practice recommendations. *Cancer Cytopathol*. 2020;128(2):117-128.

doi: 10.1002/cncy.22292

25. Sauter JL, Grogg KL, Vrana JA, Law ME, Halvorson JL, Henry MR. Young investigator challenge: Validation and optimization of immunohistochemistry protocols for use on client cell block specimens. *Cancer Cytopathol*. 2016;124(2):89-100.

doi: 10.1002/cncy.21625

26. Jain D, Nambirajan A, Borczuk A, *et al*. Immunocytochemistry for predictive biomarker testing in lung cancer cytology. *Cancer Cytopathol*. 2019;127(5):325-339.

doi: 10.1002/cncy.22126

27. Echeveste JI, Labiano T, Tejerina E, Argueta A, De Andrea C, Lozano MD. Challenges of ICC and FISH in the field of targeted therapies from cell block to smears. *J Mol Pathol*. 2021;2(1):55-65.

doi: 10.3390/jmp2010007

28. Sharma R, Sundaram S, Verma, R. Immunocytochemistry in oncology: An essential tool. *J Cancer Res Ther*. 2020;16(6):1421-1430.

doi: 10.4103/jcrt.JCRT_60_20

29. Clive RT, Shang-Rong S, Nancy JB. Techniques of immunohistochemistry: Principles, pitfalls, and standardization. In: David JD, editor. *Diagnostic Immunohistochemistry*. 3rd ed. Englewood: US: Suanders; 2011. p. 1-44.

doi: 10.1016/B978-0-443-06652-8.50007-7

30. Thermo Fisher Scientific. *Antibodies for Immunocytochemistry (ICC)*; 2024. Available from: https://www.thermofisher.com/ng/en/home/life-science/antibodies/primary-antibodies/antibodies-applications/antibodies-icc.html [Last accessed on 2024 Aug 16].

31. Oboma Y, Beredugo S, Archibong AM, Zipamone E. *Citrus aurantifolia* (Lime) juice extract reverses poly cystic ovary in Cadmium chloride exposed sprague dawley rats. *Gen Intern Med Clin Innov*. 2020;5:1-4.

doi: 10.31579/2640-1088/078

32. Oboma YI, Ngokere AA. Effect of formalin fixation on DNA purity and quantity, nucleic acid, and amplicon size in cervical human papilloma virus detection. *Afr J Cell Pathol*. 2018;10(4):47-53.

doi: 10.5897/AJCPath2018.0009

33. Novus Biologicals. *Immunocytochemistry (ICC) Handbook*. Available from: https://www.novusbio.com/support/immunocytochemistry-icc-handbook [Last accessed on 2024 Aug 20].

34. Schutter WM, Esajas V, Tan NY, Hogervorst, F. Accuracy of imaging techniques for detection of benign versus malignant ovarian masses: A systematic review and meta-analysis. *Eur Radiol*. 2018;28(10):4257-4266.

doi: 10.1007/s00330-018-5413-9

35. Li J, Wang H, Zhou X, Zheng Y, Zhang Y, Zhou Y. Diagnostic value of immunocytochemical biomarkers in ovarian masses. *J Obstet Gynaecol Res*. 2019;45(3):559-567.

doi: 10.1111/jog.13888

36. Lee JH, Kim HJ, Lee JY, Kim SH, Kim SY, Kim TH. Diagnostic value of immunocytochemical markers for the detection of malignant ovarian tumors. *J Gynecol Oncol*. 2018;29(5):e69.

doi: 10.3802/jgo.2018.29.e69

37. Metovica J, Righib L, Delsedimea L, Volanteb M, Papottia M. Role of immunocytochemistry in the cytological diagnosis of pulmonary tumors. *Acta Cytol*. 2019;63(1):2-14.

doi: 10.1159/000503757

38. Dudás B, Lane M, Mupparaju N, Kim HM, Merchenthaler I. A Forgotten principle in immunocytochemistry: Optimal dilution. *J Histochem Cytochem*. 2022;70(11-12):759-765.

doi: 10.1369/00221554221133723

39. Roy-Chowdhuri S. Immunocytochemistry of cytology specimens for predictive biomarkers in lung cancer. *Transl Lung Cancer Res*. 2020;9(3):898-905.

doi: 10.21037/tlcr.2020.02.17

40. Grayson K, Gregory E, Khan G, Guinn BA. Urine biomarkers for early detection of ovarian cancer-are we there yet? *Biomarkers Cancer*. 2019;11:1-8.

doi: 10.1177/1179299X19873209

41. Nolen BM, Lokshin AE. Biomarker testing for ovarian cancer: Clinical utility of multiplex assays. *Mol Diagn Ther*. 2013;17(3):139-146.

doi: 10.1007/s40291-013-0039-6

42. Nowak M, Stachowiak ŁG, Stetkiewicz T, Wilczyński JR. Current clinical application of serum biomarkers to detect ovarian cancer. *Prz Menopauzalny*. 2015;14(4):254-259.

doi: 10.5114/pm.2015.53113

43. Atallah GA, Abd Aziz NH, Teik CK, Shafiee MN, Kampan NC. New predictive biomarkers for ovarian cancer. *Diagnostics* (*Basel*). 2021;11(3):465.

doi: 10.3390/diagnostics11030465

44. Ye B, Skates S, Mok SC, *et al*. Proteomic-based discovery and characterization of glycosylated eosinophil-derived neurotoxin and COOH-terminal osteopontin fragments for ovarian cancer in urine. *Clin Cancer Res*. 2006;12(2):432-441.

doi: 10.1158/1078-0432.CCR-05-1406

45. Singer G, Oldt R 3rd, Cohen Y, *et al*. Mutations in BRAF and KRAS characterize the development of low-grade ovarian serous carcinoma. *J Natl Cancer Inst*. 2003;95(6):484-486.

doi: 10.1093/jnci/95.6.484

46. Schummer M, Ng WV, Bumgarner RE, *et al*. Comparative hybridization of an array of 21 500 ovarian cDNAs for the discovery of genes overexpressed in ovarian carcinomas. *Gene*. 1999;238(2):375-385.

doi: 10.1016/S0378-1119(99)00379-4

47. Konstantinopoulos PA, Lheureux S, Moore KN. PARP inhibitors for ovarian cancer: Current indications, future combinations, and novel assets in development to target DNA damage repair. *Am Soc Clin Oncol Educ Book*. 2020;40:e116-e131.

doi: 10.1200/EDBK_292956

48. Kobayashi M, Sawada K, Kimura T. Potential of integrin inhibitors for treating ovarian cancer: A literature review. *Cancers* (*Basel*). 2017;9(7):83.

doi: 10.3390/cancers9010008

49. Luo LY, Katsaros D, Scorilas A, *et al*. Prognostic value of human kallikrein 10 expression in epithelial ovarian carcinoma. *Clin Cancer Res*. 2001;7(8):2372-2379.

50. Bao LH, Sakaguchi H, Fujimoto J, Tamaya T. Osteopontin in metastatic lesions as a prognostic marker in ovarian cancers. *J Biomed Sci*. 2007;14(3):373-381.

doi: 10.1007/s11373-006-9136-0

51. Brakora K, Lee H, Yusuf R, *et al*. Utility of osteopontin as a biomarker in recurrent epithelial ovarian cancer. *Gynecol Oncol*. 2004;93(2):361-365.

doi: 10.1016/j.ygyno.2003.12.026

52. Tanaka Y, Kobayashi H, Suzuki M, Kanayama N, Suzuki M, Terao, T. Upregulation of bikunin in tumor-infiltrating macrophages as a factor of favorable prognosis in ovarian cancer. *Gynecol Oncol*. 2004;94(3):725-734.

doi: 10.1016/j.ygyno.2004.04.013

53. Matsuzaki H, Kobayashi H, Yagyu T, *et al*. Plasma bikunin as a favorable prognostic factor in ovarian cancer. *J Clin Oncol*. 2005;23(7):1463-1472.

doi: 10.1200/JCO.2005.04.112

54. Hartenbach EM, Olson AT, Goswitz JJ, *et al*. Vascular endothelial growth factor (VEGF) expression and survival in human epithelial ovarian carcinomas. *Cancer Lett*. 1997;121(2):169-175.

doi: 10.1016/S0304-3835(97)00425-8

55. James NE, Chichester C, Ribeiro JR. Beyond the biomarker: Understanding the diverse roles of human epididymis protein 4 in the pathogenesis of epithelial ovarian cancer. *Front Oncol*. 2018;8:124.

doi: 10.3389/fonc.2018.00124

56. Drapkin R, Von Horsten HH, Lin Y, *et al*. Human epididymis protein 4 (HE4) Is a secreted glycoprotein that is overexpressed by serous and endometrioid ovarian carcinomas. *Cancer Res*. 2005;65(6):2162-2169.

doi: 10.1158/0008-5472.CAN-04-3812

57. Li XH, Chen XJ, Ou WB, *et al*. Knockdown of creatine kinase B inhibits ovarian cancer progression by decreasing glycolysis. *Int J Biochem Cell Biol*. 2013;45(5):979-986.

doi: 10.1016/j.biocel.2013.01.015

58. Huddleston HG, Wong K, Welch WR, Berkowitz RS, Mok SC. Clinical applications of microarray technology: Creatine kinase B is an up-regulated gene in epithelial ovarian cancer and shows promise as a serum marker. *Gynecol Oncol*. 2005;96(1):77-83.

doi: 10.1016/j.ygyno.2004.08.041

59. Tamir A, Gangadharan A, Balwani S, *et al*. The serine protease prostasin (PRSS8) is a potential biomarker for early detection of ovarian cancer. *J Ovarian Res*. 2016;9(1):1-13.

doi: 10.1186/s13048-016-0215-5

60. Mok SC, Chao J, Skates S, *et al*. Prostasin, a potential serum marker for ovarian cancer: Identification through microarray technology. *J Natl Cancer Inst*. 2001;93(19):1458-1464.

doi: 10.1093/jnci/93.19.1458

61. McIntosh MW, Drescher C, Karlan B, *et al*. Combining CA 125 and SMR serum markers for diagnosis and early detection of ovarian carcinoma. *Gynecol Oncol*. 2004;95(1):9-15.

doi: 10.1016/j.ygyno.2004.07.039

62. Chang K, Pastan I. Molecular cloning of mesothelin, a differentiation antigen present on mesothelium, mesotheliomas, and ovarian cancers. *Proc Natl Acad Sci* U S A. 1996;93(1):136-140.

doi: 10.1073/pnas.93.1.136

63. Huang CY, Cheng WF, Lee CN, *et al*. Serum mesothelin in epithelial ovarian carcinoma: A new screening marker and prognostic factor. *Anticancer Res*. 2006;26(6B):4721-4728.

64. Zheng X, Chen S, Li L, *et al*. Evaluation of HE4 and TTR for diagnosis of ovarian cancer: Comparison with CA-125. *J Gynecol Obstet Hum Reprod*. 2018;47(6):227-230.

doi: 10.1016/j.jogoh.2018.02.002

65. Rastogi M, Gupta S, Sachan, M. Biomarkers towards ovarian cancer diagnostics: Present and future prospects. *Braz Arch Biol Technol*. 2016;59:e16160070.

doi: 10.1590/1678-4324-2016160070

66. Macuks R, Baidekalna I, Gritcina J, Avdejeva A, Donina S. Apolipoprotein A1 and transferrin as biomarkers in ovarian cancer diagnostics. *Acta Chir Latv*. 2010;10:16.

doi: 10.2478/v10163-011-0003-3

67. Ahmed N, Oliva KT, Barker G, *et al*. Proteomic tracking of serum protein isoforms as screening biomarkers of ovarian cancer. *Proteomics.* 2005;5(17):4625-4636.

doi: 10.1002/pmic.200401268

68. Su F, Lang J, Kumar A, *et al*. Validation of candidate serum ovarian cancer biomarkers for early detection. *Biomark Insights*. 2007;2:369-375.

doi: 10.4137/bmi.s288

69. Gadomska H, Grzecocińska B, Janecki J, Nowicka G, Powolny M, Marianowski L. Serum lipids concentration in women with benign and malignant ovarian tumours. *Eur J Obstet Gynecol Reprod Biol.* 2005;120(1):87-90.

doi: 10.1016/j.ejogrb.2004.10.011

70. Davis M. A comprehensive review of the diagnostic and treatment methods for ovarian cancer. *Eur J Eng Res Sci.* 2018;3(2):13-19.

doi: 10.24018/ejers.2018.3.2.89

71. Katchman BA, Chowell D, Wallstrom G, *et al*. Autoantibody biomarkers for the detection of serous ovarian cancer. *Gynecol Oncol.* 2017;146(1):129-136.

doi: 10.1016/j.ygyno.2017.04.005

72. Devarajappa GB, Kopparapu VN, Kasireddy LR, Mekala SC, Yaraganti G. Biomarkers for early detection of ovarian cancer: A review. *Asian Pac J Cancer Biol.* 2023;9(1):81-85.

doi: 10.31557/APJCB.2023.9.1.81-85

73. Simon I, Zhuo S, Corral L, *et al*. B7-H4 is a novel membrane bound protein and a candidate serum and tissue biomarker for ovarian cancer. *Cancer Res.* 2006;66(3):1570-1575.

doi: 10.1158/0008-5472.CAN-05-2959

74. Cvetkovic D, Pisarcik D, Lee C, Hamilton TC, Abdollahi A. Altered expression and loss of heterozygosity of the LOT1 gene in ovarian cancer. *Gynecol Oncol.* 2004;95(3):449-455.

doi: 10.1016/j.ygyno.2004.07.027

75. Zhao X, Zhou Y, Chen YU, Yu F. miR-494 inhibits ovarian cancer cell proliferation and promotes apoptosis by targeting FGFR2. *Oncol Lett.* 2016;11(6):4245-4251.

doi: 10.3892/ol.2016.4616

76. Montagnana M, Benati M, Danese E. Circulating biomarkers in epithelial ovarian cancer diagnosis: From present to future perspective. *Ann Transl Med*. 2017;5(13):276.

doi: 10.21037/atm.2017.05.13

77. Iorio MV, Visone R, Di LG, *et al*. MicroRNA signatures in human ovarian cancer. *Cancer Res.* 2007;67(18):8699-8707.

doi: 10.1158/0008-5472.CAN-07-1581

78. Steffensen KD, Alvero AB, Yang Y, *et al*. Prevalence of epithelial ovarian cancer stem cells correlates with recurrence in early-stage ovarian cancer. *J Oncol*. 2011;2011:620523.

doi: 10.1155/2011/620523

79. Sarojini S, Tamir A, Lim H, *et al*. Early detection biomarkers for ovarian cancer. *J Oncol*. 2012;2012:709049.

doi: 10.1155/2012/709049

80. Chen YL, Chang MC, Huang CY, *et al*. Serous ovarian carcinoma patients with high alpha-folate receptor had reducing survival and cytotoxic chemo-response. *Mol Oncol.* 2012;6(3):360-369.

doi: 10.1016/j.molonc.2012.04.004

81. Yuan Y, Nymoen DA, Dong HP, *et al*. Expression of the folate receptor genes FOLR1 and FOLR3 differentiates ovarian carcinoma from breast carcinoma and malignant mesothelioma in serous effusions. *Hum Pathol.* 2009;40(10):1453-1460.

doi: 10.1016/j.humpath.2009.04.003

82. Zhu C, Wei Y, Wei X. AXL receptor tyrosine kinase as a promising anti-cancer approach: Functions, molecular mechanisms and clinical applications. *Mol Cancer*. 2019;18(1):153.

doi: 10.1186/s12943-019-1078-2

83. Hernandez L, Friedman ER, Moore RG. Emerging biomarkers for the diagnosis of ovarian cancer. *Clin Chem.* 2021;67(4):679-689.

doi: 10.1093/clinchem/hvaa275

84. Sundfeldt K, Piontkewitz Y, Ivarsson K. The role of Ki-67 in the diagnostic pathway of ovarian tumors. *Gynecol Oncol.* 2019;154(1):31-36.

doi: 10.1016/j.ygyno.2019.04.017

85. Zhao D, Wu Y, Song Y. The role of p53 in ovarian cancer diagnosis and prognosis. *J Ovarian Res.* 2021;14(1):1.

doi: 10.1186/s13048-020-00757-8

86. Bast RC, Hennessy B, Mills GB. The biology of ovarian cancer: New opportunities for translation. *Nat Rev Cancer*. 2009;9(6):415-428.

doi: 10.1038/nrc2644

87. Kaijser J, Sayasneh A, Van Holsbeke, C. Presurgical diagnosis of adnexal tumors using combined biomarkers. *Br J Cancer*. 2019;120(6):706-712.

doi: 10.1038/s41416-019-0401-1

88. Xu HL, Gong TT, Liu FH, *et al*. Artificial intelligence performance in image-based ovarian cancer identification: A systematic review and meta-analysis. *EClinicalMedicine*. 2022;53:101662.

doi: 10.1016/j.eclinm.2022.101662

89. Brule AJ, Buist MR, Massuger LF, Rotteveel J, Vergote I, Trimbos JB. Comparison of CA125, HE4, and a multimodal immunocytochemical assay for ovarian cancer risk stratification. *Gynecol Oncol*. 2018;151(2):353-360.

doi: 10.1016/j.ygyno.2018.09.012

90. Leandersson P, Åkesson A, Hedenfalk I, Malander S, Borgfeldt C. A multiplex biomarker assay improves the diagnostic performance of HE4 and CA125 in ovarian tumor patients. *PLoS One*. 2020;15(10):e0240418.

doi: 10.1371/journal.pone.0240418

91. Wang Y, Coleman RL. The future of ovarian cancer screening. *J Clin Oncol*. 2021;39(23):2639-2646.

doi: 10.1200/JCO.21.00048

92. Holst S, Heeren RM. New horizons in ovarian cancer diagnostics: YKL-40 and mesothelin as potential markers. *Nat Rev Clin Oncol*. 2020;17(10):615-627.

doi: 10.1038/s41571-020-0379-3

93. Dijmărescu AL, Gheorman V, Manolea MM, *et al*. Serological and immunohistochemical biomarkers for discrimination between benign and malignant ovarian tumors. *Rom J Morphol Embryol*. 2019;60(4):1163-1174.

ACCSCIENCE PUBLISHING

Tumor Discovery

REVIEW ARTICLE

Cyclin-dependent kinase 4/6 inhibitor resistance mechanisms and strategies for subsequent treatment in breast cancer: A comprehensive review

Yuling Zhang[1], Bingfeng Chen[2], Rendong Zhang[2], Jundong Wu[2,3]*, and Chunfa Chen[2,3]*

[1]Department of Medical Quality Management, Cancer Hospital of Shantou University Medical College, Shantou, Guangdong, China

[2]The Breast Center, Cancer Hospital of Shantou University Medical College, Shantou, Guangdong, China

[3]The Research Laboratory for Breast Cancer Diagnosis and Treatment, Cancer Hospital of Shantou University Medical College, Shantou, Guangdong, China

***Corresponding authors:**
Jundong Wu
(wujun-dong@163.com)
Chunfa Chen
(chenchunfa@stu.edu.cn)

Citation: Zhang Y, Chen B, Zhang R, Wu J, Chen C. Cyclin-dependent kinase 4/6 inhibitor resistance mechanisms and strategies for subsequent treatment in breast cancer: A comprehensive review. *Tumor Discov*. 2025;4(1):27-36.
doi: 10.36922/td.7107

Received: December 8, 2024

Revised: January 8, 2025

Accepted: January 14, 2025

Published online: February 5, 2025

Abstract

Cyclin-dependent kinase 4 and 6 (CDK4/6) inhibitors have transformed the therapeutic landscape for hormone receptor-positive, human epidermal growth factor receptor 2-negative breast cancer, demonstrating significant efficacy in both early and advanced stages of the disease. Combined with endocrine therapy, these inhibitors have dramatically improved survival outcomes. However, resistance to CDK4/6 inhibitors inevitably develops, posing a significant challenge in clinical management. Resistance to CDK4/6 inhibitors can develop through inherent and acquired fashions, and their mechanisms are explored in this comprehensive review. Inherent resistance arises from pre-existing genetic or signaling pathway alterations that diminish cancer cell sensitivity to CDK4/6 inhibitors. Acquired resistance, on the other hand, develops over time through mechanisms, such as the activation of alternative signaling pathways or changes in the tumor microenvironment. The review also examines potential biomarkers for predicting resistance, especially circulating tumor DNA markers, and discusses strategies to overcome resistance. These include combination therapies targeting multiple pathways simultaneously, sequential approaches to delay the onset of resistance, and the development of next-generation CDK4/6 inhibitors with improved efficacy and reduced resistance potential. Understanding resistance mechanisms and developing effective countermeasures are crucial for optimizing patient outcomes and extending the clinical benefits of CDK4/6 inhibitors in cancer therapy. Leveraging these insights will enable clinicians to personalize treatment strategies, ultimately enhancing the long-term effectiveness of CDK4/6 inhibitors in managing breast cancer.

Keywords: CDK4/6 inhibitors; Endocrine resistance; Breast cancer; Drug resistance mechanisms; Treatment strategies

1. Introduction

Breast cancer is the most prevalent malignant tumor in women, constituting approximately 11.6% of all cancer diagnoses worldwide. In 2022, nearly 2.5 million new breast cancer cases were recorded globally, representing roughly a quarter of all cancer cases.[1] It is categorized into three subtypes depending on the presence of estrogen receptor (ER), progesterone receptor, and human epidermal growth factor receptor 2 (HER2): hormone receptor (HR)-positive, HER2-positive, and triple-negative. Among these, HR-positive breast cancer accounts for approximately 60% to 70% of all cases. Although HR-positive breast cancer is generally associated with a better prognosis compared to other subtypes, patients with this subtype still experience two distinct peaks of recurrence – one occurring within the first 1 – 3 years and another even after 10 years – underscoring the urgent need for novel therapeutic strategies to improve long-term patient outcomes.[2,3]

Building on the foundation of endocrine therapy, cyclin-dependent kinase 4 and 6 (CDK4/6) inhibitors have emerged as powerful targeted therapies, particularly for HR-positive breast cancer. CDK4 and CDK6 are crucial regulators of the G1-to-S phase transition in the cell cycle, a process essential for cellular proliferation.[4] These kinases form complexes with D-type cyclins, particularly cyclin D1, which phosphorylate and inactivate the retinoblastoma (RB) tumor suppressor protein. This phosphorylation releases E2F transcription factors, enabling the transcription of genes required for DNA synthesis and cell cycle progression.[5] By blocking CDK4/6 activity, these drugs prevent the phosphorylation of RB, thereby inhibiting cell cycle progression and tumor growth.

The combination of CDK4/6 inhibitors with endocrine therapy has significantly benefited both early-stage and advanced HR-positive/HER2-negative breast cancer, transforming the treatment paradigm. Clinical trials such as NATALEE and MONARCH E have expanded treatment options for patients with early HR-positive/HER2-negative breast cancer, demonstrating the potential of CDK4/6 inhibitors to reduce recurrence risk and improve overall survival (OS).[6,7] Furthermore, advanced clinical trials, such as PALOMA-2,[8] MONALEESA-7[9] and -3,[10] and MONARCH-3[11] have shown that this combination therapy significantly improves progression-free survival (PFS) for patients with metastatic HR-positive/HER2-negative breast cancer.

However, resistance to CDK4/6 inhibitor therapy remains a significant clinical challenge, resulting in disease progression in some early-stage patients and nearly all advanced-stage patients. Understanding the underlying mechanisms of resistance is crucial for improving patient outcomes, developing novel therapies, and optimizing treatment sequencing.[5,12-14] This review aims to provide a comprehensive summary of current resistance mechanisms to CDK4/6 inhibitors and explore potential approaches to overcome such resistance.

2. The operational mechanism and clinical application of CDK4/6 inhibitors

As illustrated in Figure 1, CDK4/6 kinases are pivotal in governing cell cycle progression, especially during the transition from the G1 phase to the S phase. They form complexes with cyclin D1 proteins, which then phosphorylate the RB protein, which is a key tumor suppressor.[15] Phosphorylation of RB disrupts its interaction with E2F transcription factors, thereby releasing E2F to activate the transcription of genes essential for DNA replication and cell cycle progression.[15] In HR-positive/HER2-negative breast cancer, CDK4/6 inhibitors are used in conjunction with anti-estrogen therapies, including aromatase inhibitors (AIs), fulvestrant, and tamoxifen, to achieve a synergistic effect.[16] This combination has become the standard of care for advanced HR-positive/HER2-negative breast cancer.[17] Currently, four selective CDK4/6 inhibitors have been approved, including palbociclib, ribociclib, dalpiciclib, and abemaciclib.[5,18] These agents specifically target CDK4/6 kinase and exhibit comparable inhibitory effects on both kinases. Palbociclib, dalpiciclib, and ribociclib share structural similarities and display similar kinase inhibitory activities. These drugs are typically administered on a three-week-on, one-week-off schedule to mitigate myelosuppression, their primary dose-limiting toxicity.[5,18] In contrast, abemaciclib exhibits a distinct inhibitory profile, with higher selectivity for CDK4 compared to CDK6, consistent with its reported high potency against CDK4.[5] In addition, abemaciclib inhibits multiple other kinases, including CDK1, CDK2, CDK5, CDK9, and albeit at lower potencies.[16] The predominant toxicities of abemaciclib are diarrhea and fatigue.[5] A comparative summary of the mechanisms and side effect profiles of these four CDK4/6 inhibitors is shown in Table 1.

3. Mechanisms of resistance to CDK4/6 inhibitors

Resistance to CDK4/6 inhibitors can be broadly categorized into two types: intrinsic and acquired, each driven by distinct mechanisms that contribute to treatment failure, particularly in HR-positive/HER2-negative breast cancer. Intrinsic resistance arises from pre-existing genetic or molecular alterations that render tumor cells inherently unresponsive to CDK4/6 inhibition. In contrast, acquired resistance develops over time as adaptive changes in tumor

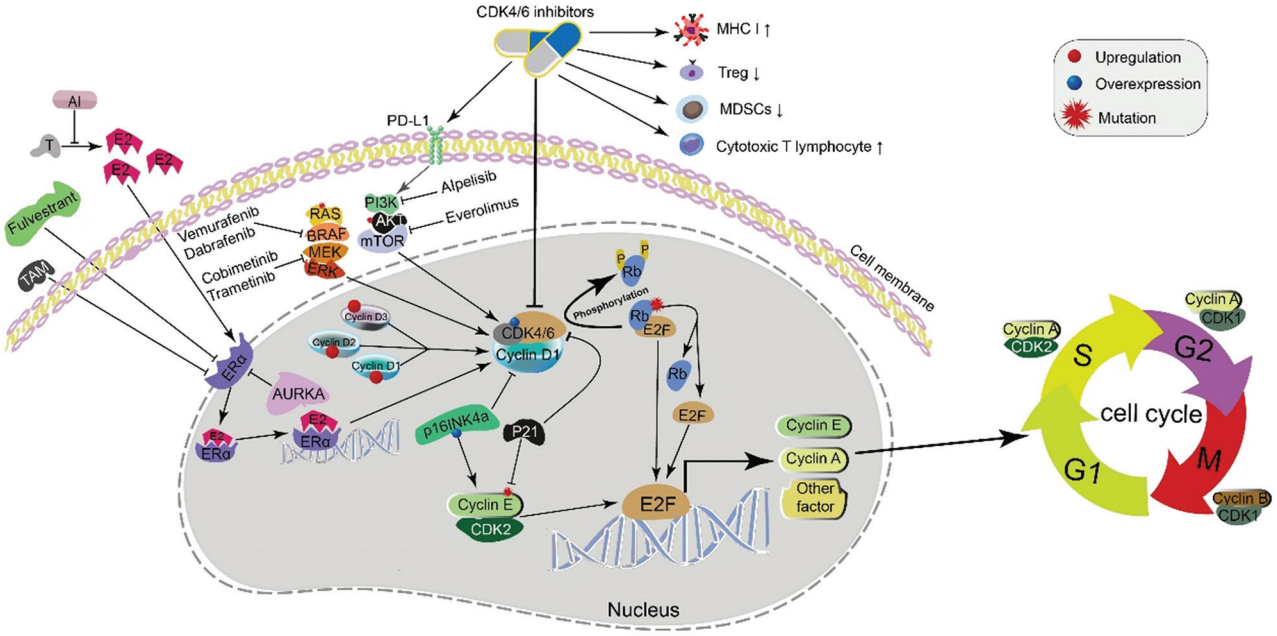

Figure 1. Schematic diagram illustrating the mechanisms of action and resistance of CDK4/6 inhibitors in combination with endocrine therapy. Abbreviations: CDK4/6: Cyclin-dependent kinase 4 and 6; MHC1: Major histocompatibility complex class 1; MDSCs: Myeloid-derived suppressor cells; Treg: Regulatory T cell; TAM: Tamoxifen; T: Testosterone; AI: Aromatase inhibitors; E2: Estradiol; PD-L1: Programmed death-ligand 1; ERα: Estrogen receptor alpha; E2F: E2F transcription factor; Rb: Retinoblastoma; AURKA: Aurora kinase A; RAS: Rat sarcoma; BRAF: B-Raf protooncogene; MEK: Mitogen-activated protein kinase kinase; ERK: Extracellular signal-regulated kinase; mTOR: Mammalian target of rapamycin.

biology occur during treatment. Understanding these resistance mechanisms is crucial for devising effective strategies to overcome them and improve patient outcomes.

3.1. Intrinsic resistance mechanisms

Intrinsic resistance refers to the inherent ability of some tumors to resist CDK4/6 inhibitors from the outset. One of the most significant mechanisms involves the loss or mutation of the RB protein, a critical cell cycle regulator.[17] Tumors lacking functional RB bypass CDK4/6 inhibition, allowing uninterrupted cell cycle progression.[12,19] In addition, overexpression of CDK4 or CDK6 can independently drive cell cycle progression by promoting RB phosphorylation, thereby enabling tumor cells to evade the inhibitory effects of CDK4/6 inhibitors.[19,20] Similarly, the upregulation of cyclins, particularly cyclin D1, D2, or D3, contributes to resistance by forming hyperactive complexes with CDK4/6 that are less susceptible to inhibition.[20] In some tumors, especially ER-positive breast cancer, non-canonical activation of CDK2 facilitates S-phase entry despite CDK4/6 inhibition. This mechanism allows cancer cells to sustain proliferation even in the presence of inhibitors.[12,21] Furthermore, paradoxical resistance can arise from the overexpression of p16INK4a proteins. Although p16INK4a typically inhibits CDK4/6 activity, its overexpression disrupts normal cell cycle regulation and activates alternative pathways that support tumor growth.[20,21] A detailed schematic representation of these pathways is demonstrated in Figure 1.

3.2. Acquired resistance mechanisms

Acquired resistance to CDK4/6 inhibitors typically develops after an initial period of therapeutic sensitivity, primarily due to genetic and epigenetic alterations within the tumor. Common mutations in genes such as the RB protein, protein kinase B (AKT), rat sarcoma, aurora kinase A (AURKA), and cyclin E have been identified as key drivers of resistance. These mutations activate alternative signaling pathways that bypass CDK4/6 activity, thereby diminishing the efficacy of treatment.[22] As illustrated in Figure 1, tumors can engage compensatory pathways such as phosphoinositide 3-kinase (PI3K)/AKT or mitogen-activated protein kinase (MAPK) signaling, to sustain cell survival and proliferation despite CDK4/6 inhibition. This adaptive rewiring of signaling networks undermines the long-term effectiveness of CDK4/6 inhibitors.[12,22] In addition, changes in ER status, including loss or downregulation, have been associated with reduced responsiveness to combined endocrine therapy and CDK4/6 inhibition.[22] Epigenetic modifications further contribute to acquired resistance by altering gene expression profiles, enabling tumors to adapt their growth

Table 1. Comparison of the mechanisms of four CDK4/6 inhibitors

CDK4/6 inhibitor	Primary target	Mechanism type	IC50 values	Binding affinity	Additional targets	Cellular effect	Dosing schedule	Main Side effects	References
Palbociclib	CDK4/6	ATP-competitive	Similar potency for CDK4 and CDK6	Similar affinity for CDK4/cyclin D3 and CDK6/cyclin D1	Highly specific for CDK4/6	Cytostasis only	21 days on/ 7 days off	Neutropenia	5,16,50,51
Ribociclib	CDK4/6	ATP-competitive	CDK4: 10 nM CDK6: 39 nM	5-fold greater affinity for CDK4/ cyclin D3	Highly specific for CDK4/6	Cytostasis only	21 days on/ 7 days off	Neutropenia, QTc prolongation	5,16,46,50,51
Abemaciclib	CDK4/6	ATP-competitive	CDK4: 2 nM, CDK6: 10 nM	9-fold greater affinity for CDK4/ cyclin D3; 14 times more potent against CDK4 than CDK6	Also inhibits CDK1, CDK2, CDK5, CDK9, and other kinases	Both cytostasis and cytotoxicity	Continuous dosing	Diarrhea, fatigue	5,16,50-52
Dalpiciclib	CDK4/6	ATP-competitive	CDK4: 12.4 nM, CDK6: 9.9 nM	Shows selectivity toward CDK4 and CDK6	Specific for CDK4/6	Induces G1 arrest and cellular senescence	21 days on/ 7 days off	Neutropenia, leukopenia	18,53-55

Abbreviations: ATP: Adenosine triphosphate; CDK: Cyclin-dependent kinase; CDK4/6: Cyclin-dependent kinase 4 and 6; QTc: Corrected QT interval.

and survival strategies in response to ongoing therapy. These modifications may include DNA methylation, histone acetylation, or chromatin remodeling, which collectively promote tumor plasticity and resistance.[21,22]

3.3. Immune-mediated resistance mechanisms

Recent research has identified immune-mediated mechanisms as a significant contributor to acquired resistance against CDK4/6 inhibitors. These inhibitors have been shown to reprogram transcriptional activity in both tumor and immune cells, enhancing tumor immunogenicity and fostering an immune-enriched tumor microenvironment.[23] However, tumors can counteract these effects by upregulating immune checkpoint proteins, such as programmed cell death-ligand 1, and disrupting antigen presentation mediated by the major histocompatibility complex (MHC). These adaptations enable immune evasion and establish immunosuppressive conditions within the tumor microenvironment.[24,25] This resistance is further exacerbated by a decrease in regulatory T cells (Tregs) and myeloid-derived suppressor cells (MDSCs), which play a pivotal role in maintaining anti-tumor immunity (Figure 1).[26] Paradoxically, while CDK4/6 inhibitors reduce Tregs and MDSCs, the resulting immune dysregulation can promote tumor adaptation. Tumors may also undergo phenotypic changes as a form of adaptive resistance, allowing them to evade immune surveillance even after an initial response to CDK4/6 inhibitor therapy.[23,25]

4. Novel biomarkers for predicting resistance

Circulating tumor DNA (ctDNA) analysis has emerged as a highly promising method for tracking treatment responses and identifying resistance mechanisms to CDK4/6 inhibitors. Sequential ctDNA assessments demonstrate high sensitivity (75%) and specificity (92%) in detecting disease progression, often identifying an increase in tumor DNA approximately three months before radiological evidence of progression.[27] This non-invasive approach is particularly valuable for monitoring treatment responses in challenging scenarios, such as bone metastases or small-sized target lesions, where traditional imaging modalities may have limitations.[27,28]

Compared to conventional serum tumor markers, such as carcinoembryonic antigen or cancer antigen 15-3, ctDNA analysis offers superior sensitivity for monitoring tumor response to CDK4/6 inhibitors.[27] Moreover, ctDNA has proven effective in detecting acquired genetic alterations associated with resistance to these inhibitors. For example, loss of function in the *RB* gene is strongly

associated with resistance, with *RB* mutations detected through ctDNA linked to poorer PFS in patients treated with palbociclib and fulvestrant.[27-29] Similarly, mutations in the Kirsten rat sarcoma viral oncogene homolog gene, detectable through ctDNA, are significantly associated with resistance to palbociclib, leading to earlier tumor relapse and reduced efficacy.[28] In addition, upregulation of *c-myc* has been observed in palbociclib-resistant cell lines, with clinical data showing that 5 – 9% of patients receiving abemaciclib developed new *MYC* genetic alterations during treatment.[29,30]

Longitudinal ctDNA analysis has identified other acquired mutations linked to resistance, including phosphatidylinositol-4,5-bisphosphate 3-kinase catalytic subunit alpha (*PIK3CA*) and tumor protein p53 (*TP53*) alterations.[31] Impressively, rising levels of *PIK3CA*-mutated ctDNA were detected 4 – 17 months before imaging evidence of progression. Moreover, genomic complexity metrics such as blood tumor mutational burden derived from ctDNA have been shown to predict early progression during combined endocrine therapy and CDK4/6 inhibition.[32] The ctDNA marker is detailed in the schematic diagram Figure 2.

5. Strategies to overcome resistance

Combining CDK4/6 inhibitors with endocrine therapy is now the standard of care for advanced HR-positive/HER2-negative breast cancer, significantly improving PFS and OS compared to endocrine therapy alone.[4,8-11] The MONALEESA-2 trial exemplifies this, demonstrating prolonged PFS and improved OS when ribociclib was added to letrozole in patients with advanced HR-positive/HER2-negative breast cancer.[4]

To address resistance, combining CDK4/6 inhibitors with inhibitors of the PI3K/AKT/mechanistic target of the rapamycin (mTOR) pathway has emerged as a promising strategy, as this pathway is frequently activated in resistant tumors.[15] mTOR inhibitors, such as everolimus have shown potential in restoring sensitivity to endocrine therapy when co-administered with AIs.[33] Similarly, PI3K inhibitors, such as alpelisib, combined with fulvestrant, have demonstrated prolonged PFS in patients with PIK3CA-mutated advanced luminal breast cancer.[33]

Vemurafenib is a selective BRAF inhibitor that targets the B-Raf proto-oncogene, serine/threonine kinase (*BRAF*) V600E mutation, effectively suppressing tumor growth by inhibiting the MAPK/extracellular signal-regulated kinase (ERK) signaling pathway, which is hyperactivated in BRAF-mutant cancers. However, resistance to vemurafenib often arises due to reactivation of the MAPK pathway through mechanisms such as cyclin D1 upregulation or alternative signaling pathways. Studies indicate that combining CDK4/6 inhibitors with vemurafenib can overcome resistance by targeting cyclin D1–CDK4/6 signaling, inducing cell cycle arrest, and delaying tumor progression.[34] Dabrafenib, another selective BRAF

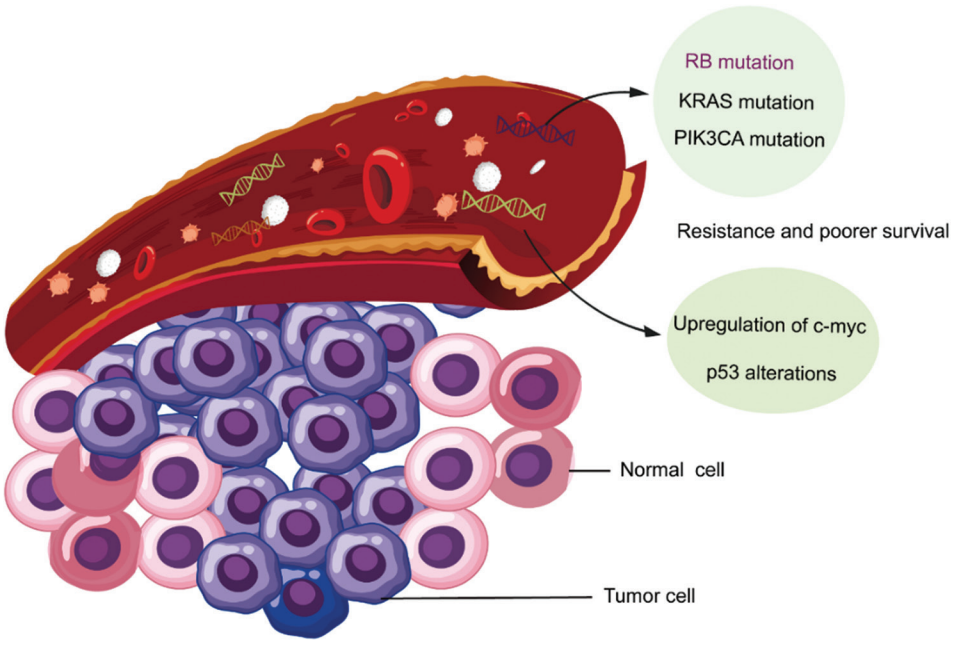

Figure 2. Detection of circulating tumor DNA as a predictive marker for resistance to CDK4/6 inhibitors.
Abbreviations: RB: Retinoblastoma; PIK3CA: Phosphatidylinositol-4,5-bisphosphate 3-kinase catalytic subunit alpha.

inhibitor, blocks MAPK pathway activation by inhibiting mutated BRAF kinase activity (e.g., V600E and V600K mutations). Resistance mechanisms include upregulation of CDK4 and cyclin D1, which bypass CDK4/6 inhibition and reactivate cell cycle progression.[35] Pre-clinical models have demonstrated that combining dabrafenib with CDK4/6 inhibitors significantly reduces tumor growth by simultaneously targeting the MAPK and cell cycle pathways.[36] This dual inhibition prevents compensatory activation of cyclin D1–CDK4 signaling, which is a key driver of dabrafenib resistance.

Cobimetinib is a selective MEK1/2 inhibitor that blocks downstream ERK activation in the MAPK pathway. Resistance to cobimetinib often involves reactivation of ERK further downstream or activation of parallel pathways, such as PI3K/AKT. Pre-clinical studies suggest that combining cobimetinib with CDK4/6 inhibitors enhances anti-tumor efficacy by simultaneously targeting both MAPK and cell cycle pathways.[37] This combination is particularly effective in tumors with cyclin D1 amplification or p16INK4a loss. Trametinib is an allosteric MEK1/2 inhibitor that prevents phosphorylation and activation of ERK, effectively blocking MAPK signaling. Resistance mechanisms include reactivation of the MAPK pathway or compensatory activation of alternative survival pathways, such as PI3K/AKT/mTOR. The combination of trametinib with CDK4/6 inhibitors has demonstrated synergistic effects in pre-clinical models by inhibiting both MAPK and cell cycle pathways.[37,38] This dual inhibition restores sensitivity to trametinib-resistant cells by suppressing proliferation and inducing apoptosis.

An emerging approach involves combining CDK4/6 inhibitors with immunotherapy to enhance anti-tumor immunity. This combination increases T-cell infiltration and activation within the tumor microenvironment. Clinical trials are currently underway to assess the efficacy of this combination across various cancer types.[28]

Sequential therapeutic approaches systematically administer various treatments to optimize therapeutic efficacy and delay resistance. For example, the sequential application of CDK4/6 inhibitors and endocrine therapy may mitigate or postpone resistance development.[39] Novel CDK inhibitors are under development to address the limitations of existing CDK4/6 inhibitors by offering enhanced selectivity and potency. These inhibitors aim to demonstrate efficacy against tumors that have developed resistance.[14] In addition, dual inhibitors targeting multiple CDKs and other cell cycle regulatory kinases are being investigated as potential strategies to overcome resistance.[40]

A pivotal strategy involves identifying and targeting alternative pathways that sustain cell proliferation in resistant tumors. Inhibition of cyclin E-CDK2 signaling has demonstrated potential in overcoming resistance to CDK4/6 inhibitors in certain cases.[15] Other promising targets implicated in resistance include components of the MAPK pathway, AURKA, and cyclin E.[15,28] These strategies aim to prolong the effectiveness of CDK4/6 inhibitors and improve patient outcomes in resistant tumors. Continued research and clinical trials are expected to refine these methodologies and may reveal additional strategies to counteract resistance.

6. Treatment options following CDK4/6 inhibitor resistance

The selection of subsequent treatments after resistance to CDK4/6 inhibitors poses a significant challenge. Several strategies are being explored to optimize outcomes for patients with HR-positive/HER2-negative breast cancer. One common approach involves switching endocrine agents, such as transitioning from an AI to fulvestrant, or vice versa, which may provide clinical benefits in some cases.[39,41] In addition, the combination of exemestane and everolimus has shown efficacy in patients who progressed on CDK4/6 inhibitors, with median PFS ranging from 4.2 to 5.8 months across various studies.[42]

For targeted therapies, PI3K inhibitors, such as alpelisib combined with fulvestrant, have demonstrated a median PFS of 5.6 – 8.0 months in patients with *PIK3CA* mutations following CDK4/6 inhibitor treatment.[42,43] Similarly, AKT inhibitors, such as capivasertib plus fulvestrant have shown a median PFS of 5.5 months in AKT-altered tumors following CDK4/6 inhibitor treatment.[43] Emerging evidence also supports continuing the same CDK4/6 inhibitor while switching the endocrine partner in select cases.[42,44] Limited data suggest potential benefits in switching to a different CDK4/6 inhibitor, such as abemaciclib, after progression on palbociclib or ribociclib.[42]

Innovative therapies are under investigation for resistant breast cancer. Antibody-drug conjugates and poly ADP-ribose polymerase inhibitors have shown promise in clinical trials.[45,46] Chemotherapy remains an option for patients with a visceral crisis or rapid disease progression, although it is generally less favored due to its toxicity profiles.[42,47] Recent studies indicate that trastuzumab deruxtecan is a viable alternative for HR-positive, HER2-low, or HER2-ultra-low metastatic breast cancer patients who have received one or more lines of endocrine therapy. This agent has achieved a median PFS of 13.2 months, approximately five months longer than chemotherapy.[48]

The optimal sequencing of treatments after CDK4/6 inhibitor resistance continues to evolve. Treatment selection should be personalized based on prior therapies,

mutation status, and individual patient factors. Ongoing clinical trials are evaluating novel agents and combinations to further improve outcomes for patients with CDK4/6 inhibitor-resistant breast cancer.[45,46]

7. Future directions in research and clinical practice

Ongoing clinical trials are focused on developing novel strategies to overcome resistance to CDK4/6 inhibitors. These include combination therapies pairing CDK4/6 inhibitors with immune checkpoint inhibitors across various cancer types, leveraging the immunomodulatory effects of CDK4/6 inhibitors to enhance anti-tumor immunity.[23] As shown in Figure 1, CDK4/6 inhibitors increase MHC class I expression, reduce Tregs, and promote cytotoxic T lymphocyte activation, creating a tumor microenvironment conducive to immunotherapy.

In addition, researchers are exploring innovative dosing regimens, such as intermittent dosing or lead-in periods, to optimize efficacy while minimizing toxicity.[23] Expanding the scope of CDK4/6 inhibitors beyond advanced HR-positive/HER2-negative breast cancer is another area of interest. Trials are assessing their efficacy in diverse breast cancer subtypes and clinical scenarios, including early-stage disease and tumors with unique molecular profiles.[4]

In terms of resistance detection, emerging technologies like ctDNA analysis are being utilized for their non-invasive nature in detecting genetic alterations associated with resistance. ctDNA has proven effective in identifying *RB* mutations, *MYC* amplifications, and cyclin E overexpression – key markers of resistance to CDK4/6 inhibitors – often months before radiological progression.[27,30] This ability of early detection allows for more informed treatment decisions and personalized therapeutic strategies.[49] Genomic profiling is also being employed to uncover novel genetic alterations linked to resistance, including loss-of-function mutations in FAT atypical cadherin 1, which may contribute to bypassing CDK4/6 inhibition.[49]

Personalized medicine approaches are at the forefront of current research, with biomarker-driven treatment selection playing a pivotal role. Reliable biomarkers such as RB status or cyclin E protein expression levels are being investigated to predict response to CDK4/6 inhibitors.[12,49] Adaptive treatment strategies are also under investigation, which involve modifying therapy based on early molecular or clinical indicators of response or resistance. For example, switching to alternative therapies or adding targeted agents like PI3K/AKT/mTOR inhibitors may counter specific resistance mechanisms in tumors with pathway activation.[12,13] Furthermore, personalized combination therapies targeting multiple pathways are being developed based on individual tumor molecular profiles. For instance, combining CDK4/6 inhibitors with PI3K/AKT/mTOR pathway inhibitors has shown promise in overcoming resistance by addressing compensatory signaling pathways frequently activated in resistant tumors.

8. Conclusion

CDK4/6 inhibitors have revolutionized the treatment landscape for HR-positive/HER2-negative breast cancer, significantly improving PFS and OS. However, resistance to these therapies remains a critical clinical challenge. Ongoing research into resistance mechanisms, the development of predictive biomarkers to guide treatment, and novel therapeutic strategies offer hope for enhancing treatment efficacy and extending benefits to a broader range of patients.

Acknowledgments

None.

Funding

None.

Conflict of interest

The authors declare they have no competing interests.

Author contributions

Conceptualization: Jundong Wu, Chunfa Chen
Visualization: Bingfeng Chen, Rendong Zhang, Chunfa Chen
Writing–original draft: Yuling Zhang, Chunfa Chen
Writing–review & editing: Jundong Wu, Chunfa Chen

Ethics approval and consent to participate

Not applicable.

Consent for publication

Not applicable.

Availability of data

Not applicable.

References

1. Bray F, Laversanne M, Sung H, *et al*. Global cancer statistics 2022: GLOBOCAN estimates of incidence and mortality worldwide for 36 cancers in 185 countries. *CA Cancer J Clin*. 2024;74(3):229-263.

doi: 10.3322/caac.21834

2. Dar H, Johansson A, Nordenskjold A, *et al.* Assessment of 25-year survival of women with estrogen receptor-positive/ERBB2-negative breast cancer treated with and without tamoxifen therapy: A secondary analysis of data from the stockholm tamoxifen randomized clinical trial. *JAMA Netw Open*. 2021;4(6):e2114904.

doi: 10.1001/jamanetworkopen.2021.14904

3. Chua AV Jr., Sheng H, Liang E, *et al*. Epidemiology of early vs late recurrence among women with early stage estrogen receptor-positive breast cancer in the Pathways Study. *J Natl Cancer Inst*. 2024;116(10):1621-31.

doi: 10.1093/jnci/djae128

4. Wang X, Zhao S, Xin Q, Zhang Y, Wang K, Li M. Recent progress of CDK4/6 inhibitors' current practice in breast cancer. *Cancer Gene Ther*. 2024;31(9):1283-1291.

doi: 10.1038/s41417-024-00747-x

5. Knudsen ES, Witkiewicz AK. The strange case of CDK4/6 inhibitors: Mechanisms, resistance, and combination strategies. *Trends Cancer*. 2017;3(1):39-55.

doi: 10.1016/j.trecan.2016.11.006

6. Rastogi P, O'Shaughnessy J, Martin M, *et al*. Adjuvant abemaciclib plus endocrine therapy for hormone receptor-positive, human epidermal growth factor receptor 2-negative, high-risk early breast cancer: Results from a preplanned monarchE overall survival interim analysis, including 5-year efficacy outcomes. *J Clin Oncol*. 2024;42(9):987-993.

doi: 10.1200/JCO.23.01994

7. Hortobagyi GN, Lacko A, Sohn J, *et al*. A phase III trial of adjuvant ribociclib plus endocrine therapy versus endocrine therapy alone in patients with HR-positive/HER2-negative early breast cancer: final invasive disease-free survival results from the NATALEE trial. *Ann Oncol*. 2024;36(2):149-157.

doi: 10.1016/j.annonc.2024.10.015

8. Li H, Wu Y, Zou H, *et al*. Clinical efficacy of CDK4/6 inhibitor plus endocrine therapy in HR-positive/HER2-0 and HER2-low-positive metastatic breast cancer: A secondary analysis of PALOMA-2 and PALOMA-3 trials. *EBioMedicine*. 2024;105:105186.

doi: 10.1016/j.ebiom.2024.105186

9. Lu YS, Im SA, Colleoni M, *et al*. Updated overall survival of ribociclib plus endocrine therapy versus endocrine therapy alone in pre- and perimenopausal patients with HR+/HER2- advanced breast cancer in MONALEESA-7: A phase III randomized clinical trial. *Clin Cancer Res*. 2022;28(5):851-859.

doi: 10.1158/1078-0432.CCR-21-3032

10. Neven P, Fasching PA, Chia S, *et al*. Updated overall survival from the MONALEESA-3 trial in postmenopausal women with HR+/HER2- advanced breast cancer receiving first-line ribociclib plus fulvestrant. *Breast Cancer Res*. 2023;25(1):103.

doi: 10.1186/s13058-023-01701-9

11. Goetz MP, Toi M, Huober J, *et al*. Abemaciclib plus a nonsteroidal aromatase inhibitor as initial therapy for HR+, HER2- advanced breast cancer: final overall survival results of MONARCH 3. *Ann Oncol*. 2024;35(8):718-727.

doi: 10.1016/j.annonc.2024.04.013

12. Xu XQ, Pan XH, Wang TT, *et al*. Intrinsic and acquired resistance to CDK4/6 inhibitors and potential overcoming strategies. *Acta Pharmacol Sin*. 2021;42(2):171-178.

doi: 10.1038/s41401-020-0416-4

13. Xue Y, Zhai J. Strategy of combining CDK4/6 inhibitors with other therapies and mechanisms of resistance. *Int J Clin Exp Pathol*. 2024;17(7):189-207.

doi: 10.62347/HGNI4903

14. Du Q, Guo X, Wang M, Li Y, Sun X, Li Q. The application and prospect of CDK4/6 inhibitors in malignant solid tumors. *J Hematol Oncol*. 2020;13(1):41.

doi: 10.1186/s13045-020-00880-8

15. Watt AC, Goel S. Cellular mechanisms underlying response and resistance to CDK4/6 inhibitors in the treatment of hormone receptor-positive breast cancer. *Breast Cancer Res*. 2022;24(1):17.

doi: 10.1186/s13058-022-01510-6

16. George MA, Qureshi S, Omene C, Toppmeyer DL, Ganesan S. Clinical and pharmacologic differences of CDK4/6 inhibitors in breast cancer. *Front Oncol*. 2021;11:693104.

doi: 10.3389/fonc.2021.693104

17. Pandey K, An HJ, Kim SK, *et al*. Molecular mechanisms of resistance to CDK4/6 inhibitors in breast cancer: A review. *Int J Cancer*. 2019;145(5):1179-1188.

doi: 10.1002/ijc.32020

18. Chen X, Shen K. Dalpiciclib in advanced breast cancer. *Lancet Oncol*. 2023;24(6):578-579.

doi: 10.1016/S1470-2045(23)00228-0

19. Huang J, Zheng L, Sun Z, Li J. CDK4/6 inhibitor resistance mechanisms and treatment strategies (Review). *Int J Mol Med*. 2022;50(4):128.

doi: 10.3892/ijmm.2022.5184

20. Chang CM, Lam HYP. Mechanism of CDK4/6 inhibitor resistance in hormone receptor-positive breast cancer and alternative treatment strategies. *Anticancer Res*. 2023;43(12):5283-5298.

doi: 10.21873/anticanres.16732

21. Zhou FH, Downton T, Freelander A, Hurwitz J, Caldon CE, Lim E. CDK4/6 inhibitor resistance in estrogen receptor positive breast cancer, a 2023 perspective. *Front Cell Dev*

Biol. 2023;11:1148792.

doi: 10.3389/fcell.2023.1148792

22. Wander SA, Cohen O, Gong X, *et al*. The genomic landscape of intrinsic and acquired resistance to cyclin-dependent kinase 4/6 inhibitors in patients with hormone receptor-positive metastatic breast cancer. *Cancer Discov*. 2020;10(8):1174-1193.

doi: 10.1158/2159-8290.CD-19-1390

23. Lelliott EJ, Sheppard KE, McArthur GA. Harnessing the immunotherapeutic potential of CDK4/6 inhibitors in melanoma: Is timing everything? *NPJ Precis Oncol*. 2022;6(1):26.

doi: 10.1038/s41698-022-00273-9

24. Sun M, Dong L, Wang Y, *et al*. The role of targeting CDK4/6 in cancer immunotherapy. *Holistic Integr Oncol*. 2024;3(1):32.

doi: 10.1007/s44178-024-00100-0

25. Teh JLF, Aplin AE. Arrested developments: CDK4/6 inhibitor resistance and alterations in the tumor immune microenvironment. *Clin Cancer Res*. 2019;25(3):921-927.

doi: 10.1158/1078-0432.CCR-18-1967

26. Deng J, Wang ES, Jenkins RW, *et al*. CDK4/6 inhibition augments antitumor immunity by enhancing T-cell activation. *Cancer Discov*. 2018;8(2):216-233.

doi: 10.1158/2159-8290.CD-17-0915

27. Chin YM, Shibayama T, Chan HT, *et al*. Serial circulating tumor DNA monitoring of CDK4/6 inhibitors response in metastatic breast cancer. *Cancer Sci*. 2022;113(5):1808-1820.

doi: 10.1111/cas.15304

28. Krasniqi E, Goeman F, Pulito C, *et al*. Biomarkers of response and resistance to CDK4/6 inhibitors in breast cancer: Hints from liquid biopsy and microRNA exploration. *Int J Mol Sci*. 2022;23(23):14534.

doi: 10.3390/ijms232314534

29. Goetz MP, Hamilton EP, Campone M, *et al*. Landscape of baseline and acquired genomic alterations in circulating tumor DNA with abemaciclib alone or with endocrine therapy in advanced breast cancer. *Clin Cancer Res*. 2024;30(10):2233-2244.

doi: 10.1158/1078-0432.CCR-22-3573

30. Asghar US, Kanani R, Roylance R, Mittnacht S. Systematic review of molecular biomarkers predictive of resistance to CDK4/6 inhibition in metastatic breast cancer. *JCO Precis Oncol*. 2022;6:e2100002.

doi: 10.1200/PO.21.00002

31. Kindt CK, Alves CL, Ehmsen S, *et al*. Genomic alterations associated with resistance and circulating tumor DNA dynamics for early detection of progression on CDK4/6 inhibitor in advanced breast cancer. *Int J Cancer*. 2024;155(12):2211-2222.

doi: 10.1002/ijc.35126.

32. Davis AA, Luo J, Zheng T, *et al*. Genomic complexity predicts resistance to endocrine therapy and CDK4/6 inhibition in hormone receptor-positive (HR+)/HER2-negative metastatic breast cancer. *Clin Cancer Res*. 2023;29(9):1719-1729.

doi: 10.1158/1078-0432.CCR-22-2177.

33. Li Z, Zou W, Zhang J, *et al*. Mechanisms of CDK4/6 inhibitor resistance in luminal breast cancer. *Front Pharmacol*. 2020;11:580251.

doi: 10.3389/fphar.2020.580251

34. Yoshida A, Lee EK, Diehl JA. Induction of therapeutic senescence in vemurafenib-resistant melanoma by extended inhibition of CDK4/6. *Cancer Res*. 2016;76(10):2990-3002.

doi: 10.1158/0008-5472.CAN-15-2931

35. Hirai N, Hatanaka Y, Hatanaka KC, *et al*. Cyclin-dependent kinase 4 upregulation mediates acquired resistance of dabrafenib plus trametinib in BRAF V600E-mutated lung cancer. *Transl Lung Cancer Res*. 2021;10(9):3737-3744.

doi: 10.21037/tlcr-21-415

36. Nassar KW, Hintzsche JD, Bagby SM, *et al*. Targeting CDK4/6 represents a therapeutic vulnerability in acquired BRAF/MEK inhibitor-resistant melanoma. *Mol Cancer Ther*. 2021;20(10):2049-2060.

doi: 10.1158/1535-7163.MCT-20-1126

37. Lelliott EJ, McArthur GA, Oliaro J, Sheppard KE. Immunomodulatory effects of BRAF, MEK, and CDK4/6 inhibitors: Implications for combining targeted therapy and immune checkpoint blockade for the treatment of melanoma. *Front Immunol*. 2021;12:661737.

doi: 10.3389/fimmu.2021.661737

38. Cheng K, Zhou Z, Chen Q, *et al*. CDK4/6 inhibition sensitizes MEK inhibition by inhibiting cell cycle and proliferation in pancreatic ductal adenocarcinoma. *Sci Rep*. 2024;14(1):8389.

doi: 10.1038/s41598-024-57417-z

39. Sonke GS, van Ommen-Nijhof A, Wortelboer N, *et al*. Early versus deferred use of CDK4/6 inhibitors in advanced breast cancer. *Nature*. 2024;636:474-480.

doi: 10.1038/s41586-024-08035-2

40. Wells CI, Vasta JD, Corona CR, *et al*. Quantifying CDK inhibitor selectivity in live cells. *Nat Commun*. 2020;11(1):2743.

doi: 10.1038/s41467-020-16559-0

41. Bidard FC, Hardy-Bessard AC, Dalenc F, *et al*. Switch to fulvestrant and palbociclib versus no switch in advanced breast cancer with rising ESR1 mutation during aromatase inhibitor and palbociclib therapy (PADA-1): A randomised,

open-label, multicentre, phase 3 trial. *Lancet Oncol*. 2022;23(11):1367-1377.

doi: 10.1016/S1470-2045(22)00555-1

42. Ye M, Xu H, Ding J, Jiang L. Therapy for hormone receptor-positive, human epidermal growth receptor 2-negative metastatic breast cancer following treatment progression via CDK4/6 inhibitors: A literature review. *Breast Cancer (Dove Med Press)*. 2024;16:181-197.

doi: 10.2147/BCTT.S438366

43. Müller VJE. Current and upcoming treatment strategies after CDK4/6 inhibitors for patients with ER+/HER2- advanced. *Breast Cancer*. 2023;11(1):33-43.

44. Kalinsky K, Accordino MK, Chiuzan C, *et al*. Randomized phase II trial of endocrine therapy with or without ribociclib after progression on cyclin-dependent kinase 4/6 inhibition in hormone receptor-positive, human epidermal growth factor receptor 2-negative metastatic breast Cancer: MAINTAIN trial. *J Clin Oncol*. 2023;41(24):4004-4013.

doi: 10.1200/JCO.22.02392

45. Ma J, Chan JJ, Toh CH, Yap YS. Emerging systemic therapy options beyond CDK4/6 inhibitors for hormone receptor-positive HER2-negative advanced breast cancer. *NPJ Breast Cancer*. 2023;9(1):74.

doi: 10.1038/s41523-023-00578-3

46. Mittal A, Molto Valiente C, Tamimi F, *et al*. Filling the gap after CDK4/6 inhibitors: Novel endocrine and biologic treatment options for metastatic hormone receptor positive breast cancer. *Cancers (Basel)*. 2023;15(7):2015.

doi: 10.3390/cancers15072015

47. Benvenuti C, Gaudio M, Jacobs F, *et al*. Clinical review on the management of breast cancer visceral crisis. *Biomedicines*. 2023;11(4):1083.

doi: 10.3390/biomedicines11041083

48. Bardia A, Hu X, Dent R, *et al*. Trastuzumab deruxtecan after endocrine therapy in metastatic breast cancer. *N Engl J Med*. 2024;391:2110-2122.

doi: 10.1056/NEJMoa2407086

49. McCartney A, Migliaccio I, Bonechi M, *et al*. Mechanisms of resistance to CDK4/6 inhibitors: Potential implications and biomarkers for clinical practice. *Front Oncol*. 2019;9:666.

doi: 10.3389/fonc.2019.00666

50. Johnston S, Emde A, Barrios C, *et al*. Cyclin-dependent kinase 4 and 6 (CDK4/6) inhibitors: Existing and emerging differences. *JNCI Cancer Spectr*. 2023;7(4):pkad045.

doi: 10.1093/jncics/pkad045

51. Thill M, Schmidt M. Management of adverse events during cyclin-dependent kinase 4/6 (CDK4/6) inhibitor-based treatment in breast cancer. *Ther Adv Med Oncol*. 2018;10:1758835918793326.

doi: 10.1177/1758835918793326

52. Gelbert LM, Cai S, Lin X, *et al*. Preclinical characterization of the CDK4/6 inhibitor LY2835219: *In-vivo* cell cycle-dependent/independent anti-tumor activities alone/ in combination with gemcitabine. *Invest New Drugs*. 2014;32(5):825-837.

doi: 10.1007/s10637-014-0120-7

53. Xu B, Zhang Q, Zhang P, *et al*. Dalpiciclib or placebo plus fulvestrant in hormone receptor-positive and HER2-negative advanced breast cancer: A randomized, phase 3 trial. *Nat Med*. 2021;27(11):1904-1909.

doi: 10.1038/s41591-021-01562-9

54. Sheikh MS, Satti SA. The emerging CDK4/6 inhibitor for breast cancer treatment. *Mol Cell Pharmacol*. 2021;13(3):9-12.

55. Long F, He Y, Fu H, *et al*. Preclinical characterization of SHR6390, a novel CDK 4/6 inhibitor, *in vitro* and in human tumor xenograft models. *Cancer Sci*. 2019;110(4):1420-1430.

doi: 10.1111/cas.13957

ACCSCIENCE PUBLISHING

Tumor Discovery

REVIEW ARTICLE

WD repeat domain 4 in tumorigenesis: Molecular mechanisms, cancer-type specific roles, and therapeutic potential

Xun Zou[1], Ling Tao[2], and Bin Liu[1]*

[1]Jiangsu Key Laboratory of Marine Pharmaceutical Compound Screening, College of Pharmacy, Jiangsu Ocean University, Lianyungang, Jiangsu, China

[2]Department of Nutrition and Food Hygiene, School of Public Health, Institute of Nutrition, Zhongshan Hospital, Fudan University, Shanghai, China

Abstract

WD repeat domain 4 (WDR4) is an essential member of the WD-repeat protein family, known for its regulatory roles in cellular processes critical to cancer development, including RNA modification, protein stability, cell cycle progression, and apoptosis. Studies have shown that WDR4 plays a pivotal role in tumorigenesis across various cancer types, with a particular focus on breast cancer in this study, where its overexpression is closely associated with aggressive tumor characteristics and poorer patient outcomes. As a scaffold protein, WDR4 is involved in N7-methylguanosine tRNA methylation and ubiquitin-mediated protein degradation, thereby regulating RNA stability, protein synthesis, and cell survival. This review provides a comprehensive analysis of WDR4's molecular mechanisms, its oncogenic functions across different cancer types, and its interactions with other key factors in the tumor microenvironment, further exploring its potential role in tumor progression. As research on WDR4 progresses, we not only gain a deeper understanding of its complex role in tumor biology but also uncover new therapeutic avenues. In particular, the potential of WDR4 as a biomarker and therapeutic target is increasingly recognized. Despite the challenges faced in its clinical application, such as the difficulty in developing targeted therapies and managing side effects, the future prospects of WDR4 in cancer diagnosis and treatment remain promising, and it is expected to emerge as an effective therapeutic target in the near future.

Keywords: WD repeat domain 4; Tumorigenesis; RNA modification; Tumor microenvironment; Cancer-type specificity; Targeted therapy

***Corresponding author:**
Bin Liu
(liubin@jou.edu.cn)

Citation: Zou X, Tao L, Liu B. WD repeat domain 4 in tumorigenesis: Molecular mechanisms, cancer-type specific roles, and therapeutic potential. *Tumor Discov*. 2025;4(1):37-46. doi: 10.36922/td.5830

Received: November 9, 2024

1st revised: December 31, 2024

2nd revised: January 16, 2025

Accepted: January 21, 2025

Published online: February 5, 2025

1. Introduction

1.1. Molecular and functional overview of WD repeat domain 4 (WDR4)

WDR4 belongs to the WD-repeat protein family, defined by the presence of WD40 repeat motifs that enable extensive protein-protein interactions.[1] These WD40 domains form a stable beta-propeller structure (Figure 1), providing WDR4 with a large interaction surface that supports its role as a scaffold protein in critical cellular pathways. Located on chromosome 21q22.3, *WDR4* encodes a protein consisting of 311 amino acids,

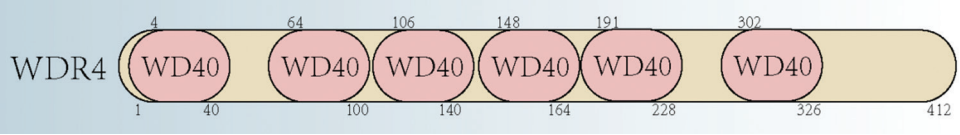

Figure 1. The protein structure of WDR4. WDR4 is composed of multiple WD40 domains
Abbreviations: WDR4: WD repeat domain 4.

that contributes to essential processes in normal cellular function and disease states, including transcriptional regulation, signal transduction, protein degradation, and cell cycle progression.[2]

Functionally, WDR4 plays a pivotal role in RNA metabolism, particularly in m7G modification of transfer RNA (tRNA).[3] This post-transcriptional modification is critical for stabilizing tRNA, enhancing translation fidelity, and ensuring efficient protein synthesis.[4,5] In the biological characteristics of malignant tumor cells, the stability of RNA molecules and the efficiency of their translation processes constitute the fundamental mechanisms driving the rapid proliferation and growth of cancer cells. By modulating tRNA methylation, WDR4 affects RNA stability and translation efficiency, driving the increased protein synthesis required for oncogenesis.[6,7] Consequently, the dysregulation of WDR4 leads to a cellular environment conducive to tumorigenesis, positioning WDR4 as a significant factor in malignant transformation.[8,9]

In addition to its role in RNA modification, recent studies have shown that WDR4 regulates protein stability through interactions with the ubiquitin-proteasome system.[10] Specifically, WDR4 facilitates the degradation of tumor suppressor proteins and enhances the stability of proteins involved in cell cycle progression and resistance to apoptosis.[11] This mechanism may promote tumor cell proliferation and survival by selectively modulating the degradation and maintenance of critical proteins.[12,13] Therefore, WDR4 plays a crucial role not only through RNA modification pathways but also by influencing protein stability, making it a potential therapeutic target in cancer biology.

This dual role in RNA modification and protein stability enables WDR4 to regulate several tumor-promoting processes, underscoring its potential as a therapeutic target in oncology.

1.2. Relevance of WDR4 in cancer

The oncogenic functions of WDR4 in multiple malignancies have been studied, including hepatocellular carcinoma (HCC),[14-16] lung cancer,[17-19] head and neck squamous cell carcinoma,[20] adrenocortical carcinoma,[21] prostate adenocarcinoma,[22,23] esophageal squamous cell carcinoma,[24] hepatoblastoma,[25] and Wilms tumor,[26] where its overexpression or polymorphism has been linked to tumor progression, metastasis, and poor patient prognosis. In HCC, high expression of WDR4 is associated with aggressive disease features, including advanced tumor stage and reduced survival, as it supports RNA modifications that promote the synthesis of oncogenic proteins by forming a complex with methyltransferase like 1 (METTL1), which cooperatively regulates the m7G modification of mRNA in HCC cells. WDR4 effectively modulates both the expression of mRNA and the protein levels of the *METTL1* gene. Moreover, the impact of WDR4 on tRNA m7G levels directly mediates the translation of TRIM28, which in turn enhances the stemness of cancer stem cells. This process contributes to the development of resistance to lenvatinib and promotes tumor progression in HCC. In lung cancer, WDR4 has been shown to influence cell cycle regulation and apoptosis, facilitating rapid cell division and enhanced survival under conditions of cellular stress. Similarly, in head and neck squamous cell carcinoma, elevated expression of WDR4 is linked to disease progression by regulating RNA translation through RNA modification. This process impacts critical signaling pathways, including the PI3K/AKT/mTOR pathway, which are essential for promoting oncogenic protein synthesis.[20] This regulation facilitates tumor growth and may contribute to the aggressive behavior characteristic of this malignancy.

This multifaceted role of WDR4 across cancer types suggests that its oncogenic mechanisms may vary depending on the specific molecular context and the surrounding tumor microenvironment. Understanding the precise molecular functions and signaling interactions of WDR4 in different types of cancer is essential to identifying its potential as a therapeutic target and designing targeted strategies to selectively inhibit its activity in cancer cells.

2. Molecular mechanisms of WDR4 in tumorigenesis

2.1. Structural and functional aspects of WDR4

The oncogenic mechanisms of WDR4 in cancer are mainly attributable to its unique structural properties, particularly its WD40 repeat domains,[27] which form a stable beta-propeller structure capable of binding diverse cellular partners, such as METTL1.[28] This structure enables WDR4 as a scaffold protein that coordinates cellular complexes in RNA modification and protein turnover pathways.

2.1.1. RNA modification and tumorigenesis

WDR4's role in RNA metabolism is particularly evident in its involvement in M7G modification of tRNA, which stabilizes tRNA molecules and improves translation fidelity.[29] Dysregulation of this modification in cancer cells contributes to rapid protein synthesis, supporting the increased cellular proliferation and metabolic demand associated with tumorigenesis.[6] In HCC, WDR4 overexpression has been shown to enhance m7G modification, resulting in the translation of oncogenic proteins that promote cell survival and proliferation.[30] By specifically improving the translation efficiency of these tumor-promoting proteins, WDR4 drives cellular processes that support malignancy, highlighting its potential as an oncogene in RNA metabolism.

2.1.2. Interaction with the ubiquitin-proteasome system

WDR4 also interacts with the ubiquitin-proteasome system, influencing protein stability by promoting the degradation of tumor suppressor proteins. For instance, in cancer, WDR4 facilitates the ubiquitination and degradation of p53, a crucial tumor suppressor, enabling cancer cells to evade apoptosis.[11] This ability to degrade tumor suppressors while stabilizing cell cycle regulators allows WDR4 to support cell proliferation and survival, which are critical for tumor progression. WDR4-mediated ubiquitination of protein tyrosine phosphatase, non-receptor type 23 (PTPN23) leads to its proteasomal degradation, thereby inhibiting the lysosomal transport and degradation of wild-type epidermal growth factor receptor (EGFR), EGFR mutants, and c-MET. Through this mechanism, WDR4 maintains EGFR and c-MET signaling, promoting the proliferation, migration, invasion, stemness, and metastasis of non-small cell lung cancer. In addition, WDR4-mediated ubiquitination of promyelocytic leukemia (PML) enhances lung tumor growth. Specifically, the degradation of PML induced by WDR4 triggers the secretion of a series of cell surface or secreted factors, including CD73, urokinase-type plasminogen activator receptor, and serum amyloid A2, which initiate paracrine signaling that stimulates cell migration, invasion, and metastasis.[13] WDR4-induced ubiquitination and degradation of Arhgap17 activate Rac1, which prevents the cell cycle exit of granule neuron precursor (GNP), thus supporting GNP proliferation and ultimately facilitating cell cycle progression, a process essential for cerebellar development and motor function.[31] By modulating the ubiquitin-proteasome pathway, WDR4 effectively tilts the balance between cell survival and apoptosis in favor of tumor progression. However, current research suggests that WDR4's role in protein degradation might be interconnected with its function in tRNA modification, although the exact mechanisms may differ. Figure 2 illustrates the molecular mechanisms of WDR4 in tumorigenesis.

2.2. Regulation of cell cycle and apoptosis

WDR4's influence on cell cycle progression and apoptosis is fundamental to its role in tumorigenesis. Through interactions with cell cycle regulators and apoptotic pathways, WDR4 promotes cell proliferation while inhibiting programmed cell death, creating a cellular environment conducive to tumor growth.

2.2.1. Cell cycle control

In several types of cancer, WDR4 overexpression is associated with increased levels of cell cycle-promoting proteins, particularly those that regulate the G1/S transition.[32,33] In lung cancer, WDR4's impact on cyclin D1 levels accelerates cell cycle progression by promoting the G1/S phase transition, enabling tumor cells to sustain high proliferation rates.[34] In addition, WDR4's influence on other cyclins and cyclin-dependent kinases may further reinforce its role in cell cycle regulation, contributing to continuous tumor growth.

2.2.2. Modulation of apoptosis

WDR4's role in apoptosis resistance is evident in its interactions with pro- and anti-apoptotic factors.[35,36] In head and neck squamous cell carcinoma, WDR4 downregulates or degrades p53, reducing cellular sensitivity to apoptosis-inducing signals.[20] Furthermore, WDR4 is associated with the upregulation of anti-apoptotic proteins, such as BCL-2, which inhibit apoptotic signaling pathways and protect cancer cells from programmed cell death.[36,37] This ability to modulate apoptosis is essential for cancer cell survival, particularly under stress conditions, such as nutrient deprivation or exposure to chemotherapy.[38,39] Figure 3 illustrates the molecular mechanisms underlying the inhibitory effects of WDR4 on the cell cycle and apoptosis of cancer cells.

3. WDR4 is associated with multiple oncogenic pathways

3.1. PI3K/AKT/mTOR pathway

The PI3K/AKT/mTOR signaling pathway is a crucial intracellular regulatory network that plays a key role in regulating fundamental biological processes such as cell growth, proliferation, survival, metabolism, and motility. Abnormal activation of this pathway is closely associated with the development of various diseases, particularly cancer, diabetes, and neurodegenerative diseases.[40-42] PI3K (phosphoinositide 3-kinase) is an enzyme that catalyzes the phosphorylation of phosphoinositides and their

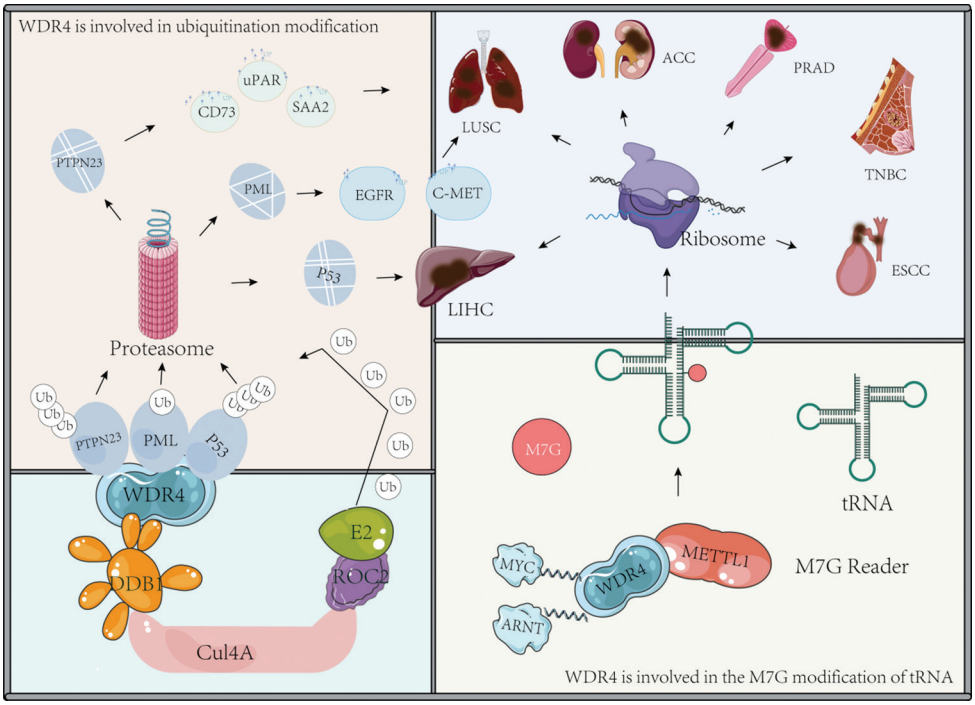

Figure 2. Molecular mechanisms of WDR4 in tumorigenesis. WDR4 can ubiquitinate and degrade multiple important proteins such as PML, PTPN23, and P53. It can also form a complex with METTL1 as a reader of M7G modification, promoting various types of cancers.
Abbreviations: ACC: Adrenocortical carcinoma; ARNT: Aryl hydrocarbon receptor nuclear translocator; EGFR: Epidermal growth factor receptor; ESCC: Esophageal squamous cell carcinoma; LIHC: Liver hepatocellular carcinoma; LUSC: Lung squamous cell carcinoma; METTL1: Methyltransferase like 1; PML: Promyelocytic leukemia; PRAD: Prostate adenocarcinoma; PTPN23: Protein tyrosine phosphatase non-receptor type 23; SAA2: Serum amyloid A2; TNBC: Triple-negative breast cancer; uPAR: Urokinase-type plasminogen activator receptor; WDR4: WD repeat domain 4.

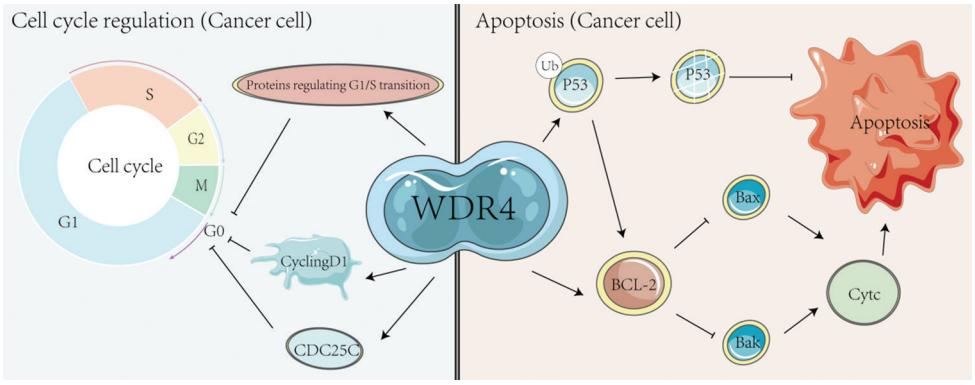

Figure 3. Molecular mechanisms underlying the inhibitory effects of WDR4 on the cell cycle and apoptosis of cancer cells.
Abbreviations: Bak: Bcl-2-associated x protein; Bax: Bcl-2-associated x protein; BCL-2: B-cell lymphoma 2; CDC25C: Cell division cycle 25C; WDR4: WD repeat domain 4.

derivatives, primarily initiating downstream signaling by generating phosphoinositide (3,4,5)-trisphosphate (PIP3) on the cell membrane.[43,44] PI3K activates this signaling pathway by interacting with receptor proteins on the cell membrane, such as growth factor receptors.

PI3K phosphorylates phosphoinositides on the cell membrane to produce PIP3, and the accumulation of PIP3 provides binding sites for downstream kinases like AKT, thus activating AKT.[45] This process is a core step in the PI3K/AKT/mTOR signaling pathway. Through the activation of AKT, this pathway regulates multiple cellular functions, including protein synthesis, metabolic regulation, cell cycle control, and anti-apoptotic actions. Moreover, the PI3K/AKT/mTOR pathway plays an essential role in the initiation and progression of various cancers by regulating cell proliferation and survival.[46]

In liver cancer, studies have shown that WDR4 may regulate the protein level of CCNB1, influencing the activation of the PI3K/AKT signaling pathway and promoting tumor progression.[12] In head and neck squamous cell carcinoma, it has been found that m7G tRNA modification mediates the interaction with the PI3K/AKT/mTOR pathway, regulating the mRNA expression profile and further promoting cancer progression.[20] This suggests the significant role of tRNA modifications in tumor metabolism and biological processes. In addition, in esophageal squamous cell carcinoma, WDR4 regulates m7G modification to affect tRNA expression, activating the RPTOR/ULK1/autophagy pathway and contributing to cancer development.[24] These findings indicate that WDR4, as a critical regulatory factor, plays a significant role in the onset and progression of various cancers through its regulation of the PI3K/AKT/mTOR signaling pathway.

3.2. MAPK pathway

The mitogen-activated protein kinase (MAPK) pathway is a critical intracellular signaling pathway involved in various physiological processes, including cell growth, differentiation, stress response, apoptosis, and metabolism.[47,48] The activation of the MAPK pathway is typically triggered by external stimuli such as growth factors, cytokines, and environmental stress.[49] On activation, this pathway regulates downstream transcription factors and other effector molecules, thereby influencing the function and fate of the cell.[50-52]

In pancreatic cancer, the MAPK pathway plays a significant role in regulating cell proliferation and survival.[53] The functional role of WDR4 in influencing protein stability may extend to the components of the MAPK pathway, thereby enhancing their stability and facilitating their activation. By modulating MAPK signaling, WDR4 supports tumor cell growth and metastasis, positioning it as a potential therapeutic target in MAPK-driven pancreatic cancer.

3.3. WNT/β-catenin pathway and epithelial-mesenchymal transition (EMT) pathway

The WNT/β-catenin pathway is a central signaling mechanism that regulates various physiological processes, including development, stem cell maintenance, and tissue homeostasis.[50,54] Dysregulation of this pathway is a key feature in the pathogenesis of many diseases, particularly cancer.[55,56]

The EMT is a biological process in which epithelial cells, which are normally tightly bound and organized in layers, lose their cell-cell adhesion properties and acquire mesenchymal characteristics.[57-59] These include increased motility, invasiveness, and the ability to degrade components of the extracellular matrix.[60] EMT is essential during embryogenesis, tissue development, and wound healing, and plays a significant role in cancer metastasis.[61,62]

In nasopharyngeal carcinoma, the expression of WDR4 is significantly elevated, leading to a notable increase in the translation efficiency of m7G-modified codon-containing mRNA. This enhanced translation efficiency activates the WNT/β-catenin signaling pathway, thereby influencing the EMT process.[63]

3.4. EGFR pathway

The EGFR pathway is a critical cellular signaling pathway that plays a fundamental role in regulating biological processes such as cell proliferation, survival, migration, and differentiation. EGFR is a transmembrane receptor belonging to the receptor tyrosine kinase family.[64-66]

In addition to its regulation through the E3 ubiquitin ligase-mediated degradation of PTPN23,[12] as previously discussed, WDR4 has been shown to influence tRNA modification by regulating the M7G cap in HCC.[14] This tRNA modification enhances resistance to lenvatinib, a first-line tyrosine kinase inhibitor used in the treatment of advanced liver cancer.[67] Specifically, WDR4 promotes the translation of genes involved in the EGFR signaling pathway, contributing to the development of drug resistance.

Furthermore, in bladder cancer, WDR4, in collaboration with METTL1, modulates tRNA modifications to regulate the translation of EGFR and EGF-containing fibulin-like extracellular matrix protein 1 (EFEMP1).[68] This process activates the EGFR signaling pathway, emphasizing the significant role of tRNA modifications and their interaction with key oncogenic signaling pathways in cancer progression and drug resistance. Figure 4 illustrates the key role of WDR4 in the pathway.

4. Clinical implications and therapeutic potential of WDR4

4.1. WDR4 as a prognostic and predictive biomarker

Elevated WDR4 expression across multiple cancers correlates with poor clinical outcomes, underscoring its potential as a prognostic and predictive biomarker. High levels of WDR4 expression in patient samples correlate with increased metastasis, reduced survival rates, and resistance to standard therapies, suggesting its use as a biomarker for assessing tumor aggressiveness and therapeutic resistance.

4.2. Therapeutic targeting of WDR4

Several approaches are applied to target WDR4's oncogenic activity, including small-molecule inhibitors, RNA interference, gene editing, and combination therapies.

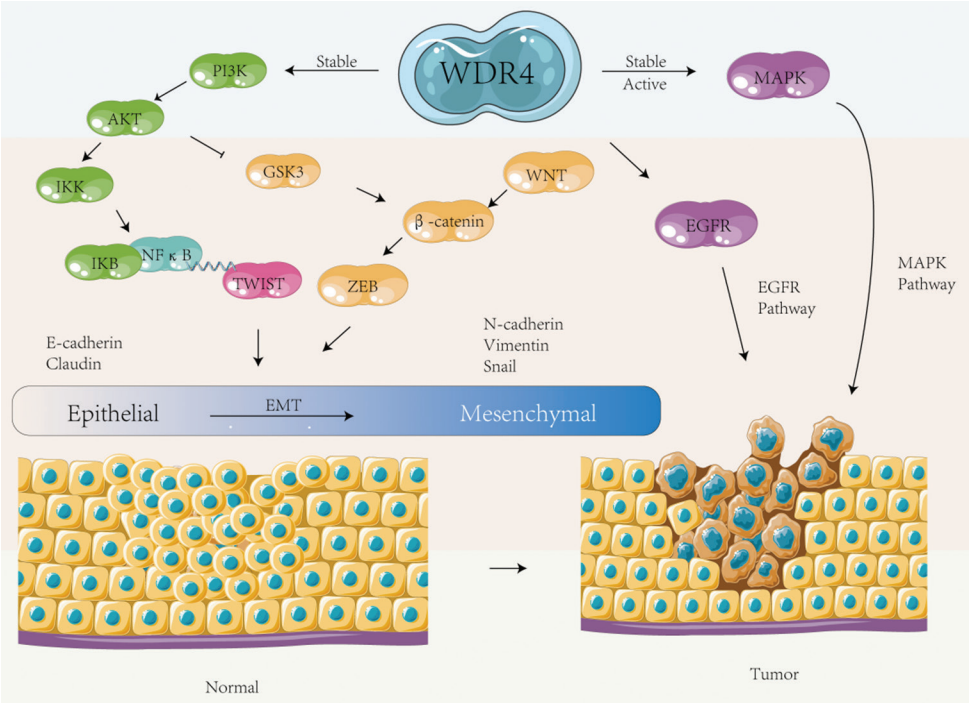

Figure 4. The key role of WDR4 in signaling pathway. WDR4 has the ability to modulate several signaling pathways, thereby contributing to the onset and progression of cancer.
Abbreviations: AKT: Protein kinase B; EGFR: Epidermal growth factor receptor; EMT: Epithelial-mesenchymal transition; GSK3: Glycogen synthase kinase 3; IKB: Inhibitor of kappa B; IKK: IκB kinase; MAPK: Mitogen-activated protein kinase; NFκB: Nuclear factor kapp B; TWIST: Twist family BHLH transcription factor; WDR4: WD repeat domain 4; WNT: WD repeat domain 4; ZEB: Zinc finger E-box binding homeobox.

4.2.1. Small-molecule inhibitors

Developing small molecules that specifically inhibit WDR4's scaffold function or its involvement in RNA modification could hinder its tumor-promoting functions. However, achieving high specificity is challenging due to WDR4's role in normal cellular processes. Structure-based drug design and high-throughput screening could help identify compounds with optimal selectivity, minimizing off-target effects and preserving normal cellular functions.[69]

4.2.2. RNA interference and antisense oligonucleotides

RNA interference and antisense oligonucleotides targeting WDR4 mRNA offer a means to selectively reduce its expression in cancer cells, without affecting normal tissues. Pre-clinical studies have shown that silencing WDR4 in HCC and lung cancer models reduces tumor cell proliferation, and invasion, and promotes apoptosis.[14,17] Optimizing delivery systems, such as nanoparticle-based delivery, could improve these RNA-based therapies' tumor specificity and efficacy.[70]

4.2.3. Gene editing using CRISPR/Cas9

CRISPR/Cas9-mediated gene editing provides a precise approach to knocking out or reducing WDR4 expression in cancer cells. CRISPR-based WDR4 silencing in triple-negative breast cancer and HCC models has shown promise in reducing tumor growth and metastasis. Viral and non-viral vectors, such as lipid nanoparticles, are being explored to improve delivery efficiency, although managing off-target effects and ensuring specificity remain critical.[18]

4.2.4. Combination therapy approaches

Combining WDR4-targeted therapies with other treatments, such as cell cycle inhibitors, PI3K/mTOR pathway inhibitors, or immune checkpoint inhibitors, could enhance therapeutic efficacy. For example, in cancers where WDR4 stabilizes PI3K/Akt/mTOR pathway components, combination therapies with PI3K inhibitors may improve outcomes by inhibiting complementary survival pathways.

4.3. Challenges in clinical translation

Translating therapies targeting WDR4 into clinical practice faces several challenges. These include ensuring treatment selectivity to avoid toxicity in normal tissues, addressing tumor heterogeneity, and deepening our understanding of WDR4's role in normal physiology. To effectively overcome

these obstacles and fully realize the therapeutic potential of WDR4, advanced drug design, and innovative delivery systems will be critical. Specifically, developing highly selective inhibitors or modulators will help minimize side effects on non-tumor cells. In addition, personalized therapeutic strategies may be more effective in addressing the heterogeneity of different tumor types. Further research into the function of WDR4 in normal cells and tissues is warranted to explore strategies for avoiding unwanted side effects and for achieving precision treatment. Therefore, integrating basic research with clinical needs and fostering multidisciplinary collaboration in drug development are key steps toward the successful clinical translation of WDR4-targeted therapies.

5. Future directions for WDR4 research in cancer

To validate the therapeutic potential of WDR4-targeting strategy, future research should focus on mapping its interaction networks, developing precise preclinical models, exploring combination therapy approaches, and investigating its role in cancer stem cells and drug resistance. Understanding how WDR4 influences cancer biology and its interactions within the tumor microenvironment will be essential to unlock its potential as a therapeutic target.

6. Conclusion

Given its roles in RNA modification, protein stability, cell cycle regulation, and immune modulation, WDR4 represents a promising target in cancer therapy. Its overexpression and association with aggressive tumor phenotypes underscore its potential as both a biomarker and a therapeutic target. Advances in structural biology, preclinical modeling, and combination therapies could transform WDR4 into a cornerstone of cancer treatment, offering new hope for patients with aggressive and treatment-resistant cancers. Continued research into its molecular functions and interactions will be critical for translating WDR4-targeted therapies from bench to bedside.

Acknowledgments

None.

Funding

This study was supported by the National Natural Science Foundation of China (82273167, 82304124), Jiangsu Province Basic Research Program Natural Science Foundation (Outstanding Youth Fund Project, BK20220063), the Key Program of Basic Science (Natural Science) of Jiangsu Province (22KJA350001), and the Key Disciplines in the Three-year Plan of Shanghai Municipal Public Health System (2023 – 2025) (GWVI-11.1-42).

Conflict of interest

The authors declare that they have no competing interests.

Author contributions

Conceptualization: All authors
Visualization: Xun Zou
Writing – original draft: All authors
Writing – review & editing: Bin Liu, Ling Tao

Ethics approval and consent to participate

Not applicable.

Consent for publication

Not applicable.

Availability of data

Not applicable.

References

1. Cheng W, Gao A, Lin H, Zhang W. Novel roles of METTL1/WDR4 in tumor via m^7G methylation. *Mol Ther Oncolytics*. 2022;26:27-34.

   doi: 10.1016/j.omto.2022.05.009

2. Michaud J, Kudoh J, Berry A, *et al*. Isolation and characterization of a human chromosome 21q22.3 gene (WDR4) and its mouse homologue that code for a WD-repeat protein. *Genomics*. 2000;68(1):71-79.

   doi: 10.1006/geno.2000.6258

3. Dedon PC, Begley TJ. Dysfunctional tRNA reprogramming and codon-biased translation in cancer. *Trends Mol Med*. 2022;28(11):964-978.

   doi: 10.1016/j.molmed.2022.09.007

4. Zhang X, Zhu WY, Shen SY, Shen JH, Chen XD. Biological roles of RNA m7G modification and its implications in cancer. *Biol Direct*. 2023;18(1):58.

   doi: 10.1186/s13062-023-00414-5

5. Tang Q, Li L, Wang Y, *et al*. RNA modifications in cancer. *Br J Cancer*. 2023;129(2):204-221.

   doi: 10.1038/s41416-023-02275-1

6. Zhang Y, Xu W, Peng C, *et al*. Exploring the role of m7G modification in Cancer: Mechanisms, regulatory proteins, and biomarker potential. *Cell Signal*. 2024;121:111288.

   doi: 10.1016/j.cellsig.2024.111288

7. Luo Y, Yao Y, Wu P, Zi X, Sun N, He J. The potential role of N^7-methylguanosine (m7G) in cancer. *J Hematol Oncol*.

2022;15(1):63.

doi: 10.1186/s13045-022-01285-5

8. Cai M, Yang C, Wang Z. N7-methylguanosine modification: From regulatory roles to therapeutic implications in cancer. *Am J Cancer Res*. 2023;13(5):1640-1655.

9. Du D, He J, Ju C, *et al*. When N^7-methyladenosine modification meets cancer: Emerging frontiers and promising therapeutic opportunities. *Cancer Lett*. 2023;562:216165.

doi: 10.1016/j.canlet.2023.216165

10. Wang YT, Chen RH. PML degradation fosters an immunosuppressive and pro-metastatic tumor microenvironment. *Mol Cell Oncol*. 2017;4(6):e1364212.

doi: 10.1080/23723556.2017.1364212

11. Singh S, Yeat NY, Wang YT, *et al*. PTPN23 ubiquitination by WDR4 suppresses EGFR and c-MET degradation to define a lung cancer therapeutic target. *Cell Death Dis*. 2023;14(10):671.

doi: 10.1038/s41419-023-06201-4

12. Xia P, Zhang H, Xu K, *et al*. MYC-targeted WDR4 promotes proliferation, metastasis, and sorafenib resistance by inducing CCNB1 translation in hepatocellular carcinoma. *Cell Death Dis*. 2021;12(7):691.

doi: 10.1038/s41419-021-03973-5

13. Wang YT, Chen J, Chang CW, *et al*. Ubiquitination of tumor suppressor PML regulates prometastatic and immunosuppressive tumor microenvironment. *J Clin Invest*. 2017;127(8):2982-2997.

doi: 10.1172/JCI89957

14. Huang M, Long J, Yao Z, *et al*. METTL1-Mediated m7G tRNA modification promotes lenvatinib resistance in hepatocellular carcinoma. *Cancer Res*. 2023;83(1):89-102.

doi: 10.1158/0008-5472.CAN-22-0963

15. Zhu S, Wu Y, Zhang X, *et al*. Targeting N^7-methylguanosine tRNA modification blocks hepatocellular carcinoma metastasis after insufficient radiofrequency ablation. *Mol Ther*. 2023;31(6):1596-1614.

doi: 10.1016/j.ymthe.2022.08.004

16. Dong R, Wang C, Tang B, *et al*. WDR4 promotes HCC pathogenesis through N^7-methylguanosine by regulating and interacting with METTL1. *Cell Signal*. 2024;118:111145.

doi: 10.1016/j.cellsig.2024.111145

17. Ma J, Han H, Huang Y, *et al*. METTL1/WDR4-mediated m(7)G tRNA modifications and m(7)G codon usage promote mRNA translation and lung cancer progression. *Mol Ther*. 2021;29(12):3422-3435.

doi: 10.1016/j.ymthe.2021.08.005

18. Liu Y, Jiang B, Lin C, *et al*. m7G-related gene NUDT4 as a novel biomarker promoting cancer cell proliferation in lung adenocarcinoma. *Front Oncol*. 2022;12:1055605.

doi: 10.3389/fonc.2022.1055605

19. Duan HP, Yan JH, Nie L, Wang Y, Xie H. A noval prognostic signature of the N7-methylguanosine (m7G)-related miRNA in lung adenocarcinoma. *BMC Pulm Med*. 2023;23(1):14.

doi: 10.1186/s12890-022-02290-7

20. Chen J, Li K, Chen J, *et al*. Aberrant translation regulated by METTL1/WDR4-mediated tRNA N7-methylguanosine modification drives head and neck squamous cell carcinoma progression. *Cancer Commun* (*Lond*). 2022;42(3):223-244.

doi: 10.1002/cac2.12273

21. Xu F, Cai D, Liu S, *et al*. N7-methylguanosine regulatory genes well represented by METTL1 define vastly different prognostic, immune and therapy landscapes in adrenocortical carcinoma. *Am J Cancer Res*. 2023;13(2):538-568.

22. Zhai Q, Hou Y, Ye Y, *et al*. Expression pattern and prognostic value of key regulators for N7-methylguanosine RNA modification in prostate cancer. *Acta Biochim Biophys Sin (Shanghai)*. 2023;55(4):561-573.

doi: 10.3724/abbs.2023017

23. Mei W, Jia X, Xin S, *et al*. A N^7-methylguanine-related gene signature applicable for the prognosis and microenvironment of prostate cancer. *J Oncol*. 2022;2022:8604216.

doi: 10.1155/2022/8604216

24. Han H, Yang C, Ma J, *et al*. N^7-methylguanosine tRNA modification promotes esophageal squamous cell carcinoma tumorigenesis via the RPTOR/ULK1/autophagy axis. *Nat Commun*. 2022;13(1):1478.

doi: 10.1038/s41467-022-29125-7

25. He S, Zhu J, Xiao Z, *et al*. WDR4 gene polymorphisms increase hepatoblastoma susceptibility in girls. *J Cancer*. 2022;13(12):3342-3347.

doi: 10.7150/jca.76255

26. Deng L, Hua RX, Deng C, *et al*. WDR4 gene polymorphisms and Wilms tumor susceptibility in Chinese children: A five-center case-control study. *J Cancer*. 2023;14(8):1293-1300.

doi: 10.7150/jca.83747

27. Jain BP, Pandey S. WD40 repeat proteins: Signalling scaffold with diverse functions. *Protein J*. 2018;37(5):391-406.

doi: 10.1007/s10930-018-9785-7

28. Alexandrov A, Martzen MR, Phizicky EM. Two proteins that form a complex are required for 7-methylguanosine modification of yeast tRNA. *RNA*. 2002;8(10):1253-1266.

doi: 10.1017/s1355838202024019

29. Li J, Wang L, Hahn Q, *et al*. Structural basis of regulated m^7G tRNA modification by METTL1-WDR4. *Nature*. 2023;613(7943):391-397.

doi: 10.1038/s41586-022-05566-4

30. Li R, Liu X, Deng K, Wang X. M^7G methylated core genes (METTL1 and WDR4) and associated RNA risk signatures are associated with prognosis and immune escape in HCC. *BMC Med Genomics*. 2023;16(1):179.

doi: 10.1186/s12920-023-01614-8

31. Wu PR, Chiang SY, Midence R, *et al*. Wdr4 promotes cerebellar development and locomotion through Arhgap17-mediated Rac1 activation. *Cell Death Dis*. 2023;14(1):52.

doi: 10.1038/s41419-022-05442-z

32. Patel DA, Patel SS, Patel HD. Advances in synthesis and biological evaluation of CDK2 inhibitors for cancer therapy. *Bioorg Chem*. 2024;143:107045.

doi: 10.1016/j.bioorg.2023.107045

33. Rubin SM, Sage J, Skotheim JM. Integrating old and new paradigms of G1/S control. *Mol Cell*. 2020;80(2):183-192.

doi: 10.1016/j.molcel.2020.08.020

34. Zhang H, Lin J, Yahaya BH. Comprehensive analysis of co-expressed genes with TDP-43: Prognostic and therapeutic potential in lung adenocarcinoma. *J Cancer Res Clin Oncol*. 2024;150(2):44.

doi: 10.1007/s00432-023-05554-9

35. Dong S, Alahari SK. Small molecule Mcl-1 inhibitor for triple negative breast cancer therapy. *Front Cell Dev Biol*. 2024;12:1408107.

doi: 10.3389/fcell.2024.1408107

36. Nguyen D, Osterlund E, Kale J, Andrews DW. The C-terminal sequences of Bcl-2 family proteins mediate interactions that regulate cell death. *Biochem J*. 2024;481(14):903-922.

doi: 10.1042/BCJ20210352

37. Cauwelier C, De Ridder I, Bultynck G. Recent advances in canonical versus non-canonical Ca^{2+}-signaling-related anti-apoptotic Bcl-2 functions and prospects for cancer treatment. *Biochim Biophys Acta Mol Cell Res*. 2024;1871(5):119713.

doi: 10.1016/j.bbamcr.2024.119713

38. Ummarino A, Cala N, Allavena P. Extrinsic and cell-intrinsic stress in the immune tumor micro-environment. *Int J Mol Sci*. 2024;25(22):12403.

doi: 10.3390/ijms252212403

39. Zhang Z, Su M, Jiang P, Wang X, Tong X, Wu G. Unlocking apoptotic pathways: Overcoming tumor resistance in CAR-T-cell therapy. *Cancer Med*. 2024;13(19):e70283.

doi: 10.1002/cam4.70283

40. Wang S, Liu C, Yang C, *et al*. PI3K/AKT/mTOR and PD1/CTLA4/CD28 pathways as key targets of cancer immunotherapy (review). *Oncol Lett*. 2024;28(6):567.

doi: 10.3892/ol.2024.14700

41. Peng Y, Wang Y, Zhou C, Mei W, Zeng C. PI3K/Akt/mTOR pathway and its role in cancer therapeutics: Are we making headway? *Front Oncol*. 2022;12:819128.

doi: 10.3389/fonc.2022.819128

42. Meuten TK, Dean GA, Thamm DH. Review: The PI3K-AKT-mTOR signal transduction pathway in canine cancer. *Vet Pathol*. 2024;61(3):339-356.

doi: 10.1177/03009858231207021

43. Zhang HP, Jiang RY, Zhu JY, *et al*. PI3K/AKT/mTOR signaling pathway: An important driver and therapeutic target in triple-negative breast cancer. *Breast Cancer*. 2024;31(4):539-551.

doi: 10.1007/s12282-024-01567-5

44. Leiphrakpam PD, Are C. PI3K/Akt/mTOR signaling pathway as a target for colorectal cancer treatment. *Int J Mol Sci*. 2024;25(6):3178.

doi: 10.3390/ijms25063178

45. Hao C, Wei Y, Meng W, Zhang J, Yang X. PI3K/AKT/mTOR inhibitors for hormone receptor-positive advanced breast cancer. *Cancer Treat Rev*. 2025;132:102861.

doi: 10.1016/j.ctrv.2024.102861

46. Browne IM, Okines AFC. Resistance to targeted inhibitors of the PI3K/AKT/mTOR pathway in advanced oestrogen-receptor-positive breast cancer. *Cancers* (*Basel*). 2024;16(12):2259.

doi: 10.3390/cancers16122259

47. Zhao P, Zhang X, Dong J, Li L, Meng X, Gao L. *In vitro* study of the pro-apoptotic mechanism of amino acid Schiff base copper complexes on anaplastic thyroid cancer. *Eur J Pharm Sci*. 2025;206:107005.

doi: 10.1016/j.ejps.2025.107005

48. Zhang F, Wu X, Jiao T, *et al*. Genomic characterization reveals distinct mutational landscape of acral melanoma in East Asian. *J Genet Genomics*. 2025.

doi: 10.1016/j.jgg.2024.12.018

49. You YL, Byun HJ, Chang Y, *et al*. *Euglena gracilis*-derived racilis, 24.12.018es particulate matter ($PM_{2.5}$)-induced airway inflammation by modulating nuclear factor kappa B, mitogen-activated protein kinase, and nuclear factor erythroid 2-related factor 2 signaling pathways in A549 cells and BALB/c mice. *Int J Biol Macromol*. 2025;296:139671.

doi: 10.1016/j.ijbiomac.2025.139671

50. Wu S, Nasser BSA, Ll NG, *et al*. The regulatory role of integrin in gastric cancer tumor microenvironment and drug resistance. *Prog Biophys Mol Biol*. 2025;195:130-136.

doi: 10.1016/j.pbiomolbio.2025.01.001

51. Lu Q, Tang X, Tao B, *et al*. Multifunctional hyaluronic acid microneedle patch enhances diabetic wound healing in

diabetic infections. *Int J Biol Macromol*. 2025;296:139685.

doi: 10.1016/j.ijbiomac.2025.139685

52. Liang C, Liu J, Jiang M, Zhu Y, Dong P. The advancement of targeted regulation of hepatic stellate cells using Traditional Chinese medicine for the treatment of liver fibrosis. *J Ethnopharmacol*. 2025;341:119298.

doi: 10.1016/j.jep.2024.119298

53. Wang Y, Xiong G, Cai W, Tao Q. METTL1 facilitates ameloblastoma invasive growth via MAPK signaling pathway. *Gene*. 2024;905:148234.

doi: 10.1016/j.gene.2024.148234

54. Wang M, Zheng Y, Hao Q, *et al*. Hypoxic BMSC-derived exosomal miR-210-3p promotes progression of triple-negative breast cancer cells via NFIX-Wnt/beta-catenin signaling axis. *J Transl Med*. 2025;23(1):39.

doi: 10.1186/s12967-024-05947-5

55. Utpal BK, Roy SC, Zehravi M, *et al*. Polyphenols as Wnt/M, i M, -5pathway modulators: A promising strategy in clinical neurodegeneration. *Anim Model Exp Med*. 2025.

doi: 10.1002/ame2.12525

56. Singhai H, Raikwar S, Rathee S, Jain SK. Emerging combinatorial drug delivery strategies for breast cancer: A comprehensive review. *Curr Drug Targets*. 2025.

doi: 10.2174/0113894501352081241211090911

57. Ye TT, Chen WH, Pei J, Jia YX, Wu HY. Expression and clinical significance of NEK2 and EMT related molecules in oral squamous cell carcinoma. *Shanghai Kou Qiang Yi Xue*. 2023;32(6):640-644.

doi: 10.19439/j.sjos.2023.06.014

58. Ye F, Xie L, Liang L, *et al*. Mechanisms and therapeutic strategies to combat the recurrence and progression of hepatocellular carcinoma after thermal ablation. *J Interv Med*. 2023;6(4):160-169.

doi: 10.1016/j.jimed.2023.10.004

59. Yang HW, Chun-Yu Ho D, Liao HY, *et al*. Resveratrol inhibits arecoline-induced fibrotic properties of buccal mucosal fibroblasts via miR-200a activation. *J Dent Sci*. 2024;19(2):1028-1035.

doi: 10.1016/j.jds.2023.06.027

60. Wang R, Zhu F, Gao G, *et al*. B-cell specific Moloney murine leukemia virus insertion site 1 contributes to invasion, metastasis, and poor prognosis in salivary adenoid cystic carcinoma. *J Dent Sci*. 2024;19(1):21-31.

doi: 10.1016/j.jds.2023.06.014

61. Poryazova E, Serteva D, Markov D, Chonov V, Markov G. Expression of snail and twist compared with clinical and pathological parameters in patients with gastric cancer. *Folia Med (Plovdiv)*. 2023;65(3):393-398.

doi: 10.3897/folmed.65.e84132

62. Pek JH, Quah LJJ, Teng KPD, Yeo YWM, Lee CYJ. Developing the disaster medical responderndecourse in Singapore. *Western Pac Surveill Response J*. 2023;14(6 Spec edition):1-6.

doi: 10.5365/wpsar.2023.14.6.1009

63. Chen B, Jiang W, Huang Y, *et al*. N^7-methylguanosine tRNA modification promotes tumorigenesis and chemoresistance through WNT/ters in patients with gastric cancer. noma. cin*Oncogene*. 2022;41(15):2239-2253.

doi: 10.1038/s41388-022-02250-9

64. Sabbah DA, Hajjo R, Sweidan K. Review on epidermal growth factor receptor (EGFR) structure, signaling pathways, interactions, and recent updates of EGFR inhibitors. *Curr Top Med Chem*. 2020;20(10):815-834.

doi: 10.2174/1568026620666200303123102

65. Talukdar S, Emdad L, Das SK, Fisher PB. EGFR: An essential receptor tyrosine kinase-regulator of cancer stem cells. *Adv Cancer Res*. 2020;147:161-188.

doi: 10.1016/bs.acr.2020.04.003

66. Singh D, Attri BK, Gill RK, Bariwal J. Review on EGFR inhibitors: Critical updates. *Mini Rev Med Chem*. 2016;16(14):1134-1166.

doi: 10.2174/1389557516666160321114917

67. Al-Salama ZT, Syed YY, Scott LJ. Lenvatinib: A review in hepatocellular carcinoma. *Drugs*. 2019;79(6):665-674.

doi: 10.1007/s40265-019-01116-x

68. Ying X, Liu B, Yuan Z, *et al*. METTL1-m^7 G-EGFR/EFEMP1 axis promotes the bladder cancer development. *Clin Transl Med*. 2021;11(12):e675.

doi: 10.1002/ctm2.675

69. Nai F, Flores Espinoza MP, Invernizzi A, *et al*. Small-Molecule Inhibitors of the m7G-RNA Writer METTL1. *ACS Bio Med Chem Au*. 2024;4(2):100-110.

doi: 10.1021/acsbiomedchemau.3c00030

70. Zhao W. Ling-Ling Chen: RNA has its own features; don't study it as a protein. *Natl Sci Rev*. 2024;11(2):nwad287.

doi: 10.1093/nsr/nwad287

ACCSCIENCE PUBLISHING

Tumor Discovery

ORIGINAL RESEARCH ARTICLE

Systemic drug repurposing for pancreatic cancer based on genetic and epigenetic network analysis using a systems biology approach and deep neural learning of drug-target interactions

Yi-Hsin Tsai and Bor-Sen Chen*

Laboratory of Automatic Control, Signal Processing and Systems Biology, Department of Electrical Engineering, Institute of Electronic Engineering, National Tsing Hua University, Hsinchu, Taiwan, China

Abstract

Pancreatic cancer is a malignant tumor associated with a high mortality rate. This research presents a systems biology approach to explore the mechanisms of pancreatic ductal adenocarcinoma (PDAC), aiming to identify significant biomarkers that can serve as drug targets. We propose a systematic drug repurposing strategy that incorporates a deep neural network (DNN)-based drug-target interaction (DTI) model along with drug design specifications to develop a potential multi-molecule drug for PDAC treatment. We first established candidate protein-protein interaction networks and gene regulatory networks using big data mining techniques. Real PDAC and non-PDAC genome-wide genetic and epigenetic networks (GWGENs) were systematically identified using their corresponding microarray data through system identification and system order detection methods. The top 6,000 core GWGENs of PDAC and non-PDAC were extracted using the Principal Network Projection method. Subsequently, we annotated the core GWGENs using the Kyoto Encyclopedia of Genes and Genomes pathways to construct their respective core signaling pathways. By comparing upstream microenvironmental factors, core signaling pathways, and downstream aberrant cellular functions between PDAC and non-PDAC, we investigated the carcinogenic mechanisms of PDAC. Notably, c-MYC, forkhead box O3, and tumor suppressor p53 were identified as significant biomarkers for potential drug targets. Furthermore, the DNN-based DTI model predicted the interaction probabilities between candidate molecular drugs and these biomarkers. Based on drug design specifications such as regulatory ability, sensitivity, and toxicity, suitable multi-molecular potential drugs were selected. Ultimately, gemcitabine and MK-2206 were identified as a promising multi-molecular drug combination for PDAC treatment.

Keywords: Pancreatic cancer mechanisms; Systems biology; Big data mining; Genome-wide genetic and epigenetic networks; Kyoto Encyclopedia of Genes and Genomes pathways; Deep neural network-based drug-target interaction model; Drug design specifications; Principal network projection

***Corresponding author:**
Bor-Sen Chen
(bschen@ee.nthu.edu.tw)

Citation: Tsai Y, Chen B. Systemic drug repurposing for pancreatic cancer based on genetic and epigenetic network analysis using a systems biology approach and deep neural learning of drug-target interactions. *Tumor Discov*. 2025;4(1):47-67.
doi: 10.36922/td.4709

Received: August 30, 2024

Revised: October 8, 2024

Accepted: October 24, 2024

Published online: November 20, 2024

1. Introduction

Pancreatic ductal adenocarcinoma (PDAC), often referred to as the "king of cancers," is the most common type of pancreatic cancer.[1] It is primarily characterized by a lack of significant symptoms in its early stages, making timely diagnosis challenging. Even when symptoms do emerge, they are frequently mistaken for other health conditions, typically indicating an advanced stage of the disease. Scholars predict that by 2030, pancreatic cancer will become the second leading cause of cancer-related deaths,[2] resulting in an estimated 46,000 deaths annually by 2040.[3] Despite numerous technological advancements in cancer treatment, the 5-year survival rate for PDAC patients remains only 12.2%.[4] A major contributing factor to this low survival rate is that pancreatic cancer is often diagnosed at an advanced stage, which severely limits the opportunities for surgical intervention. Compared to other cancers, pancreatic cancer has a relatively high mortality rate, influenced by various factors such as geographic region,[5] case numbers, and medical standards. The overall survival rate for PDCA is relatively low, primarily because tumors are often diagnosed at advanced stages and due to factors such as tumor location, size, and metastasis that affect treatment efficacy. Specific survival rate data may vary by region and treatment modality, reflecting the varying prevalence of pancreatic cancer across different populations. This variability is also influenced by various risk factors, including smoking, high-fat diets, obesity, and genetic factors.[6] Therefore, there is a pressing global need for enhanced preventive measures and genetic diagnostics to address this significant health challenge.[7]

The carcinogenic mechanisms underlying PDAC involve multiple gene mutations, abnormalities in signaling pathways, and the influence of the tumor microenvironment. Common gene mutations in PDAC include *KRAS*, *CDKN2A*, *TP53*, and *SMAD4*.[8] These mutations disrupt signaling pathways, leading to uncontrolled cell proliferation, inhibition of apoptosis, and promotion of tumor growth and metastasis.

Current treatment options for pancreatic cancer include surgical resection, radiation therapy, chemotherapy, immunotherapy, and targeted drugs. However, not all patients are suitable for surgery.[9] Common chemotherapy regimens often fail due to drug resistance, resulting from complex interactions among pancreatic cells, cancer cells, and the tumor microenvironment.[10] Consequently, clinical outcomes remain poor, and effective treatment methods are still lacking. Moreover, drug development typically takes at least 10 years and requires substantial funding.[11] Biopharmaceutical companies must invest heavily in research to identify drug targets, assess efficacy, consider side effects, and conduct extensive preclinical and clinical trials. Given the high failure rate in clinical trials,[12] there is a need for a more efficient drug development system. Recent advancements in deep learning have shown promise in drug discovery, with neural network methods being applied to predict drug-target interactions (DTI).[13-16] DTI data from various databases can help elucidate the relationships between drugs and their targets.[13,14] By framing drug and target features as a binary classification problem, DTI models based on deep neural networks (DNNs) can predict the interactions between drugs and targets (biomarkers), thereby identifying candidate multi-molecular drugs for specific diseases.[15,16] This approach, known as drug repurposing, utilizes existing drugs for new therapeutic purposes, potentially expediting the progression to preclinical and clinical trials.[17]

Before employing the DNN-based DTI model to predict potential multi-molecular drugs for PDAC biomarkers, we adopted a systems biology approach using whole-genome microarray data from PDAC and health controls to study their genome-wide genetic and epigenetic networks (GWGENs) for investigating the carcinogenic mechanisms of PDAC. The first step involved mining large databases to establish candidate GWGENs. Next, using system identification and systematic order detection techniques on the corresponding genome-wide microarray data of PDAC and healthy controls to eliminate false positive interactions and regulations, we obtained real GWGENs for PDAC and healthy controls. Given that the Kyoto Encyclopedia of Genes and Genomes (KEGG) pathway annotations currently encompass only up to 6,000 nodes of GWGENs, the principal network projection (PNP) method was employed to individually extract the top 6,000 important nodes as core GWGENs from the real GWGENs of both PDAC and healthy controls. Then, we annotated the real GWGENs using KEGG pathways to construct core signaling pathways for both PDAC and healthy controls. By comparing the similarities and differences between the core signaling pathways of PDAC and healthy controls, along with their downstream cellular functional abnormalities, we investigated the carcinogenic mechanisms of PDAC and identified significant biomarkers, including c-MYC, forkhead box O3 (FOXO3), and tumor suppressor p53 (TP53), as potential drug targets. Finally, we combined the features of selected biomarkers with those of molecular drugs to train the DNN-based DTI model, predicting the probability of interaction between candidate molecular drugs and the identified drug targets (biomarkers). Based on drug design specifications, such as regulatory capacity, sensitivity, and toxicity, we identified potential drugs, ultimately selecting the combination of MK-2206 and gemcitabine as a promising multi-molecular drug approach to target key biomarkers for PDAC treatment.

2. Materials and methods

2.1. Overview of PDAC and healthy control genome-wide genetic and epigenetic networks using systems biology approach

In this study, we aim to establish the GWGENs of PDAC and non-PDAC core genomes. Microarray data for PDAC and non-PDAC were obtained from the National Center for Biotechnology Information (NCBI) under accession number GSE183795. Four processes were then conducted to identify the core signaling pathways of candidate GWGENs, as illustrated in Figure 1 and detailed below.

i. Construction of candidate GWGENs: We utilized a data mining approach to construct Boolean matrices representing candidate protein-protein interaction networks (PPINs) and candidate gene regulatory networks (GRNs), which include interactions among proteins, and regulation among genes, microRNAs (miRNAs), and long non-coding RNAs (lncRNAs). Specifically, if an interaction or regulation exists between two nodes, it is denoted as 1; if not, it is denoted as 0.
ii. Identification of real GWGENs: We employed PDAC and non-PDAC (control) microarray data to construct real GWGENs, identifying parameters for protein-protein interaction (PPI) models and GRN regulatory models by solving constrained linear least squares parameter estimation problems. To address potential false positive interactions in candidate GWGEN, we pruned these false positives using the Akaike Information Criterion (AIC) system order identification method, obtaining real GWGENs for PDAC and non-PDAC.
iii. Extraction of core GWGENs: We applied the PNP method to extract core GWGENs from the real GWGENs. The PNP method calculates the projection value of each node in the real GWGEN to capture 85% of the network's energy, sorting the projection values of all nodes from highest to lowest. Given the maximum allowable annotated node count of 6,000 (as per KEGG pathways), we selected the top 6,000 significant nodes to form the core GWGEN.
iv. Construction and comparison of core signaling pathways: We annotated the KEGG pathways of PDAC and non-PDAC of core GWGENs based on relevant literature, completing the construction of core signaling pathways for each. We then compared the upstream microenvironmental factors, core signaling pathways, and corresponding downstream aberrant cellular functions between PDAC and non-PDAC to explore the oncogenic molecular mechanisms of PDAC and identify potential biomarkers as drug targets for PDAC therapeutics.

2.2. Constructing candidate genome-wide genetic and epigenetic networks for PDAC and healthy controls based on big data mining

In this research, we obtained microarray data from the NCBI under accession number GSE183795. The dataset was divided into two groups: the disease group, comprising 139 PDAC samples, and the healthy control group, consisting of 105 non-PDAC samples.

The candidate GWGENs include candidate PPINs and candidate GRNs. We represented the candidate GWGEN using a binary Boolean matrix, where a value of 1 is assigned if an interaction or regulation exists for a node, and 0 if it does not. To construct the candidate PPINs, we consulted various databases, including the Database of Interacting Proteins (DIP),[18] IntAct,[19] the Biological General Repository for Interaction Datasets (BioGRID),[20] and the Molecular INTeraction Database (MINT).[21] For the candidate GRNs, we utilized multiple resources such as the Human Transcriptional Regulation Interaction Database (HTRIdb),[22] the integrated transcription factor platform (ITFP),[23] TRANSFAC,[24] CircuitDB,[25] TargetScanHuman,[26] and StarBase.[27]

2.3. Establishing a system model for identifying real genome-wide genetic and epigenetic networks for PDAC and healthy controls based on candidate genome-wide genetic and epigenetic networks

To investigate the oncogenic molecular mechanisms of PDAC, we referenced relevant databases and utilized PDAC microarray data to construct candidate GWGENs.[28] Following the establishment of these candidate GWGENs, we employed PDAC microarray data to discern the real GWGENs for PDAC and non-PDAC samples. This process required the development of a stochastic system model to enable candidate GWGENs to capture stochastic interactions and regulations, such as protein-protein interactions, as well as the regulation of transcription factors (TFs), miRNAs, and lncRNA. Additionally, the stochastic model should account for residuals from the initial model establishment and stochastic noise resulting from experimental measurements. Furthermore, the main protein interaction model in Equation I and the miRNA regulation models in Equations II–IV were designed as bilinear interaction models based on the product of the concentrations of the interacting proteins in Equation I or the regulations of miRNAs on their target mRNAs, miRNAs or lncRNAs in Equations II–IV. However, for simplification, we presented the interaction and regulation coefficients as linear in PPINs and GRNs.[28]

First, we established a system model of the interactions involving the w-th protein and other proteins in the candidate PPINs, presented as follows:

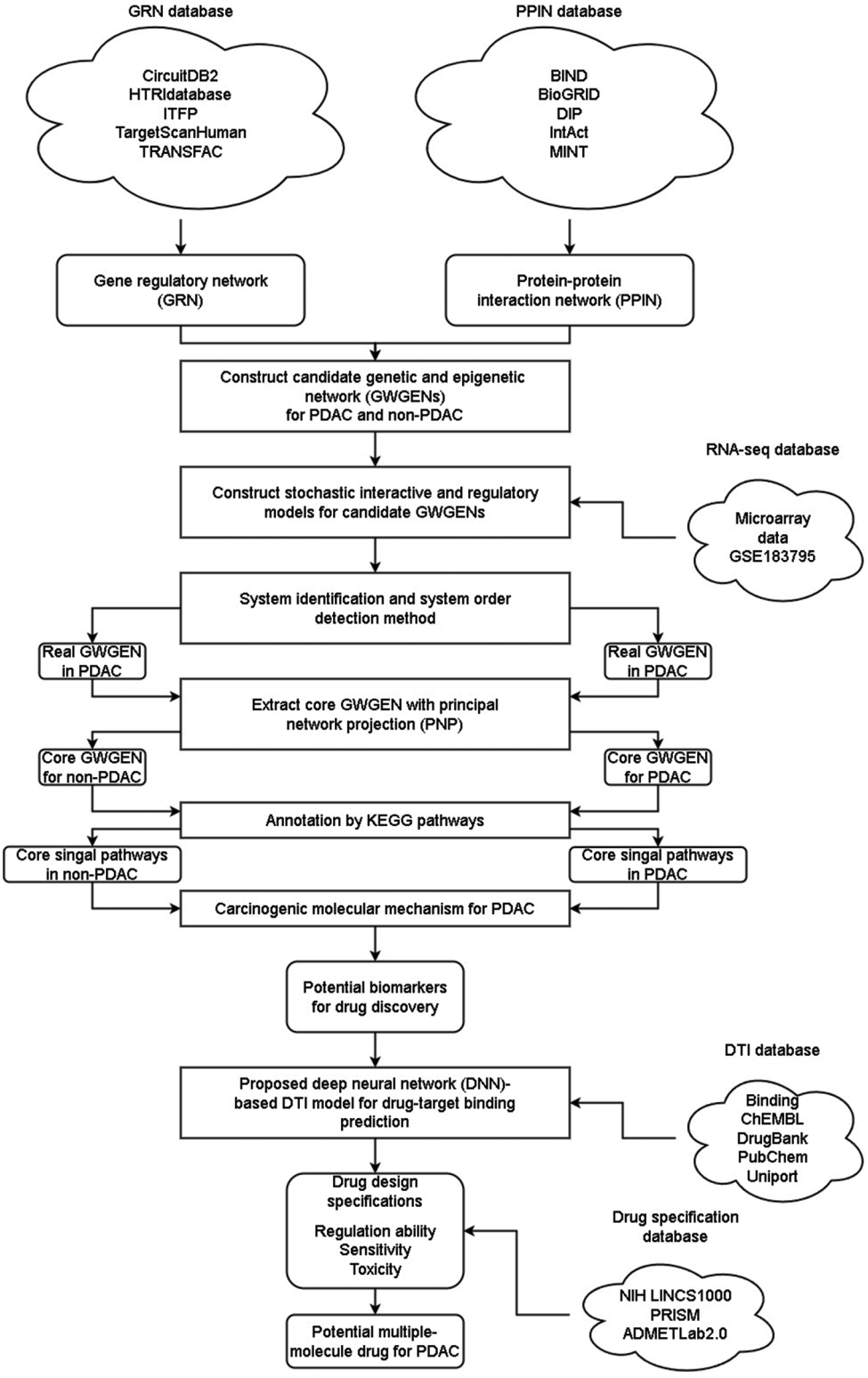

Figure 1. Flowchart of the systems biology approach to investigate the carcinogenic molecular mechanisms and systematic drug design for PDAC
Abbreviations: BioGRID: Biological General Repository for Interaction Datasets; DIP: Database of Interacting Proteins; DTI: Drug-target interaction; HTRI: Human Transcriptional Regulation Interaction; ITFP: Integrated Transcription Factor Platform; KEGG: Kyoto Encyclopedia of Genes and Genomes; MINT: Molecular INTeraction Database; PDAC: Pancreatic ductal adenocarcinoma; PRISM: Pharmaceutical Regulatory Information System.

$$p_w[n] = \sum_{r=1}^{R_w} \pi_{w-r} p_w[n] p_r[n] + \beta_{w-PPIN} + \delta_{w-PPIN}[n] \quad \text{(I)}$$

for w = 1,2…,W-1,W，n = 1,2…,N-1,N

among which p_w [n] and p_r [n] denote the expression levels of the w-th protein and the r-th protein in the n-th sample, respectively; π_{w_r} represents the interaction ability between the r-th protein and the w-th protein; R_w is the total number of proteins interacting with the w-th protein; W denotes the total number of proteins in the candidate PPIN; N is the number of data samples (PDAC or non-PDAC); β_{w_PPIN} indicates the basal expression level of the w-th protein, reflecting changes due to interactions such as acetylation, phosphorylation, or unknown histone modifications that cannot be modeled in (1); δ_{w_PPIN} [n] accounts for random noise affecting the w-th protein in the n-th sample due to modeling residuals, experimental measurement errors, or environmental interference.

After establishing the PPI system model, we also developed a regulatory system model to describe the relationships between genes and their regulators, including TFs, miRNAs, and lncRNAs. The transcriptional regulation system model for the x-th gene in the n-th sample can be expressed as:[28]

$$g_x[n] = \sum_{s=1}^{S_x} \alpha_{x-s} t_s[n] + \sum_{u=1}^{U_x} \gamma_{x-u} l_u[n] - \sum_{v=1}^{V_x} \varepsilon_{x-v} m_v[n] g_x[n] + \beta_x + \delta_x[n] \quad \text{(II)}$$

for x = 1,2…,X-1,X, n = 1,2…,N-1,N

where g_x [n] indicates the expression level of the x-th gene in the n-th sample; S_x, U_x, and V_x represent the total number of TFs, lncRNAs, and miRNAs binding to the x-th gene, respectively; t_s [n], l_n [n], and m_v [n] denote the expression levels of the s-th TF, the u-th lncRNA, and the v-th miRNA in the n-th sample, respectively; α_{x_s} symbolizes the transcriptional regulatory ability of the s-th TF on the x-th gene; γ_{x_u} signifies the transcriptional regulatory ability of the u-th lncRNA on the x-th gene; $\varepsilon_{x\_y} > 0$ indicates the post-transcriptional regulatory ability of the v-th miRNA in degrading the x-th gene's miRNA; X is the total number of genes in the candidate GWGEN; N is the number of data samples (PDAC or non-PDAC); β_x represents the basal expression level of the x-th gene, influenced by modifications such as methylation, phosphorylation, acetylation, or unknown gene regulatory effects; δ_x [n] accounts for the random noise affecting the x-th gene in the n-th sample due to modeling residuals and measurement errors.

Next, we established the regulatory system model for lncRNA. The transcriptional regulation system model for the y-th lncRNA in the n-th sample is described as:

$$l_y[n] = \sum_{s=1}^{S_y} \zeta_{y-s} t_s[n] + \sum_{u=1}^{U_y} \psi_{y-u} l_u[n] - \sum_{v=1}^{V_y} \kappa_{y-v} m_v[n] l_y[n] + \beta_y + \delta_y[n] \quad \text{(III)}$$

for y = 1,2…,Y-1,Y, n = 1,2…,N-1,N

where l_y [n] indicates the expression level of the y-th lncRNA in the n-th sample; S_y, U_y, and V_y represent the total numbers of TFs, lncRNAs, and miRNAs binding to the y-th lncRNA, respectively; t_s [n], l_u [n], and m_v [n] denote the expression levels of the s-th TF, the u-th lncRNA, and the v-th miRNA in the n-th sample, respectively; ζ_{y_s} symbolizes the transcriptional regulatory ability of the s-th TF on the y-th lncRNA; ψ_{y_u} signifies the transcriptional regulatory ability of the u-th lncRNA on the y-th lncRNA; $k_{y\_v} > 0$ represents the post-transcriptional regulatory ability of the v-th miRNA in degrading the y-th lncRNA's miRNA; Y is the total number of lncRNAs in the candidate GWGEN; N is the number of data samples (PDAC or non-PDAC); β_y reflects the expression basal level of the y-th lncRNA, influenced by modifications such as phosphorylation, acetylation, or unknown gene regulatory effects; δ_y [n] captures the random noise affecting the y-th lncRNA in the n-th sample due to modeling residuals and measurement errors.

Finally, we established the miRNA regulatory system model in a similar manner. The transcriptional regulation system model for the z-th miRNA in the n-th sample can be described by the following equation:

$$m_z[n] = \sum_{s=1}^{S_z} \lambda_{z-s} t_s[n] + \sum_{u=1}^{U_z} \mu_{z-u} l_u[n] - \sum_{v=1}^{V_z} \rho_{z-v} m_v[n] m_z[n] + \beta_z + \delta_z[n] \quad \text{(IV)}$$

for z = 1,2…,Z-1,Z, n = 1,2…,N-1,N

where m_z [n] represents the expression level of the z-th miRNA in the n-th sample; S_z, U_z, and V_z indicate the total number of TFs, lncRNAs, and miRNAs binding to the z-th miRNA, respectively; t_s [n], l_u [n], and m_v [n] denote the expression levels of the s-th TF, the u-th lncRNA, and the v-th miRNA in the n-th sample, respectively; λ_{z_s} symbolizes the transcriptional regulatory ability of the s-th TF on the z-th miRNA; μ_{z_u} signifies the transcriptional regulatory ability of the u-th lncRNA on the z-th miRNA; $\rho_{z\_v} > 0$ represents the post-transcriptional regulatory ability of the v-th miRNA in degrading the z-th miRNA's miRNA; Z is the total number of miRNAs in the candidate GWGEN; N is the number of data samples (PDAC or non-PDAC); β_z indicates the change in the expression of the z-th miRNA due to phosphorylation, acetylation, or unknown gene regulatory effects; δ_z [n] accounts for the random noise affecting the z-th miRNA in the n-th sample due to model residuals and experimental measurement errors.

2.4. Elimination of false positives from candidate genome-wide genetic and epigenetic networks for real genome-wide genetic and epigenetic networks of PDAC and healthy controls based on system identification and order detection methods

Based on the stochastic system models of protein interaction and gene regulations described above, we constructed four interaction and regulation models for candidate GWGENs, including the candidate PPI model, candidate gene regulation model, candidate lncRNA regulation model, and candidate miRNA regulation model in Equations I–IV. Next, we pruned false positive interactions and regulations, from these candidate GWGENs using system identification and order detection methods, utilizing microarray data from both PDAC and non-PDAC samples to estimate the corresponding real GWGENs.

Equations I–IV can be reformulated as the following linear regression equations to obtain parameter vectors for interactions and gene regulations.

$$p_w[n]=\left[p_w[n]p_1[n]p_w[n]p_2[n]\cdots p_w[n]p_{R_w}[n]1\right]\times\begin{bmatrix}\pi_{w-1}\\ \pi_{w-2}\\ \vdots\\ \pi_{w-R_w}\\ \beta_{w-PPIN}\end{bmatrix}+\delta_{w-PPIN}[n]=\boldsymbol{\phi}_w[n]\cdot\theta_w+\delta_{w-PPIN}[n] \quad (V)$$

for w =1,2…,W-1,W, n = 1,2…,N-1,N

$$g_x[n]=\begin{bmatrix}t_1[n]\cdots t_{S_x}[n]\,l_1[n]\\ \cdots l_{U_x}[n]\,m_1[n]g_x[n]\cdots\\ m_{V_x}[n]g_x[n]1\end{bmatrix}\times\begin{bmatrix}\alpha_{x-1}\\ \vdots\\ \alpha_{x-S_x}\\ \gamma_{x-1}\\ \vdots\\ \gamma_{x-U_x}\\ -\varepsilon_{x-1}\\ \vdots\\ -\varepsilon_{x-V_x}\\ \beta_x\end{bmatrix}+\delta_x[n]=\phi_x[n]\cdot\theta_x+\delta_x[n] \quad (VI)$$

for x = 1,2…,X-1,X, n = 1,2…,N-1,N

$$l_y[n]=\begin{bmatrix}t_1[n]\cdots t_{S_y}[n]\,l_1[n]\cdots l_{U_y}\\ [n]\,m_1[n]\,l_y[n]\cdots\\ m_{V_y}[n]l_y[n]\,1\end{bmatrix}\times\begin{bmatrix}\zeta_{y-1}\\ \vdots\\ \zeta_{y-S_y}\\ \psi_{y-1}\\ \vdots\\ \psi_{y-U_y}\\ -\kappa_{y-1}\\ \vdots\\ -\kappa_{y-V_y}\\ \beta_y\end{bmatrix}+\delta_y[n]=\phi_y[n]\cdot\theta_y+\delta_y[n] \quad (VII)$$

for y =1,2…,Y-1,Y, n = 1,2…,N-1,N

$$m_z[n]=\begin{bmatrix}t_1[n]\cdots t_{S_z}[n]\,l_1[n]\cdots l_{U_z}\\ [n]\,m_1[n]\,m_z[n]\cdots\\ m_{V_z}[n]\,m_z[n]\,1\end{bmatrix}\times\begin{bmatrix}\lambda_{z-1}\\ \vdots\\ \lambda_{z-S_z}\\ \mu_{z-1}\\ \vdots\\ \mu_{z-U_z}\\ -\rho_{z-1}\\ \vdots\\ -\rho_{z-V_z}\\ \beta_z\end{bmatrix}+\delta_z[n]=\phi_z[n]\cdot\theta_z+\delta_z[n] \quad (VIII)$$

for z =1,2…,Z-1,Z, n = 1,2…,N-1,N

Next, with N representing microarray data samples, we can express these as linear Equations V–VIII:

$$\begin{bmatrix} p_w[1] \\ p_w[2] \\ \vdots \\ p_w[N] \end{bmatrix} = \begin{bmatrix} \phi_w[1] \\ \phi_w[2] \\ \vdots \\ \phi_w[N] \end{bmatrix} \theta_w + \begin{bmatrix} \delta_w[1] \\ \delta_w[2] \\ \vdots \\ \delta_w[N] \end{bmatrix} \quad \text{(IX)}$$

for w =1,2…,W-1,W, n = 1,2…,N-1,N

$$\begin{bmatrix} g_x[1] \\ g_x[2] \\ \vdots \\ g_x[N] \end{bmatrix} = \begin{bmatrix} \phi_x[1] \\ \phi_x[2] \\ \vdots \\ \phi_x[N] \end{bmatrix} \theta_x + \begin{bmatrix} \delta_x[1] \\ \delta_x[2] \\ \vdots \\ \delta_x[N] \end{bmatrix} \quad \text{X)}$$

for x = 1,2…,X-1,X, n = 1,2…,N-1,N

$$\begin{bmatrix} l_y[1] \\ l_y[2] \\ \vdots \\ l_y[N] \end{bmatrix} = \begin{bmatrix} \phi_y[1] \\ \phi_y[2] \\ \vdots \\ \phi_y[N] \end{bmatrix} \theta_y + \begin{bmatrix} \delta_y[1] \\ \delta_y[2] \\ \vdots \\ \delta_y[N] \end{bmatrix} \quad \text{(XI)}$$

for y =1,2…,Y-1,Y, n = 1,2…,N-1,N

$$\begin{bmatrix} m_z[1] \\ m_z[2] \\ \vdots \\ m_z[N] \end{bmatrix} = \begin{bmatrix} \phi_z[1] \\ \phi_z[2] \\ \vdots \\ \phi_z[N] \end{bmatrix} \theta_z + \begin{bmatrix} \delta_z[1] \\ \delta_z[2] \\ \vdots \\ \delta_z[N] \end{bmatrix} \quad \text{(XII)}$$

for z = 1,2…,Z-1,Z, n = 1,2…,N-1,N

Further Equations IX–XII can be represented by the following algebraic equations individually:

$$P_w = \Phi_w \cdot \Theta_w + \Delta_w \ \ for\ w = 1,2\ldots,W-1,W \quad \text{(XIII)}$$

$$G_x = \Phi_x \cdot \Theta_x + \Delta_x \ \ for\ x = 1,2\ldots,X-1,X \quad \text{(XIV)}$$

$$L_y = \Phi_y \cdot \Theta_y + \Delta_y \ \ for\ y = 1,2\ldots,Y-1,Y \quad \text{(XV)}$$

$$M_z = \Phi_z \cdot \Theta_z + \Delta_z \ \ for\ z = 1,2\ldots,Z-1,Z \quad \text{(XVI)}$$

where Φ_w is the linear regression matrix for proteins, Φ_x is the linear regression matrix for genes, Φ_y is the linear regression matrix for lncRNAs, and Φ_z is the linear regression matrix for miRNAs.

Next, we employed a constrained linear least-squares parameter estimation method to estimate parameter vectors Φ_w, Φ_x, Φ_y and Φ_z. Specifically, we imposed constraints to ensure that the degrading effects of miRNAs on post-transcriptional genes, lncRNAs, and miRNAs are negative. The parameter estimation problem for the GWGENs of PDAC and non-PDAC can be solved by the following constrained least-squares parameter estimation problem equations:

$$\hat{\Theta}_w = \underset{\Theta_w}{\operatorname{argmin}} \frac{1}{2} \Phi_w \cdot \Theta_w - P_{w2}^2 \quad \text{(XVII)}$$

$$\hat{\Theta}_x = \underset{\Theta_x}{\operatorname{argmin}} \frac{1}{2} \Phi_x \cdot \Theta_x - G_{x2}^2 \quad \text{(XVIII)}$$

$$subject\ to \left[\begin{array}{ccc|ccc|ccc|c} 0 & \cdots & 0 & 0 & \cdots & 0 & 1 & \cdots & 0 & 0 \\ \vdots & \ddots & \vdots & \vdots & \ddots & \vdots & \vdots & \ddots & \vdots & \vdots \\ 0 & \cdots & 0 & 0 & \cdots & 0 & 0 & \cdots & 1 & 0 \\ \multicolumn{3}{c|}{\underbrace{\qquad\qquad}_{S_x}} & \multicolumn{3}{c|}{\underbrace{\qquad\qquad}_{U_x}} & \multicolumn{3}{c|}{\underbrace{\qquad\qquad}_{V_x}} & \end{array}\right] \cdot \Theta_x \le \begin{bmatrix} 0 \\ \vdots \\ 0 \end{bmatrix}$$

$$\hat{\Theta}_y = \underset{\Theta_y}{\operatorname{argmin}} \frac{1}{2} \Phi_y \cdot \Theta_y - L_{y2}^2 \quad \text{(XIX)}$$

$$subject\ to \left[\begin{array}{ccc|ccc|ccc|c} 0 & \cdots & 0 & 0 & \cdots & 0 & 1 & \cdots & 0 & 0 \\ \vdots & \ddots & \vdots & \vdots & \ddots & \vdots & \vdots & \ddots & \vdots & \vdots \\ 0 & \cdots & 0 & 0 & \cdots & 0 & 0 & \cdots & 1 & 0 \\ \multicolumn{3}{c|}{\underbrace{\qquad\qquad}_{S_y}} & \multicolumn{3}{c|}{\underbrace{\qquad\qquad}_{U_y}} & \multicolumn{3}{c|}{\underbrace{\qquad\qquad}_{V_y}} & \end{array}\right] \cdot \Theta_y \le \begin{bmatrix} 0 \\ \vdots \\ 0 \end{bmatrix}$$

$$\hat{\Theta}_z = \underset{\Theta_z}{\operatorname{argmin}} \frac{1}{2} \Phi_z \cdot \Theta_z - M_{z2}^2 \quad \text{(XX)}$$

$$subject\ to \left[\begin{array}{ccc|ccc|ccc|c} 0 & \cdots & 0 & 0 & \cdots & 0 & 1 & \cdots & 0 & 0 \\ \vdots & \ddots & \vdots & \vdots & \ddots & \vdots & \vdots & \ddots & \vdots & \vdots \\ 0 & \cdots & 0 & 0 & \cdots & 0 & 0 & \cdots & 1 & 0 \\ \multicolumn{3}{c|}{\underbrace{\qquad\qquad}_{S_z}} & \multicolumn{3}{c|}{\underbrace{\qquad\qquad}_{U_z}} & \multicolumn{3}{c|}{\underbrace{\qquad\qquad}_{V_z}} & \end{array}\right] \cdot \Theta_z \le \begin{bmatrix} 0 \\ \vdots \\ 0 \end{bmatrix}$$

Given that the regulatory effects of miRNAs on post-transcriptional genes, lncRNAs, and other miRNAs must be negative, we utilized the MATLAB Optimization Toolbox to solve the constrained least-squares parameter estimation problems with their added constraints in Equations XVII–XX. This approach allowed us to derive optimal estimated parameter vectors for PPIs, as well as for gene, lncRNA, and miRNA regulations within the GWGENs for both PDAC and non-PDAC.

To address the issue of numerous false positive interactions identified among the candidate GWGENs, we

employed the systematic order detection method using the AIC to prune these inaccuracies and derive real GWGENs for both PDAC and non-PDAC.[29]

The system order detection scheme, based on the AIC method, estimates the number of interactions among proteins and the number of regulations involving genes, lncRNAs, and miRNAs within the candidate GWGENs as follows:

$$AIC\left(R_w\right)=\log\left(\Omega_w^2\right)+\frac{2\left(1+R_w\right)}{N} \quad \text{(XXI)}$$

$$\text{where } \Omega_w^2=\sqrt[2]{\frac{\left(\Phi_w\cdot\hat{\Theta}_w-P_w\right)^T\left(\Phi_w\cdot\hat{\Theta}_w-P_w\right)}{N}}$$

where the parameter vector $\hat{\Theta}_w$ can be obtained from Equation (XVII) using the least-squares method. Ω_w represents the residual estimation of the w-th protein model, and R_w is the number of interactions (i.e., the model's complexity) with the w-th protein.

$$AIC\left(S_x,U_x,V_x\right)=\log\left(\Omega_x^2\right)+\frac{2\left(S_x+U_x+V_x+1\right)}{N} \quad \text{(XXII)}$$

$$\textit{where } \Omega_x^2=\sqrt[2]{\frac{\left(\Phi_x\cdot\hat{\Theta}_x-G_x\right)^T\left(\Phi_x\cdot\hat{\Theta}_x-G_x\right)}{N}}$$

where the parameter vector $\hat{\Theta}_x$ can be obtained from Equation (XVIII) using the least-squares method. Ω_x represents the residual estimation of the x-th gene model, while S_x, U_x, and V_x represent the number of gene, lncRNA, and miRNA regulations acting on the x-th gene, respectively.

$$AIC\left(S_y,U_y,V_y\right)=\log\left(\Omega_y^2\right)+\frac{2\left(S_y+U_y+V_y+1\right)}{N} \quad \text{(XXIII)}$$

$$\textit{with } \Omega_y^2=\sqrt[2]{\frac{\left(\Phi_y\cdot\hat{\Theta}_y-L_y\right)^T\left(\Phi_y\cdot\hat{\Theta}_y-L_y\right)}{N}}$$

where the parameter vector $\hat{\Theta}_y$ can be obtained from Equation (XIX) using the least-squares method. Ω_y represents the residual estimation of the y-th lncRNA model, whereas S_y, U_y, and V_y represent the number of genes, lncRNA, and miRNA regulations acting on the y-th lncRNA, respectively.

$$AIC\left(S_z,U_z,V_z\right)=\log\left(\Omega_z^2\right)+\frac{2\left(S_z+U_z+V_z+1\right)}{N} \quad \text{(XXIV)}$$

$$\textit{where } \Omega_z^2=\sqrt[2]{\frac{\left(\Phi_z\cdot\hat{\Theta}_z-M_z\right)^T\left(\Phi_z\cdot\hat{\Theta}_z-M_z\right)}{N}}$$

where the parameter vector $\hat{\Theta}_z$ can be obtained from Equation XX using the least-squares method. Ω_z represents the residual estimation of the z-th miRNA model, and S_z, U_z, and V_z respectively represent the number of gene, lncRNA, and miRNA regulations acting on the z-th miRNA, respectively.

The AIC method was used to assess the complexity of stochastic models and their fit to data. A smaller value of AIC indicates a better model fit while accounting for the model's complexity. To obtain the real GWGEN, we had to minimize four AIC Equations XXI–XXIV:

$$R_w^*=\underset{R_w}{\operatorname{argmin}}\,AIC\left(R_w\right) \quad \text{(XXV)}$$

$$S_x^*,U_x^*,V_x^*=\underset{S_x,U_x,V_x}{\operatorname{argmin}}\,AIC\left(S_x,U_x,V_x\right) \quad \text{(XXVI)}$$

$$S_y^*,U_y^*,V_y^*=\underset{S_y,U_y,V_y}{\operatorname{argmin}}\,AIC\left(S_y,U_y,V_y\right) \quad \text{(XXVII)}$$

$$S_z^*,U_z^*,V_z^*=\underset{S_z,U_z,V_z}{\operatorname{argmin}}\,AIC\left(S_z,U_z,V_z\right) \quad \text{(XXVIII)}$$

R_w^* represents the actual quantity of protein interactions with the w-th protein. S_x^*, U_x^*, and V_x^* represent the actual number of regulatory TFs, lncRNAs, and miRNAs on the x-th gene, respectively. S_y^*, U_y^*, and V_y^* indicate the actual quantities of regulations between TFs, lncRNAs, and miRNAs on the y-th lncRNA, respectively. S_z^*, U_z^*, and V_z^* denote the actual number of regulatory TFs, lncRNAs, and miRNAs on the z-th miRNA, respectively. By minimizing the AIC, we successfully identified the true number of interactions for each protein and the actual number of regulations for each gene, miRNA and lncRNA, effectively pruning false positives from the candidate GWGENs, and thus obtaining the real GWGENs for both PDAC and non-PDAC, as depicted in Figure S1.

2.5. Extracting core genome-wide genetic and epigenetic networks from real genome-wide genetic and epigenetic networks using the principal network projection method

By employing the AIC method to prune false positive interactions and regulations from candidate GWGENs, real GWGENs for both PDAC and non-PDAC were obtained. However, due to the complexity of real GWGENs from both PDAC and non-PDAC, the carcinogenic molecular mechanisms of PDAC have not yet been fully confirmed. Therefore, it was necessary to leverage KEGG pathways to elucidate the signaling pathways underlying real GWGENs of both PDAC and non-PDAC. Since the current KEGG database can only annotate networks containing up to 6,000 nodes,

we focused on extracting the top 6,000 significant nodes (i.e., core GWGENs) from both the PDAC and non-PDAC real GWGENs using the PNP method. Subsequently, KEGG pathways were utilized to annotate these core GWGENs.

The PNP method we employed involves performing singular value decomposition (SVD) on the real GWGENs, as shown in Figure S1, followed by extracting the top 6,000 ranked nodes to construct the core GWGENs, as depicted in Figure S2. To perform SVD, we first constructed the network matrix *K* for the real GWGEN:

$$K=\begin{bmatrix} k_{protein\leftrightarrow protein} & 0 & 0 \\ k_{TF\rightarrow gene} & k_{lncRNA\rightarrow gene} & k_{miRNA\rightarrow gene} \\ k_{TF\rightarrow lncRNA} & k_{lncRNA\rightarrow lncRNA} & k_{miRNA\rightarrow lncRNA} \\ k_{TF\rightarrow miRNA} & k_{lncRNA\rightarrow miRNA} & k_{miRNA\rightarrow miRNA} \end{bmatrix} \quad \text{(XXIX)}$$

$$K\in\mathbb{R}^{(W+X+Y+Z)\times(X+Y+Z)}$$

where the submatrix $k_{protein\leftrightarrow protein}$ represents the estimated interaction abilities between proteins in the PPIN. Since protein interactions are bidirectional, these are represented by double-headed arrows. The respective submatrices $k_{TF\rightarrow gene}$, $k_{lncRNA\rightarrow gene}$, and $k_{miRNA\rightarrow gene}$ represent the estimated regulatory network of TFs, lncRNAs, and miRNAs that regulate or transcribe genes. Additionally, the submatrices $k_{TF\rightarrow lncRNA}$, $k_{lncRNA\rightarrow lncRNA}$, and $k_{miRNA\rightarrow lncRNA}$ represent estimated networks of TFs, lncRNAs, and miRNAs involved in regulating or transcribing lncRNAs, respectively. Finally, the submatrices $k_{TF\rightarrow miRNA}$, $k_{lncRNA\rightarrow miRNA}$, and $k_{miRNA\rightarrow miRNA}$ represent the estimated regulations of TFs, lncRNAs, and miRNAs in miRNA transcription, respectively.

Below is the detailed description of the network matrix *K* for real GWGENs of PDAC and non-PDAC:

$$K=\begin{bmatrix} \hat{\pi}_{1-1} & \cdots & \hat{\pi}_{1-r} & \cdots & \hat{\pi}_{1-Rw} & & 0 & \cdots & 0 & \cdots & 0 & & 0 & \cdots & 0 & \cdots & 0 & \\ \vdots & \ddots & \vdots & \iddots & \vdots & & \vdots & \ddots & \vdots & \iddots & \vdots & & \vdots & \ddots & \vdots & \iddots & \vdots & \\ \hat{\pi}_{w-1} & \cdots & \hat{\pi}_{w-r} & \cdots & \hat{\pi}_{w-Rw} & & 0 & \cdots & 0 & \cdots & 0 & & 0 & \cdots & 0 & \cdots & 0 & \\ \vdots & \iddots & \vdots & \ddots & \vdots & & \vdots & \iddots & \vdots & \ddots & \vdots & & \vdots & \iddots & \vdots & \ddots & \vdots & \\ \hat{\pi}_{W-1} & \cdots & \hat{\pi}_{W-r} & \cdots & \hat{\pi}_{W-Rw} & & 0 & \cdots & 0 & \cdots & 0 & & 0 & \cdots & 0 & \cdots & 0 & \\ \hat{\alpha}_{1-1} & \cdots & \hat{\alpha}_{1-s} & \cdots & \hat{\alpha}_{1-Sx} & \hat{\gamma}_{1-1} & \cdots & \hat{\gamma}_{1-u} & \cdots & \hat{\gamma}_{1-Ux} & -\hat{\varepsilon}_{1-1} & \cdots & -\hat{\varepsilon}_{1-v} & \cdots & -\hat{\varepsilon}_{1-Vx} \\ \vdots & \ddots & \vdots & \iddots & \vdots & \vdots & \ddots & \vdots & \iddots & \vdots & \vdots & \ddots & \vdots & \iddots & \vdots \\ \hat{\alpha}_{x-1} & \cdots & \hat{\alpha}_{x-s} & \cdots & \hat{\alpha}_{x-Sx} & \hat{\gamma}_{x-1} & \cdots & \hat{\gamma}_{x-u} & \cdots & \hat{\gamma}_{x-Ux} & -\hat{\varepsilon}_{x-1} & \cdots & -\hat{\varepsilon}_{x-v} & \cdots & -\hat{\varepsilon}_{x-Vx} \\ \vdots & \iddots & \vdots & \ddots & \vdots & \vdots & \iddots & \vdots & \ddots & \vdots & \vdots & \iddots & \vdots & \ddots & \vdots \\ \hat{\alpha}_{X-1} & \cdots & \hat{\alpha}_{X-s} & \cdots & \hat{\alpha}_{X-Sx} & \hat{\gamma}_{X-1} & \cdots & \hat{\gamma}_{X-u} & \cdots & \hat{\gamma}_{X-Ux} & -\hat{\varepsilon}_{X-1} & \cdots & -\hat{\varepsilon}_{X-v} & \cdots & -\hat{\varepsilon}_{X-Vx} \\ \hat{\zeta}_{1-1} & \cdots & \hat{\zeta}_{1-s} & \cdots & \hat{\zeta}_{1-Sy} & \hat{\psi}_{1-1} & \cdots & \hat{\psi}_{1-u} & \cdots & \hat{\psi}_{1-Uy} & -\hat{\kappa}_{1-1} & \cdots & -\hat{\kappa}_{1-v} & \cdots & -\hat{\kappa}_{1-Vy} \\ \vdots & \ddots & \vdots & \iddots & \vdots & \vdots & \ddots & \vdots & \iddots & \vdots & \vdots & \ddots & \vdots & \iddots & \vdots \\ \hat{\zeta}_{y-1} & \cdots & \hat{\zeta}_{y-s} & \cdots & \hat{\zeta}_{y-Sy} & \hat{\psi}_{y-1} & \cdots & \hat{\psi}_{y-u} & \cdots & \hat{\psi}_{y-Uy} & -\hat{\kappa}_{y-1} & \cdots & -\hat{\kappa}_{y-v} & \cdots & -\hat{\kappa}_{y-Vy} \\ \vdots & \iddots & \vdots & \ddots & \vdots & \vdots & \iddots & \vdots & \ddots & \vdots & \vdots & \iddots & \vdots & \ddots & \vdots \\ \hat{\zeta}_{Y-1} & \cdots & \hat{\zeta}_{Y-s} & \cdots & \hat{\zeta}_{Y-Sy} & \hat{\psi}_{Y-1} & \cdots & \hat{\psi}_{Y-u} & \cdots & \hat{\psi}_{Y-Uy} & -\hat{\kappa}_{Y-1} & \cdots & -\hat{\kappa}_{Y-v} & \cdots & -\hat{\kappa}_{Y-Vy} \\ \hat{\lambda}_{1-1} & \cdots & \hat{\lambda}_{1-s} & \cdots & \hat{\lambda}_{1-Sz} & \hat{\mu}_{1-1} & \cdots & \hat{\mu}_{1-u} & \cdots & \hat{\mu}_{1-Uz} & -\hat{\rho}_{1-1} & \cdots & -\hat{\rho}_{1-v} & \cdots & -\hat{\rho}_{1-Vz} \\ \vdots & \ddots & \vdots & \iddots & \vdots & \vdots & \ddots & \vdots & \iddots & \vdots & \vdots & \ddots & \vdots & \iddots & \vdots \\ \hat{\lambda}_{z-1} & \cdots & \hat{\lambda}_{z-s} & \cdots & \hat{\lambda}_{z-Sz} & \hat{\mu}_{z-1} & \cdots & \hat{\mu}_{z-u} & \cdots & \hat{\mu}_{z-Uz} & -\hat{\rho}_{z-1} & \cdots & -\hat{\rho}_{z-v} & \cdots & -\hat{\rho}_{z-Vz} \\ \vdots & \iddots & \vdots & \ddots & \vdots & \vdots & \iddots & \vdots & \ddots & \vdots & \vdots & \iddots & \vdots & \ddots & \vdots \\ \hat{\lambda}_{Z-1} & \cdots & \hat{\lambda}_{Z-s} & \cdots & \hat{\lambda}_{Z-Sz} & \hat{\mu}_{Z-1} & \cdots & \hat{\mu}_{Z-u} & \cdots & \hat{\mu}_{Z-Uz} & -\hat{\rho}_{Z-1} & \cdots & -\hat{\rho}_{Z-v} & \cdots & -\hat{\rho}_{Z-Vz} \end{bmatrix} \quad \text{(XXX)}$$

Next, we applied SVD to the network matrix *K* for the real GWGENs of PDAC and non-PDAC as follows:

$$\boldsymbol{K}=\boldsymbol{\mathcal{U}}\sum\boldsymbol{\mathcal{V}}^{\boldsymbol{T}}$$

$$\boldsymbol{\mathcal{U}}\in\mathbb{R}^{(\boldsymbol{W}+\boldsymbol{X}+\boldsymbol{Y}+\boldsymbol{Z})\times(\boldsymbol{W}+\boldsymbol{X}+\boldsymbol{Y}+\boldsymbol{Z})}$$

$$\sum\in\mathbb{R}^{(\boldsymbol{W}+\boldsymbol{X}+\boldsymbol{Y}+\boldsymbol{Z})\times(\boldsymbol{X}+\boldsymbol{Y}+\boldsymbol{Z})}$$

$$\boldsymbol{\mathcal{V}}\in\mathbb{R}^{(\boldsymbol{X}+\boldsymbol{Y}+\boldsymbol{Z})\times(\boldsymbol{X}+\boldsymbol{Y}+\boldsymbol{Z})} \quad \text{(XXXI)}$$

$$where\ \sum=\begin{bmatrix} \sigma_1 & 0 & \cdots & 0 & \cdots & 0 \\ 0 & \sigma_2 & \cdots & 0 & \cdots & 0 \\ \vdots & \vdots & \ddots & \vdots & \ddots & \vdots \\ 0 & 0 & \cdots & \sigma_i & \cdots & 0 \\ \vdots & \vdots & \ddots & \vdots & \ddots & \vdots \\ 0 & 0 & \cdots & 0 & \cdots & \sigma_{(X+Y+Z)} \\ 0 & 0 & \cdots & 0 & \cdots & 0 \\ \vdots & \vdots & \ddots & \vdots & \ddots & \vdots \\ 0 & 0 & \cdots & 0 & \cdots & 0 \end{bmatrix} \quad \text{(XXXII)}$$

in which the singular values σ_I are arranged in decreasing order, i.e., $\sigma^1 \geq \sigma_2 \ldots \geq \sigma_{(X+Y+Z)} \geq 0$.

Based on energy considerations, we chose to retain the first *J* singular values from the singular matrix Σ in network matrix *K*, ensuring they account for at least 85% of the total energy in the real GWGEN.

Subsequently, we retained the first *J* rows of the singular matrices *u* and *v*, establishing the significant structural component of the network, which contains at least 85% of the total energy in the real GWGEN,[30] as indicated below:

$$E_j=\frac{\sum_{i=1}^{J}\sigma_i^2}{\sum_{c=1}^{X+Y+Z}\sigma_c^2}\geq 0.85 \quad \text{(XXXIII)}$$

Next, we projected each row of the network matrix *K* (representing the interactions or regulations of each node in the real GWGEN) onto the first *J* significant singular vectors. The 2-norm of the projection value for each protein, gene, miRNA, and lncRNA node corresponds to the first *J* principal singular vectors of both PDAC and non-PDAC real GWGENs as described below:

$$Project\left(a,b\right)=K_a\cdot V_b^T$$

$$P_{2-norm}\left(a\right)=\sqrt[2]{\sum_{b=1}^{J}Project\left(a,b\right)^2} \quad \text{(XXXIV)}$$

for a = 1,2…, (W + X + Y + Z), b =1,2…, J-1, J

where *Project*(*a*,*b*) represents the projection value of the *a*-th node onto the *b*-th principal singular vector;

K_a denotes the a-th row of the matrix K; V_b indicates the b-th principal singular vector; P_{2_norm} (a) represents the square root of the sum of the squared projection values of the a-th node onto the first J singular vectors, reflecting the significance of the node within the real GWGEN from the network energy perspective.

Using the 2-norm projection value P_{2_norm} (a), we extracted the top 6,000 ranked nodes, which we classified as important nodes to construct the core GWGENs for PDAC and non-PDAC, as shown in Figure S2. We then utilized KEGG pathways to annotate the core GWGENs of both PDAC and non-PDAC, helping to identify the core signaling pathways for both conditions, as presented in Figure 2. In addition, considering information loss of real GWGEN, we actually obtained nearly identical signaling pathways of PDAC under different SVD truncation thresholds (75%, 85%, and 95%), demonstrating that filtering off insignificant singular values did not substantially affect the KEGG pathway annotations. By comparing the core signaling pathways of PDAC and non-PDAC in Figure 2, we aim to investigate the carcinogenic mechanisms of PDAC. Based on these insights, we identified key biomarkers, listed in Table 1, which may serve as potential drug targets for drug repurposing to treat PDAC.

2.6. Predicting drug candidates using deep neural network-based drug-target interaction model and screening by design specifications for treating PDAC

After identifying three important biomarkers implicated in the carcinogenic mechanisms of PDAC as candidate drug targets, we trained a DNN-DTI model to predict potential molecular drugs targeting these biomarkers. We utilized drug-target interaction data from several databases such as KEGG,[31] BIDD,[32] UniProt,[33] DrugBank,[34] PubChem,[35] ChEMBL,[36] and STITCH.[37] After identifying potential molecular drugs for PDAC and considering their regulatory ability, sensitivity, and toxicity as design specifications, we proceeded with drug repurposing and design.

Before training the DNN-DTI model, we preprocessed the DTI data. We gathered relevant interaction data from the aforementioned databases and converted the drug-

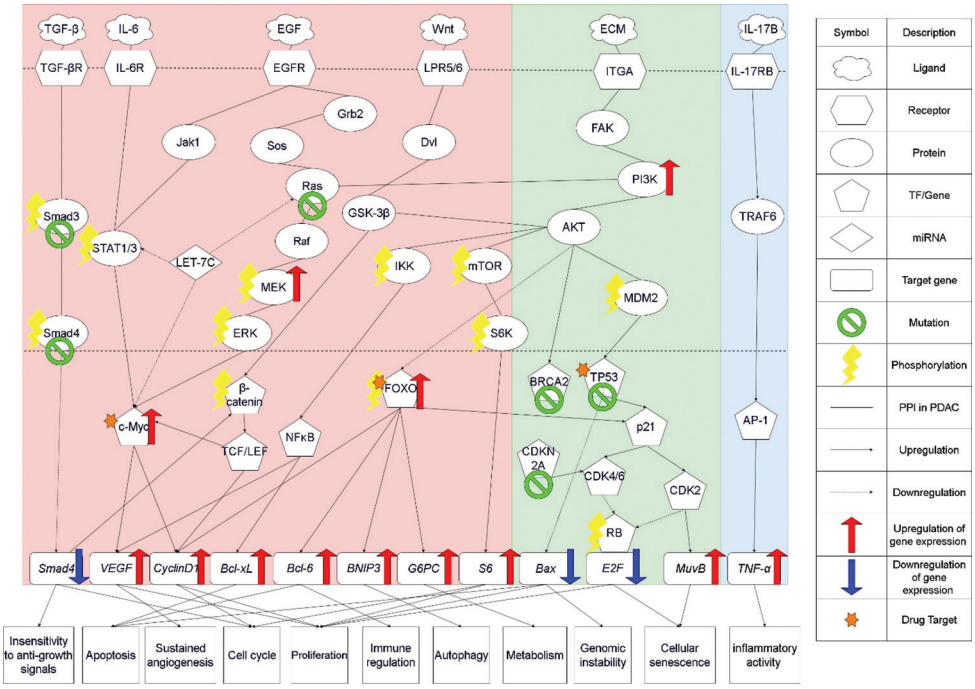

Figure 2. Shared and distinct core signaling pathways and downstream cellular functional impairments between PDAC and healthy controls
Abbreviations: AKT: Protein kinase B; AP-1: Activator protein 1; BNIP: BCL2 interacting protein 3; BRCA: Breast cancer gene; CDK: Cyclin-dependent kinase; ECM: Extracellular matrix; EGF: Epidermal growth factor; EGFR: Epidermal growth factor receptor; ERK: Extracellular signal-regulated kinase 1; FAK: Focal adhesion kinase; FOXO: Forkhead box O; GSK: Glycogen synthase kinase; G6PC: Glucose-6-phosphatase; IKK: IκB kinase; IL: Interleukin; IL-XR: Interleukin X receptor; ITGA: Integrin alpha; Jak1: Janus kinase 1; LEF: Lymphoid enhancer factor; LPR: Low-density-lipoprotein-receptor-related-protein; MDM2: Mouse double minute 2; MEK: Mitogen-activated extracellular signal-regulated kinase; mTOR: Mammalian target of rapamycin; NFκB: Nuclear factor κ B; PDAC: Pancreatic ductal adenocarcinoma; PI3K: Phosphoinositide 3-kinase; PPI: Protein-protein interaction; RB: Retinoblastoma protein; STAT: Signal transducer and activator of transcription; S6K: Ribosomal protein S6 kinase; TCF: T cell factor; TF: Transcription factor; TGF-β: Transforming growth factor β; TβR: Transforming growth factor β receptor; TNF-α: Tumor necrosis factor α; TRAF6: Tumor necrosis factor receptor-associated factor 6; VEGF: Vascular endothelial growth factor.

Table 1. Information on candidate molecular drugs for selected pancreatic ductal adenocarcinoma biomarkers based on their regulatory capacity, sensitivity, and toxicity

Target biomarker : c-MYC(+)			
Potential drug	**Regulation ability (L1000)**	**Sensitivity (PRISM)**	**Toxicity (LC50, mol/kg)**
Tipranavir	−1.33845971	−0.283941421	4.556
Tolcapone	−0.072789862	−0.26251132	4.78
Gemcitabine	−0.544798394	−2.417963872	2.381
Target biomarker : FOXO3(+)			
Potential drug	**Regulation ability (L1000)**	**Sensitivity (PRISM)**	**Toxicity (LC50, mol/kg)**
Atracurium	−0.238786879	−0.468347976	5.587
MK-2206	−0.503738765	0.772406631	5.561
ARN-509	−0.93691652	0.02300543	3.673
Target biomarker : TP53(*)			
Potential drug	**Regulation ability (L1000)**	**Sensitivity (PRISM)**	**Toxicity (LC50, mol/kg)**
Gemcitabine	−0.537988045	−2.417963872	2.381
Guanadrel	−0.915635131	−0.411395434	2.38
Bemegride	−3.718984186	1.008142951	1.532

Notes: *Denotes the mutation; +denotes overexpression on the corresponding biomarker.
Abbreviations: FOXO3: Forkhead box O3; LC50: Lethal concentration 50%; PRISMA: Pharmaceutical Regulatory Information System; TP53: Tumor suppressor p53.

target pairs into feature vectors to enable input into the DNN model. To generate the feature vectors, we used the Protein Feature Server and PyBioMed tool in a Python 3.7 environment. The drug features encompass widely utilized structural and physicochemical data, while the target features are derived from the structural and physicochemical characteristics of proteins and peptides, determined from their amino acid sequences. Each drug-target pair was combined into a single feature vector. The feature vector for the *i*-th drug-target pair in DTI databases can be presented as:

$$q^{i}_{drug-target} = \left[d_1, d_2, \ldots, d_{A-1}, d_A, t_1, t_2, \ldots, t_{B-1}, t_B\right]^i = \left[D, T\right]^i \quad \text{(XXXV)}$$

for i=1,2…,180315, $A + B = 1359$

The total feature vector dataset consists of 180,315 entries, including 80,291 experimentally validated DTIs and 100,024 unvalidated interactions. To address the imbalance in the dataset, we downsampled the unvalidated interactions to match the number of validated entries. Before training the DNN-DTI model, we standardized and transformed the drug-target interaction data because of variations in units among the different feature vectors. Standardization highlights the differences between each feature vector. The standardization of the features is shown as follows:

$$d^{*}_{a} = \frac{d_a - \mu_a}{\sigma_a} \quad for\ a = 1,2\ldots,A-1, A \quad \text{(XXXVI)}$$

where d_a represents the a-th drug feature, and d^{*}_{a} indicates the a-th drug feature after standardization; σ_a and μ_a refer to the standard deviation and mean of the a-th drug feature, respectively. A denotes the total number of drug features.

Similarly,

$$t^{*}_{b} = \frac{t_b - \mu_b}{\sigma_b} \quad for\ b = 1,2\ldots,B-1, B \quad \text{(XXXVII)}$$

where t_b denotes the b-th target feature, and t^{*}_{b} represents the b-th target feature after standardization; σ_b and μ_b refer to the standard deviation and mean of the b-th target feature, respectively; B represents the total number of target features.

Given that the DNN-based DTI model (Figure 3) requires 996 input nodes, the total (A+B) feature vector dimension needed to be reduced so that these drug-target feature vectors can be input to train the DNN-DTI model. By selecting the top 85% significant features for both drugs and targets using the principal component analysis (PCA), we reduced the dimensionality of the features from 1,359 to 996. This reduction aligns with the model's input layer dimension and enhances training performance.[38]

All the aforementioned data preprocessing steps were performed to enable the DNN-DTI model to effectively learn from feature data of drug-target interactions. After completing the data preprocessing, we split the dataset into

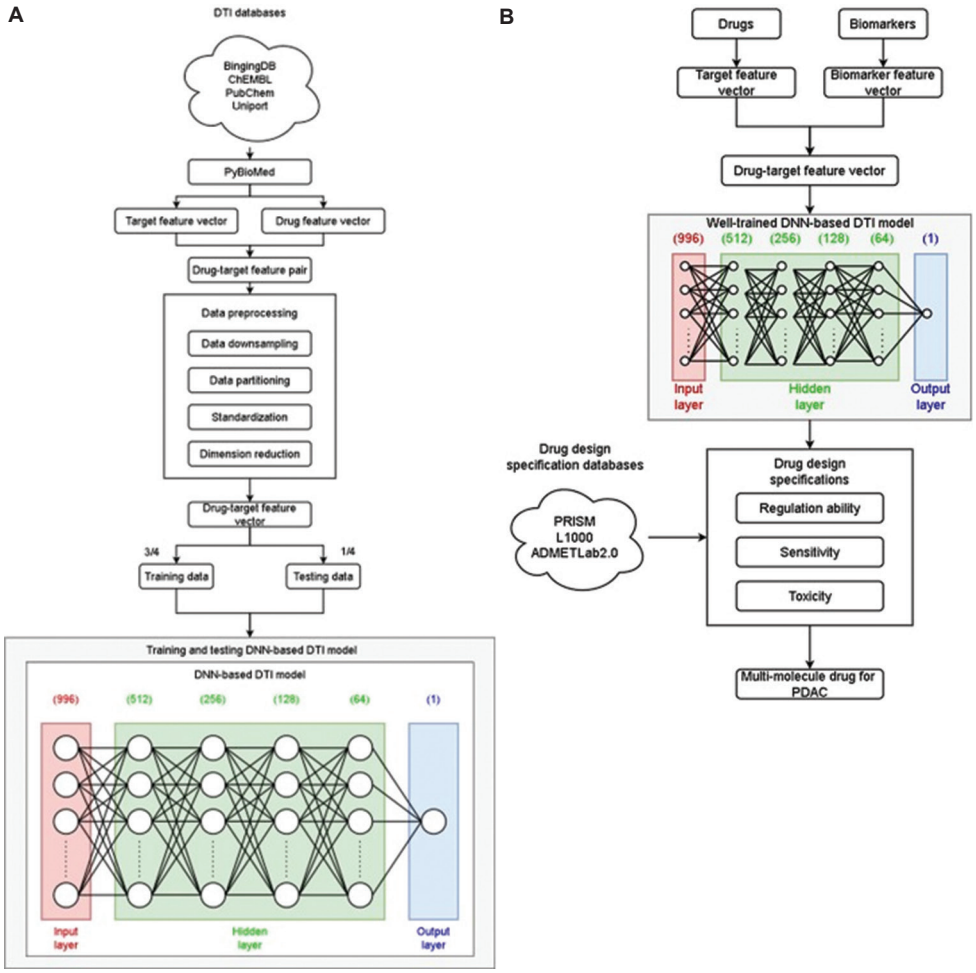

Figure 3. Flowchart of the systematic drug repurposing approach for treating PDAC. (A) Pre-training process of the deep neural network-based drug-target interaction model using drug-target interaction databases. (B) Prediction of candidate molecular drugs for PDAC biomarkers and selection of multi-molecular drug combination based on three drug design specifications
Abbreviations: DNN: Deep neural network; DTI: Drug-target interaction; PDAC: Pancreatic ductal adenocarcinoma.

75% for training and 25% for testing. We then utilized the DNN-DTI model to predict the probability of drug-target interactions. The architecture of the DNN model comprises an input layer with 996 neurons, followed by hidden layers with 512, 256, 128, and 64 neurons, respectively. The rectified linear unit (ReLU) activation function was applied in the hidden layers, and a dropout rate of 0.2 was set to prevent overfitting. The output layer consists of a single neuron with a sigmoid activation function, as drug-target interaction prediction is a binary classification problem. The mathematical formula for each layer is as follows:

$$O_n = A\left(w \times I_n + b\right) \quad \text{(XXXVIII)}$$

where A is the activation function (either ReLU or Sigmoid); I_n and O_n represent the input and output of the n-th feature vector, respectively; w and b are the weight vector and bias vector, respectively.

The output represents the probability of a drug-target interaction, ensuring the result lies within (0,1). The following binary cross-entropy was chosen as the loss function to address the binary classification problem of drug-target interactions:

$$C_n\left(p_n, \hat{p}_n\right) = -\left[p_n \log \hat{p}_n + \left(1 - p_n\right)\log\left(1 - \hat{p}_n\right)\right] \quad \text{(XXXIX)}$$

$$L\left(w, b\right) = \frac{1}{N}\sum_{n=1}^{N} C_n\left(p_n, \hat{p}_n\right) \quad \text{(XL)}$$

where n represents the nth sample, N is the total number of samples, p_n is the empirical probability of a positive interaction, $1-p_n$ is the empirical probability of a negative interaction, $\hat{p}_n$ is the estimated probability of a positive interaction, and $\hat{p}_n$ is the estimated probability of a negative interaction. The loss function computed the average loss $L(w, b)$ over all samples by averaging the loss $C_n\left(p_n, \hat{p}_n\right)$.

Finally, we used backpropagation and the Adam optimal learning algorithm with a learning rate of 0.001 to train the DNN-based DTI model. We set the number of epochs to 100 and the batch size to 100. The gradient update algorithm is given as follows:

$$\theta = \begin{bmatrix} w \\ b \end{bmatrix} \tag{XLI}$$

$$\theta^* = arg\min_{\theta} L(\theta) \tag{XLII}$$

$$\theta^{f-1} - \theta^f = \eta \nabla L\left(\theta^{f-1}\right) \tag{XLIII}$$

$$with\ \nabla L\left(\theta^{f-1}\right) = \begin{bmatrix} \frac{\partial L\left(\theta^{f-1}\right)}{\partial w} \\ \frac{\partial L\left(\theta^{f-1}\right)}{\partial b} \end{bmatrix}$$

where f represents the f-th iteration of the DNN training process, η is the learning rate, and ∇ denotes the gradient operator.

To evaluate the model, we employed five-fold cross-validation and used receiver operating characteristic (ROC) curves for the binary classification problem. The area under the ROC curve (AUC) is an important evaluation metric, where a higher AUC value indicates a better prediction of drug-target interaction. The formulas for calculating the ROC curves and AUC are as follows:

$$\text{TPR}\left(\text{True Positive Rate}\right) = \frac{TP}{TP + FN} \tag{XLIV}$$

$$\text{TNR}\left(\text{True Negative Rate}\right) = \frac{TN}{FP + TN} \tag{XLV}$$

$$\text{FPR}\left(\text{False Positive Rate}\right) = \frac{FP}{TN + FP} \tag{XLVI}$$

$$\text{FNR}\left(\text{False Negative Rate}\right) = \frac{FN}{FN + TP} \tag{XLVII}$$

where *TP* means the judgment is true and it is indeed true; *TN* means the judgment is false and it is indeed false; *FP* means the judgment is true, but it is actually false; *FN* means the judgment is false, but it is actually true.

Utilizing predictions from the DNN-based DTI model, we obtained three candidate molecular drugs for each key biomarker, as shown in Table 1. These drugs were screened based on some drug design specifications to identify potential molecular targets for PDAC. In this study, we considered pharmacological properties such as regulatory ability, sensitivity, and toxicity as key design specifications, and selected suitable candidate drugs from Table 1 based on these criteria. Specifically, we assessed the regulatory ability of drugs by referring to the LINCS L1000 level 5 dataset, which allowed us to identify drugs capable of regulating gene expression to normal levels. A regulatory ability value >0 indicates upregulation of gene expression, while a value <0 suggests downregulation. We also selected compounds with small absolute sensitivity values from the Pharmaceutical Regulatory Information System (PRISM) database to minimize interference with normal cells. Most importantly, in considering drug toxicity, we used tools from the ADMETlab 2.0 website and focused on LC50 values. LC50 represents the concentration at which 50% of organisms are lethally affected, and higher LC50 values indicate lower toxicity. Therefore, we selected compounds with higher LC50 values.

In conclusion, we followed three drug design specifications — toxicity, regulatory ability, and sensitivity — to screen potential molecular drugs for the biomarkers of PDAC, ultimately identifying two potential molecular drugs. These drugs were then combined into multi-target therapy for treating PDAC, as shown in Table 2. Ultimately, we successfully identified a suitable combination of molecular drugs for the treatment of PDAC.

3. Results

3.1. Overview of the systems biology approach to PDAC mechanisms and systematic drug repurposing and design

In this study, a systems biology approach was employed to investigate the carcinogenic mechanism of PDAC, utilizing big data mining and genome-wide microarray data. This approach led to the identification of crucial biomarkers of PDAC carcinogenesis, which were subsequently targeted for drug repurposing. A DNN-based DTI model was trained using DTI databases to predict potential drugs targeting these biomarkers. These molecular drugs were designed based on drug design specifications and their ability to restore the cellular functions of pancreatic cancer cells. Finally, the selected molecular drugs were considered as a multi-molecular therapeutic strategy of PDAC. The flowchart outlining the systems biology approach and drug repurposing process for PDAC is depicted in Figure 1.

Initially, to understand the carcinogenic mechanisms underlying PDAC and identify important biomarkers for therapeutic targeting, candidate GWGENs were constructed using a big database mining approach. The following databases were used: starBase,[27] DIP,[18] CircuitDB,[25] BioGRID,[20] IntAct,[19] HTRIdatabase,[22] ITFP,[23] MINT,[21] TRANSFAC,[24] and TargetScanHuman.[26] The candidate GWGENs are represented as a Boolean matrix,

Table 2. Filtering potential molecular drugs for pancreatic ductal adenocarcinoma based on three drug design specifications: regulatory ability, sensitivity, and toxicity, derived from the candidate molecular drugs listed in Table 1

Target drug	c-MYC (+)	FOXO3 (+)	TP53 (*)	Sensitivity (PRISM)	Toxicity (LC50, mol/kg)
MK-2206		↓		0.772406631	5.561
Gemcitabine	↓		✓	2.417963872	2.381

Notes: ✓ denotes drug-target interaction; ↓ denotes downregulation of the biomarker by the molecular drug.
Abbreviations: FOXO3: Forkhead box O3; LC50: Lethal concentration 50%; PRISMA: Pharmaceutical Regulatory Information System; TP53: Tumor suppressor p53.

where interactions between proteins and genes were encoded as 1 (interaction) and 0 (no interaction). The nodes in the GWGENs include proteins, genes, miRNAs, and lncRNAs.

Next, using systematic identification and order detection methods, false positives were removed from the candidate GWGENs based on whole-genome microarray data GSE183795, resulting in the construction of the real GWGEN for both PDAC and healthy controls, as shown in Figure S1. Although the number of nodes was reduced after the false positives were filtered out from candidate GWGENs, the real GWGENs for both PDAC and healthy controls remained too complex for direct annotation using KEGG pathway analysis. To simplify this, the number of nodes in GWGENs was reduced to 6,000 using the PNP method. The 6,000 significant nodes from the real GWGENs of PDAC and healthy controls were extracted, forming the core GWGENs for PDAC and healthy controls, as depicted in Figure S2.

For KEGG pathway enrichment analysis to interpret the carcinogenic mechanisms of PDAC, the DAVID functional annotation tool was employed, supported by references from PDAC-related literature. Based on the KEGG pathway annotations, core signaling pathways for PDAC and healthy controls were established, allowing the investigation of the mechanisms involved in PDAC carcinogenesis, as illustrated in Figure 2.

Based on these core signaling pathways, key biomarkers of PDAC carcinogenesis were identified as potential drug targets, which were implicated in downstream cellular dysfunctions associated with PDAC. Using the DNN-based DTI model trained with data from the DTI databases, the systematic drug repurposing and design process for PDAC therapy was carried out, as shown in Figure 3. The DTI databases served as the training set for the DNN model, which predicted candidate molecular drugs for PDAC drug targets. These candidate drugs were screened according to drug design specifications, including regulatory ability, sensitivity, and toxicity, to identify a suitable combination of molecular drugs for PDAC treatment.

3.2. Core signaling pathways of carcinogenic mechanisms of PDAC

Tumors are more likely to accelerate their development in an appropriate microenvironment. The microenvironment of PDAC involves complex interactions between tissues, blood vessels, immune cells, cytokines, and other molecules surrounding pancreatic cancer cells.[39] The characteristics of this microenvironment include fibrosis, immune cell infiltration, angiogenesis, and the presence of various cytokines and growth factors.[40,41] To identify relevant signaling pathways based on their cellular functions, we consulted existing research literature. Key pathways involved in pancreatic fibrosis include transforming growth factor β, Wnt, and phosphoinositide 3-kinase (PI3K)-protein kinase B (AKT) signaling pathways.[42] Pathways associated with immune cell infiltration include Janus kinase-signal transducer and activator of transcription (STAT) pathway, PI3K-AKT, and mammalian target of rapamycin (mTOR) signaling pathways.[43] Additionally, the mitogen-activated protein kinase, PI3K-AKT, and mTOR signaling pathways have been implicated in the creation of new blood vessels (angiogenesis).[44] These six signaling pathways provide a comprehensive framework for investigating the oncogenic mechanisms of PDAC.

Through KEGG enrichment pathway analysis and annotation of the core GWGENs of PDAC and healthy controls, we identified the core signaling pathways involved in PDAC carcinogenesis, as shown in Figure 2. By examining the core signaling pathways and their downstream target genes, we explored the carcinogenic mechanisms of PDAC and identified key biomarkers as drug targets. This approach ultimately aided in the discovery of multi-molecular drugs for the treatment of PDAC.

3.3. Core signaling pathways in healthy controls

In healthy controls, the core signaling pathways primarily include PI3K-AKT, TP53, and interleukin 17 (IL-17) signaling pathways. The TP53 pathway plays a crucial role in regulating the cell cycle by modulating the expression and activity of genes such as *p21*, *CDK4/6*, *CDK2*, *BAX*, *E2F*, and *MUVB*. These interactions influence cell

proliferation and survival. The IL-17 signaling pathway involves proteins such as activator protein 1 (AP-1) and tumor necrosis factor receptor-associated factor 6 (TRAF6), which work together to regulate the expression of downstream genes. Additionally, tumor necrosis factor α (TNF-α) is a key cytokine involved in immune responses and inflammation regulation. Signaling through the IL-17 pathway often triggers the production of *TNFα*, thereby impacting the inflammatory responses. The activation of the IL-17 signaling pathway is regulated by genes including *IL17B*, *IL17RB*, *TRAF6*, AP-1, and *TNFα*.

Through KEGG pathway enrichment analysis and annotation of the core GWGENs for both PDAC and healthy controls, as shown in Figure 2, we obtained the core signaling pathways and their downstream target genes. This analysis provides a deeper understanding of the carcinogenic mechanisms of PDAC. By comparing the core signaling pathways and their downstream target genes between PDAC and healthy controls, we identified significant biomarkers as drug targets, thus facilitating the discovery of more effective multi-molecular drugs for treating PDAC. Furthermore, recent studies have suggested that miRNAs may be the answer to cancer treatment. Based on the core GWGENs of healthy controls, we identified miRNA LET-7C. According to recent research, miRNA LET-7C regulates key genes such as *Ras, STAT1/3*, and *c-MYC* in the core signaling pathways of PDAC.[45]

3.4. Selection of drug targets by investigating the pathogenesis of PDAC and systematic drug repurposing via deep neural network-based drug-target interactions model

Based on the core signaling pathways of PDAC patients and the abnormal downstream cellular dysfunctions compared with the healthy controls in Figure 2, we selected key biomarkers, such as c-MYC, FOXO3, and TP53, as drug targets. Our aim is to identify potential multi-molecular drugs that could restore the abnormal expression of these key biomarkers to normal levels for the treatment of PDAC.

c-MYC, a TF located downstream of the MAPK signaling pathway, is important in regulating cell growth, proliferation, and apoptosis.[46] Research indicates that overexpression of c-MYC is strongly associated with the development of PDAC and plays a significant role in its early transformation.[47] Excessive activation of c-MYC promotes the proliferation of PDAC cells, thereby accelerating tumor growth.[48] Moreover, c-MYC inhibits apoptosis in PDAC cells, further enhancing tumor progression.[49] Thus, downregulating c-MYC can effectively inhibit PDAC cell proliferation and survival, offering therapeutic potential.[50] Additionally, c-MYC contributes to PDAC resistance to chemotherapy. Research has demonstrated that overexpression of MYC enhances the resistance of PDAC cells to chemotherapy,[51] thereby reducing treatment efficacy. By regulating c-MYC to restore cellular function, the sensitivity of PDAC cells to existing treatments can be enhanced, thereby improving therapeutic outcomes.

Forkhead box O3 is a TF that plays a crucial role in regulating cell proliferation, apoptosis, and metabolism.[52] It has been shown to significantly involve in the development and progression of PDAC.[53] Dysregulation of FOXO3 is closely linked to the onset and progression of PDAC, with its expression in PDAC being much higher than in normal tissues, although the precise mechanism remains unclear.[54] Scholars speculate that FOXO3 may be upregulated or degraded in cancer tissues, leading to its accumulation in the nucleus and increased expression levels. In normal tissues, FOXO3 is transcribed at low levels and rapidly degraded.[55] In our study, FOXO3 regulates several target genes, and our goal is to restore FOXO3 to normal expression levels to mitigate downstream cellular dysfunction.

The *TP53* gene encodes the tumor suppressor protein p53, one of the most commonly mutated genes in PDAC.[56] TP53 regulates the expression of many genes involved in cell cycle control, apoptosis, and senescence, as well as influencing the immune microenvironment of PDAC. Inactivation of the *TP53* gene disrupts these processes, leading to altered immune responses.[56] Research indicates that the loss of *TP53* expression allows cells harboring the *KRASG12D* mutation to survive, promoting tumor formation and metastasis.[57] Our goal is to restore cellular function to normal by targeting mutated TP53, thereby achieving therapeutic effects.

After selecting these important biomarkers of PDAC carcinogenesis as potential drug targets, we obtained DTI data from databases such as KEGG,[31] BIDD,[32] UniProt,[33] DrugBank,[34] PubChem,[35] ChEMBL,[36] and STITCH.[37] Using these data, we trained a DNN-based DTI model to predict molecular drugs for these targets. The training dataset consists of 180,315 drug-target interactions, including 80,291 experimentally verified drug-target interactions and 100,024 unverified interactions. To address the potential imbalance between the two categories in the training dataset, we randomly selected an equal number of drug-target interactions from each database. Before training the DNN-DTI model, the interaction data were transformed and standardized, followed by dimensionality reduction using PCA, which reduced the transformed features from 1,359 to 996. This step is necessary to match the input layer dimensions of the model. As shown in Figure 3, the input layer of the DNN-DTI model consists of 996 nodes, followed by four hidden layers of

512, 256, 128, and 64 nodes, respectively, each using the ReLU activation function. The output layer consists of a single node with sigmoid activation function. To prevent overfitting during training, we added a dropout layer. After training the DNN-DTI model to predict candidate molecular drugs for these drug targets, we evaluated the model's learning effectiveness. Figures S3 and S4 show the accuracy and loss during the training process, respectively. The five-fold cross-validation was employed to assess the model's performance, achieving an average accuracy of 98.3% and a standard deviation of 0.138%, as shown in Table S1. Additionally, the AUC was used to evaluate the model's classification performance, as shown in Figure S5. An AUC of 0.5 represents random guessing, while an AUC of 1 indicates perfect classification. The DNN-DTI model achieved an AUC of 0.980, indicating that its predictive ability is much superior to random guessing and close to perfect classification. This highly efficient DNN-based DTI model enables us to accurately predict the probability of interactions between drugs and the selected biomarkers.

To identify suitable potential drugs, we considered three drug design specifications to ensure the rationality and effectiveness of the candidate multi-molecular drugs predicted by the DNN-DTI model. These specifications include regulatory ability, sensitivity, and toxicity, among other pharmacological properties. The regulatory ability of the drugs was assessed using the LINCS L1000 level 5 dataset, guiding the selection of drugs that could restore key biomarkers to their normal expression levels.[58] A regulatory ability value >0 indicates an increase in gene expression, while a value <0 indicates a decrease. Additionally, the sensitivity of the drugs was assessed using the PRISM dataset,[59] and we selected drugs with small absolute sensitivity values to avoid excessive chemical perturbation from potential drugs. Finally, we evaluated the drug toxicity using tools from the ADMETlab 2.0 website, which calculates LC50.[60] A higher LC50 value indicates lower toxicity, which helps avoid life-threatening from low drug doses. Table 1 presents the candidate molecular drugs predicted by the DNN-DTI model for the selected biomarkers, listing their relevant pharmacological properties, such as regulatory ability, sensitivity, and toxicity. Based on these drug design specifications, we selected two potential molecular drugs, MK-2206 and gemcitabine, which have adequate regulatory ability, normal sensitivity (small absolute value), and weaker toxicity, as shown in Table 2. These drugs were combined into a multi-molecular therapeutic strategy for PDAC.

4. Discussion

Currently, treatment options for exocrine ductal adenocarcinoma, also known as PDAC, include surgical resection, radiotherapy, chemotherapy, immunotherapy, and targeted therapy. However, not all patients are suitable candidates for surgery, and standard chemotherapy regimens may be ineffective due to the complex interactions between healthy pancreatic cells, cancer cells, and the tumor microenvironment, leading to drug resistance and suboptimal therapeutic outcomes. Therefore, there is a pressing need to explore new treatment approaches.

Given the substantial financial costs and time required for the discovery of new drugs, repurposing existing drugs for new therapeutic indications has become an attractive alternative. Drug repurposing involves identifying new uses for already-approved drugs beyond their original medical indications.[17]

In this study, we employed database mining and genome-wide microarray data from PDAC and healthy controls, utilizing systems biology approaches to identify their core GWGENs. These networks were annotated using the KEGG database to establish the core signaling pathways of PDAC and the associated downstream cellular dysfunctions, as shown in Figure 2. After investigating the oncogenic mechanisms of PDAC and identifying key biomarkers suitable for drug targeting, we trained a DNN-based DTI model using data from DTI databases to predict the probability of interaction between these biomarkers and candidate molecular drugs. The model was validated using five-fold cross-validation, as shown in Table S1, and the drug repurposing flowchart is presented in Figure 3. We subsequently screened potential drugs as a multi-molecular therapy based on drug design specifications, focusing on sensitivity, toxicity, and regulatory capability. Ultimately, we predicted a combination of potential molecular drugs, MK-2206 and gemcitabine, to modulate the overexpression of c-MYC and FOXO3, as well as the mutation of TP53, as shown in Table 2.

Gemcitabine is one of the most widely used treatments for PDAC. As a deoxycytidine nucleoside analog,[10] it inhibits DNA chain elongation by phosphorylation after entering the cells, leading to cell apoptosis and death. However, the therapeutic effect of gemcitabine is limited by its unstable metabolism and the potential for drug resistance.[61] As a result, it is often used in combination with other drugs, such as Fluorouracil and paclitaxel,[62,63] to enhance treatment efficacy. Studies have pointed out that gemcitabine can induce the activation of mutated p53, leading to cancer cell death,[64] as the drug causes the accumulation of *Bax* downstream of TP53, which induces apoptosis.[65,66] In our research, we referenced the LINCS L1000 level 5 dataset and found that gemcitabine can reduce the expression c-MYC.[67] However, the high expression of c-MYC may induce resistance to gemcitabine.[68] Therefore,

Table 3. Overview of potential multi-molecular drugs screened for pancreatic ductal adenocarcinoma treatment based on three drug design specifications using a systematic drug discovery approach

Target drug	c-MYC	FOXO3	TP53	Sensitivity (PRISM)	Toxicity (LC50, mol/kg)
MK-2206		•		0.772406631	5.561
Gemcitabine	•		•	2.417963872	2.381
MK-2206			Gemcitabine		

Note: • Denotes drug targeting on the corresponding biomarker.
Abbreviations: FOXO3: Forkhead box O3; LC50: Lethal concentration 50%; PRISMA: Pharmaceutical Regulatory Information System; TP53: Tumor suppressor p53.

we selected gemcitabine as a potential drug for further evaluation.

MK-2206 is an AKT inhibitor. Abnormal activation of the PI3K/AKT signaling pathway affects cell metabolism and survival, cell cycle progression, apoptosis regulation, protein synthesis, and genome instability.[69] Since the PI3K/AKT pathway is frequently dysregulated in many cancers, MK-2206 inhibits AKT and downregulates FOXO3,[70,71] thereby exhibiting anti-tumor activity and increasing cancer cell sensitivity to chemotherapy and radiotherapy. MK-2206 is often used in combination with other chemotherapy drugs to improve therapeutic efficacy.[72] Current studies show that MK-2206 is well tolerated and can effectively block AKT signaling,[73] making it a promising candidate for repurposing as a potential drug for PDAC treatment.

However, this study has several limitations. First, the analysis was based on GSE183795 microarray data, and the quality and completeness of this dataset directly influence the accuracy of the results. If the dataset contains significant noise or incomplete data, it may lead to erroneous conclusions. Second, the findings of this study are primarily based on mathematical modeling and bioinformatics analysis, and lack direct experimental validation. Predictions made without experimental confirmation may face challenges in practical application, highlighting the need for further laboratory experiments to confirm the results. While there is limited experimental research on the combination treatment of MK-2206 and gemcitabine, existing studies suggest that this combination may be effective.[74,75] Additionally, although our study predicts multi-drug combination, the actual pharmacodynamic interactions and effects of this combination need to be verified through *in vivo* and *in vitro* experiments. It is also important to consider potential synergistic or antagonistic effects between the drugs, which may not have been fully captured in the model predictions.

These limitations should be addressed in future research to enhance the reliability and applicability of drug repurposing strategies in PDAC treatment.

5. Conclusion

In this research, we employed a systems biology approach to construct candidate GWGENs by mining large-scale databases. We then applied system identification and order detection methods to eliminate false positive interactions within candidate GWGENs, thereby generating the real GWGENs for PDAC and healthy controls. Using the principal network projection method, we extracted the core GWGENs for both PDAC and healthy controls. To elucidate the oncogenic mechanisms of PDAC, we annotated the core GWGENs with KEGG pathways to identify core signaling pathways in PDAC and healthy controls. By comparing the core signal pathways between PDAC and healthy controls, we investigated the association between these pathways and downstream cellular dysfunctions in PDAC, identifying key biomarkers involved in the carcinogenesis of PDAC as potential drug targets. With these drug targets, we utilized a DNN-based DTI model to predict the probability of interaction between the drugs and their targets. Based on the drug's regulatory ability, sensitivity, and toxicity, we selected a potential multi-molecular drug combination. Ultimately, we identified MK-2206 and gemcitabine as a promising combination for PDAC treatment, targeting significant biomarkers such as c-MYC, FOXO3, and TP53, as shown in Table 3. While the Drug Interaction Checker suggests that there is no known interaction between these

two drugs, their interaction in clinical treatment for PDAC still requires further clinical and experimental verification.

Conclusion

In conclusion, we integrated systems biology methods with deep learning techniques to systematically repurpose existing drugs for PDAC therapy. By utilizing systems biology to identify drug targets through large-scale databases and genome-wide microarray data from both PDAC and non-PDAC samples, and applying deep learning for the DTI model to identify potential molecular drugs based on three drug design specifications, we have developed a systematic approach to accelerate drug development for PDAC. We hope that this drug repurposing strategy can be applied to other diseases in the future, further advancing the field of systems drug development.

Acknowledgments

None.

Funding

None.

Conflict of interest

The authors declare they have no competing interests.

Author contributions

Conceptualization: All authors
Formal analysis: All authors
Investigation: Yi-Hsin Tsai
Methodology: All authors
Writing – original draft: Yi-Hsin Tsai
Writing – review & editing: All authors

Ethics approval and consent to participate

Not applicable.

Consent for publication

Not applicable.

Availability of data

The RNA-sequencing datasets from PDAC patients and healthy controls can be obtained from GSE183795 (https://www.ncbi.nlm.nih.gov/geo/query/acc.cgi?acc=GSE183795, accessed on 10 March 2023).

References

1. Ma Y, Wu Q, Li X, Gu X, Xu J, Yang J. Pancreatic cancer: From bench to bedside. *Ann Transl Med*. 2016;4(23):458.

   doi: 10.21037/atm.2016.11.57

2. Rahib L, Smith BD, Aizenberg R, Rosenzweig AB, Fleshman JM, Matrisian LM. Projecting cancer incidence and deaths to 2030: The unexpected burden of thyroid, liver, and pancreas cancers in the United States. *Cancer Res*. 2014;74(11):2913-2921.

   doi: 10.1158/0008-5472.Can-14-0155

3. Rahib L, Wehner MR, Matrisian LM, Nead KT. estimated projection of US cancer incidence and death to 2040. *JAMA Netw Open*. 2021;4(4):e214708.

   doi: 10.1001/jamanetworkopen.2021.4708

4. Strobel O, Lorenz P, Hinz U, *et al*. Actual five-year survival after upfront resection for pancreatic ductal adenocarcinoma: Who beats the odds? *Ann Surg*. 2022;275(5):962-971.

   doi: 10.1097/sla.0000000000004147

5. Sung H, Ferlay J, Siegel RL, *et al*. Global cancer statistics 2020: GLOBOCAN estimates of incidence and mortality worldwide for 36 cancers in 185 countries. *CA Cancer J Clin*. 2021;71(3):209-249.

   doi: 10.3322/caac.21660

6. Lynch SM, Vrieling A, Lubin JH, *et al.* Cigarette smoking and pancreatic cancer: A pooled analysis from the pancreatic cancer cohort consortium. *Am J Epidemiol*. 2009;170(4):403-413.

   doi: 10.1093/aje/kwp134

7. Mela A, Rdzanek E, Tysarowski A, *et al*. The impact of changing the funding model for genetic diagnostics and improved access to personalized medicine in oncology. *Expert Rev Pharmacoecon Outcomes Res*. 2023;23(1):43-54.

   doi: 10.1080/14737167.2023.2140139

8. Park W, Chawla A, O'Reilly EM. Pancreatic cancer: A review. *JAMA*. 2021;326(9):851-862.

   doi: 10.1001/jama.2021.13027

9. Elsayed M, Abdelrahim M. The latest advancement in pancreatic ductal adenocarcinoma therapy: A review article for the latest guidelines and novel therapies. *Biomedicines*. 2021;9(4):389.

   doi: 10.3390/biomedicines9040389

10. Zeng S, Pöttler M, Lan B, Grützmann R, Pilarsky C, Yang H. Chemoresistance in pancreatic cancer. *Int J Mol Sci*. 2019;20(18):4504.

    doi: 10.3390/ijms20184504

11. Hughes J, Rees S, Kalindjian S, Philpott K. Principles of early drug discovery. *Br J Pharmacol*. 2011;162(6):1239-1249.

    doi: 10.1111/j.1476-5381.2010.01127.x

12. Weaver MF, Hopper JA, Gunderson EW. Designer drugs 2015: Assessment and management. *Addict Sci Clin Pract*. 2015;10(1):8.

    doi: 10.1186/s13722-015-0024-7

13. Zhan YP, Chen BS. Drug target identification and drug repurposing in psoriasis through systems biology approach, DNN-based DTI model and genome-wide microarray data. *Int J Mol Sci*. 2023;24(12):10033.

doi: 10.3390/ijms241210033

14. Wang CT, Chen BS. Drug discovery for periodontitis treatment based on big data mining, systems biology, and deep learning methods. *SynBio*. 2023;1(1):116-143.

doi: 10.3390/synbio1010009

15. Hsu BW, Chen BS. Genetic and epigenetic host-virus network to investigate pathogenesis and identify biomarkers for drug repurposing of human respiratory syncytial virus via real-world two-side RNA-Seq data: Systems biology and deep-learning approach. *Biomedicines*. 2023;11(6):1531.

doi: 10.3390/biomedicines11061531

16. Lin YC, Chen BS. Identifying drug targets of oral squamous cell carcinoma through a systems biology method and genome-wide microarray data for drug discovery by deep learning and drug design specifications. *Int J Mol Sci*. 2022;23(18):10409.

doi: 10.3390/ijms231810409

17. Kulkarni VS, Alagarsamy V, Solomon VR, Jose PA, Murugesan S. Drug repurposing: An effective tool in modern drug discovery. *Russ J Bioorg Chem*. 2023;49(2):157-166.

doi: 10.1134/s1068162023020139

18. Salwinski L, Miller CS, Smith AJ, Pettit FK, Bowie JU, Eisenberg D. The database of interacting proteins: 2004 update. *Nucleic Acids Res*. 2004;32(suppl_1):D449-D451.

doi: 10.1093/nar/gkh086

19. Orchard S, Ammari M, Aranda B, *et al*. The MIntAct project--IntAct as a common curation platform for 11 molecular interaction databases. *Nucleic Acids Res*. 2013;42(D1):D358-D363.

doi: 10.1093/nar/gkt1115

20. Stark C, Breitkreutz BJ, Reguly T, Boucher L, Breitkreutz A, Tyers M. BioGRID: A general repository for interaction datasets. *Nucleic Acids Res*. 2006;34(suppl_1):D535-D539.

doi: 10.1093/nar/gkj109

21. Zanzoni A, Montecchi-Palazzi L, Quondam M, Ausiello G, Helmer-Citterich M, Cesareni G. MINT: A molecular INTeraction database. *FEBS Lett*. 2002;513(1):135-140.

doi: 10.1016/S0014-5793(01)03293-8

22. Bovolenta LA, Acencio ML, Lemke N. HTRIdb: An open-access database for experimentally verified human transcriptional regulation interactions. *BMC Genomics*. 2012;13(1):405.

doi: 10.1186/1471-2164-13-405

23. Zheng G, Tu K, Yang Q, *et al*. ITFP: An integrated platform of mammalian transcription factors. *Bioinformatics*. 2008;24(20):2416-2417.

doi: 10.1093/bioinformatics/btn439

24. Wingender E, Chen X, Hehl R, *et al*. TRANSFAC: An integrated system for gene expression regulation. *Nucleic Acids Res*. 2000;28(1):316-319.

doi: 10.1093/nar/28.1.316

25. Friard O, Re A, Taverna D, De Bortoli M, Corá D. CircuitsDB: A database of mixed microRNA/transcription factor feed-forward regulatory circuits in human and mouse. *BMC Bioinformatics*. 2010;11(1):435.

doi: 10.1186/1471-2105-11-435

26. Agarwal V, Bell GW, Nam JW, Bartel DP. Predicting effective microRNA target sites in mammalian mRNAs. *Elife*. 2015;4:e05005.

doi: 10.7554/eLife.05005

27. Li JH, Liu S, Zhou H, Qu LH, Yang JH. StarBase v2.0: Decoding miRNA-ceRNA, miRNA-ncRNA and protein-RNA interaction networks from large-scale CLIP-Seq data. *Nucleic Acids Res*. 2013;42(D1):D92-D97.

doi: 10.1093/nar/gkt1248

28. Chen BS, Wu CC. Systems biology as an integrated platform for bioinformatics, systems synthetic biology, and systems metabolic engineering. *Cells*. 2013;2(4):635-688.

doi: 10.3390/cells2040635

29. Sakamoto Y, Ishiguro M, Kitagawa G. Akaike information criterion statistics. *Dordrecht Netherlands D Reidel*. 1986;81(10.5555):26853.

30. Chang S, Wang LHC, Chen BS. Investigating core signaling pathways of hepatitis b virus pathogenesis for biomarkers identification and drug discovery via systems biology and deep learning method. *Biomedicines*. 2020;8(9):320.

doi: 10.3390/biomedicines8090320

31. Kanehisa M, Goto S. KEGG: Kyoto encyclopedia of genes and genomes. *Nucleic Acids Res*. 2000;28(1):27-30.

doi: 10.1093/nar/28.1.27

32. Wang Y, Zhang S, Li F, *et al*. Therapeutic target database 2020: Enriched resource for facilitating research and early development of targeted therapeutics. *Nucleic Acids Res*. 2019;48(D1):D1031-D1041.

doi: 10.1093/nar/gkz981

33. Consortium TU. UniProt: A hub for protein information. *Nucleic Acids Res*. 2014;43(D1):D204-D212.

doi: 10.1093/nar/gku989

34. Knox C, Law V, Jewison T, *et al*. DrugBank 3.0: A comprehensive resource for 'Omics' research on drugs. *Nucleic Acids Res*. 2010;39(suppl_1):D1035-D1041.

doi: 10.1093/nar/gkq1126

35. Kim S, Thiessen PA, Bolton EE, *et al*. PubChem substance and compound databases. *Nucleic Acids Res*. 2015;44(D1):D1202-D1213.

doi: 10.1093/nar/gkv951

36. Gaulton A, Hersey A, Nowotka M, *et al*. The ChEMBL database in 2017. *Nucleic Acids Res*. 2016;45(D1):D945-D954.

doi: 10.1093/nar/gkw1074

37. Kuhn M, von Mering C, Campillos M, Jensen LJ, Bork P. STITCH: Interaction networks of chemicals and proteins. *Nucleic Acids Res*. 2007;36(suppl_1):D684-D688.

doi: 10.1093/nar/gkm795

38. Ringnér M. What is principal component analysis? *Nat Biotechnol*. 2008;26(3):303-304.

doi: 10.1038/nbt0308-303

39. Huber M, Brehm CU, Gress TM, *et al*. The immune microenvironment in pancreatic cancer. *Int J Mol Sci*. 2020;21(19):7307.

doi: 10.3390/ijms21197307

40. Truong LH, Pauklin S. Pancreatic cancer microenvironment and cellular composition: Current understandings and therapeutic approaches. *Cancers* (*Basel*). 2021;13(19):5028.

doi: 10.3390/cancers13195028

41. Cortesi M, Zanoni M, Pirini F, *et al*. Pancreatic cancer and cellular senescence: Tumor microenvironment under the spotlight. *Int J Mol Sci*. 2022;23(1):254.

doi: 10.3390/ijms23010254

42. Arneth B. Tumor microenvironment. *Medicina* (*Kaunas*). 2020;56(1):15.

doi: 10.3390/medicina56010015

43. Stopa KB, Kusiak AA, Szopa MD, Ferdek PE, Jakubowska MA. Pancreatic cancer and its microenvironment-recent advances and current controversies. *Int J Mol Sci*. 2020;21(9):3218.

doi: 10.3390/ijms21093218

44. Javadrashid D, Baghbanzadeh A, Derakhshani A, *et al*. Pancreatic cancer signaling pathways, genetic alterations, and tumor microenvironment: The barriers affecting the method of treatment. *Biomedicines*. 2021;9(4):373.

doi: 10.3390/biomedicines9040373

45. Ma Y, Shen N, Wicha MS, Luo M. The roles of the let-7 family of MicroRNAs in the regulation of cancer stemness. *Cells*. 2021;10(9):2415.

doi: 10.3390/cells10092415

46. Hessmann E, Schneider G, Ellenrieder V, Siveke JT. MYC in pancreatic cancer: Novel mechanistic insights and their translation into therapeutic strategies. *Oncogene*. 2016;35(13):1609-1618.

doi: 10.1038/onc.2015.216

47. Wolfer A, Ramaswamy S. MYC and metastasis. *Cancer Res*. 2011;71(6):2034-2037.

doi: 10.1158/0008-5472.Can-10-3776

48. Liu YH, Gan YX, Chen JZ, Jiang YX, Huang F, Tang D. Targeting MYC to combat pancreatic cancer. *J Explor Rese Pharmacol*. 2022;7(3):164-178.

doi: 10.14218/jerp.2021.00015

49. Wirth M, Mahboobi S, Krämer OH, Schneider G. Concepts to target MYC in pancreatic cancer. *Mol Cancer Ther*. 2016;15(8):1792-1798.

doi: 10.1158/1535-7163.Mct-16-0050

50. Ala M. Target c-Myc to treat pancreatic cancer. *Cancer Biol Ther*. 2022;23(1):34-50.

doi: 10.1080/15384047.2021.2017223

51. Farrell AS, Joly MM, Allen-Petersen BL, *et al*. MYC regulates ductal-neuroendocrine lineage plasticity in pancreatic ductal adenocarcinoma associated with poor outcome and chemoresistance. *Nature Commun*. 2017;8(1):1728.

doi: 10.1038/s41467-017-01967-6

52. Fujiwara-Tani R, Sasaki T, Bhawal UK, *et al*. Nuclear MAST4 suppresses FOXO3 through interaction with AKT3 and induces chemoresistance in pancreatic ductal carcinoma. *Int J Mol Sci*. 2024;25(7):4056.

doi: 10.3390/ijms25074056

53. Luo X, Yang Z, Liu X, *et al*. The clinicopathological significance of forkhead box P1 and forkhead box O3a in pancreatic ductal adenocarcinomas. *Tumor Biol*. 2017;39(5):1010428317699129.

doi: 10.1177/1010428317699129

54. Feng S, Jiang ZJ, Yu D, Li J, Liu G, Sun JJ. FOXO3a expression and its diagnostic value in pancreatic ductal adenocarcinoma. *Int J Clin Exp Pathol*. 2018;11(11):5422-5429.

55. Yu S, Yu Y, Sun Y, *et al*. Activation of FOXO3a suggests good prognosis of patients with radically resected gastric cancer. *Int J Clin Exp Pathol*. 2015;8(3):2963-2970.

56. McCubrey JA, Yang LV, Abrams SL, *et al*. Effects of TP53 mutations and mirs on immune responses in the tumor microenvironment important in pancreatic cancer progression. *Cells*. 2022;11(14):2155.

doi: 10.3390/cells11142155

57. Stefanoudakis D, Frountzas M, Schizas D, Michalopoulos NV, Drakaki A, Toutouzas KG. Significance of TP53, CDKN2A, SMAD4 and KRAS in pancreatic cancer. *Curr Issues Mol Biol*. 2024;46(4):2827-2844.

doi: 10.3390/cimb46040177

58. Subramanian A, Narayan R, Corsello SM, *et al*. A next

generation connectivity map: L1000 platform and the first 1,000,000 profiles. *Cell*. 2017;171(6):1437-1452.e17.

doi: 10.1016/j.cell.2017.10.049

59. Corsello SM, Nagari RT, Spangler RD, *et al*. Discovering the anti-cancer potential of non-oncology drugs by systematic viability profiling. *Nat Cancer*. 2020;1(2):235-248.

doi: 10.1038/s43018-019-0018-6

60. Xiong G, Wu Z, Yi J, *et al*. ADMETlab 2.0: An integrated online platform for accurate and comprehensive predictions of ADMET properties. *Nucleic Acids Res*. 2021;49(W1):W5-W14.

doi: 10.1093/nar/gkab255

61. Amrutkar M, Gladhaug IP. Pancreatic cancer chemoresistance to gemcitabine. *Cancers* (*Basel*). 2017;9(11):157.

doi: 10.3390/cancers9110157

62. Adamska A, Domenichini A, Falasca M. Pancreatic ductal adenocarcinoma: Current and evolving therapies. *Int J Mol Sci*. 2017;18(7):1338.

doi: 10.3390/ijms18071338

63. Coppola A, Farolfi T, La Vaccara V, *et al*. Neoadjuvant treatments for pancreatic ductal adenocarcinoma: Where we are and where we are going. *J Clin Med*. 2023;12(11):3677.

doi: 10.3390/jcm12113677

64. Kielb SJ, Shah NL, Rubin MA, Sanda MG. Functional p53 mutation as a molecular determinant of paclitaxel and gemcitabine susceptibility in human bladder cancer. *J Urol*. 2001;166(2):482-487.

65. Hill R, Rabb M, Madureira PA, *et al*. Gemcitabine-mediated tumour regression and p53-dependent gene expression: Implications for colon and pancreatic cancer therapy. *Cell Death Dis*. 2013;4(9):e791.

doi: 10.1038/cddis.2013.307

66. Achanta G, Pelicano H, Feng L, Plunkett W, Huang P. Interaction of p53 and DNA-PK in response to nucleoside analogues: Potential role as a sensor complex for DNA damage. *Cancer Res*. 2001;61(24):8723-8729.

67. Cao P, Zhang W, Qiu J, Tang Z, Xue X, Feng T. Gemcitabine inhibits the progression of pancreatic cancer by restraining the WTAP/MYC chain in an m6A-dependent manner. *Cancer Res Treat*. 2024;56(1):259-271.

doi: 10.4143/crt.2022.1600

68. Yao J, Huang M, Shen Q, *et al*. c-Myc-PD-L1 axis sustained gemcitabine-resistance in pancreatic cancer. *Front Pharmacol*. 2022;13:851512.

doi: 10.3389/fphar.2022.851512

69. Ebrahimi S, Hosseini M, Shahidsales S, *et al*. Targeting the Akt/PI3K signaling pathway as a potential therapeutic strategy for the treatment of pancreatic cancer. *Curr Med Chem*. 2017;24(13):1321-1331.

doi: 10.2174/0929867324666170206142658

70. Konopleva MY, Walter RB, Faderl SH, *et al*. Preclinical and early clinical evaluation of the oral AKT inhibitor, MK-2206, for the treatment of acute myelogenous leukemia. *Clin Cancer Res*. 2014;20(8):2226-2235.

doi: 10.1158/1078-0432.Ccr-13-1978

71. Simioni C, Martelli AM, Cani A, *et al*. The AKT inhibitor MK-2206 is cytotoxic in hepatocarcinoma cells displaying hyperphosphorylated AKT-1 and synergizes with conventional chemotherapy. *Oncotarget*. 2013;4(9):1496-1506.

doi: 10.18632/oncotarget.1236

72. Hirai H, Sootome H, Nakatsuru Y, *et al*. MK-2206, an allosteric akt inhibitor, enhances antitumor efficacy by standard chemotherapeutic agents or molecular targeted drugs *in vitro* and *in vivo*. *Mol Cancer Ther*. 2010;9(7):1956-1967.

doi: 10.1158/1535-7163.Mct-09-1012

73. Yap TA, Yan L, Patnaik A, *et al*. First-in-man clinical trial of the oral pan-AKT inhibitor MK-2206 in patients with advanced solid tumors. *J Clin Oncol*. 2011;29(35):4688-4695.

doi: 10.1200/jco.2011.35.5263

74. Wang Z, Luo G, Qiu Z. Akt inhibitor MK-2206 reduces pancreatic cancer cell viability and increases the efficacy of gemcitabine. *Oncol Lett*. 2020;19(3):1999-2004.

doi: 10.3892/ol.2020.11300

75. Elnaggar MS, Sminia P, Shehata S, Fedrigo C, Peters G. 1676P - gemcitabine, PI3kinase-Akt pathway inhibition and radiation in human glioma cell lines. *Ann Oncol*. 2012;23:ix537.

doi: 10.1016/S0923-7534(20)34222-8

ACCSCIENCE PUBLISHING

Tumor Discovery

ORIGINAL RESEARCH ARTICLE

Molecular characterization of colorectal cancer: Insights from miRNA, mRNA, and protein analysis

Hersh Abdul Ham-Karim[1]*, Narmeen Ahmad[2], Alan Shwan[3], and Mohammad Ilyas[4]

[1]Department of Dentistry, College of Medicine, Komar University of Science and Technology, Chaq-Chaq-Qualaraisi, Sulaimani City, Iraq

[2]Kurdistan Institution for Strategic Studies and Scientific Research, Qirga, Sulaimani, KRG, Iraq

[3]Department of Medical Laboratory Analysis, College of Medical Science, Cihan University, Sulaimani, Iraq

[4]Nottingham Molecular Pathology Node, University of Nottingham, Nottingham, United Kingdom

(This article belongs to the *Special Issue: Colorectal Cancer: Best Tools for Diagnosis to Management Strategies*)

Abstract

Recent research highlights the significant roles of microRNAs (miRNAs) in various diseases, particularly cancer, where they serve as diagnostic and prognostic markers. This study focuses on colorectal cancer (CRC) by examining the expression of six specific miRNAs, miR-20a, miR-21, miR-29a, miR-31, miR-92a, and miR-224, in 81 tumor samples compared to matched normal tissues. We assessed the expression levels of six target genes, *SMAD4*, *PTEN*, *TGFBRII*, *BCL2*, *KLF4*, and *RASA1*, using reverse transcription quantitative polymerase chain reaction and immunohistochemistry. Our results indicated a significant upregulation of miR-20a, miR-21, miR-29a, and miR-31 in tumor samples, alongside a decrease in *TGFBRII* mRNA expression. Correlation analyses demonstrated that high levels of miR-20a were inversely related to both mRNA and protein levels of PTEN. Elevated expressions of miR-21 and miR-224 were associated with lower mRNA and protein levels of TGFBRII. Furthermore, increased levels of miR-29a and miR-31 showed an inverse relationship with mRNA and protein levels of RASA1. These findings suggest a strong link between upregulated miRNAs and downregulated target genes, indicating their significant roles in CRC carcinogenesis. Notably, the upregulation of miR-20a, miR-21, miR-29a, and miR-31 may serve as effective biomarkers for differentiating CRC from normal mucosa, potentially enhancing screening strategies in the general population.

Keywords: Colorectal cancer; microRNA; mRNA; Immunohistochemistry

***Corresponding author:**
Hersh Abdul Ham-Karim
(hersh.abdul@komar.edu.iq)

Citation: Ham-Karim H, Ahmad N, Shwan A, Ilyas M. Molecular characterization of colorectal cancer: Insights from miRNA, mRNA, and protein analysis. *Tumor Discov*. 2025;4(1):68-78. doi: 10.36922/td.4631

Received: August 22, 2024

1st revised: October 22, 2024

2nd revised: November 2, 2025

Accepted: November 7, 2024

Published online: November 28, 2024

1. Introduction

Colorectal cancer (CRC) stands as a prominent gastrointestinal malignancy globally, with more than 1.2 million new cases reported annually. It holds the position of being the third most common cancer worldwide and significantly contributes to cancer-

related deaths.[1] In recent years, there has been a notable emergence of new favorable subsets of cancers of unknown primary origin, including CRC of unknown origin. This new clinical entity is treated as CRC and has contributed to the rising incidence rates of CRC. Understanding these trends is crucial, as they may influence the sociodemographic factors and clinical aspects that ultimately affect the quality of life in patients undergoing surgical treatment for CRC.[2] There is significant evidence affirming the vital role of screening and early detection in combating CRC, effectively reducing its incidence and mortality rates.[3] For example, the 5-year survival rate is as high as 93.2% for TNM stage I as compared to only 8.1% for stage IV.[4] However, existing screening tools such as (i) colonoscopy screening, which is currently the most reliable screening tool, has been hampered because of its invasive nature and high cost; and (2) the fecal occult blood test, which has low sensitivity and requires dietary restriction, impedes compliance and use. In addition, studies have investigated several molecular biomarkers for CRC detection, such as carcinoembryonic antigen (CEA), and shown that high CEA levels are associated with CRC progression. However, its utility in the disease screening is limited due to the serum level of CEA not being elevated after the tumor has invaded the serosa membrane.[5,6]

Given these factors, there is a pressing need for specific molecular markers to improve the diagnosis of CRC. Recently, researchers have concentrated on microRNAs (miRNAs) because of their involvement in essential cellular processes such as development, cell cycle advancement, differentiation, proliferation, and apoptosis.[7] Aberrant expression of miRNAs, which function as either tumor suppressors or oncogenes, has been implicated in various cancers. Moreover, miRNAs exhibit discriminatory potential across cancer types, predicting outcomes in hematological and solid malignancies.[8] Notably, the differential expression of miRNAs between CRC tumors and adjacent normal tissue underscores their promise in early diagnostic and prognostic applications.[9]

Biomarker testing is now a standard part of CRC investigation, particularly regarding major genetic mutations like RAS, which are associated with tumor aggressiveness and chemotherapy response. In addition, growing evidence indicates that inflammation contributes to CRC progression, prompting studies on the predictive and prognostic roles of various blood-based inflammatory markers, such as the neutrophil–lymphocyte ratio, lymphocyte–monocyte ratio, and platelet–lymphocyte ratio. Furthermore, miRNAs act as both tumor suppressors and oncogenes, with ongoing research exploring their diagnostic, prognostic, and predictive implications. For instance, FOLFOX resistance in advanced CRC is linked to the altered expression of serum miRNAs, such as miR-19a. In metastatic CRC, miR-126 upregulation has been associated with resistance to bevacizumab, while overexpression of miR-31, miR-100, and miR-125b, along with miR-7 downregulation, correlates with resistance to cetuximab.[10]

In this study, we have selected a panel of six miRNAs (miR-20a, miR-21, miR-29a, miR-31, miR-92a, and miR-224), previously implicated in CRC and proposed as diagnostic and prognostic markers. These miRNAs have shown promise in CRC research, with multiple studies highlighting their dysregulation and potential clinical significance.[11-16] For instance, Sun *et al.*[17] showed that miR-31 significantly contributes to the activation of the RAS signaling pathway by inhibiting the translation of RASA1. This action enhances the growth of CRC cells and promotes tumor development. MiR-92a has been found to be upregulated in CRC and associated with tumor growth, migration and invasion via suppression of PTEN.[18] MiR-29a has been associated with CRC progression and poor prognosis, acting by downregulating genes involved in apoptosis and extracellular matrix remodeling.[19] Our experiments suggest that miR-20a disrupts the homeostasis of the colonic epithelium by interfering with the regulation of Myc/p21 by transforming growth factor beta (TGF-β), a process that is crucial for malignant transformation.[20] Colorectal tumors with elevated levels of miR-21 exhibited microsatellite instability and demonstrated a diminished response to 5-fluorouracil-based chemotherapy,[21] Our investigation aims to elucidate whether this miRNA panel: (i) orchestrates the activation of common signaling pathways pivotal in CRC carcinogenesis, as gauged by mRNA and protein expression levels of genes targeted by these miRNAs, and (ii) holds potential as screening biomarkers for CRC.

2. Methods

2.1. Selection criteria

In this study, we utilized paired formalin-fixed paraffin-embedded (FFPE) cases, consisting of primary CRC tissues and corresponding normal mucosa samples obtained from 81 patients. The normal tissue specimens comprised margin blocks and tissue immediately adjacent to the tumor, exclusively sourced from mucosal tissue. All patients underwent surgical procedures at Queen's Medical Centre (QMC) in Nottingham, United Kingdom, between 2012 and 2014. Case selection criteria included the availability of comprehensive clinicopathological data and the presence of at least 50% tumor cells in the tumor block. Notably, all tissue samples analyzed in this study

originated from adenocarcinomas and were acquired through surgical interventions.

2.2. Macrodissection

To mitigate potential confounding effects from stromal cells, tumor specimens underwent macrodissection following evaluation by a pathologist to ensure a minimum of 50% tumor tissue content, as recommended in literature.[22] Two 20 μm-thick serial sections were excised from each paraffin block. After identifying tumor regions on unstained sections from hematoxylin–eosin-stained slides, macrodissection was carried out. Total RNA and miRNA were subsequently isolated using the miRNeasy FFPE kit (Qiagen, Hilden, Germany).

2.3. Quantitative reverse-transcription polymerase chain reaction (RT-qPCR)

After synthesizing cDNA with the miScript II RT Kit and the QuantiTec Reverse Transcription Kit (Qiagen, Hilden, Germany) for miRNA and mRNA, respectively, the targeted genes were quantified using the miScript SYBR Green PCR kit (Qiagen) on a 7500 Fast Real-Time PCR System (Applied Biosystems, Thermo Fisher, USA). The primer sequences and their efficiencies, determined through assay optimization, are provided in Supplementary File. The ΔΔCt method was employed for relative quantification of mRNA, comparing miRNA and mRNA expression in normal versus CRC tissues. RNU6B and HPRT were used as reference genes for miRNA and mRNA, respectively.[23,24]

2.4. Evaluation of protein expression

2.4.1. Immunohistochemistry

2.4.1.1. TMA

After validating antibody specificity and determining optimal concentrations, we assessed protein expression in CRC tissue using Tissue Microarray (TMA) sections. Western blotting analysis confirmed the specificity of the antibodies (Supplementary file Figure S1). TMAs facilitate high-throughput evaluation of biomarker expression across numerous tissue samples, comprising paraffin blocks with minute tissue specimens arranged in an array configuration. The antibodies employed are listed in Supplementary File. TMA sections were prepared at the Nottingham Health Science Biobank, QMC, Nottingham, UK. We stained 4-μm paraffin-embedded CRC TMA sections using Novolink Polymer Detection Systems (Leica Microsystems, Germany) with anti-SMAD4, anti-KLF4, anti-RASA1, anti-PTEN, anti-TGFBRII, and anti-BCL2 antibodies. Each run included positive and negative controls to validate experimental success. Detailed immunohistochemistry staining procedures are provided in Supplementary File.

2.4.1.2. Assessment of protein expression

Following initial validation under a light microscope, TMA slides were scanned at 20× magnification using a Nanozoomer Digital Pathology scanner (Hamamatsu Photonics, Japan). Protein expression in tumor cells was assessed semi-quantitatively using the H-score method, which combines the percentage of positive tumor cells with staining intensity (0 for negative, 1 for weak, 2 for moderate, and 3 for strong staining).[25] To ensure consistency, all slides underwent independent evaluation by a second scorer, and the intraclass correlation coefficient (ICC) was employed to assess inter-scorer agreement.

2.5. Statistical analysis

Statistical analysis was conducted using the SPSS version 22 software package (IBM acquired SPSS Inc. USA). Categorical data were assessed for statistical significance using the Chi-square test, while continuous data were analyzed for differences between datasets using the Wilcoxon test. Fisher's exact test was employed to explore associations between unpaired tumor groups. Spearman's correlation was used to detect correlations between targets. For multiple corrections testing, the Bonferroni step-down (Holm) correction was applied. In both statistical analyses, $P < 0.05$ was considered statistically significant. In this study, we used the Wilcoxon test, a non-parametric method robust to outliers and suitable for non-normally distributed data. Outliers, identified as data points outside the 10th and 90th percentiles in Figure 1, were retained in the analysis without additional transformation or removal. This approach provides an accurate representation of the dataset, accommodating natural data variation without the influence of strict distributional assumptions.

3. Results

3.1. MiRNA quantification

3.1.1. Cutoff point for miRNAs detection

Before analyzing mRNA expression levels, we sought to establish a cutoff point to distinguish high and low expression levels. Initially, RNA was extracted from 20 individual pure normal colon tissues and pooled with equal volumes. Subsequently, the expression levels of all miRNAs and mRNAs were assessed in each normal colon tissue sample compared to the pooled sample. On average, the minimum fold expression for all mRNAs in normal colon tissues was 0.6, while the maximum was 1.8. Downregulation was defined as <0.6 fold, and upregulation as >1.8 fold. This method provided a robust benchmark for distinguishing between high and low mRNA expression in subsequent analyses. For the miRNAs, the average minimum fold change in expression for all miRNAs in

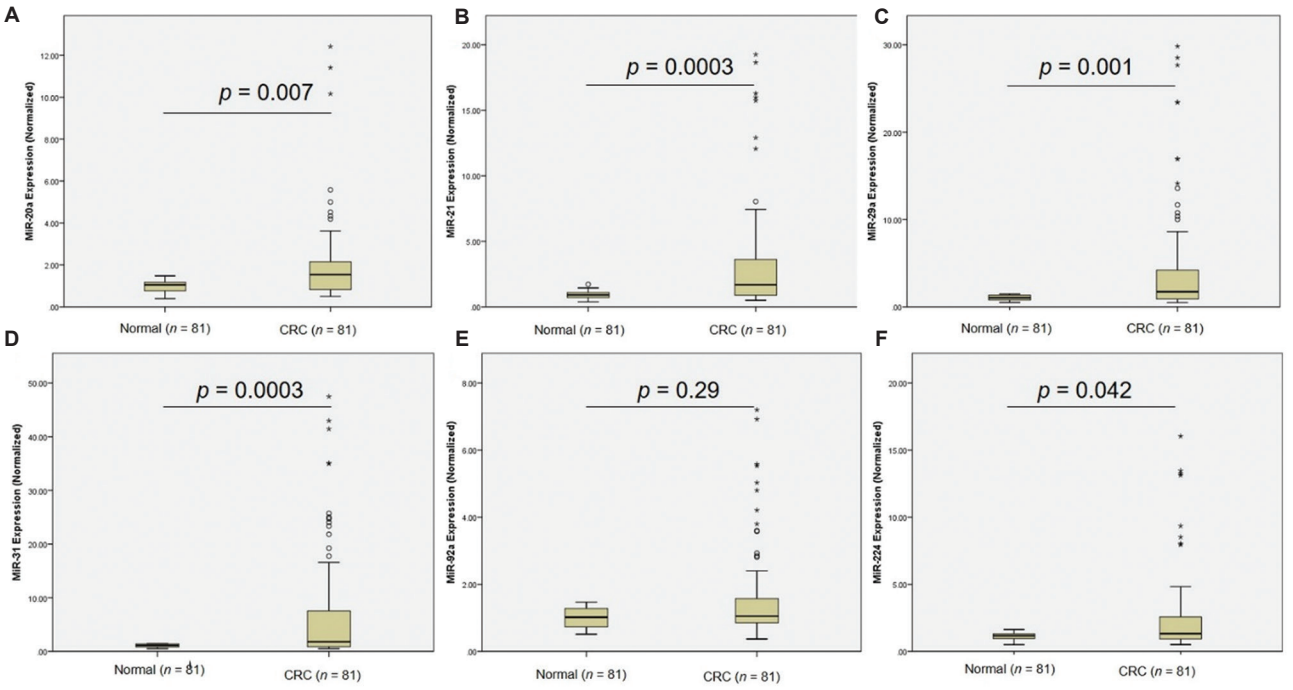

Figure 1. miRNA selection and validation by quantitative reverse-transcription polymerase chain reaction analysis. Box plots of plasma levels of (A) miR-20a, (B) miR-21 (C) miR29a, (D) miR-31, (E) miR-92a and (F) miR-224 in healthy normal subjects (n = 81) and patients with colorectal cancer (n = 81). Expression levels of the miRNAs (log10 scale at y-axis) are normalized to *RNU6B*. The lines inside the boxes denote the medians. The boxes mark the interval between the 25th and 75th percentiles. The whiskers denote the interval between the 10th and 90th percentiles. Filled circles indicate data points outside the 10th and 90th percentiles. Statistically significant differences were determined using Wilcoxon tests. Open circle and asterisks represent data points that are outside the 10th and 90th percentiles. These are often referred to as outliers, indicating individual measurements that fall significantly outside the typical range for the respective groups.
Abbreviation: miRNA: MicroRNA.

normal colon tissue was 0.5, while the maximum was 1.5 (with values below 0.5 indicating downregulation and those above 1.5 indicating upregulation).

3.1.2. miRNA quantification by real-time RT-qPCR

To measure the expression of miRNAs including (miR-20a, 21, 29a, 31, 92a and 224), the study screened miRNA levels in 81 CRC samples and matched normal mucosa through RT-qPCR assay, normalized to *RNU6B*. All assays were done in triplicate and the cycle threshold (Ct) value of all targets in all samples were <27 (range 16.1 – 26.8) with standard deviation (SD) < 0.5 between replicates Ct value. The miRNAs with significantly different expression in the CRC samples compared with the normal mucosa were identified by Wilcoxon test (because data are not normally distributed), with an expression fold >1.5. Among the studied miRNAs, four exhibited notably higher expression levels in CRC samples compared to normal mucosa (Figure 1): miR-31 demonstrated an average 10.83-fold higher expression in CRC than in adjacent normal colon tissue (fold range: 0.52 – 161.69, P = 0.0003); miR-29a showed an average 8.11-fold higher expression in CRC compared to adjacent normal colon tissue (fold range: 0.52 – 108.36, P = 0.001); miR-21 displayed a 6.42-fold higher expression in CRC than in normal tissue (fold range: 0.5 – 63.84, P = 0.0003); and miR-20a exhibited a 3.27-fold higher expression in CRC than in normal tissue (fold range: 0.53 – 109.16, P = 0.007). In addition, miR-92a showed a 2.2-fold higher expression in CRC than in normal tissue (fold range: 0.37 – 34.8, P = 0.2), and miR-224 exhibited a 2.68-fold higher expression in CRC than in normal tissue (fold range: 0.51 – 19.35, P = 0.042). However, after applying the Bonferroni correction for multiple testing, miR-224 lost statistical significance (P = 0.22), while significance persisted for miR-20a (P = 0.04), miR-21 (P = 0.001), miR-29a (P = 0.006), and miR-31 (P = 0.001) (Table 1).

3.1.3. Association of the expression of biomarkers and clinicopathological variables

Pearson's Chi-square test was applied to identify association between miRNAs and clinicopathological features, and the results showed that normal miRNA92a expression was associated with grade two (χ^2 = 7.037, d.f. = 2, P = 0.03). High miRNA21 expression was associated with Duke's B stage (χ^2 = 6.115, d.f. = 2, P = 0.04). However,

Table 1. Expression profiles of candidate microRNAs

Gene	Fold of change	*P*	*P*-value of Bonferroni correction test
miRNA20a	3.27	0.007	0.04
miRNA21	6.42	0.003	0.001
miRNA29a	8.11	0.001	0.006
miRNA31	10.83	0.003	0.001
miRNA92a	2.2	0.29	0.87
miRNA224	2.68	0.042	0.22

following multiple correction testing using the Bonferroni correction, they both failed to retain significance ($P = 0.28$ and $P = 0.36$, respectively) (Table 2).

3.2. mRNA quantification by real-time RT-qPCR

Significant differences in mRNA expression between CRC samples and normal mucosa were identified through a paired *t*-test. Downregulation was defined as <0.6 fold, while upregulation was set at >1.8 fold. All assays were meticulously conducted in triplicate, and replicates with a Ct standard deviation >0.5 were excluded to ensure data integrity. Among the six examined targets, *RASA1* ($P = 0.002$, fold change of 0.66 ± SD 0.74, 95% confidence interval [CI] 0.5 – 0.82) and *TGFBRII* ($P = 0.0001$, fold change of 0.46 ± SD 0.78, 95% CI 0.29 – 0.63) exhibited significantly lower expression levels in tumor samples compared to normal tissues. Conversely, *BCL2* showed a significantly higher expression level ($P = 0.05$, fold change of 3.72 ± SD 8.2, 95% CI 1.93 – 5.53). For *SMAD4* ($P = 0.12$, fold change of 0.98 ± SD 0.92, 95% CI 0.78 – 1.18), *PTEN* ($P = 0.22$, fold change of 0.97 ± SD 0.91, 95% CI 0.77 – 1.17), and *KLF4* ($P = 0.8$, fold change of 1.16 ± SD 1.6, 95% CI 0.81 – 1.51), mRNA expression levels were relatively similar in tumor and normal tissues. However, after meticulous multiple correction testing using the Bonferroni correction, *RASA1* and *TGFBRII* retained significance ($P = 0.01$ and $P = 0.006$, respectively), highlighting their robust association with CRC. Conversely, *BCL2* failed to maintain statistical significance ($P = 0.2$) (Table 3).

3.3. Protein evaluation

3.3.1. Optimization of primary antibodies for immunohistochemical staining

Before conducting immunohistochemical staining on CRC tissues, we validated the specificity of antibodies against SMAD4, TGFBRII, RASA1, and KLF4 through Western blotting. These antibodies target proteins with molecular weights of 65 kDa (SMAD4), 75 kDa (TGFBRII), 140 kDa (RASA1), and 55 kDa (KLF4). Western blotting confirmed the presence of the

Table 2. Association between microRNAs expression and clinicopathological variables

Variable	miRNA expression		*P*	*P*-value of Bonferroni correction test
	Normal (%)	High (%)		
miR-20a				
Tumor grade				
Well	1 (2.6)	1 (2.3)	0.8	0.2
Good	34 (89.5)	40 (93.0)		
Poor	3 (7.9)	2 (4.7)		
Nodal state				
pN 0	21 (55.3)	29 (67.4)	0.3	0.7
pN I	12 (31.6)	12 (27.9)		
pN II	5 (13.2)	2 (4.7)		
Dukes' stage				
A	5 (13.2)	7 (16.3)	0.5	0.9
B	16 (42.1)	22 (51.2)		
C	17 (44.7)	14 (32.6)		
EMVI				
0	15 (39.5)	26 (60.5)	0.1	0.3
1	22 (57.9)	16 (37.2)		
2	1 (2.6)	1 (2.3)		
miR-21				
Tumor grade				
Well	2 (6.3)	0 (0.0)	0.1	0.3
Good	29 (90.6)	45 (91.8)		
Poor	1 (3.1)	4 (8.2)		
Nodal state				
pN 0	15 (46.9)	35 (71.4)	0.08	0.2
pN I	13 (40.6)	11 (22.4)		
pN II	4 (12.5)	3 (6.1)		
Dukes' stage				
A	2 (6.3)	10 (20.4)	0.04	0.1
B	13 (40.6)	25 (51.0)		
C	17 (53.1)	14 (28.6)		
EMVI				
0	12 (37.5)	29 (59.2)	0.05	0.1
1	20 (62.5)	18 (36.7)		
2	0 (0.0)	2 (4.1)		
miR-29a				
Tumor grade				
Well	1 (2.8)	1 (2.2)	0.9	0.9
Good	33 (91.7)	41 (91.1)		
Poor	2 (5.6)	3 (6.7)		

(Cont'd...)

Table 2. *(Continued)*

Variable	miRNA expression		*P*	*P*-value of Bonferroni correction test
	Normal (%)	High (%)		
Nodal state				
pN 0	22 (61.1)	28 (62.2)	0.6	0.9
pN I	12 (33.3)	12 (26.7)		
pN II	2 (5.6)	5 (11.1)		
Dukes' stage				
A	4 (11.1)	8 (17.8)	0.6	0.9
B	18 (50.0)	20 (44.4)		
C	14 (38.9)	17 (37.8)		
EMVI				
0	19 (52.8)	22 (48.9)	0.4	0.8
1	17 (47.2)	21 (46.7)		
2	0 (0.0)	2 (4.4)		
miR-31				
Tumor grade				
Well	1 (2.9)	1 (2.1)	0.1	0.3
Good	29 (85.3)	45 (95.7)		
Poor	4 (11.8)	1 (2.1)		
Nodal state				
pN 0	22 (64.7)	28 (59.6)	0.1	0.3
pN I	7 (20.6)	17 (36.2)		
pN II	5 (14.7	2 (4.3)		
Dukes' stage				
A	2 (5.9)	10 (21.3)	0.1	0.3
B	19 (55.9)	19 (40.4)		
C	13 (38.2)	18 (38.3)		
EMVI				
0	14 (41.2)	27 (57.4)	0.3	0.7
1	19 (55.9)	19 (40.4)		
2	1 (2.9)	1 (2.1)		
miR-92a				
Tumor grade				
Well	1 (1.8)	1 (4.2)	0.03	0.2
Good	55 (96.5)	19 (79.2)		
Poor	1 (1.8)	4 (16.7)		
Nodal state				
pN 0	38 (66.7)	12 (50.0)	0.2	0.6
pN I	14 (24.6)	10 (41.7)		
pN II	5 (8.8)	2 (8.3)		
Dukes' stage				
A	9 (15.8)	3 (12.5)	0.3	0.7
B	29 (50.9)	9 (37.5)		
C	19 (33.3)	12 (50.0)		
EMVI				
0	31 (54.4)	10 (41.7)	0.3	0.7
1	24 (42.1)	14 (58.3)		
2	2 (3.5)	0 (0.0)		
miR-224				
Tumor grade				
Well	1 (2.3)	1 (2.7)	0.4	0.8
Good	39 (88.6)	35 (94.6)		
Poor	4 (9.1)	1 (2.7)		
Nodal state				
pN 0	29 (65.9)	21 (56.8)	0.6	0.9
pN I	11 (25.0)	13 (35.1)		
pN II	4 (9.1)	3 (8.1)		
Dukes' stage				
A	6 (13.6)	6 (16.2)	0.5	0.9
B	23 (52.3)	15 (40.5)		
C	15 (34.1)	16 (43.2)		
EMVI				
0	23 (52.3)	18 (48.6)	0.9	0.9
1	20 (45.5)	18 (48.6)		
2	1 (2.3)	1 (2.7)		

Abbreviation: EMVI: Extramural vascular invasion.

expected bands for each antibody in specific cell lysates: SMAD4 in SW480, RASA1 in HT29 and Lovo, KLF4 in HT29, and TGFBRII in HT29 and SW480 (Figure S1 in Supplementary File). These results validated the specificity of the antibodies for staining target proteins within CRC TMAs via immunohistochemistry. Other antibodies used in our study, sourced from our group and the histopathological department at Nottingham QMC, underwent similar validation procedures. In addition, we optimized the concentration of each antibody for immunohistochemical staining. For example, anti-SMAD4 at 1:100 exhibited optimal staining without background, while concentrations of 1:50 and 1:200 were either too high or too low for detection. Similarly, optimal concentrations were determined for TGFBRII (1:400), RASA1 (1:40), and KLF4 (1:100). Staining for BCL2 and PTEN was performed separately by the histopathology department at QMC. Further details on the staining optimization process can be found in Table 1 and Figure S2 (in Supplementary file).

3.3.2. Protein expression of target genes

In a primary operable invasive CRC patient cohort, we conducted an evaluation to delve deeper into the expression of miRNA target genes, including SMAD4, PTEN, TGFBRII, BCL2, KLF4, and RASA1. Staining patterns for all markers displayed heterogeneity both within and between tumor cores, ranging from weak to intense staining (Figure 2). Three cores per case were stained, and the average scores of these cores were used for subsequent analysis. The H-score, representing staining intensity, was determined for each marker. SMAD4 exhibited a median H-score of 85 (range: 0 – 300), PTEN had a median H-score of 95 (range: 0 – 300), TGFBRII had a median H-score of 70 (range: 0 – 225), BCL2 had a median H-score of 125 (range: 0 – 300), KLF4 had a median H-score of 90 (range: 0 – 300), and RASA1 had a median H-score of 65 (range: 0 – 200).

Table 3. Expression profiles of candidate target genes of microRNAs

Gene	Fold of change of tumor tissue versus normal tissue	*P*	*P*-value of Bonferroni multiple correction
SMAD4	0.98	0.12	
PTEN	0.97	0.22	
BCL2	3.72	0.05	0.2
TGFBRII	0.46	0.001	0.006
KLF4	1.18	0.8	
RASA1	0.66	0.002	0.01

As previously mentioned, excellent concordance between scorers was observed, as indicated by the single-measure ICC for SMAD4, PTEN, TGFBRII, BCL2, KLF4, and RASA1, which ranged from 0.71 to 0.82. Specimens were categorized into low and high expression groups based on mean scores. For instance, 63% of CRC cases exhibited low expression of SMAD4, while 37% displayed high expression relative to normal mucosa. Similarly, 83% of CRC cases demonstrated low expression of PTEN, with 17% characterized by high expression. For TGFBRII, 80% of CRC cases were categorized as low expression, while 20% showed high expression compared to normal mucosa. In the case of BCL2, 58% of CRC specimens had low expression, whereas 42% exhibited high expression. For KLF4, 44% of CRC cases exhibited low expression, while 56% displayed high expression. Lastly, 75% of CRC cases demonstrated low expression of RASA1, and 25% exhibited high expression compared to normal mucosa. Chi-square test was conducted to assess the correlation between mRNA and protein level of the markers used in this study. Results demonstrated a significant correlation between mRNA and protein levels of SMAD4 (r = 0.466,

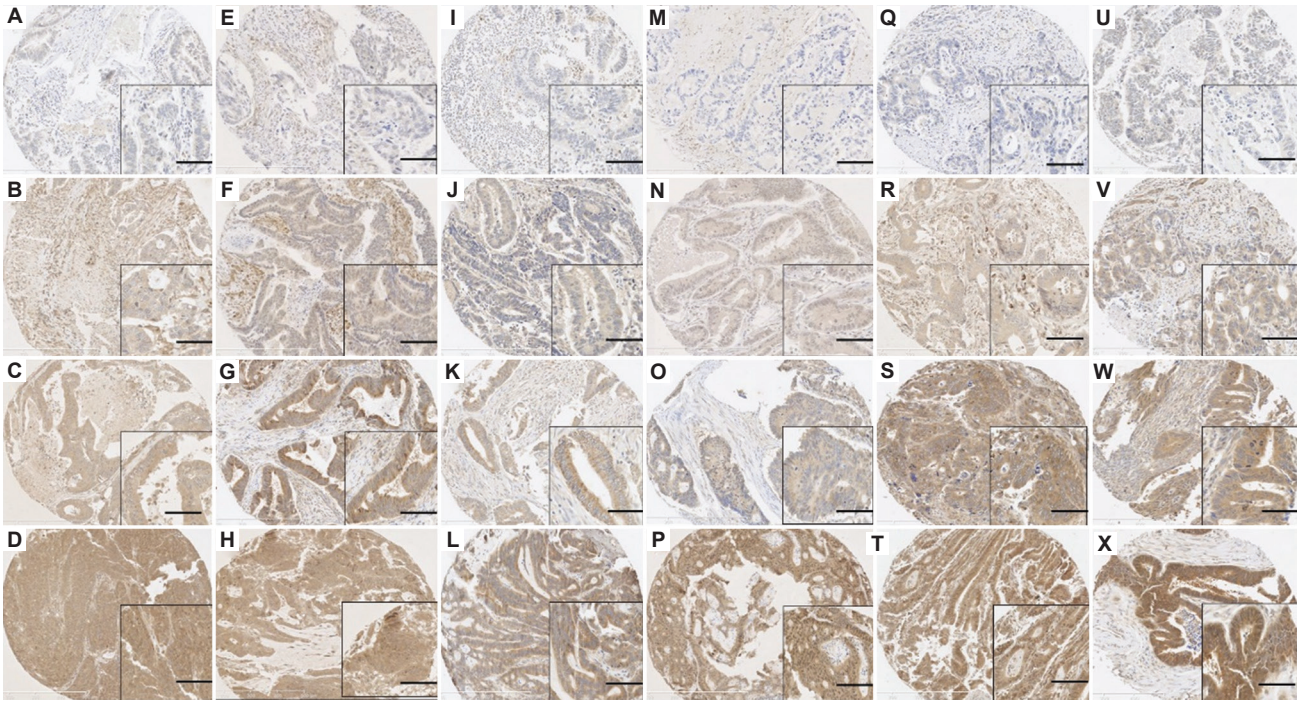

Figure 2. Representative photomicrographs of various staining intensity of markers in colorectal tissue: (A-D) SMAD4, (E-H) PTEN, (I-L) BCL2, (M-P) TGFBRII, (Q-T) KLF4, and (U-X) RASA1. Photomicrographs were viewed at ×100 magnification, whereas images at the inset boxes were at ×200 magnification; scale bar = 100 μm.

$P < 0.0001$), TGFBRII I (r = 0.708, $P < 0.0001$), BCL2 (r = 0.623, $P < 0.0001$), and RASA1 (r = 0.728, $P < 0.0001$). No correlation was observed between mRNA and protein levels of PTEN (r = −0.085, $P = 0.450$), and KLF4 (r = 0.114, $P = 0.313$).

3.4. Association the expression of biomarkers (target genes) and miRNAs

Spearman's rank-order correlation was performed to evaluate the relationship between the markers examined in this study. High expression levels of miR-21 and miR-224 were found to be associated with lower levels of *TGFBRII* mRNA (r = −0.358, $P = 0.001$; and r = −0.276, $P = 0.01$, respectively) as well as TGFBRII protein (r = −0.328, $P = 0.003$; and r = −0.319, $P = 0.004$, respectively). Furthermore, increased expression of both miR-29a and miR-31 showed an inverse correlation with *RASA1* mRNA levels (r = −0.217, $P = 0.01$; and r = −0.276, $P = 0.01$, respectively) and RASA1 protein levels (r = −0.222, $P = 0.004$; and r = −0.209, $P = 0.01$, respectively) (Table 4). A significant correlation was also observed between miR-20a and miR-29 (r = 0.380, $P = 0.0001$) as well as miR-31 (r = 0.403, $P = 0.0001$). In addition, a notable correlation was found between miR-21 and miR-29a (r = 0.526, $P = 0.0001$) and miR-31 (r = 0.285, $P = 0.01$). Moreover, a strong correlation was noted between miR-29a and miR-31 (r = 0.275, $P = 0.01$) and miR-92a (r = 0.324, $P = 0.003$). Significant correlations were also observed between miR-31 and miR-224 (r = 0.328, $P = 0.003$) and between miR-92a and miR-224 (r = 0.382, $P = 0.0001$) (Table 5).

Table 4. Association between mRNAs and target genes (mRNA and protein)

Variable	*TGFBRII* mRNA	TGFBRII protein	*RASA1* mRNA	RASA1 protein
miR-21 CC	−0.358	−0.328		
P	0.001	0.003		
miR-29a CC			−0.217	−0.222
P			0.01	0.004
miR-31 CC			−0.276	−0.209
P			0.01	0.01
miR-224 CC	−0.276	−0.319		
P	0.01	0.004		

Abbreviation: CC: Correlation coefficient; mRNA: microRNAs.

Table 5. Association between microRNAs

Variables	miR-29a	miR-31	miR-92a	miR-224
miR-20a CC	0.380	0.403		
P	0.0001	0.0001		
miR-21 CC	0.526	0.285		
P	0.0001	0.01		
miR-29a CC		0.275	0.324	
P		0.01	0.003	
miR-31 CC				0.328
P				0.003
miR-92a CC				0.382
P				0.0001

Abbreviation: CC: Correlation coefficient.

4. Discussion

CRC remains a significant global health burden, with substantial morbidity and mortality rates worldwide. Unraveling the intricate molecular mechanisms underlying CRC pathogenesis is crucial for advancing our understanding of the disease and identifying novel therapeutic targets and diagnostic biomarkers. In this comprehensive study, we employed a multidimensional approach, integrating miRNA quantification, mRNA profiling, and protein evaluation, to evaluate their potential as biomarkers for CRC detection.

The dysregulation of miRNAs, small non-coding RNAs that modulate gene expression, is a hallmark of CRC tumorigenesis.[26,27] Our study revealed abnormal expression patterns of several miRNAs in CRC tissues compared to adjacent normal mucosa. Notably, miR-31, miR-29a, miR-21, and miR-20a were significantly upregulated in CRC samples, indicating their roles as oncogenic drivers in CRC progression.[28-30] These findings support the growing evidence implicating these miRNAs in CRC pathogenesis and highlight their potential as diagnostic and prognostic biomarkers.

Despite the relatively small sample size, we explored clinical associations, though no significant correlations between miRNA expression and clinicopathological features were identified. This is contrary to findings by others, such as Schepeler *et al.*[31] who reported increased miR-31 levels in stage IV tumors, and Zhou *et al.*[32] who observed a correlation between miR-92a expression and advanced clinical stage.

In addition, our study identified potential mRNA targets of dysregulated miRNAs in CRC. Through mRNA quantification analysis, we observed differential expression patterns of genes involved in critical signaling pathways dysregulated in CRC. Specifically, *RASA1* and *TGFBRII*, tumor suppressor genes in Ras and TGF-β pathways, respectively, were significantly downregulated in CRC tissues.[33,34] Conversely, *BCL2*, an anti-apoptotic gene, showed upregulation in CRC samples, consistent with its role in promoting cell survival and chemoresistance.[35]

The immunohistochemical evaluation of target protein expression provided further insights into the molecular alterations within CRC tissues. The observed heterogeneity in protein expression patterns underscores the dynamic

nature of CRC tumors and the diverse cellular phenotypes within the tumor microenvironment. Importantly, the correlations between mRNA and protein levels for selected markers, including SMAD4, TGFBRII, BCL2, and RASA1, highlight the transcriptional regulation of protein expression in CRC.[17,36] These findings underscore the importance of integrating multiple omics approaches to comprehensively characterize the molecular landscape of CRC.

Although this study did not include functional validation experiments, the high correlation between miRNAs and their target genes suggests that the selected miRNAs could play roles in CRC carcinogenesis by regulating key signaling pathways. For example, the inverse correlations between miR-21, miR-224, and TGFBRII highlight their role in suppressing TGFBRII expression, thus potentiating TGF-β signaling dysregulation in CRC.[37] Similarly, the inverse associations between miR-29a, miR-31, and RASA1 underscore their regulatory role in modulating RASA1 expression, consequently influencing Ras signaling pathway activation in CRC.[14,38] In addition, the lack of correlation between mRNA and protein levels of PTEN, coupled with the strong correlation between miR-20a and reduced PTEN protein expression, suggests that miR-20a may regulate PTEN at the post-transcriptional level. These findings suggest that these miRNAs may play a role in CRC tumorigenesis by modulating key tumor suppressor genes, although further mechanistic studies are required to confirm these interactions.

This study has several strengths, such as the use of matched tumor and normal mucosa tissues, which minimizes the influence of non-tumorous miRNAs. However, there are also limitations, including the relatively small sample size, the lack of validation using alternative methods, and the absence of mutation screening.

5. Conclusion

Our findings suggest that upregulation of miR-20a, miR-21, miR-29a, and miR-31 may contribute to CRC progression by targeting genes involved in key signaling pathways. While these miRNAs show potential as diagnostic biomarkers, further research is needed to validate their clinical utility and explore their roles in CRC pathways. Future studies should focus on investigating the interactions between miRNAs, gene mutations, and other CRC-related pathways to better understand the molecular mechanisms driving CRC.

Acknowledgments

None.

Funding

This work was funded by Universities of Nottingham for Mohammed Ilyas.

Conflict of interest

The authors declare that they have no competing interests.

Author contributions

Conceptualization: Hersh Ham-Karim, Mohammad Ilyas
Formal analysis: Hersh Ham-Karim, Alan Shwan
Investigation: Hersh Ham-Karim, Narmeen Ahmad, Alan Shwan
Methodology: Hersh Ham-Karim
Writing – original draft: Hersh Ham-Karim, Mohammad Ilyas
Writing – review & editing: Mohammad Ilyas

Ethics approval and consent to participate

Access to tissues and ethics approval were granted by Nottingham Health Sciences Biobank, which has approval as an IRB from North West, Greater Manchester Central Research Ethics Committee (REC reference: 15/NW/0685).

Consent for publication

No patient consent was needed.

Availability of data

All datasets on which the conclusions of this paper rely have been presented in the main manuscript and in the supplementary file. In addition, raw data can be accessed on request.

References

1. Rawla P, Sunkara T, Barsouk A. Epidemiology of colorectal cancer: Incidence, mortality, survival, and risk factors. *Prz Gastroenterol*. 2019;14(2):89-103.

   doi: 10.5114/pg.2018.81072

2. Olivier T, Fernandez E, Labidi-Galy I, *et al*. Redefining cancer of unknown primary: Is precision medicine really shifting the paradigm? *Cancer Treat Rev*. 2021;97:102204.

   doi: 10.1016/j.ctrv.2021.102204

3. Ždralević M, Raonić J, Popovic N, *et al.* The role of miRNA in colorectal cancer diagnosis: A pilot study. *Oncol Lett*. 2023;25(6):267.

   doi: 10.3892/ol.2023.13853

4. Kim SM, Choi HS, Byun JS. Overall 5-year survival rate and prognostic factors in patients with stage IB and IIA cervical cancer treated by radical hysterectomy and pelvic lymph node dissection. *Int J Gynecol Cancer*. 2000;10(4):305-312.

doi: 10.1046/j.1525-1438.2000.010004305.x

5. Coleman D, Kuwada S. miRNA as a Biomarker for the early detection of colorectal cancer. Genes *(*Basel*)*. 2024;15(3):338.

doi: 10.3390/genes15030338

6. Kral J, Kojecky V, Stepan M, *et al.* The experience with colorectal cancer screening in the Czech Republic: The detection at earlier stages and improved clinical outcomes. *Public Health*. 2020;185:153-158.

doi: 10.1016/j.puhe.2020.05.021

7. Ji Y, Jialin G, Hongqun Z, Houxi X. Identification and validation of Key miRNAs for colon cancer based on miRNA-gene integration analysis. *Int J Gen Med*. 2023;(16):5703-5718.

doi: 10.2147/IJGM.S440340

8. Sadeghi S, Lotfi M, Soltani N, *et al*. Recent advances on high-efficiency of microRNAs in different types of lung cancer: A comprehensive review. *Cancer Cell Int*. 2023;23(1):284.

doi: 10.1186/s12935-023-03133-z

9. Sado AI, Batool W, Ahmed A, *et al*. Role of microRNA in colorectal carcinoma (CRC): A narrative review. *Ann Med Surg* (*Lond*). 2023;86(1):308-318.

doi: 10.1097/MS9.0000000000001494

10. Koncina E, Haan S, Rauh S, Letellier E. Prognostic and predictive molecular biomarkers for colorectal cancer: Updates and challenges. *Cancers* (*Basel*). 2020;12(2):319.

doi: 10.3390/cancers12020319

11. Cheng D, Zhao S, Tang H, *et al.* MicroRNA-20a-5p promotes colorectal cancer invasion and metastasis by downregulating Smad4. *Oncotarget*. 2016;7(29):45199-45213.

doi: 10.18632/oncotarget.9900

12. Sun LH, Tian D, Yang ZC, Li JL. Exosomal miR-21 promotes proliferation, invasion and therapy resistance of colon adenocarcinoma cells through its target PDCD4. *Sci Rep.* 2020;10(1):8271.

doi: 10.1038/s41598-020-65207-6

13. Wang J, Chen X, Xie C, *et al.* MicroRNA miR-29a inhibits colon cancer progression by downregulating B7-H3 expression: Potential molecular targets for colon cancer therapy. *Mol Biotechnol*. 2021;63(9):849-861

doi: 10.1007/s12033-021-00348-1

14. Kent OA, Mendell JT, Rottapel R. Transcriptional regulation of miR-31 by Oncogenic KRAS mediates metastatic phenotypes by repressing RASA1. *Mol Cancer Res.* 2016;14(3):267-277.

doi: 10.1158/1541-7786.MCR-15-0456

15. Li Y, Li K, Lou X, *et al.* HNRNPA2B1-mediated microRNA-92a upregulation and section acts as a promising noninvasive diagnostic biomarker in colorectal cancer. *Cancers* (*Basel*). 2023;15(4):1367.

doi: 10.3390/cancers15051367

16. Li T, Lai Q, Wang S, *et al.* MicroRNA-224 sustains Wnt/β-catenin signaling and promotes aggressive phenotype of colorectal cancer. *J Exp Clin Cancer Res*. 2016;35:21.

doi: 10.1186/s13046-016-0287-1. Erratum in: *J Exp Clin Cancer Res*. 2021;40(1):143.

doi: 10.1186/s13046-021-01945-3

17. Sun D, Yu F, Ma Y, *et al.* MicroRNA-31 activates the RAS pathway and functions as an oncogenic MicroRNA in human colorectal cancer by repressing RAS p21 GTPase activating protein 1 (RASA1). *J Biol Chem*. 2013;288(13):9508-9518.

doi: 10.1074/jbc.M112.367763

18. Zhang G, Zhou H, Xiao H, Liu Z, Tian H, Zhou T. MicroRNA-92a functions as an oncogene in colorectal cancer by targeting PTEN. *Dig Dis Sci.* 2014;59(1):98-107.

doi: 10.1007/s10620-013-2858-8

19. Mo WY, Cao SQ. MiR-29a-3p: A potential biomarker and therapeutic target in colorectal cancer. *Clin Transl Oncol*. 2023;25(3):563-577.

doi: 10.1007/s12094-022-02978-6

20. Sokolova V, Fiorino A, Zoni E, *et al.* The effects of miR-20a on p21: Two mechanisms blocking growth arrest in TGF-β-responsive colon carcinoma. *J Cell Physiol*. 2015;230(12):3105-3114.

doi: 10.1002/jcp.25051

21. Michas A, Michas V, Anagnostou E. The clinical significance of MicroRNAs in colorectal cancer signaling pathways: A review. *Glob Med Genet*. 2023;10(4):315-323.

doi: 10.1055/s-0043-1777094

22. Chretien AS, Harlé A, Meyer-Lefebvre M, *et al.* Optimization of routine KRAS mutation PCR-based testing procedure for rational individualized first-line-targeted therapy selection in metastatic colorectal cancer. *Cancer Med*. 2013;2(1):11-20.

doi: 10.1002/cam4.47

23. Díaz R, Silva J, García JM, *et al.* Deregulated expression of miR-106a predicts survival in human colon cancer patients. *Genes Chromosomes Cancer*. 2008;47(9):794-802.

doi: 10.1002/gcc.20580

24. Ng EK, Chong WW, Jin H, *et al.* Differential expression of microRNAs in plasma of patients with colorectal cancer: A potential marker for colorectal cancer screening. *Gut*. 2009;58(10):1375-1381.

doi: 10.1136/gut.2008.167817

25. Abd El-Rehim DM, Ball G, Pinder SE, *et al.* High-throughput protein expression analysis using tissue microarray technology of a large well-characterised series identifies biologically distinct classes of breast cancer

confirming recent cDNA expression analyses. *Int J Cancer*. 2005;116(3):340-350.

doi: 10.1002/ijc.21004

26. Pandey S, Jain A, Vagha S. Insights into colorectal carcinoma: A comprehensive review of MicroRNA expression patterns. *Cureus*. 2024;16(3):e56739.

doi: 10.7759/cureus.56739

27. Muhammad S, Kaur K, Huang R, *et al*. MicroRNAs in colorectal cancer: Role in metastasis and clinical perspectives. *World J Gastroenterol*. 2014;20(45):17011-17019.

doi: 10.3748/wjg.v20.i45.17011

28. Al-Nakhle HH. Unraveling the multifaceted role of the miR-17-92 cluster in colorectal cancer: From mechanisms to biomarker potential. *Curr Issues Mol Biol*. 2024;46(3):1832-1850.

doi: 10.3390/cimb46030120

29. Santos DAR, Gaiteiro C, Santos M, Santos L, Dinis-Ribeiro M, Lima L. MicroRNA biomarkers as promising tools for early colorectal cancer screening-a comprehensive review. *Int J Mol Sci*. 2023;24(13):11023.

doi: 10.3390/ijms241311023

30. Fellizar A, Refuerzo V, Ramos JD, Albano PM. Expression of specific microRNAs in tissue and plasma in colorectal cancer. *J Pathol Transl Med*. 2023;57(3):147-157.

doi: 10.4132/jptm.2022.02.19

31. Schepeler T, Reinert JT, Ostenfeld MS, *et al*. Diagnostic and prognostic microRNAs in stage II colon cancer. *Cancer Res*. 2008;68(15):6416-6424.

doi: 10.1158/0008-5472.CAN-07-6110

32. Zhou T, Zhang G, Liu Z, Xia S, Tian H. Overexpression of miR-92a correlates with tumor metastasis and poor prognosis in patients with colorectal cancer. *Int J Colorectal Dis*. 2013;28(1):19-24.

doi: 10.1007/s00384-012-1528-1

33. Liu C, Yu C, Song G, *et al*. Comprehensive analysis of miRNA-mRNA regulatory pairs associated with colorectal cancer and the role in tumor immunity. *BMC Genomics*. 2023;24(1):724

doi: 10.1186/s12864-023-09635-4

34. Prakash S, Alisha G. MicroRNAs: Potential biomarkers for diagnosis and prognosis of different cancers. *Transl Cancer Res*. 2020;9(9):5798-5818.

doi: 10.21037/tcr-20-1294

35. Ramesh P, Medema JP. BCL-2 family deregulation in colorectal cancer: Potential for BH3 mimetics in therapy. *Apoptosis*. 2020;25(5-6):305-320.

doi: 10.1007/s10495-020-01601-9

36. Yu T, Ma P, Wu D, Shu Y, Gao W. Functions and mechanisms of microRNA-31 in human cancers. *Biomed Pharmacother*. 2018;108:1162-1169.

doi: 10.1016/j.biopha.2018.09.132

37. Ahadi A. The significance of microRNA deregulation in colorectal cancer development and the clinical uses as a diagnostic and prognostic biomarker and therapeutic agent. *Noncoding RNA Res*. 2020;5(3):125-134.

doi: 10.1016/j.ncrna.2020.08.003

38. Sasso CV, Lhamyani S, Hevilla F, *et al*. Modulation of miR-29a and miR-29b Expression and their target genes related to inflammation and renal fibrosis by an oral nutritional supplement with probiotics in malnourished hemodialysis patients. Int J Mol Sci. 2024;*25*:1132.

doi: 10.3390/ijms25021132

ACCSCIENCE PUBLISHING

Tumor Discovery

ORIGINAL RESEARCH ARTICLE

Covalent docking-based virtual screening and molecular dynamics simulations identify C02b as a potential *KRAS*(G12C) inhibitor

Safiye Merve Bostancioglu[1]* and Ahmet Acar[2]*

[1]Department of Biology, Faculty of Arts and Sciences, Marmara University, Goztepe Campus, Istanbul, Turkey

[2]Department of Biological Sciences, Middle East Technical University, Universiteler Mah., Ankara, Turkey

Abstract

Decades of efforts to target the "undruggable" *Kirsten rat sarcoma viral oncogene homolog* (*KRAS*) oncoprotein yielded promising results in 2021 with the approval of Sotorasib, a *KRAS*(G12C) inhibitor for non-small cell lung cancer patients with the *KRAS*(G12C) variant. Before Sotorasib's approval, developing *KRAS*(G12C) covalent inhibitors faced challenges, particularly their inability to preserve the *KRAS* protein in the GDP-bound state, which hindered clinical trial progression. Considering the importance of developing inhibitors targeting *KRAS*(G12C), we aimed to identify compounds analogous to Sotorasib, resulting in the discovery of a total of 174 Sotorasib scaffold-compounds. We then performed covalent docking-based virtual screening to examine the binding affinity of Sotorasib-like compounds to *KRAS*(G12C). Four compounds showed comparable binding energies according to Glide score to Sotorasib for targeting *KRAS*(G12C). Subsequently, molecular dynamics (MD) simulations were conducted for these four compounds, spanning 100 ns, 300 ns, and 500 ns durations, to identify the most stable complex with the lowest root-mean-square deviation (RMSD), similar to the *KRAS*(G12C)-Sotorasib reference complex. Additional dynamic cross-correlation matrix and PCA were performed as post-MD analyses to investigate the movements of two switches and the flexible regions of *KRAS*(G12C)-Sotorasib and -C02b complexes. As a result, among these four compounds, *KRAS*(G12C)-C02b was found as the optimal candidate. Further investigations beyond this study may provide more insight into C02b's inhibitory effect on *KRAS*(G12C), offering a deeper understanding of its potential as a therapeutic agent.

Keywords: *KRAS*(G12C); Sotorasib-like compounds; Molecular dynamics simulations

***Corresponding authors:**
Safiye Merve Bostancioglu (mervebostancioglu@marun.edu.tr); Ahmet Acar (acara@metu.edu.tr)

Citation: Acar A, Bostancioglu SM. Covalent docking-based virtual screening and molecular dynamics simulations identify C02b as a potential *KRAS*(G12C) inhibitor. *Tumor Discov*. 2025;4(1):79-98. doi: 10.36922/td.5163

Received: October 15, 2024

Revised: November 30, 2024

Accepted: December 9, 2024

Published online: December 26, 2024

1. Introduction

Cancer is a complex disease characterized by the number of key hallmarks, including sustained proliferative signaling, evasion of growth suppressors, resistance to cell death, enabling replicative immortality, inducing angiogenesis, activation of invasion and metastasis, deregulation of cellular energetics, avoidance of immune destruction, promotion of inflammation, genome instability and mutation, and alteration of

the tumor microenvironment.[1,2] These characteristics collectively contribute to the development and progression of cancer, making it a difficult and complex disease to treat. Understanding these characteristics is critical for developing cancer therapies that target specific aspects of the disease's biology, as cancer is greatly influenced by evolutionary principles, particularly through tumor evolution.[3-6] Genetic mutations and natural selection drive the development of diverse cell populations within a tumor, resulting in genetic diversity and heterogeneity.[7] This diversity enables cancer cells to adapt to various environmental challenges, such as treatments or changes in the microenvironment, resulting in the survival of drug-resistant and more aggressive cell clones.[8-11]

Kirsten rat sarcoma viral oncogene homolog (*KRAS*) signaling regulates important cellular functions through a network of intracellular signaling pathways.[12] *KRAS* functions normally as a molecular switch, cycling between an inactive (GDP-bound) and active (GTP-bound) form. When activated, GTP-bound *KRAS* drives downstream signaling pathways that regulate cell growth, survival, and proliferation, such as the MAPK/ERK and PI3K/AKT pathways.[13] *KRAS* mutations, such as the common G12C mutation, maintain *KRAS* in an active state, resulting in uncontrolled signaling and cellular responses, ultimately driving cancer development and progression by promoting cell growth, inhibiting apoptosis, enhancing metastasis, and modulating the tumor microenvironment.[14]

KRAS gene mutations, particularly the G12C variant, are prevalent in a variety of cancers, including non-small cell lung cancer (NSCLC) and colorectal cancer.[15,16] *KRAS*(G12C) inhibitors are an emerging class of targeted cancer therapy that targets a specific mutation (G12C) in the *KRAS* gene.[17] *KRAS*(G12C) inhibitors aim to address a long-standing problem in cancer treatment, as *KRAS* mutations were previously considered "undruggable"[18] Sotorasib (AMG 510) was the first *KRAS*(G12C) inhibitor to receive accelerated FDA approval in May 2021 for the treatment of adult patients with NSCLC harboring the *KRAS*(G12C) mutation.[19] This marked a significant milestone in cancer therapy by introducing the first drug approved to target *KRAS* mutations. Sotorasib functions by irreversibly binding to the mutant *KRAS*(G12C), inhibiting its activity.[20] Specifically, Sotorasib forms a covalent bond with cysteine 12 in the switch II pocket of *KRAS*(G12C),[21] preventing its ability to activate downstream signaling pathways that promote cell growth and proliferation.[13]

Although Sotorasib has been approved as a drug for targeting *KRAS*(G12C),[19] there are still a limited number of virtual screening approaches to identify potential inhibitors for the *KRAS*(G12C).[22-24] Given this urging need to identify novel pharmacophores targeting the *KRAS*(G12C), we performed a covalent docking-based virtual screening in conjunction with molecular dynamics (MD) simulations to investigate the stability of *compounds* binding to the target *protein*. Based on scaffold-hopping approach with Sotorasib as a template, we identified 174 molecules exhibiting structural similarities to Sotorasib among billions of compounds. Our covalent docking-based virtual screening revealed potential putative binders of *KRAS*(G12C), namely, C01, C02a, C02b, and C03, with notable Glide score similarities to Sotorasib. MD simulations further demonstrated that the *KRAS*(G12C)-C02b complex exhibited stable binding interactions with a low root-mean-square deviation (RMSD) value, comparable to the reference FDA-approved drug Sotorasib. Moreover, the calculations of binding free energy indicated that these favorable interactions were highly preserved from the last 50 nanoseconds (ns) up to 500 ns of simulation time. To further investigate the dynamics of the *KRAS*(G12C)-Sotorasib and *KRAS*(G12C)-C02b complexes, we conducted post-MD analyses, including dynamic cross-correlation matrix (DCCM) and principal component analysis (PCA). These analyses aimed to elucidate the movements of the two switches and identify the flexible regions within the complexes. These findings suggest that C02b may serve as a promising inhibitor candidate for the *KRAS*(G12C) mutation, and further advanced studies are needed to validate its potential.

2. Materials and methods

2.1. Similarity search

Sotorasib served as a template to identify similar compounds within various chemical spaces including eXplore, Freedom Space, GalaXi, and KnowledgeSpace. The scaffold-hopping search was conducted using the infiniSee software (version 5.0.1; BioSolveIT GmbH, Sankt Augustin, Germany, 2023, www.biosolveit.de/infiniSee). The chemical spaces encompassing both building blocks and reactions allowed for the creation of a maximum number of virtual product molecules. Scaffold Hopper was executed using the infiniSee software.[25] The acrylamide warhead was selected from Sotorasib[22] (Figure A1 in Appendix). The target similarity was set at 1.00 to ensure a precise match, while a minimum similarity threshold was established at 90% to guarantee a significant level of similarity. Furthermore, a total diversity score of 1.00 was ensured to uncover compounds with a high degree of similarity with Sotorasib. As a result, 174 compounds containing the acrylamide warhead and showing structural similarities to Sotorasib were identified and saved in the structure-data file (SDF) format.

2.2. Protein and ligand preparation

The 174 compounds containing the acrylamide warhead were prepared and optimized for molecular docking using LigPrep.[26,27] Compounds were obtained using Epik at pH 7.0 ± 1.0.[28] The protein structure of the inactive GDP-bound state of human *KRAS*(G12C) (PDB ID: 6OIM) was retrieved from the Protein Data Bank, with a resolution of 1.65 Å.[29] Protein preparation was performed using the protein preparation wizard in Maestro,[30] which fixed all the missing residues and atoms of the protein structure. Several crucial steps in the preparation included introducing hydrogen atoms, refining hydrogen bond networks, and addressing missing side chains through the utilization of Prime. Subsequently, water molecules were eliminated, and a restrained minimization employing the OPLS3e force field was carried out.[31] The resulting optimized protein structure was then utilized for the subsequent docking process.

2.3. Covalent dockingbased virtual screening

A set of 174 pharmacophores similar to Sotorasib was employed in covalent docking-based virtual screening (CovDock-VS)[32] against the *KRAS*(G12C) target (PDB ID: 6OIM). The reactive residue Cys12 was specifically selected, and grid generation for docking was created as a cubic grid box centered at the coordinates (x, y, and z) of Sotorasib, with a length of 12 Å. The acrylamide electrophilic warhead group, identical to the template drug Sotorasib, was selected for the Michael addition – a reaction responsible for the covalent bonding of ligands featuring an acrylamide functional group with the side chain of nucleophilic protein residues. Subsequently, the ligands were selected and prioritized based on their Glide scores for the binding modes of pre-reactive complexes.[33,34]

2.4. MD simulations

MD simulations were conducted on the protein-ligand complexes derived from the covalent docking-based virtual screening using GROningen MAchine for Chemical Simulations (GROMACS) 2023.1.[35] The CHARMM-GUI (Chemistry at HARvard Macromolecular Mechanics Graphical User Interface) server was used for solution building. The CHARMM36 force field[36] was applied to define atom types and assign atomic partial charges for both the ligand and protein. Furthermore, the CHARMM-GUI server was employed to generate the topology for both the *KRAS*(G12C) receptor and the promising inhibitors. For the setup of MD simulations, the protein-ligand complexes were centered in an octahedral box and solvated with the TIP3P water model. Neutralization of the complexes charge was achieved by adding 150 mM ions. The minimization process concluded when the maximum force was reduced to <10.0 kJ/mol, with a maximum duration of 100 picoseconds (ps) for the minimization steps. Subsequently, a 100 ps equilibration phase with position restraints on the protein and ligand molecules was conducted using NVT (Number of Volume and Temperature) and NPT (Number of Pressure and Temperature) ensembles. During this period, the systems were heated to 303.15 K using a modified Berendsen thermostat (V-rescale),[37,38] and pressure was maintained using C-rescale pressure coupling set to a reference pressure of 1 bar.[39] For energy minimization, NVT, and NPT relaxation simulations, short-range interactions utilized a smooth force switch with a cut-off of 1.2 nm, and long-range electrostatics were computed using the Particle-Mesh-Ewald (PME) algorithm.[40] In addition, hydrogen bonds were constrained by employing the Linear Constraint Solver algorithm.[41] Finally, MD simulations were conducted for durations of 100 ns, 300 ns, and 500 ns (Table 1) without applying restraints. A 2 femtoseconds integration time step was employed, and trajectory snapshots were captured at 1 ps intervals.

MDS analyses were performed using GROMACS, a Linux-×86_64-multicore CUDA-enabled program on an NVIDIA GeForce GTX 1060 GPU and an 8-core Intel Core i5-7000 central processing infrastructure. The computation of a single complex required approximately 100 ns of processing time per simulation day. GROMACS modules were used to analyze MD trajectories, focusing on parameters such as root RMSD/mean-square deviation fluctuation (RMSF) and hydrogen bond (H-bond) analysis. Graphs were generated using XMGrace[42] and visual molecular dynamics (VMD).[43]

The calculation of binding free energy was performed using the gmx_MMPBSA tool, which is based on Assisted Model Building with Energy Refinement MM/PB(GB)SA approach. This tool is designed for conducting end-state free energy calculations using GROMACS trajectory files. Specifically, the final 50 ns of the simulation trajectory were considered for the molecular mechanics with Generalized Born surface area (MM/GBSA) calculation.

Table 1. *KRAS*(G12C) complexes feature with their atom numbers for duration 500 ns

Atoms	*KRAS*(G12C)-Sotorasib	*KRAS*(G12C)-C02b
Protein	2,704	2,704
Ligand	72	87
Na^+	14	13
Cl^-	7	7
Water (TIP3P)	7,914	7,923

Abbreviations: TIP3P: Transferable intermolecular potential three-point; *KRAS*: *Kirsten rat sarcoma viral oncogene homolog.*

2.5. Post-MD simulations analyses

The analysis employed Bio3D,[44] an R library-based tool, to generate time-correlated DCCM for various ligand-bound forms of *KRAS*(G12C). This approach aimed to discern the localization and nature of fluctuations in C^{α} atoms within residues crucial to *KRAS*(G12C) function. Given the limitations of DCCM, which may overlook correlated but perpendicular motions, the analysis was complemented with PCA. In PCA, simulation frames are organized based on their principal components (eigenvectors), which represent the key directions capturing the most significant variability in the data. This approach allows for effective separation of structures by emphasizing dominant patterns and variations within the dataset. For both analyses, the final 400 ns of all MD simulations were utilized at 20 ps intervals per Bio3D file size constraints. This comprehensive approach provides a nuanced understanding of the dynamic behavior of *KRAS*(G12C) ligand-bound forms, integrating both normal mode analysis and PCA techniques to capture a broad spectrum of structural fluctuations.

3. Results

3.1. Covalent docking-based virtual screening

It is widely accepted that molecules with comparable chemical structures will have similar pharmacological properties. In ligand-based studies, Sotorasib, an FDA-approved drug for treating *KRAS*(G12C) protein in NSCLC, was reported to be a reliable template. To evaluate ligand interactions, we used the InfiniSee, a platform capable of examining billions of compounds across chemical spaces, including eXplore, Freedom Space, GalaXi, CHEMriya, and REAL, to identify potential chemical scaffolds similar to the template. This platform also provides access to KnowledgeSpace, a literature-based virtual chemical space with a strong emphasis on synthetic accessibility. These technological advancements offer great potential in the fields of drug discovery and chemical research due to its capacity to provide a greater spectrum of molecules, allowing the design of more effective and innovative therapeutic solutions. As a result, 174 molecules exhibiting structural similarities to Sotorasib were found from billions of compounds in the chemical spaces (Table A1 in Appendix). Subsequently, the selected compounds were further evaluated using a covalent docking-based virtual screening approach.

3.2. Covalent docking-based virtual screening identifies four compounds

For the covalent-based virtual screening approach, the X-ray structure of the *KRAS*(G12C) (PDB ID: 6OIM), forming a complex with Sotorasib, was selected.[29] The COVDOCK protocol was utilized to investigate the redocking capabilities as well as the binding of the co-crystallized Sotorasib to the *KRAS*(G12C) with GDP. As a result, we observed a similar binding mechanism to that observed in the crystallized structure, validating the covalent docking protocol (Figure 1A). Next, the binding modes of these four compounds were compared with the co-crystallized Sotorasib according to their 2-D interaction diagram (Figure 1B). The precision of the COVDOCK protocol in reproducing the binding mechanism of the co-crystallized ligand with the *KRAS*(G12C) protein has been demonstrated by prior researchers.[22,45]

The set of 174 selected compounds was then subjected to a covalent docking-based virtual screening, with their binding energies ranked according to their Glide scores. While none of the ranked compounds displayed a higher estimated binding energy compared to Sotorasib, which possesses a value of −8.1 kcal/mol, four compounds namely C01, C02a, C02b, and C03 exhibited closer and notable Glide scores of −7.8 kcal/mol, −7.5 kcal/mol, −7.3 kcal/mol, and −7.0 kcal/mol, respectively (Table 2 and Figure A1).

The comparison of binding modes for the four compounds with co-crystalized Sotorasib exhibited Pi-Pi stacking interactions with the residue TYR96. Similarly, compounds C01, C02a, C02b, and C03 exhibited similar interactions (Figure 2). Furthermore, these compounds formed hydrogen bonds with additional residues (LYS16, ALA59, and GLN61) in the binding pocket of *KRAS*(G12C) (Figure 2). Taken together, the four candidates show promise as covalent binders of *KRAS*(G12C) in its inactive GDP-bound configuration.

3.3. MD simulations of C01, C02a, C02b, C03, and Sotorasib with *KRAS*(G12C) protein

The root RMSD analysis allows us to monitor the fluctuation in the three-dimensional structure over time, offering valuable insight into the mobility of binding pocket residues during the MD simulation. RMSD is a measure used in computer simulations to determine how far a molecule or part of it has moved from its initial position. To assess possible fluctuations in the 3D structure over time, we ran simulations on various *KRAS*(G12C) protein complexes, including *KRAS*-C01, *KRAS*-C02a, *KRAS*(G12C)-C02b, *KRAS*-C03, and *KRAS*(G12C)-Sotorasib. Initially, we ran simulations for all complexes for 100 ns. Following that, we increased the simulation time for *KRAS*-C01, *KRAS*(G12C)-C02b, and *KRAS*(G12C)-Sotorasib to 300 ns. Finally, we ran simulations for *KRAS*(G12C)-C02b and *KRAS*(G12C)-Sotorasib for 500 ns. This enabled us to compare the structural stability of potential therapeutic

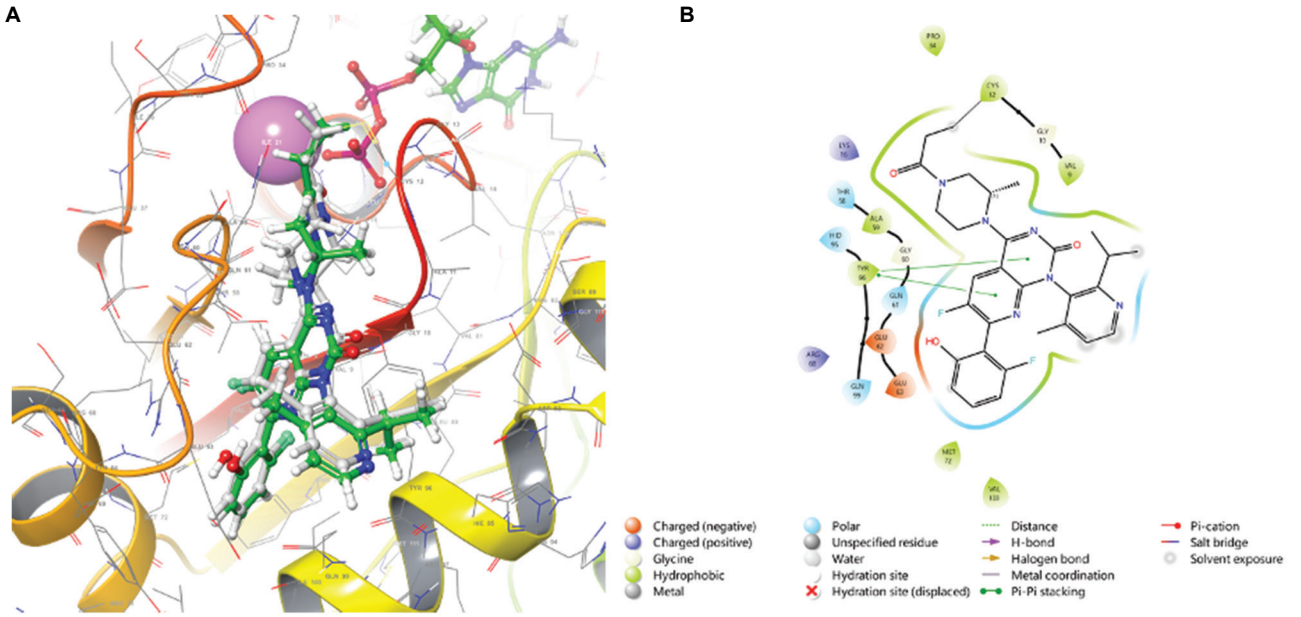

Figure 1. (A) The binding modes of the X-ray-bound Sotorasib and the re-docked Sotorasib were superimposed. (B) Amino acid interactions of Sotorasib with *Kirsten rat sarcoma viral oncogene homolog*(G12C) and compound prioritization based on molecular dynamics simulations and binding free energy calculations.

Table 2. The binding affinities and physicochemical properties of *KRAS*-C01, *KRAS*-C02a, *KRAS*(G12C)-C02b, and *KRAS*-C03 resembling the chemical scaffold of Sotorasib. TPSA: vdW polar surface area, LogP: Predicted octanol/water partition coefficient

Compound number	Compound name	Similarity	Glide score (kcal/mol)	Prime energy	Molecular weight	TPSA	LogP
	Sotorasib	1.00	−8.157	−19.6	560.6	102	4
C01	Shen_92298609_93443091_95741143	0.917	−7.801	−78.3	605.770	95.660	7.178
C02a	Shen_92298609_44473994_95741143	0.916	−7.596	−16.7	600.731	108.550	6.512
C02b	Shen_92298609_36250864_95741143	0.916	−7.347	−22.2	600.731	108.550	6.512
C03	Shen_92298609_50382533_8869305	0.916	−7.074	−5.6	611.675	130.480	4.944

Abbreviations: TPSA: Topological polar surface area.

candidates with the clinically approved drug Sotorasib using metrics such as RMSD and MM/GBSA to assess their binding strength. The 100 ns MD simulations revealed that, apart from *KRAS*-C02a and *KRAS*-C03, all complexes maintained an average RMSD value ranging from 0.2 to 0.4 nm, indicating a relatively stable simulation completion that was closely matched with their initial conformations (Figure 3). Furthermore, *KRAS*-C01 was unable to maintain its stability in subsequent 300 ns MD simulations (Figure 3). Complexes such as *KRAS*(G12C)-C02b and *KRAS*(G12C)-Sotorasib, on the other hand, successfully completed the simulation with RMSD values ranging from 0.2 to 0.4 nm (Figure 3). Continuing the 500 ns MD simulation, *KRAS*(G12C)-C02b maintained its stability until around 450 ns when its RMSD ranged from 0.3 to 0.6 nm near the end of the simulation at 500 ns (Figure 3). Of note, *KRAS*(G12C)-Sotorasib maintained an RMSD value ranging from 0.2 to 0.4 nm throughout the entire simulation. Thus, based on the RMSD of the ligand after least square fitting to the protein backbone, *KRAS*(G12C)-C02b exhibits a therapeutic candidate attribute comparable to the reference complex, *KRAS*(G12C)-Sotorasib, in that it maintains binding stability and shows no evidence of dissociation from the binding site.

To understand the fluctuations at the per residue level upon ligand binding, root mean-square fluctuation (RMSF) calculations were performed. Consistent with previously published findings,[26,31,46] it was observed that, in contrast to the entire protein, fluctuations were predominantly concentrated around switch-I (residues 30 – 38) and switch-II (residues 60 – 76). In Figure 4A, high peaks were noted in the RMSF graph within the region encompassing switch-I and switch-II loops in both complexes. Furthermore, hydrogen bond occupancy,

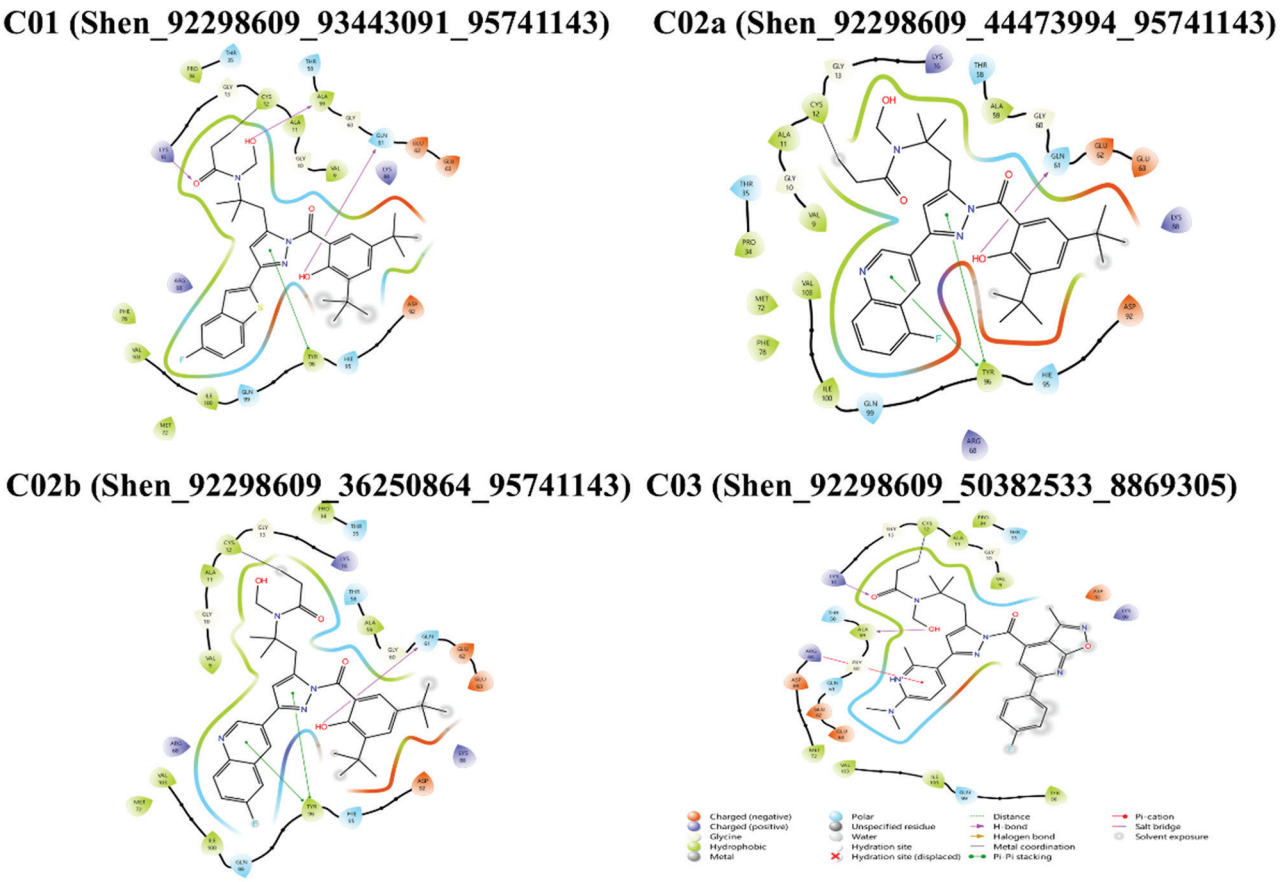

Figure 2. Amino acid interactions of the top-ranking compounds with *Kirsten rat sarcoma viral oncogene homolog*(G12C).

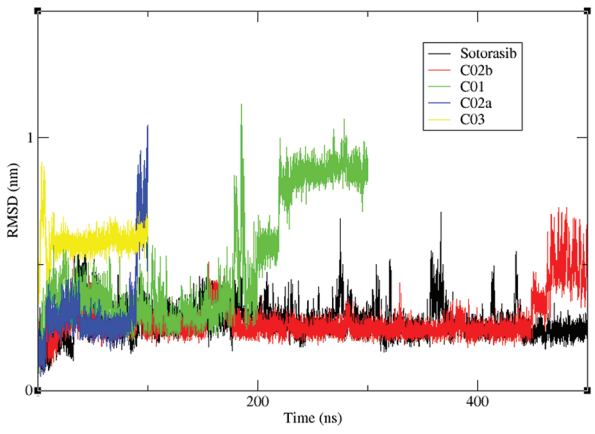

Figure 3. Lig-fit-prot RMSD graph spectrums of Sotorasib, *KRAS*-C01, *KRAS*-C02a, *KRAS*(G12C)-C02b, *KRAS*-C03, and *KRAS*(G12C)-Sotorasib in complex with *KRAS*(G12C).
Abbreviations: RMSD: Root-mean-square deviation; *KRAS*: *Kirsten rat sarcoma viral oncogene homolog.*

quantified as the average number of hydrogen bonds per time frame, was also computed for these key residues. The percentages of hydrogen bond occupancies are detailed in Figures 4B and C. The elevated rate of hydrogen bond formation between C02b and GLN61, as well as Sotorasib and ASP69, signifies a robust and dependable hydrogen-bonding profile for these interactions.

3.4. MM/GBSA calculation for evaluating binding free energy (dG)

Afterward, binding free energy (dG) was calculated using gmx_MMPBSA, and the MM/GBSA dG distribution graph was generated for the last 50 ns of the 500 ns MD simulation. For *KRAS*(G12C)-Sotorasib, the average dG was −41 kcal/mol (Figure 5A), whereas for *KRAS*(G12C)-C02b, this value was −44 kcal/mol (Figure 5B). In addition, the Delta TDC (Total DeComposition) values, illustrating the residues contributing to the binding free energy, were investigated. During the interaction with *KRAS* G12C-Sotorasib, TYR96, and GLN99 were found to contribute significantly to the binding energy, followed by ARG68 and MET72 (Figure 5C). Examination of the Delta TDC values for *KRAS*(G12C)-C02b revealed that, like in the reference complex, TYR96 and GLN99 contributed most significantly to the binding free energy, followed by GLN61 and MET72,

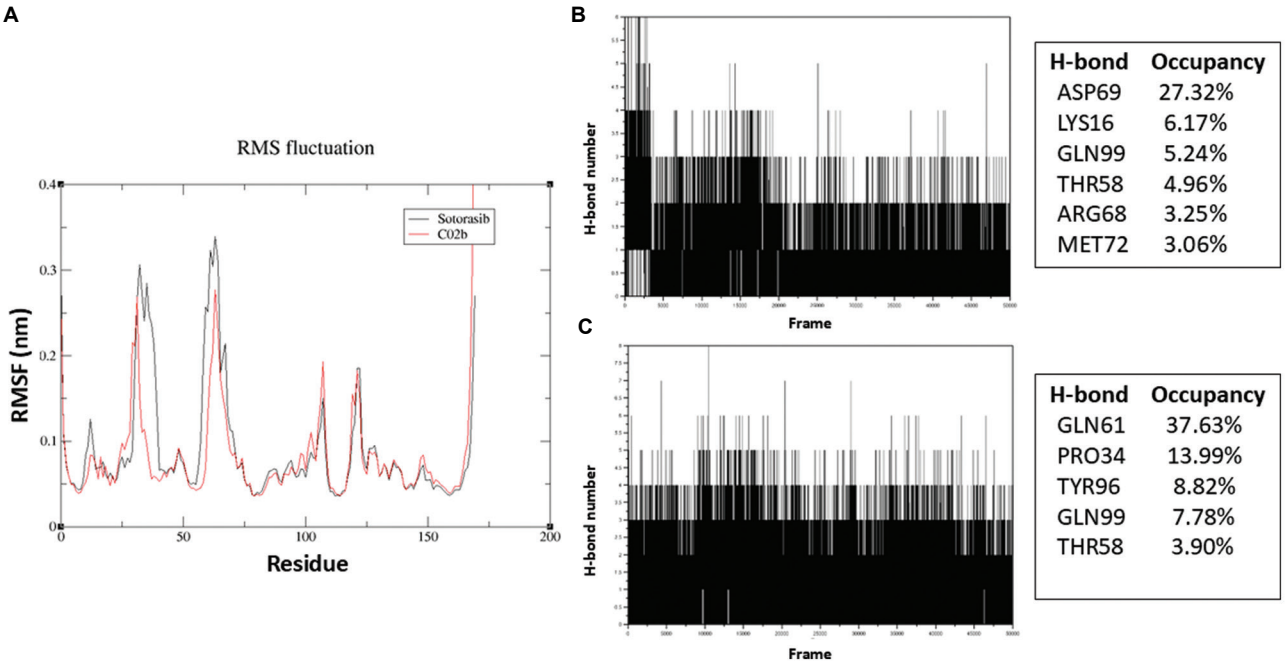

Figure 4. (A) RMSF profiles of *KRAS*(G12C) in complex with reference and hit compounds. H-bonding interactions of (B) *KRAS*(G12C)-Sotorasib and (C) *KRAS*(G12C)-C02b.
Abbreviations: RMSF: Root-mean-square fluctuation; H-bond: Hydrogen bond; *KRAS*: *Kirsten rat sarcoma viral oncogene homolog.*

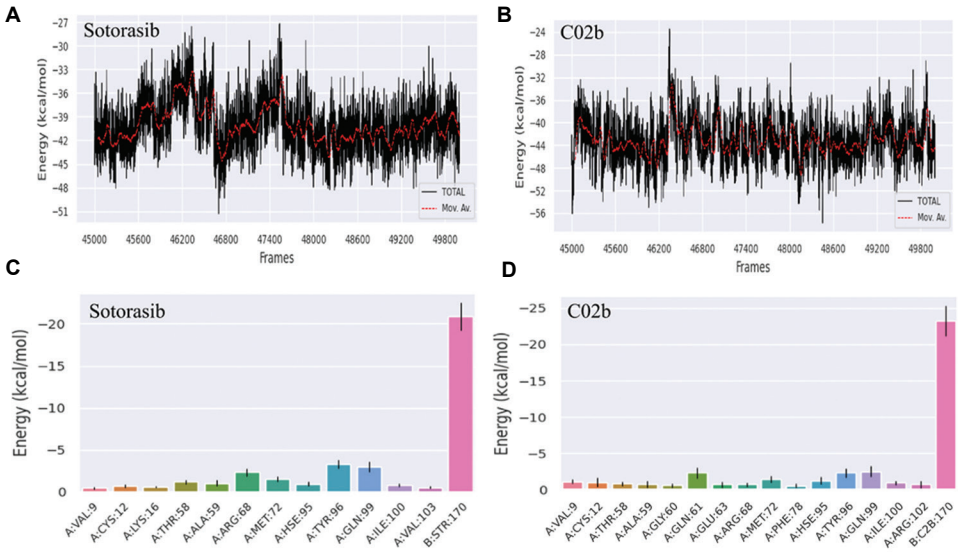

Figure 5. MM/GBSA dG distribution graph obtained for the last 50 ns of the 500 ns MD simulation for (A) Sotorasib, (B) C02b; and Delta total decomposition values for (C) STR: Sotorasib, (D) C2B: C02b.
Abbreviations: MM/GBSA: Molecular mechanics with generalized born surface area; MD: Molecular dynamics.

with a minor contribution from HIS95 (Figure 5D). It is worth reiterating that the interaction with GLN61 observed in the covalent docking results persisted throughout the 500 ns simulation. Both the *KRAS*(G12C)-C02b (Figure 6A) and *KRAS*(G12C)-Sotorasib (Figure 6B) complexes remained largely stable throughout the 500 ns trajectory, with minimal deviation from the targeted binding site, maintaining their initial positions. These findings suggest that C02b exhibits binding interactions similar to the reference FDA-approved drug Sotorasib, with highly preserved interactions. Further research into C02b, which shares similarities with Sotorasib, could potentially serve as an alternative.

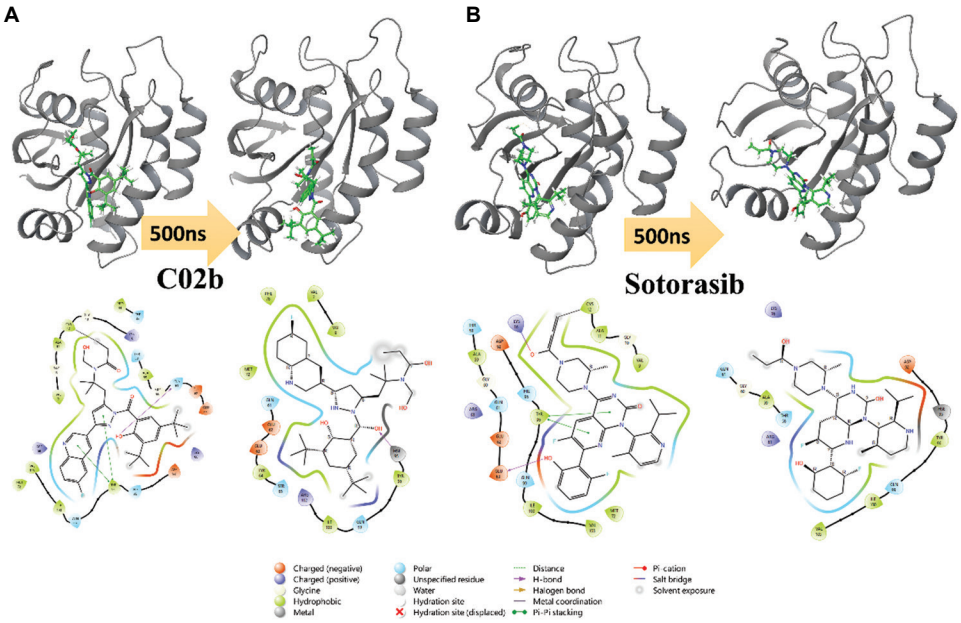

Figure 6. A schematic 2-D and 3-D representation of detailed ligand atom interactions with the protein residues at 0 ns and 500 ns. (A) C02b and (B) Sotorasib.

3.5. PCA and DCCM analysis

PCA was performed on the atomic backbone (C_α position) using three configurations: First principal component (PC1), second principal component (PC2), and third principal component (PC3). The three most representative principal components cumulatively accounted for approximately 50% of all variances among the least correlated components across all 2000 frames analyzed for *KRAS*(G12C)-ligand complexes (Figures 7-10).

In the PCA, the PC1 dominated the overall variance, accounting for more than a third of the total variance (25.45% for Sotorasib and 20.01% for C02b). PC2 accounted 12.21% for Sotorasib and 14.1% for C02b, while PC3 exhibited the lowest variability, with 5.67% for Sotorasib and 6.28% for C02b. Together, the first three components represented 43.3% and 40.5% of the total variance for Sotorasib and C02b, respectively (Figures 7 and 9).

To further elucidate the impact of Sotorasib on the structure of *KRAS*(G12C), RMSF analysis was performed to compare the flexibility of the two systems. Higher fluctuation peaks were observed in the switch-I (residues 30 – 38) and switch-II (residues 60 – 76) regions of the *KRAS*(G12C)-Sotorasib complex (Figure 8), consistent with previous observations of dynamic structural features in those regions.[46] However, for *KRAS*(G12C)-C02b, RMSF values showed a significant decrease, especially in the switch-II region (Figure 10). The 3D structures of *KRAS*(G12C)-Sotorasib and *KRAS*(G12C)-C02b revealed a noticeable reduction in flexibility in the two switch regions for the structure of *KRAS*(G12C)-C02b compared to the reference.

The correlated conformational motions of the *KRAS*(G12C)-Sotorasib and *KRAS*(G12C)-C02b complexes were examined through DCCM analysis (Figure 11). In this analysis, regions displaying high positive values (depicted in red) indicate a strong correlation in the movement of residues in the same direction. Conversely, negative regions (depicted in blue) signify robust anti-correlated motion, where residues move in opposite directions. The color intensity along the diagonal reflects the degree of movement for the corresponding atoms.

Within the reference and C02b hit complex systems, the *KRAS*(G12C)-Sotorasib complex exhibits relatively stronger correlated motions compared to the *KRAS*(G12C)-C02b complex (Figure 11). Specifically, in the DCCM of the *KRAS*(G12C)-Sotorasib complex, the flexible region is observed moving in an anti-correlated manner with both switch-I (residues 30 – 38) and switch-II (residues 60 – 76), as well as displaying anti-correlated motion with the C12 residue and switch-I. This suggests that Sotorasib brings the binding pocket closer through these anti-correlated motions of the flexible regions, including switch-I, switch-II, and the C12 residue.

On the other hand, the DCCM of the *KRAS*(G12C)-C02b complex reveals the flexible regions moving in

an anti-correlated manner with switch-I and switch-II, although the dynamic movement is less pronounced compared to the *KRAS*(G12C)-Sotorasib complex. Notably, there is no observed movement of the C12 residue in the *KRAS*(G12C)-C02b complex. These findings suggest a distinctive dynamic behavior in the correlated motions of the flexible loops and associated residues between the two complexes, highlighting the unique characteristics of Sotorasib and C02b interactions with *KRAS*(G12C).

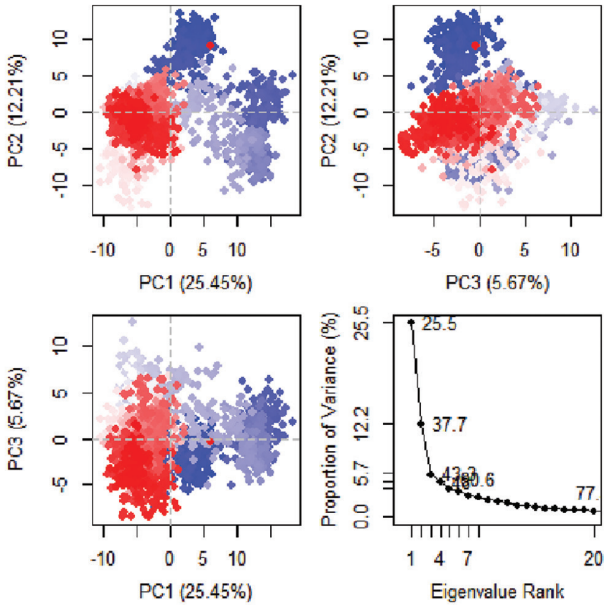

Figure 7. PCA dimension plots illustrating the first three principal components and displaying the cumulative percentages of variance covered by all eigenvectors for the *KRAS*(G12C)-Sotorasib structure. The color spectrum, transitioning from blue to red, delineates conformational alterations across the simulation. Blue dots signify the initial timesteps, white dots depict intermediate stages, and red dots denote the concluding timesteps. Abbreviations: PCA: Principal component analysis; *KRAS*: *Kirsten rat sarcoma viral oncogene homolog*.

The interaction analysis revealed notable differences between C02b and Sotorasib in their binding to the *KRAS*(G12C). C02b forms a strong and persistent interaction with GLN61 within the switch-II region, a key flexible loop implicated in *KRAS* conformational dynamics. In contrast, Sotorasib predominantly interacts with ARG68 and ASP69 in the same region. These interactions were validated through hydrogen bond occupancy analysis, which highlighted the stability and significance of the C02b-GLN61 interaction throughout the MD simulations. This distinct binding pattern of C02b suggests a potential alteration in the modulation of *KRAS*'s switch regions compared to Sotorasib, which may influence downstream signaling pathways.

Furthermore, PCA and DCCM analyses demonstrated unique dynamic behavior for the *KRAS*(G12C)-C02b complex. While Sotorasib induces a broader range of flexibility in the switch-II region, C02b exhibited reduced fluctuations in this region, potentially stabilizing the inactive GDP-bound state of *KRAS*. This stabilization is further supported by MM/GBSA binding free energy

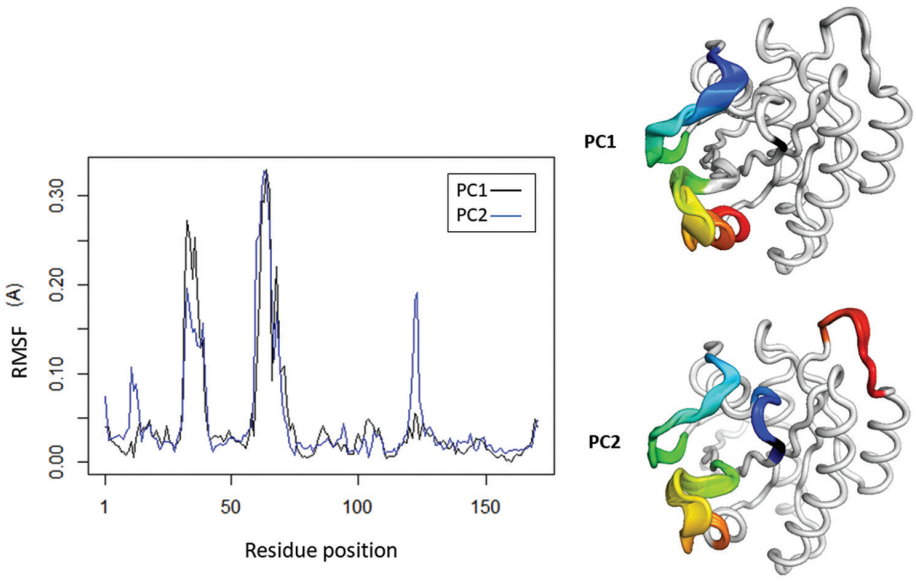

Figure 8. Flexibility analysis of the *KRAS*(G12C)-Sotorasib structure. The left side presents the RMSF values of the C^{α} atoms within the system, while the right side displays ribbon representations of the PC1 and PC2 structures. Flexible regions are highlighted with a rainbow color scheme, providing a visual cue to the dynamic nature of these segments. Notably, the C12G residue is depicted in black, and the structures were visualized using PyMOL.
Abbreviations: RMSF: Root mean-square fluctuation; *KRAS*: *Kirsten rat sarcoma viral oncogene homolog*; PC1: First principal component; PC2: Second principal component.

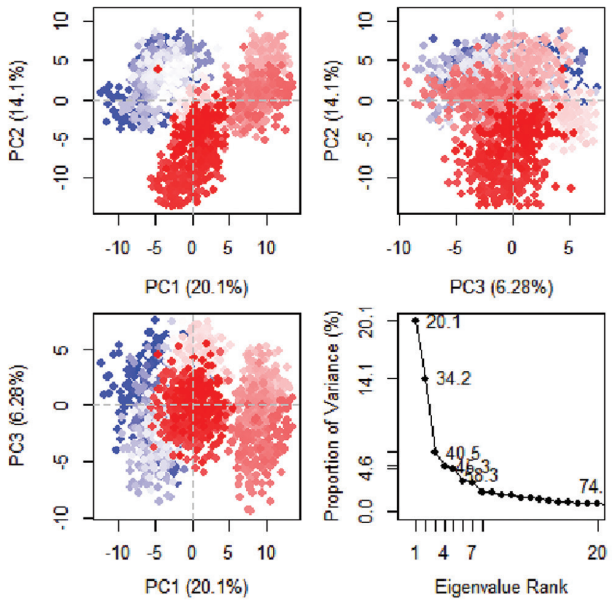

Figure 9. PCA dimension plots illustrating the first three principal components and displaying the cumulative percentages of variance covered by all eigenvectors for the *KRAS*(G12C)-C02b structure. The color spectrum, transitioning from blue to red, delineates conformational alterations across the simulation. Blue dots signify the initial timesteps, white dots depict intermediate stages, and red dots denote the concluding timesteps.
Abbreviations: PCA: Principal component analysis; *KRAS*: *Kirsten rat sarcoma viral oncogene homolog.*

calculations, which confirm the preservation of strong binding interactions for both compounds but with distinct residue-specific contributions.

4. Discussion

In this study, we present potential *KRAS*(G12C) inhibitors identified through a comprehensive approach involving covalent docking-based virtual screening and MD simulations. Our strategy started with a similarity search based on the scaffold of Sotorasib, which successfully identified 174 molecules from a vast pool of compounds. Subsequently, covalent docking-based virtual screening was performed, revealing promising *KRAS*(G12C) protein binders, namely, C01, C02a, C02b, and C03. To assess the stability of the identified complexes and putative binders, MD simulations were employed. Significantly, among the candidates, C02b demonstrated exceptional stability as an inhibitor targeting the *KRAS*(G12C) during the 500 ns MD simulation, comparable to the reference.

In a previous study, it was found that Sotorasib (AMG 510) bound to the HIS95 groove and created a connected network of 25 ligand-protein interactions through van der Waals forces.[29] This network spanned from the backbone of helix 2 (involving HIS95 and TYR96) to the backbone of the flexible switch-II loop. According to the hydrogen bond analysis performed with VMD and decomposition analysis

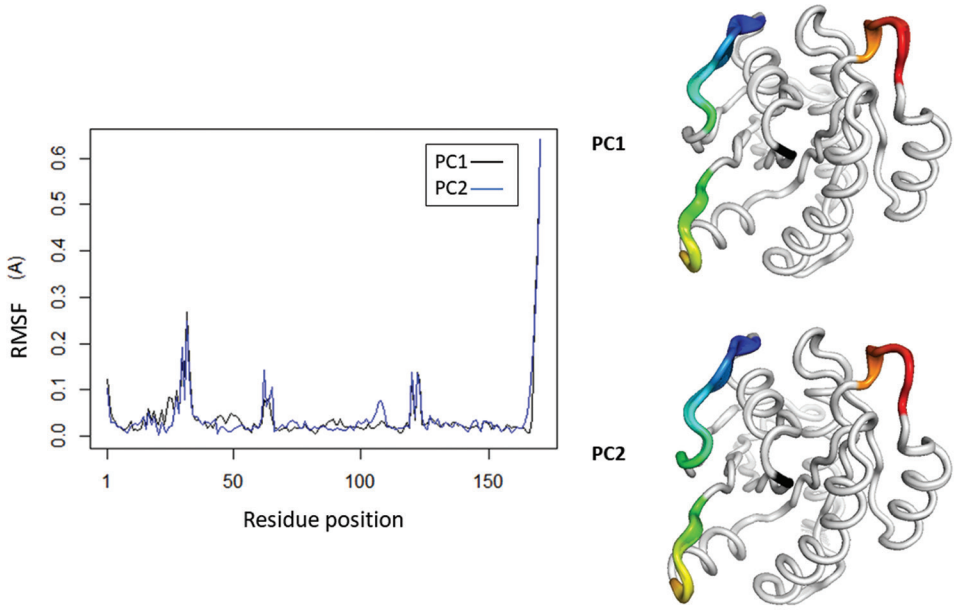

Figure 10. Flexibility analysis of *KRAS*(G12C)-C02b structure. The left side presents the RMSF values of C^{α} atoms within the system, while the right side displays ribbon representations of the PC1 and PC2 structures. Flexible regions are highlighted with a rainbow color scheme, providing a visual cue to the dynamic nature of these segments. Notably, the C12G residue is depicted in black, and the structures were visualized in PyMOL.
Abbreviations: RMSF: Root mean-square fluctuation; *KRAS*: *Kirsten rat sarcoma viral oncogene homolog*; PC1: First principal component; PC2: Second principal component.

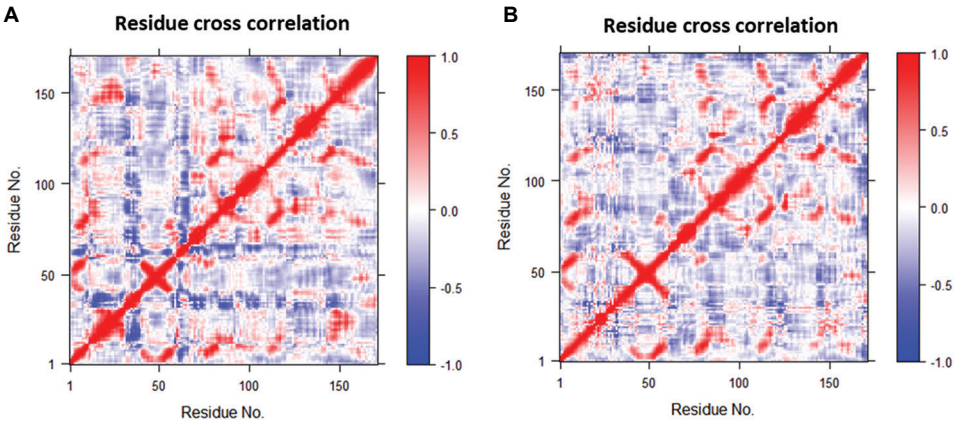

Figure 11. The post-MD simulation time-correlated DCCM plot for the *KRAS*(G12C) (A) Sotorasib and (B) *KRAS*(G12C)–C02b complexes. Blue color indicates anti-correlation and red positive correlation.
Abbreviations: DCCM: Dynamic cross-correlation matrix; MD: Molecular dynamics; *KRAS*: *Kirsten rat sarcoma viral oncogene homolog.*

using Delta TDC values in our study, the key interaction in C02b binding was observed with the GLN61 residue located in the switch-II loop. For Sotorasib, interactions were observed with ARG68 and ASP69 residues in the same loop. In addition, it was found that the TYR96 residue was crucial for both the reference and C02b interactions.

The distinct interaction of C02b with GLN61 in the switch-II region, compared to Sotorasib's interactions with ARG68 and ASP69, likely contributes to the observed differences in conformational dynamics and flexibility of the *KRAS*(G12C) complexes. Switch-II is a critical region for nucleotide exchange and downstream effector binding, and its modulation directly influences *KRAS* signaling activity. By stabilizing GLN61, C02b may better inhibit *KRAS* activation by preventing the conformational changes required for GTP loading and effector interactions. These molecular differences may translate into unique cellular outcomes. Reduced switch-II flexibility, as observed with C02b, could lead to more robust inhibition of *KRAS*-driven downstream signaling pathways, potentially altering cellular proliferation, survival, and apoptotic processes. This distinct mechanism of action highlights C02b as a promising candidate for further preclinical investigation, offering a potential advantage in overcoming resistance mechanisms associated with existing *KRAS* inhibitors like Sotorasib. Further experimental validation will be essential to confirm these findings. Comparative studies on the effects of C02b and Sotorasib in cellular models of *KRAS*(G12C)-driven cancers could provide critical insights into their impact on downstream signaling and therapeutic efficacy.

Moreover, the structural diversity of *KRAS*(G12C) inhibitors remains narrow, leaving substantial room for the development of alternative scaffolds. Such scaffolds could offer improved pharmacokinetics, enhanced binding interactions, and broader application to different tumor types harboring the *KRAS*(G12C) mutation. For instance, novel compounds with distinct binding modes may reduce side effects, enhance tolerability, or bypass resistance mechanisms arising in *KRAS* proteins with secondary mutations or altered conformations. These challenges highlight the urgent need for novel inhibitors that can either supplement or outperform existing treatments. Compounds like C02b, which demonstrate stable binding and distinct interaction profiles in computational analyses, hold promise for addressing these gaps. These novel compounds could expand the arsenal of therapeutic options, potentially improving outcomes when used alone or in combination with existing therapies.

While the current study primarily focuses on computational and simulation-based approaches, we have outlined the necessity of such biochemical analyses in the discussion section. Future work will include experimental assessments of compound selectivity using GTP-loaded *KRAS*(G12C) and wild-type *KRAS* proteins. These experiments will involve evaluating GDP/GTP exchange inhibition, covalent binding to Cys12, and downstream signaling modulation. We appreciate the reviewer's suggestion and recognize its importance for validating the therapeutic potential of C02b.

The catalytic domain of the RAS family maintains a relatively conserved conformation, apart from the two switch regions (switch-I and switch-II).[47] The conformations of these switch regions may play a crucial role in mediating interactions with other proteins.[47] Therefore, post-MD simulations analyses were carried out to evaluate the stability and flexibility of the two switches in the Sotorasib and C02b complexes targeting *KRAS*(G12C). The RMSD analysis determined the structural stability, while RMSF focused on flexibility, particularly in critical

functional regions. Throughout the 500 ns MD simulation, the *KRAS*(G12C)-C02b complex maintained low RMSD values and stability, similar to the reference complex. High peaks were observed in RMSF graph for the region containing switch-I and switch-II loops in both complexes. On the other hand, PCA identified dominant modes of motion, capturing a substantial portion of the total variance and DCCM elucidated correlated conformational motions within the complexes. The dynamic interaction of *KRAS*(G12C) and Sotorasib through a 10 microseconds MD simulation found that Sotorasib increased flexibility in the switch-I and Switch-II regions,[46] However, a previous study observed a decrease in the fluctuation of the switch-I region during an 800 ns MD simulation.[48] The disparity in these simulation results may be attributed to different simulation settings. In our RMSF analysis with PCA (Figures 8 and 10), through a 500 ns MD simulation of the dynamic interaction of *KRAS*(G12C) and Sotorasib, it was observed that Sotorasib did not stabilize *KRAS* switches in the complex.[49]

5. Conclusion

Taken together, our findings emphasize the distinctive stabilizing effects of C02b compared to Sotorasib on the conformational dynamics of *KRAS*(G12C), which may contribute to the development of potential inhibitors and highlight the importance of C02b in the development of *KRAS*(G12C) inhibitors in the preclinical setting.

Acknowledgments

None.

Funding

Ahmet Acar would like to acknowledge Republic of Türkiye The Council of Higher Education Research Universities Support Program (Grant number: ADEP-108-2022-11202).

Conflict of interest

The authors declare that they have no competing interests.

Author contributions

Conceptualization: Safiye Merve Bostancioglu, Ahmet Acar
Formal analysis: Safiye Merve Bostancioglu
Investigation: Safiye Merve Bostancioglu, Ahmet Acar
Methodology: Safiye Merve Bostancioglu, Ahmet Acar
Writing – original draft: Safiye Merve Bostancioglu, Ahmet Acar
Writing – review & editing: Safiye Merve Bostancioglu, Ahmet Acar

Ethics approval and consent to participate

Not applicable.

Consent for publication

Not applicable.

Availability of data

Data are available from the corresponding author upon reasonable request.

References

1. Hanahan D. Hallmarks of cancer: New dimensions. *Cancer Discov*. 2022;12:31-46.
   doi: 10.1158/2159-8290.CD-21-1059
2. Hanahan D, Weinberg RA. Hallmarks of cancer: The next generation. *Cell*. 2011;144:646-74.
   doi: 10.1016/j.cell.2011.02.013
3. Greaves M, Maley CC. Clonal evolution in cancer. *Nature*. 2012;481:306-313.
4. Gatenby RA, Brown JS. Integrating evolutionary dynamics into cancer therapy. *Nat Rev Clin Oncol*. 2020;17:675-86.
   doi: 10.1038/s41571-020-0411-1
5. Ermini L, Mallo D, Kleftogiannis D, *et al.* Editorial: Cancer evolution. *Front Genet*. 2023;14:1187687.
   doi: 10.3389/fgene.2023.1187687
6. Merlo LMF, Pepper JW, Reid BJ, *et al.* Cancer as an evolutionary and ecological process. *Nat Rev Cancer*. 2006;6:924-935.
   doi: 10.1038/nrc2013
7. Turajlic S, Sottoriva A, Graham T, *et al.* Resolving genetic heterogeneity in cancer. *Nat Rev Genet*. 2019;20:404-416.
   doi: 10.1038/s41576-019-0114-6
8. Yalcin GD, Yilmaz KC, Dilber T, *et al.* Investigation of evolutionary dynamics for drug resistance in 3D spheroid model system using cellular barcoding technology. *PLoS One*. 2023;18:e0291942.
   doi: 10.1371/journal.pone.0291942
9. Danisik N, Yilmaz KC, Acar A. Identification of collateral sensitivity and evolutionary landscape of chemotherapy-induced drug resistance using cellular barcoding technology. *Front Pharmacol*. 2023;14:1178489.
   doi: 10.3389/fphar.2023.1178489
10. Acar A, Nichol D, Fernandez-Mateos J, *et al.* Exploiting evolutionary steering to induce collateral drug sensitivity in cancer. *Nat Commun*. 2020;11:1923.
    doi: 10.1038/s41467-020-15596-z

11. Smalley KS, Lioni M, Noma K, *et al. In vitro* three-dimensional tumor microenvironment models for anticancer drug discovery. *Expert Opin Drug Discov*. 2008;3:1-10.

    doi: 10.1517/17460441.3.1.1

12. Downward J. Targeting RAS signalling pathways in cancer therapy. *Nat Rev Cancer*. 2003;3:11-22.

    doi: 10.1038/nrc969

13. Kim HJ, Lee HN, Jeong MS, *et al.* Oncogenic *KRAS*: Signaling and drug resistance. *Cancers* (*Basel*). 2021;13:5599.

    doi: 10.3390/cancers13225599

14. Singh G, Thakur N, Kumar U. RAS: Circuitry and therapeutic targeting. *Cell Signal*. 2023;101:110505.

    doi: 10.1016/j.cellsig.2022.110505

15. Ferrer I, Zugazagoitia J, Herbertz S, *et al. KRAS*-Mutant non-small cell lung cancer: From biology to therapy. *Lung Cancer*. 2018;124:53-64.

    doi: 10.1016/j.lungcan.2018.07.013

16. Ciardiello D, Maiorano BA, Martinelli E. Targeting *KRAS*^{G12C} in colorectal cancer: The beginning of a new era. *ESMO Open*. 2023;8:100745.

    doi: 10.1016/j.esmoop.2022.100745

17. Naim N, Moukheiber S, Daou S, *et al. KRAS*-G12C covalent inhibitors: A game changer in the scene of cancer therapies. *Crit Rev Oncol Hematol*. 2021;168:103524.

    doi: 10.1016/j.critrevonc.2021.103524

18. Molina-Arcas M, Samani A, Downward J. Drugging the undruggable: Advances on RAS targeting in cancer. *Genes* (*Basel*). 2021;12:899.

    doi: 10.3390/genes12060899

19. Skoulidis F, Li BT, Dy GK, *et al.* Sotorasib for lung cancers with *KRAS* p.G12C mutation. *N Engl J Med*. 2021;384: 2371-2381.

    doi: 10.1056/nejmoa2103695

20. Lanman BA, Parsons AT. Sotorasib (LUMA*KRAS*), an ırreversible covalent Inhibitor of *KRAS* ^{G12C}. İn: *Current Drug Synthesis*. United States: Wiley; 2022. p. 183-199.

    doi: 10.1002/9781119847281.ch10

21. Saleh K, Kordahi M, Felefly T, *et al. KRAS*-targeted therapies in advanced solid cancers: Drug the undruggable? *Pharmacogenomics*. 2021;22:587-90.

    doi: 10.2217/pgs-2021-0045

22. Kim HJ, Lee HN, Jeong MS, *et al.* Oncogenic *KRAS*: Signaling and drug resistance. *Cancers* (*Basel*). 2021;13:5599.

    doi: 10.3390/cancers13225599

23. Oyedele AQK, Ogunlana AT, Boyenle ID, *et al.* Pharmacophoric analogs of sotorasib-entrapped *KRAS* G12C in its inactive GDP-bound conformation: Covalent docking and molecular dynamics investigations. *Mol Divers*. 2023;27:1795-1807.

    doi: 10.1007/s11030-022-10534-1

24. Mortier J, Friberg A, Badock V, *et al.* Computationally empowered workflow identifies novel covalent allosteric binders for *KRAS*^{G12C}. *ChemMedChem*. 2020;15:827-832

    doi: 10.1002/cmdc.201900727

25. Nnadi CI, Jenkins ML, Gentile DR, *et al.* Novel K-Ras G12C switch-II covalent binders destabilize ras and accelerate nucleotide exchange. *J Chem Inf Model*. 2018;58:464-471.

    doi: 10.1021/acs.jcim.7b00399

26. Boehm M, Wu TY, Haussen H, *et al.* Similarity searching and scaffold hopping in synthetically accessible combinatorial chemistry spaces. *J Med Chem*. 2008;51:2468-2480.

    doi: 10.1021/jm0707727

27. Madhavi Sastry G, Adzhigirey M, Day T, *et al.* Protein and ligand preparation: Parameters, protocols, and influence on virtual screening enrichments. *J Comput Aided Mol Des*. 2013;27:221-34.

    doi: 10.1007/s10822-013-9644-8

28. *Schrödinger Release 2023-3: LigPre*. New York,: Schrödinger, LLC; 2023.

29. Shelley JC, Cholleti A, Frye LL, *et al.* Epik: A software program for pK(a) prediction and protonation state generation for drug-like molecules. *J Comput Aided Mol Des*. 2007;21:681-691.

    doi: 10.1007/s10822-007-9133-z

30. Canon J, Rex K, Saiki AY, *et al.* The clinical *KRAS*(G12C) inhibitor AMG 510 drives Anti-tumour immunity. *Nature*. 2019;575:217-223.

    doi: 10.1038/s41586-019-1694-1

31. *Schrödinger Release 2023-3: Protein Preparation Wizard; Epik*. New York: Schrödinger, LLC; 2023.

32. Roos K, Wu C, Damm W, *et al.* OPLS3e: Extending force field coverage for drug-like small molecules. *J Chem Theory Comput*. 2019;15:1863-1874.

    doi: 10.1021/acs.jctc.8b01026

33. Zhu K, Borrelli KW, Greenwood JR, *et al.* Docking covalent inhibitors: A parameter free approach to pose prediction and scoring. *J Chem Inf Model*. 2014;54:1932-1940.

    doi: 10.1021/ci500118s

34. Friesner RA, Banks JL, Murphy RB, *et al.* Glide: A New Approach for rapid, accurate docking and scoring. 1. Method and assessment of docking accuracy. *J Med Chem*. 2004;47:1739-1749.

    doi: 10.1021/jm0306430

35. Halgren TA, Murphy RB, Friesner RA, *et al.* Glide: A new approach for rapid, accurate docking and scoring. 2. enrichment factors in database screening. *J Med Chem*. 2004;47:1750-1759.

doi: 10.1021/jm030644s

36. Van Der Spoel D, Lindahl E, Hess B, *et al.* GROMACS: Fast, flexible, and free. *J Comput Chem*. 2005;26:1701-1718.

doi: 10.1002/jcc.20291

37. Best RB, Zhu X, Shim J, *et al.* Optimization of the additive CHARMM all-atom protein force field targeting improved sampling of the backbone ϕ, ψ and side-chain χ1 and χ2 Dihedral Angles. *J Chem Theory Comput*. 2012;8:3257-3273.

doi: 10.1021/ct300400x

38. Bussi G, Donadio D, Parrinello M. Canonical sampling through velocity rescaling. *J Chem Phys*. 2007;126:014101.

doi: 10.1063/1.2408420

39. Berendsen HJC, Postma JPM, Van Gunsteren WF, *et al.* Molecular dynamics with coupling to an external bath. *J Chem Phys*. 1984;81:3684-3690.

doi: 10.1063/1.448118

40. Bernetti M, Bussi G. Pressure control using stochastic cell rescaling. *J Chem Phys*. 2020;153:114107.

doi: 10.1063/5.0020514

41. Darden T, York D, Pedersen L. Particle mesh ewald: An N·log(N) method for ewald sums in large systems. *J Chem Phys*. 1993;98:10089-100920.

doi: 10.1063/1.464397

42. Hess B. P-LINCS: A parallel linear constraint solver for molecular simulation. *J Chem Theory Comput*. 2008;4: 116-122.

doi: 10.1021/ct700200b

43. Turner P. *XMGRACE, Version 5.1. 19. Center for Coastal and Land-Margin Research*. Beaverton, OR: Oregon Graduate Institute of Science and Technology; 2005.

44. Humphrey W, Dalke A, Schulten K. VMD: Visual molecular dynamics. *J Mol Graph*. 1996;14:33-8.

doi: 10.1016/0263-7855(96)00018-5

45. Grant BJ, Rodrigues APC, ElSawy KM, McCammon JA, Caves LS. Bio3d: An R package for the comparative analysis of protein structures. *Bioinformatics*. 2006;22:2695-2696.

doi: 10.1093/bioinformatics/btl461

46. Scarpino A, Ferenczy GG, Keserü GM. Comparative evaluation of covalent docking tools. *J Chem Inf Model*. 2018;58:1441-1458.

doi: 10.1021/acs.jcim.8b00228

47. Pantsar T. *KRAS*(G12C)-AMG 510 interaction dynamics revealed by all-atom molecular dynamics simulations. *Sci Rep*. 2020;10:11992.

doi: 10.1038/s41598-020-68950-y

48. Milburn MV, Tong L, DeVos AM, *et al.* Molecular switch for signal transduction: Structural differences between active and inactive forms of protooncogenic ras proteins. *Science (1979)*. 1990;247:939-945.

doi: 10.1126/science.2406906

49. Li Y, Han L, Zhang Z. Understanding the influence of AMG 510 on the structure of *KRAS*G12C empowered by molecular dynamics simulation. *Comput Struct Biotechnol J*. 2022;20:1056-1067

doi: 10.1016/j.csbj.2022.02.018

Appendices

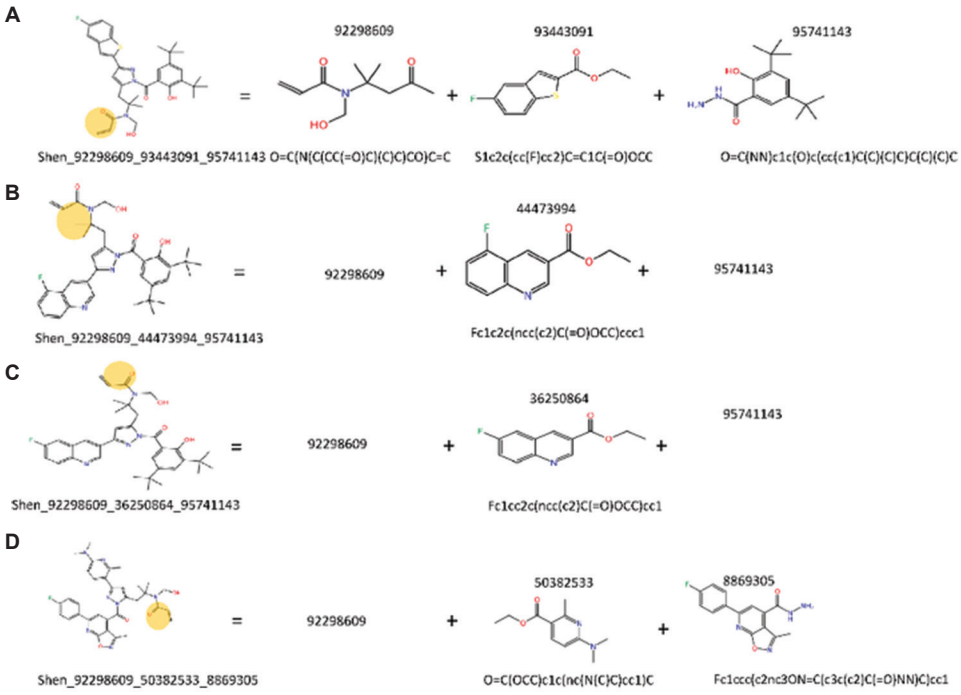

Figure A1. The acrylamide warheads and building blocks of compounds. (A) C01, (B) C02a, (C) C02b, and (D) C03.

Table A1. 174 compounds that have structural similarities to Sotorasib

No	Name
1	rxn501b____EMOL916035____EMOL4353066____EMOL45478818
2	rxn501b____EMOL485662____EMOL4353066____EMOL45478818
3	rxn508____EMOL916035____EMOL37154489____EMOL724744
4	rxn508____EMOL916035____EMOL37154489____EMOL4854098
5	rxn508____EMOL916035____EMOL37154489____EMOL300131641
6	rxn508____EMOL916035____EMOL37154489____EMOL9779925
7	rxn508____EMOL916035____EMOL37154489____EMOL2863515
8	rxn501b____EMOL882112____EMOL4353066____EMOL45478818
9	rxn508____EMOL916035____EMOL50157604____EMOL724744
10	rxn508____EMOL916035____EMOL2862529____EMOL4854098
11	rxn508____EMOL916035____EMOL50157604____EMOL2863515
12	rxn508____EMOL916035____EMOL50157604____EMOL300131641
13	rxn508____EMOL916035____EMOL2862529____EMOL300131641
14	rxn508____EMOL916035____EMOL50157604____EMOL9779925
15	rxn508____EMOL916035____EMOL2862529____EMOL2863515
16	rxn508____EMOL916035____EMOL50157604____EMOL4854098
17	rxn508____EMOL916035____EMOL2862529____EMOL9779925
18	rxn508____EMOL916035____EMOL2862529____EMOL724744
19	rxn508____EMOL916035____EMOL37154489____EMOL30070316
20	rxn508____EMOL916035____EMOL37154489____EMOL36725275
21	rxn508____EMOL916035____EMOL50157604____EMOL36725275
22	rxn508____EMOL916035____EMOL2862529____EMOL36725275
23	rxn508____EMOL916035____EMOL50157604____EMOL30070316
24	rxn508____EMOL916035____EMOL2862529____EMOL30070316
25	rxn501b____EMOL916035____EMOL4353066____EMOL48597142
26	rxn501b____EMOL916035____EMOL4353066____EMOL45478663
27	rxn508____EMOL916035____EMOL37154489____EMOL44474549
28	rxn508____EMOL916035____EMOL50157604____EMOL44474549
29	rxn508____EMOL916035____EMOL2862529____EMOL44474549
30	rxn508____EMOL916035____EMOL37154489____EMOL43633603
31	rxn508____EMOL916035____EMOL2862529____EMOL43633603
32	rxn508____EMOL916035____EMOL50157604____EMOL43633603
33	rxn508____EMOL916035____EMOL37154489____EMOL49844674
34	rxn508____EMOL916035____EMOL37154489____EMOL1522728
35	rxn508____EMOL916035____EMOL37154489____EMOL11554196
36	rxn508____EMOL916035____EMOL37154489____EMOL1885674
37	rxn508____EMOL916035____EMOL37154489____EMOL42785649
38	rxn508____EMOL916035____EMOL37154489____EMOL11488490
39	rxn508____EMOL916035____EMOL89945076____EMOL724744

(Cont'd...)

Table A1. (*Continued*)

No	Name
40	rxn508____EMOL916035____EMOL89945076____EMOL9779925
41	rxn508____EMOL916035____EMOL89945076____EMOL4854098
42	rxn508____EMOL916035____EMOL89945076____EMOL2863515
43	rxn508____EMOL916035____EMOL89945076____EMOL300131641
44	rxn508____EMOL916035____EMOL37154489____EMOL904614
45	rxn508____EMOL916035____EMOL2862529____EMOL42785649
46	rxn508____EMOL916035____EMOL50157604____EMOL49844674
47	rxn508____EMOL916035____EMOL50157604____EMOL1885674
48	rxn508____EMOL916035____EMOL2862529____EMOL11488490
49	rxn508____EMOL916035____EMOL50157604____EMOL42785649
50	rxn508____EMOL916035____EMOL50157604____EMOL11488490
51	rxn508____EMOL916035____EMOL2862529____EMOL49844674
52	rxn508____EMOL916035____EMOL2862529____EMOL1885674
53	rxn508____EMOL916035____EMOL2862529____EMOL1522728
54	rxn508____EMOL916035____EMOL50157604____EMOL11554196
55	rxn508____EMOL916035____EMOL2862529____EMOL11554196
56	rxn508____EMOL916035____EMOL50157604____EMOL1522728
57	rxn508____EMOL916035____EMOL50157604____EMOL904614
58	rxn508____EMOL916035____EMOL2862529____EMOL904614
59	rxn502b____EMOL916035____EMOL4353066____EMOL2251614
60	rxn508____EMOL916035____EMOL89945076____EMOL30070316
61	rxn508____EMOL916035____EMOL89945076____EMOL36725275
62	rxn508____EMOL485662____EMOL37154489____EMOL2863515
63	rxn508____EMOL485662____EMOL37154489____EMOL4854098
64	rxn508____EMOL485662____EMOL37154489____EMOL300131641
65	rxn508____EMOL485662____EMOL37154489____EMOL724744
66	rxn508____EMOL485662____EMOL37154489____EMOL9779925
67	rxn508____EMOL882112____EMOL37154489____EMOL2863515
68	rxn508____EMOL882112____EMOL37154489____EMOL724744
69	rxn508____EMOL882112____EMOL37154489____EMOL4854098
70	rxn508____EMOL882112____EMOL37154489____EMOL300131641
71	rxn508____EMOL882112____EMOL37154489____EMOL9779925
72	rxn508____EMOL485662____EMOL50157604____EMOL300131641
73	CSSS00161188889
74	WXDL_15A____SB1376____LN00004982____BT6378
75	Shen____92298609____48620564____44152703
76	Shen____92298609____48620700____44152703
77	Shen____92298609____93443091____44152703
78	Shen____92298609____48552545____29552264

(Cont'd...)

Table A1. (*Continued*)

No	Name
79	Shen____92298609____106083795____44152703
80	Shen____92298609____106083765____44152703
81	Shen____92298609____49239582____44152703
82	Shen____92298609____49239580____44152703
83	Shen____92298609____49239556____44152703
84	Shen____92298609____36250864____44152703
85	Shen____92298609____44473994____44152703
86	Shen____92298609____44473403____44152703
87	Shen____92298609____44473381____44152703
88	Shen____92298609____48573899____44152703
89	Shen____92298609____48552545____107053254
90	Shen____92298609____48552545____81813113
91	Shen____92298609____32456150____44152703
92	Shen____92298609____36745965____44152703
93	Shen____92298609____830425____44152703
94	Shen____92298609____42824050____44152703
95	Shen____92298609____42817358____44152703
96	Shen____92298609____25041346____44152703
97	Shen____92298609____97662126____29552264
98	Shen____92298609____36249205____29552264
99	Shen____92298609____48552545____8869305
100	Shen____92298609____36249205____107053254
101	Shen____92298609____97662126____107053254
102	Shen____92298609____56970423____44152703
103	Shen____92298609____49823880____44152703
104	Shen____92298609____36249205____81813113
105	Shen____92298609____97662126____81813113
106	Shen____92298609____50382533____29552264
107	Gray____107373053____6886343____107509511
108	Shen____92298609____53885480____44152703
109	Shen____92298609____53885502____44152703
110	Shen____92298609____44473387____44152703
111	Shen____92298609____53885486____44152703
112	Shen____92298609____42816206____44152703
113	Shen____92298609____36828355____44152703
114	Shen____92298609____53890255____44152703
115	Shen____92298609____50382533____107053254
116	Shen____92298609____50272909____29552264
117	Shen____92298609____50382533____81813113

(Cont'd...)

Table A1. (*Continued*)

No	Name
118	Shen____92298609____38501832____44152703
119	Shen____92298609____44848277____44152703
120	Shen____92298609____12814542____44152703
121	Shen____92298609____980919____44152703
122	Shen____92298609____44391072____44152703
123	Shen____92298609____520177____44152703
124	Shen____92298609____50272909____107053254
125	Shen____92298609____106068876____44152703
126	Shen____92298609____106068894____44152703
127	Shen____92298609____81802460____44152703
128	Shen____92298609____43045611____44152703
129	Shen____92298609____50272909____81813113
130	Shen____92298609____48620700____95741143
131	Shen____92298609____48620564____95741143
132	Shen____92298609____48552545____42793511
133	Shen____92298609____48620564____96426646
134	Shen____92298609____48620700____96426646
135	Shen____92298609____36249205____8869305
136	Shen____92298609____97662126____8869305
137	Shen____92298609____81802090____29552264
138	Shen____92298609____76750201____29552264
139	Shen____92298609____106978508____29552264
140	Shen____92298609____95759057____29552264
141	Shen____92298609____48552545____50495850
142	Shen____92298609____93443091____95741143
143	Shen____92298609____93443091____96426646
144	Shen____92298609____106083765____95741143
145	Shen____92298609____106083795____95741143
146	Shen____92298609____106083795____96426646
147	Shen____92298609____106083765____96426646
148	Shen____92298609____81802090____107053254
149	Shen____92298609____106978508____107053254
150	Shen____92298609____76750201____107053254
151	Shen____92298609____49253559____44152703
152	Shen____92298609____1451473____44152703
153	Shen____92298609____49253379____44152703
154	Shen____92298609____48552545____2066545
155	Shen____92298609____95759057____107053254
156	Shen____92298609____50382533____8869305

(Cont'd...)

Table A1. (*Continued*)

No	Name
157	Shen____92298609____48552545____50658478
158	Shen____92298609____49239556____95741143
159	Shen____92298609____49239582____95741143
160	Shen____92298609____49239580____95741143
161	Shen____92298609____44473381____95741143
162	Shen____92298609____44473403____95741143
163	Shen____92298609____36250864____95741143
164	Shen____92298609____44473994____95741143
165	Shen____92298609____48573899____95741143
166	Shen____92298609____76750201____81813113
167	Shen____92298609____81802090____81813113
168	Shen____92298609____106978508____81813113
169	Shen____92298609____95759057____81813113
170	Shen____92298609____49239556____96426646
171	Shen____92298609____49239580____96426646
172	Shen____92298609____49239582____96426646
173	Shen____92298609____84829545____44152703
174	Shen____92298609____44473389____44152703

ACCSCIENCE PUBLISHING

Tumor Discovery

ORIGINAL RESEARCH ARTICLE

Homoharringtonine inhibits pancreatic cancer progression via mitochondrial energy metabolism suppression and macrophages reduction

Xiaoxia Wang, Tao Wang, Xuelu Peng, Ke Zhu, Ming Ye, Jie Meng*, and Haiyan Xu*

Department of Biomedical Engineering, Institute of Basic Medical Sciences, Chinese Academy of Medical Sciences and Peking Union Medical College, Beijing, China

Abstract

Homoharringtonine (HHT) has been used in leukemia therapy since the 1970s. Its inhibitory effects on solid tumors have attracted increasing interest and have been actively explored in recent years. This study investigates the therapeutic effects and pharmacological mechanisms of HHT on pancreatic cancer, focusing on mitochondrial energy metabolism and macrophage sensitivity to HHT. HHT significantly inhibited the proliferation and colony formation of pancreatic cancer cell lines PANC-1 and Pan02 *in vitro* and suppressed tumorigenic potential *in vivo*. The mechanistic study revealed that HHT induced a significant elevation of reactive oxygen species (ROS) levels in pancreatic cancer cells over time, as evidenced by the enhanced dichlorodihydrofluorescein diacetate fluorescence and an elevated NAD^+/NADH ratio. This resulted in mitochondrial respiratory dysfunction, including reductions in basal respiration, maximal respiration, and adenosine triphosphate production. In addition, HHT caused cell cycle arrest and disrupted the cytoskeleton, thereby inhibiting cell division and proliferation. The anti-tumor effects of HHT were further evaluated using a subcutaneous pancreatic tumor-bearing mouse model, showing that HHT inhibited the proliferation of pancreatic tumor cells *in vivo*, which led to reduced tumor mass. Moreover, HHT significantly reduced the viability of macrophages both *in vitro* and *in vivo*, leading to the depletion of tumor-associated macrophages in the tumor microenvironment (TME), thereby alleviating immune suppression. In conclusion, HHT effectively inhibits pancreatic cancer progression through upregulating cellular ROS levels over time, thereby disrupting mitochondrial respiratory capacity in tumor cells and reducing macrophage populations, contributing to TME reprogramming and immune restoration.

Keywords: Pancreatic cancer; Reactive oxygen species; Mitochondrial energy metabolism; Cell cycle; Tumor microenvironment

***Corresponding authors:**
Haiyan Xu
(xuhy@pumc.edu.cn)
Jie Meng
(mengjie@ibms.pumc.edu.cn)

Citation: Wang X, Wang T, Peng X, *et al*. Homoharringtonine inhibits pancreatic cancer progression via mitochondrial energy metabolism suppression and macrophages reduction. *Tumor Discov*. 2025;4(1):99-112.
doi: 10.36922/td.7825

Received: December 17, 2024

Revised: January 20, 2025

Accepted: January 24, 2025

Published online: February 24, 2025

1. Introduction

Pancreatic cancer is a malignant tumor of the digestive system with high lethality and low cure rates. It is the sixth leading cause of cancer-related deaths in China[1] and

ranks 12th in new cases but sixth in cancer mortality worldwide.[2] Among pancreatic cancers, pancreatic ductal adenocarcinoma (PDAC) has one of the highest mortality rates among solid tumors, with an overall 5-year survival rate of <10%.[3] Pancreatic tumors treated with standard chemotherapy regimens are prone to developing drug resistance, whose mechanisms are further complicated by the genetic heterogeneity of the tumors.[4] Moreover, drug resistance in pancreatic cancer is not only driven by intrinsic tumor cell mechanisms but also by immune suppression within the tumor microenvironment (TME).[5-8] Therefore, more effective therapeutic approaches are keen to address the challenges in improving pancreatic cancer treatment outcomes.

Homoharringtonine (HHT), an alkaloid extracted from the herb *Cephalotaxus*, is a protein synthesis inhibitor that inhibits the initial elongation step of translation by binding to the A-site of the ribosome, thereby inhibiting protein synthesis.[9,10] HHT has been approved by the U.S. Food and Drug Administration for the treatment of chronic myeloid leukemia (CML) and acute myeloid leukemia (AML).[11,12] In recent years, studies on HHT have expanded to solid tumors. Several pioneering investigations have shown that HHT exerts inhibitory effects on the growth of human pancreatic cancer cells, such as inhibiting proliferation and growth of MIA-PaCa-2 and PANC-1 cells in a time- and dose-dependent manner.[13,14] In addition, HHT has been shown to induce cell cycle arrest and enhance the anticancer activity of erlotinib in MIA-PaCa-2 and B×PC-3 cells.[15] Nevertheless, despite its promising potential in pancreatic cancer therapy, the underlying molecular mechanisms and therapeutic efficacy of HHT require further investigation.

Previous studies on CML cells have indicated that HHT affects mitochondrial functions, particularly in oxygen consumption rate (OCR).[16] This implies the involvement of reactive oxygen species (ROS), which plays a crucial role in maintaining cellular homeostasis in normal cells. However, ROS dysregulation in cancer cells often leads to aberrant cell signaling and uncontrolled proliferation.[17-19] Building on this evidence, this study investigated the potential anti-tumor effects of HHT on PDAC cells and its underlying mechanism of action, focusing on mitochondrial energy metabolism in both tumor cells and stromal cells within the TME. The results showed that HHT significantly inhibited pancreatic cancer progression through significantly elevating intracellular ROS levels over time, resulting in the disruption of mitochondrial respiratory capacity, impairment of energy metabolism, and cell cycle arrest. In addition, HHT alleviated the immunosuppressive effects within the TME by reducing the viability of macrophages.

2. Materials and methods

2.1. Cells, reagents, and animal models

Human pancreatic cancer cell lines PANC-1 and SW1990, mouse pancreatic cancer cell line Pan02-mCherry, and mouse macrophage cell line RAW264.7 were purchased from the Cell Resource Center, Institute of Basic Medical Sciences, Chinese Academy of Medical Sciences and Peking Union Medical College. Cells were maintained at 37°C with 5% CO_2 in high-glucose Dulbecco's Modified Eagle Medium (DMEM, Invitrogen, USA), supplemented with 10% fetal bovine serum (FBS, Gibco, USA), 100 U/mL penicillin (Hyclone, USA), and 100 μg/mL streptomycin (Hyclone, USA). HHT was purchased from Xi'an Hao-Xuan Bio-Tech Co., Ltd. (Shanxi, China). The HHT powder was dissolved in dimethyl sulfoxide to prepare a 20 mM stock solution, which was further diluted to corresponding concentrations with DMEM complete medium for cellular experiments.

Healthy female C57BL/6 mice (6 – 8 weeks old) were purchased and bred at the animal center of the Institute of Basic Medical Sciences. All animal experiments reported were carried out in accordance with the guidelines of the committee on the Animal Care and Use of Institute of Basic Medical Sciences, Chinese Academy of Medical Sciences and Peking Union Medical College (Ethics Approval ID: ACUC-A02-2023-015). Mice were euthanized through cervical dislocation following isoflurane anesthesia in accordance with the 2020 AVMA Guidelines for the Euthanasia of Animals, ensuring humane treatment. The study adhered strictly to the ARRIVE guideline.[20]

2.2. Cell viability assay

PANC-1, SW1990, Pan02-mCherry, and RAW264.7 cells were seeded at a density of 5×10^3 cells per well and allowed to attach overnight. Subsequently, HHT concentrations ranging from 0 to 400 nM were added to the cells. After 24 or 48 h of treatment, 10 μL of cell counting kit-8 (CCK-8) reagent (Dojindo, Japan) was added, and the cells were incubated for an additional 1 – 4 h at 37°C. Absorbance was measured at 450 nm and 630 nm using a microplate reader (Thermofisher Scientific, USA). Cell viability was calculated as a percentage of the control, and the half-maximal inhibitory concentration (IC50) values were determined using GraphPad Prism software (GraphPad Software, USA).

2.3. Cell proliferation assay

PANC-1 cells were washed with phosphate-buffered saline (PBS) and resuspended in serum-free DMEM. Next, carboxyfluorescein succinimidyl ester (CFSE, Dojindo, Japan) was added to the cell suspension at 5 μM, followed

by incubation at 37°C for 10 min. Unbound CFSE was removed by centrifugation. The CFSE-labeled cells were then treated with various concentrations of HHT for 24 or 48 h. Fluorescence intensity was analyzed using an Accuri™ C6 flow cytometer (BD Biosciences, USA).

2.4. Colony-forming assay

PANC-1 and Pan02-mCherry cells were seeded into 6-well plates at a density of 2×10^3 cells per well. After overnight adherence, the cells were treated with HHT at different concentrations for 48 h, and then the culture medium was replaced with fresh medium and replenished every 3 days. After a 14-day incubation, cell colonies were fixed with 4% paraformaldehyde (PFA) and stained with crystal violet solution. The number of colonies was counted manually.

2.5. *In vivo* tumor-forming assay

Pan02-mCherry cells were cultured with HHT at 25 nM and 200 nM, respectively. After 24 h, the cells were collected, centrifuged, and counted. Untreated or HHT-treated cells were then subcutaneously injected into mice at a dose of 2×10^6/mouse, with four mice per group. Tumor sizes were recorded during the experiment. On the 23rd day post-implantation, *in vivo* imaging of mouse tumors was performed using the Xenogen IVIS Spectrum system (Caliper Life Sciences, USA). The mice were then sacrificed, and the tumors were excised and weighed.

2.6. Cell cycle assay

PANC-1 cells were treated with HHT at 25 nM, 50 nM, and 100 nM for 48 h, then collected, washed, and fixed with 70% ethanol overnight at −20°C. The cells were treated with RNase for 30 min at 37°C and stained with propidium iodide (PI) staining solution (BD Biosciences, USA) for 30 min. Flow cytometric analysis was performed using an Accuri™ C6 flow cytometer (BD Biosciences, USA), and the data were processed using ModFit LT™ software (Verity Software, USA).

2.7. Western blotting

PANC-1 cells were incubated with HHT at 50 nM and 100 nM for 48 h, then washed with cold PBS and lysed using RIPA buffer (Solarbio, China) supplemented with phenylmethylsulfonyl fluoride (PMSF, Solarbio, China) and protease inhibitors (Applygen, China). The cell lysates were centrifuged at 12,000 rpm for 15 min at 4°C, and the protein concentrations of the supernatants were determined using a BCA kit (Thermofisher Scientific, USA). Equal amounts of protein were separated on 12% SDS-PAGE gels and transferred onto 0.45 μm PVDF membranes (Merck Millipore, Germany). The membranes were blocked with 5% non-fat milk in Tris-buffered saline with 0.1% Tween-20 (TBST) for 1 h at room temperature, followed by incubation with primary antibodies overnight at 4°C. The primary antibodies used in this study included cyclin D2, cyclin-dependent kinase 1 (CDC2), cell division cycle 25c (CDC25c), p53, and GAPDH (Cell Signaling Technology, USA). After washing with TBST, the membranes were incubated with horseradish peroxidase-conjugated secondary antibodies (Biolegend, USA) for 1 h at room temperature. Protein bands were visualized using an enhanced chemiluminescence reagent (ECL, Merck Millipore, Germany) in a gel imaging system (Tanon, China). The blot quantification was performed using ImageJ software (NIH, USA). Protein expression levels were normalized to GAPDH, and relative protein expression levels were calculated.

2.8. Cytoskeleton staining assay

PANC-1 cells were treated with 50 nM HHT for 48 h. After fixation with 4% PFA, the cells were stained with Flash Phalloidin™ Red 594 (Biolegend, USA) for cytoskeleton visualization and DAPI (ZSGB-Bio, China) for nuclear staining. Cytoskeletons were observed using an Olympus FV1000MPE multiphoton laser scanning microscope (Olympus, Japan).

2.9. Intracellular ROS measurement

After treatment with HHT (50 nM, 100 nM) for various durations, PANC-1 cells were incubated with 10 μM 2',7'-dichlorodihydrofluorescein diacetate (DCFH-DA, Sigma, USA) for 30 min at 37°C. The fluorescence intensity, which represents the intracellular ROS level, was measured using a flow cytometer. Relative ROS levels were calculated by normalization to the control.

2.10. Cell OCR measurement

The OCR of PANC-1 cells was measured using an XFe24 extracellular flux analyzer (Agilent, USA). HHT-pretreated (50 nM, 24 h) and untreated cells were seeded into XFe24 cell culture microplates and allowed to adhere overnight. The medium was then replaced with XF base medium supplemented with glucose, pyruvate, and glutamine. OCR measurements were recorded after the sequential addition of oligomycin (oligo), carbonyl cyanide 4-(trifluoromethoxy) phenylhydrazone, and a combination of rotenone and antimycin A. The data were analyzed using Seahorse XFe24 software to determine basal respiration, adenosine triphosphate (ATP)-linked respiration, maximal respiration, and non-mitochondrial respiration.

2.11. ATP measurement

PANC-1 cells were treated with HHT at 50 nM and 100 nM for 24 or 48 h. ATP levels were measured using an ATP assay

kit (Beyotime, China) according to the manufacturer's instructions. Luminescence intensity was measured using a microplate reader (Thermofisher Scientific, USA) and normalized to the protein content of the cell lysates.

2.12. NAD^+/NADH measurement

PANC-1 cells were treated with HHT at 50 nM and 100 nM for 24 or 48 h. Intracellular total NAD (NAD_{total}) and NADH content were measured using a commercial assay kit (Beyotime, China) according to the manufacturer's protocol. The NAD^+/NADH ratio was calculated according to the following formula.

$$[NAD^+]/[NADH] = ([NAD_{total}] - [NADH])/[NADH]$$

2.13. *In vivo* therapeutic efficacy evaluation

First, an HHT toxicity assessment was conducted in healthy mice to determine a safe dosage for therapeutic evaluation. Briefly, healthy female C57BL/6 mice (6 – 8 weeks old, ~20 g) were randomly divided into five groups (n = 3). HHT solution was prepared in 0.4% (w/v) Soluplus® (BASF SE, Germany) in PBS, with four dosages including 0.5, 1, 2, and 4 mg/kg. A PBS solution containing 0.4% Soluplus® was used as the control. Mice were intravenously administered different dosages of HHT daily for four consecutive days. The survived mice were monitored and recorded daily for 5 days after the initial administration.

Pan02-mCherry cells were subcutaneously injected into the right axillary region of mice at the dose of 2×10^6 cells per mouse. When tumors reached about 75 mm^3, mice were randomly divided into three groups (n = 7). Meanwhile, HHT solution was prepared in 0.4% of Soluplus® (BASF SE, Germany) in PBS for the animal experiment. Mice were intravenously administered with HHT at the dosages of 0.5 and 1.0 mg/kg/day for 5 days/week over 2 weeks. The control (Ctrl) group received an injection of 0.4% of Soluplus® in PBS in the same volume. The body weight and tumor volume were measured. On the 3rd day after the final injection, mice were sacrificed, and tumors were excised, photographed, and weighed. Tumor samples were fixed in 4% PFA, embedded in paraffin, and analyzed with hematoxylin-eosin (H&E) staining and immunofluorescence staining for Ki67 and F4/80 (Servicebio, China) according to the manufacturer's instructions.

2.14. Statistical analysis

Statistical analyses were carried out using the GraphPad Prism software (version 10.1.1, GraphPad Software, USA). All data in this study were presented as mean ± standard deviation (SD). Comparisons between two groups were performed using an unpaired two-tailed Student's t-test. One-way analysis of variance (ANOVA) was used for comparisons among three or more groups defined by a single factor, whereas two-way ANOVA was used for comparisons involving two factors. The least significant difference *post hoc* test was conducted following ANOVA to compare group means. A $P < 0.05$ was considered statistically significant.

3. Results

3.1. HHT inhibited the growth and proliferation of PDAC cells *in vitro*

The cytotoxic effect of HHT on the viability of PDAC cells was evaluated using the CCK-8 assay. It was shown that the viability of PANC-1 cells was significantly inhibited by HHT in a dose- and time-dependent manner (Figure 1A). The IC50 value of HHT for PANC-1 at 24 hs was 23.11 nM. Similarly, the IC50 values for SW1990 cells and Pan02-mCherry cells at 24 h were 144.00 nM and 20.67 nM, respectively (Table S1). The effect of HHT on the proliferation of PANC-1 cells was examined using the CFSE

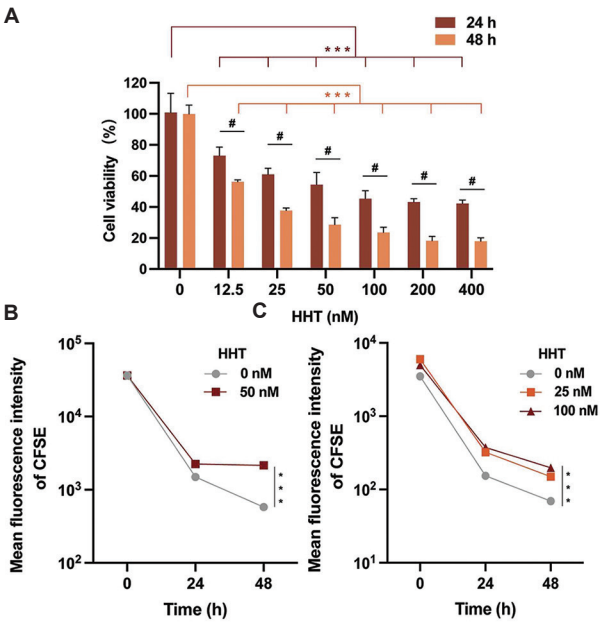

Figure 1. Effects of HHT on the viability and proliferation of pancreatic cancer cells. (A) Viability of human pancreatic cancer PANC-1 cells treated with HHT at different concentrations for 24 and 48 h, assessed by the CCK-8 assay (n = 4). (B) Proliferation of PANC-1 cells treated with HHT for 24 and 48 h, evaluated by CFSE staining assay (n = 3). PANC-1 cells were labeled with 5 μM CFSE, followed by HHT treatment at 50 nM for 24 and 48 h. (C) Long-term inhibitory effect of HHT on PANC-1 cell proliferation. Cells were pre-treated with 25 nM or 100 nM HHT for 24 h, followed by incubation in fresh, drug-free medium for another 24 and 48 h (n = 3). Note: #$P < 0.05$, ***$P < 0.001$.
Abbreviations: HHT: Homoharringtonine; CFSE: Carboxyfluorescein succinimidyl ester; CCK-8 assay: Cell counting kit-8 assay; h: Hours.

assay. The results showed that the fluorescent intensity of PANC-1 cells treated with HHT decreased much more slowly over time than that of the control (Figure 1B). Specifically, the mean fluorescent intensity of PANC-1 cells treated with 50 nM HHT was nearly 4-fold compared to the control. To determine whether the inhibitory effect persisted over time, PANC-1 cells were treated with HHT at 25 nM or 100 nM for 24 h, followed by replenishing with fresh complete medium and further incubated for another 24 or 48 h. Results showed that HHT-treated cells continued to exhibit significantly higher CFSE values, indicating that the inhibitory effect on proliferation was still evident 48 h after HHT removal (Figure 1C).

Next, crystal violet staining was used to investigate the effect of HHT on the colony-forming ability of PANC-1 and Pan02-mCherry cells. Both cell lines exhibited a significant reduction in colony formation after 48 h of incubation of HHT in a dose-dependent manner compared to untreated cells (Figure 2A). Specifically, in PANC-1 cells, 25 nM HHT inhibited colony formation by about 41%. Pan02-mCherry cells exhibited greater sensitivity to HHT treatment, with the same concentration inducing about 54% inhibition of colony formation in reference to that of control (Figure 2B). The inhibitory effect of HHT on the tumorigenic capacity of Pan02-mCherry cells was also examined *in vivo*. The tumor cells were treated with HHT at 200 nM for 24 h before implantation. On the 23rd post-implantation, the fluorescence intensity of the tumor mass in the HHT-pretreated group was lower than that of control group (Figure 2C), indicating that HHT-pretreated cells developed tumors more slowly than the control cells (Figure 2D). At the same time, the tumor weight in the HHT-pretreated group was significantly decreased compared to the control group.

3.2. HHT-induced oxidative stress and impaired mitochondrial respiration in PDAC cells

The intracellular ROS levels were measured using DCFH-DA in PANC-1 cells treated with HHT at 50 nM and 100 nM. Results showed that ROS levels remained unchanged during the first 6 h of HHT treatment but were significantly elevated after 12 h of treatment, demonstrating both dose- and time-dependent effects (Figure 3A). Notably, the ROS levels in the 100 nM group were much higher than those in the 50 nM group at 12, 24, and 48 h. Fluorescent microscopy of cells treated with HHT for 18 h (Figure 3B) confirmed these findings, showing increased cellular fluorescence with HHT treatment at both 50 nM and 100 nM, consistent with the data in Figure 3A. At the same time, NADH levels were downregulated following HHT treatment (Figure 3C), along with a significant increase of NAD^+/NADH ratio after 48 h of HHT treatment at 50 nM or 100 nM (Figure 3D), clearly indicating a state of oxidative stress.

To examine whether oxidative stress affected mitochondrial function in the tumor cells, OCR was

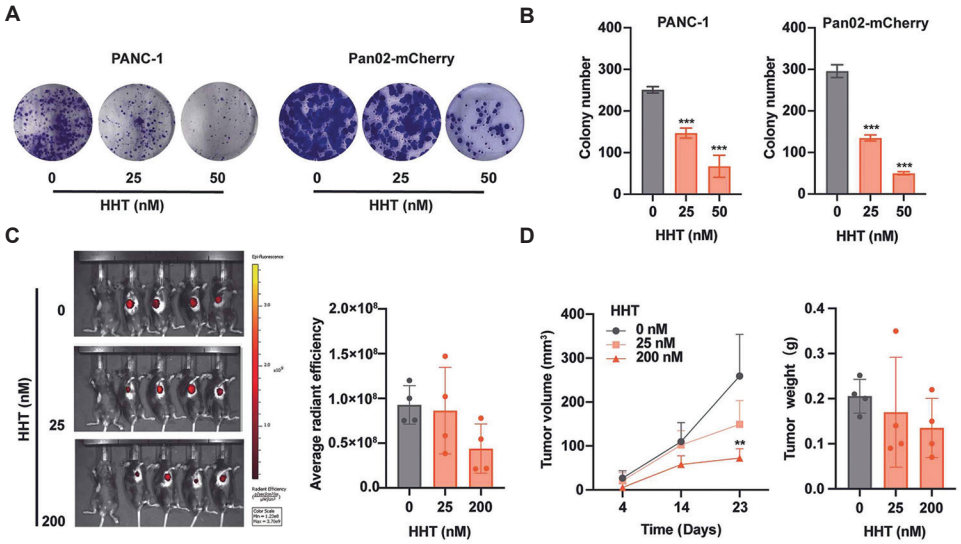

Figure 2. Effects of HHT on colony formation and tumorigenicity. (A) Representative images of cell colonies stained with crystal violet. PANC-1 and Pan02-mCherry cells were incubated in the complete medium for 14 days following treatment with 25 nM and 50 nM HTT for 48 h. (B) Quantification of colony formation in PANC-1 and Pan02-mCherry cells from the colony formation experiment in panel A ($n = 3$). ***$P < 0.001$. (C) Fluorescent imaging and intensity analysis of tumors *in vivo* on the 23rd day after inoculation. Cells were treated with 25 nM or 200 nM HTT for 24 h before inoculation. A healthy mouse without cancer cell injection was placed on the left of each image as a background control ($n = 4$). (D) Tumor volumes and weights in each group ($n = 4$).
Abbreviation: HHT: Homoharringtonine.

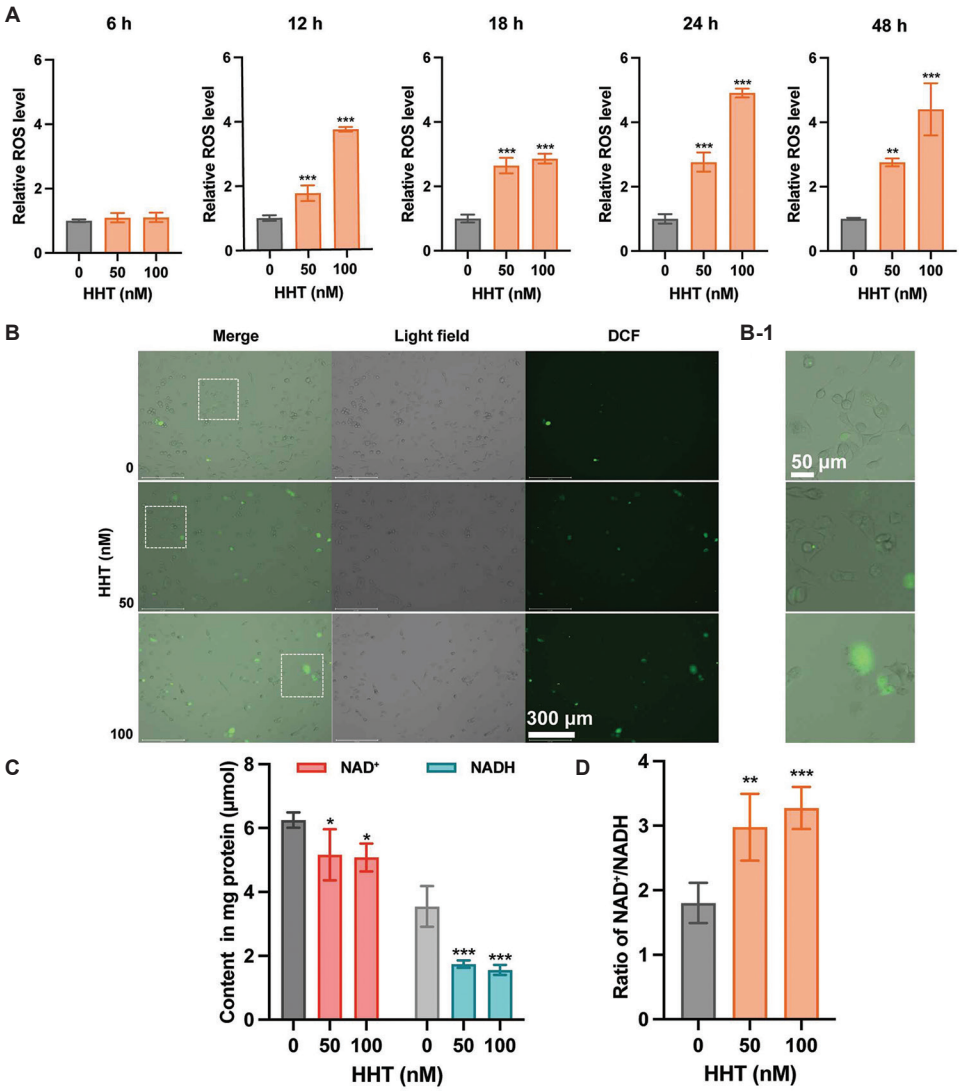

Figure 3. HHT-induced oxidative stress in PANC-1 cells. (A) Flow cytometric analysis of intracellular ROS in PANC-1 cells treated with 50 nM and 100 nM HHT at different time points (n = 3). (B) Fluorescence images of PANC-1 cells treated with 50 nM or 100 nM HHT for 18 h and stained with DCFH-DA. Panel B-1 presents a magnified view of the highlighted area in panel B, marked with dashed lines. Magnification: 4× and 12× for pane B and B1, respectively. (C) NAD^+ and NADH contents in PANC-1 cells treated with 50 nM and 100 nM HHT for 48 h (n = 4). (D) NAD^+/NADH ratio calculated from panel C. Note: $^*P < 0.05$, $^{**}P < 0.01$, $^{***}P < 0.001$.

Abbreviations: HHT: Homoharringtonine; ROS: Reactive oxygen species; NAD^+/NADH: Nicotinamide adenine dinucleotide; DCFH-DA: Dichlorodihydrofluorescein diacetate; DCF: 2′,7′-dichlorofluorescein; μmol: Micromole; h: Hours.

measured by the Seahorse XFe24 analyzer (Figure 4A). HHT treatment reduced the OCR to 61.15 pmol/min/10^4 cells, compared to 142.9 pmol/min/10^4 cells in the untreated group, indicating impaired mitochondrial respiration. Specifically, the OCR associated with ATP biosynthesis in HHT-treated cells dropped to 44.51 pmol/min/10^4 cells, compared to 109.4 pmol/min/10^4 cells in the control group, suggesting that HHT inhibited mitochondrial ATP production. Furthermore, the maximum respiration rate, as reflected by the OCR, of HHT-treated PANC-1 cells was notably lower, indicating a substantial decrease in energy generation capacity. Moreover, the spare respiratory capacity of these cells was extremely low (Figure 4B), reflecting the inability to adapt mitochondrial metabolism to stress conditions.[21] In addition, ATP levels in HHT-treated cells were measured using an ATP assay kit, showing significantly lower levels compared to those in control cells (Figure 4C), consistent with the OCR results. Taken together, HHT induced oxidative stress over time, which impaired mitochondrial respiration.

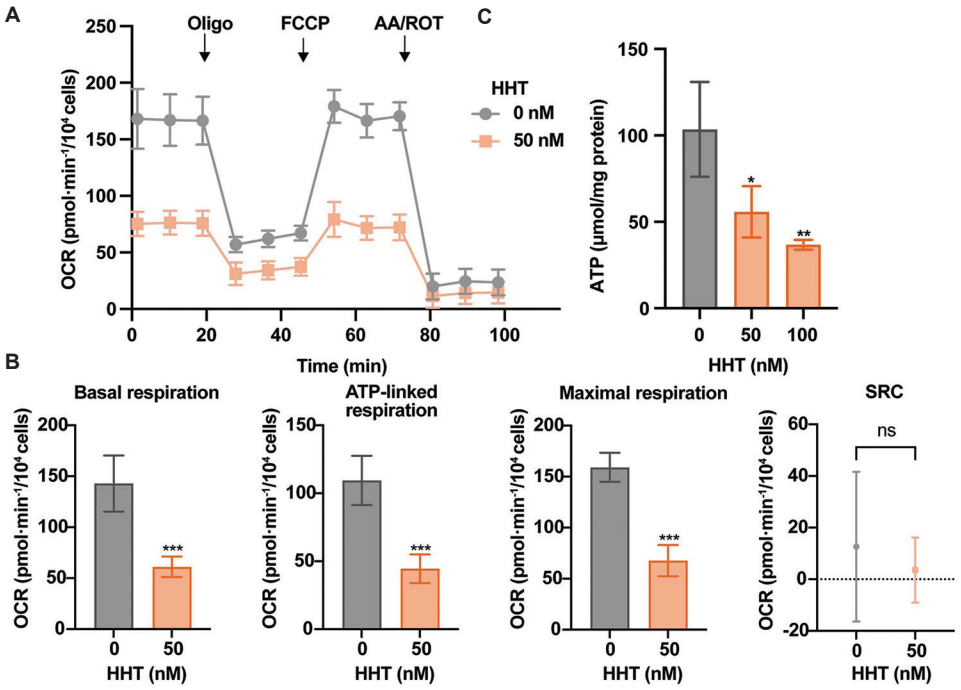

Figure 4. HHT inhibits mitochondrial respiration in PANC-1 cells. (A) OCR assay of HHT-treated cells using the Seahorse instrument (n = 5). (B) Basal OCR, ATP-linked respiration, maximal respiration, and spare respiratory capacity were calculated from OCR curves (n = 5). (C) ATP content in PANC-1 cells treated with 50 nM and 100 nM HHT for 48 h (n = 3). Note: $^{*}P < 0.05$, $^{**}P < 0.01$, $^{***}P < 0.001$.
Abbreviations: HHT: Homoharringtonine; OCR: Oxygen consumption rate; ATP: Adenosine triphosphate; Oligo: Oligomycin; FCCP: Carbonyl cyanide-p-(trifluoromethoxy) phenylhydrazone; AA/ROT: Antimycin A and rotenone; SRC: Spare respiratory capacity; pmol: Picomole; μmol: Micromole; min: Minutes; ns: Not significant.

3.3. HHT-induced cell cycle arrest

The effect of HHT on the cell cycle of PANC-1 cells treated with HHT for 48 h was investigated by flow cytometry. Results showed that HHT treatment induced cell cycle arrest in the S phase (Figure 5A). Concurrently, the expressions of CDC2, CDC25c, cyclinD2, and p53 in HHT-treated PANC-1 cells were downregulated in a dose-dependent manner (Figure 5B). Quantification results (Figure 5C), derived from the replicates of Western blotting (Figure S1-S8), revealed that nearly half of the CDC2, CDC25c, and Cyclin D2 protein levels were decreased by 50 nM of HHT. Notably, PANC-1 cells express mutant p53 (mp53 R273H), which has a reported positive correlation with CDC2 expression in PANC-1 cells.[22] Western blot analysis showed that HHT treatment significantly decreased the expression of mp53 in a dose-dependent manner, which is consistent with previously reported findings in the literature. Moreover, the effect of HHT on the cytoskeleton of PANC-1 cells was visualized using confocal microscopy. HHT-treated cells showed fewer actin fibers dispersed in the cells (Figure 5D), suggesting a connection between cytoskeletal alterations, inhibited cell division, and cell cycle arrest.

3.4. HHT-inhibited tumor growth and proliferation of PDAC cells *in vivo*

The therapeutic effect of HHT on pancreatic cancer was investigated using a mouse model subcutaneously inoculated with Pan02-mCherry cells. First, the toxicity of HHT was assessed in healthy mice (n = 3 per group) at four dosages, including 0.5 mg/kg, 1.0 mg/kg, 2.0 mg/kg, and 4.0 mg/kg (administered once per day for four consecutive days) to determine the appropriate dosages for therapeutic efficacy experiments. Doses of 0.5 mg/kg and 1.0 mg/kg did not induce mortality or obvious body weight loss during the experimental period. However, one mouse (1/3) in the 2 mg/kg group was found dead on the 4th day after the final injection, whereas all mice (3/3) in the 4 mg/kg group were found dead on the 1st day after the initial injection (Figure 6A and B). Based on these findings, 0.5 mg/kg and 1.0 mg/kg were selected for the therapeutics efficacy assay. The tumor-bearing mice were randomly divided into three groups (n = 7 per group) and intravenously administrated with HHT at 0.5 mg/kg, 1.0 mg/kg, or 0.4% of Soluplus® in PBS as the control. It was shown that HHT treatment significantly reduced the tumor volumes in a dose-dependent manner compared to the control group

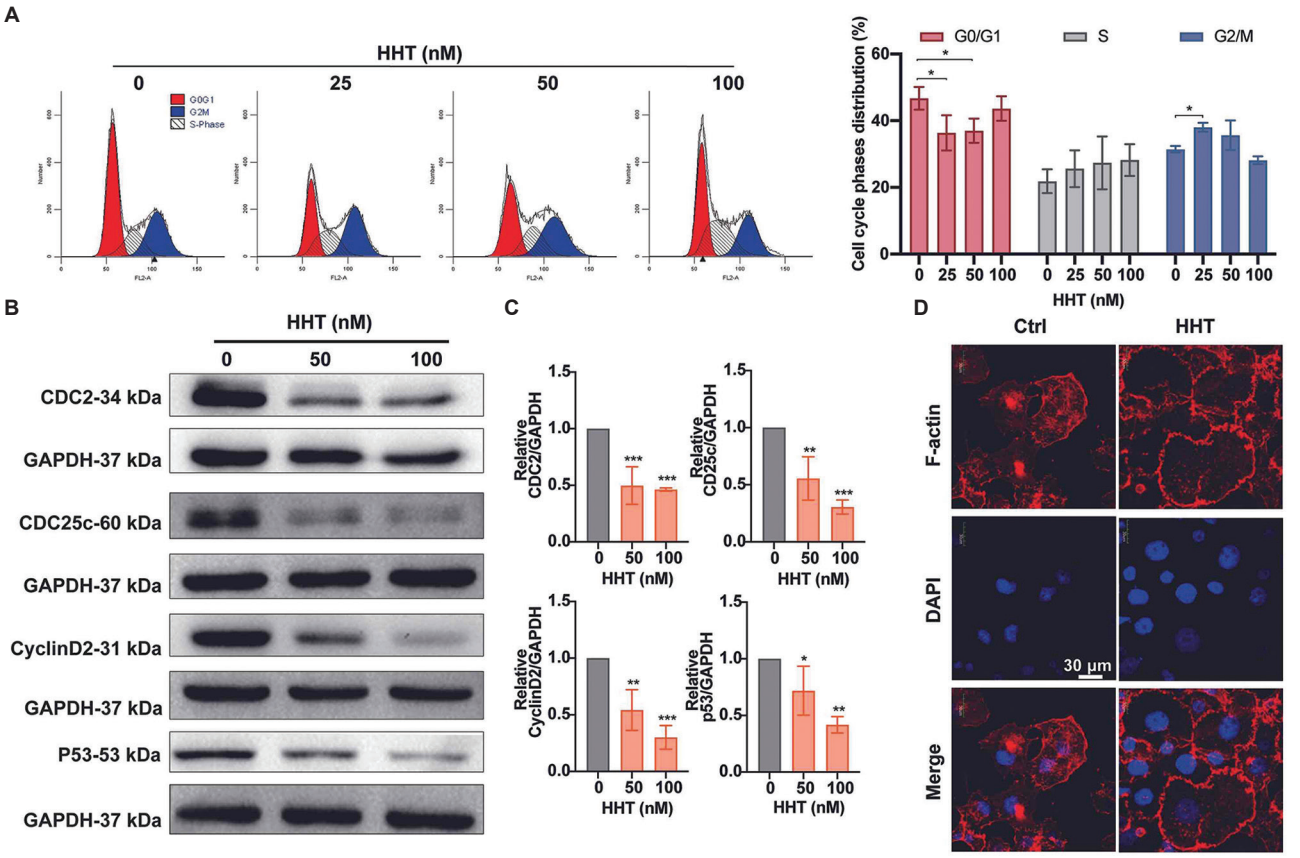

Figure 5. HHT-induced cell cycle arrest in PANC-1 cells. (A) Cell cycle analysis by flow cytometry and quantification of PANC-1 cells ($n = 3$). PANC-1 cells were treated with 25 nM, 50 nM, and 100 nM HHT for 48 h, followed by fixation and PI staining. (B) Expression levels and (C) quantification of CDC2, CDC25c, cyclin D2, and mutant p53 in PANC-1 cells treated with 50 nM and 100 nM HHT for 48 h ($n = 3$). Original blots for display and quantitation are presented in Figures S1 – S8 (supplementary file). (D) Cytoskeleton analysis of untreated (Ctrl) and or HHT-treated (50 nM, 48 h) PANC-1 cells. Actin was stained with phalloidin (red fluorescence), and nuclei were stained with DAPI (blue fluorescence). Magnification: 400× for panel D. Note: $^{*}P < 0.05$, $^{**}P < 0.01$, $^{***}P < 0.001$.

Abbreviations: HHT: Homoharringtonine; PI: Propidium iodide; CDC2: Cyclin-dependent kinase 1: CDC25c: Cell division cycle 25c; Ctrl: Control.

(Figure 6C). Concurrently, body weight measurements indicated that neither 0.5 mg/kg nor 1.0 mg/kg of HHT caused significant weight loss or systemic toxicity in mice (Figure 6D). On the 16th day after the initial HHT administration, all mice were euthanized, and the tumors from the three groups were excised, photographed, and weighed. Tumor sizes in the HHT-treated groups were notably smaller compared to those in the control group (Figure 6E). Quantification analysis of tumor weights further confirmed the inhibitory effect of HHT on tumor growth (Figure 6F).

H&E staining of tumor sections revealed that HHT treatment significantly inhibited the proliferation of pancreatic cancer cells. In the control mice, pancreatic cancer foci were observed, characterized by typical ductal carcinoma structures (asterisks) mainly distributed at the edges of the tissues. Following HHT treatment, the number of pancreatic cancer foci decreased significantly. In the mice treated with 0.5 mg/kg of HHT, tumor cells in the ductal structures were shrunken in size (asterisks) and surrounded by fibrous structures. For the 1.0 mg/kg HHT-treated group, only a few ductal carcinoma foci were observed. The tumor cells in these structures displayed unclear boundaries and lacked nuclei (asterisks), suggesting cell death (Figure 7A). Ki67 immunofluorescence staining of tumor sections further confirmed the reduced cell proliferation with HHT treatment. The Ki67-positive cells (red fluorescence) were clearly seen in the control group, whereas their numbers decreased progressively with increasing doses of HHT, demonstrating a dose-dependent reduction of tumor cell proliferation (Figure 7B). The above results show that HHT inhibits pancreatic tumor growth *in vivo* by suppressing cell proliferation.

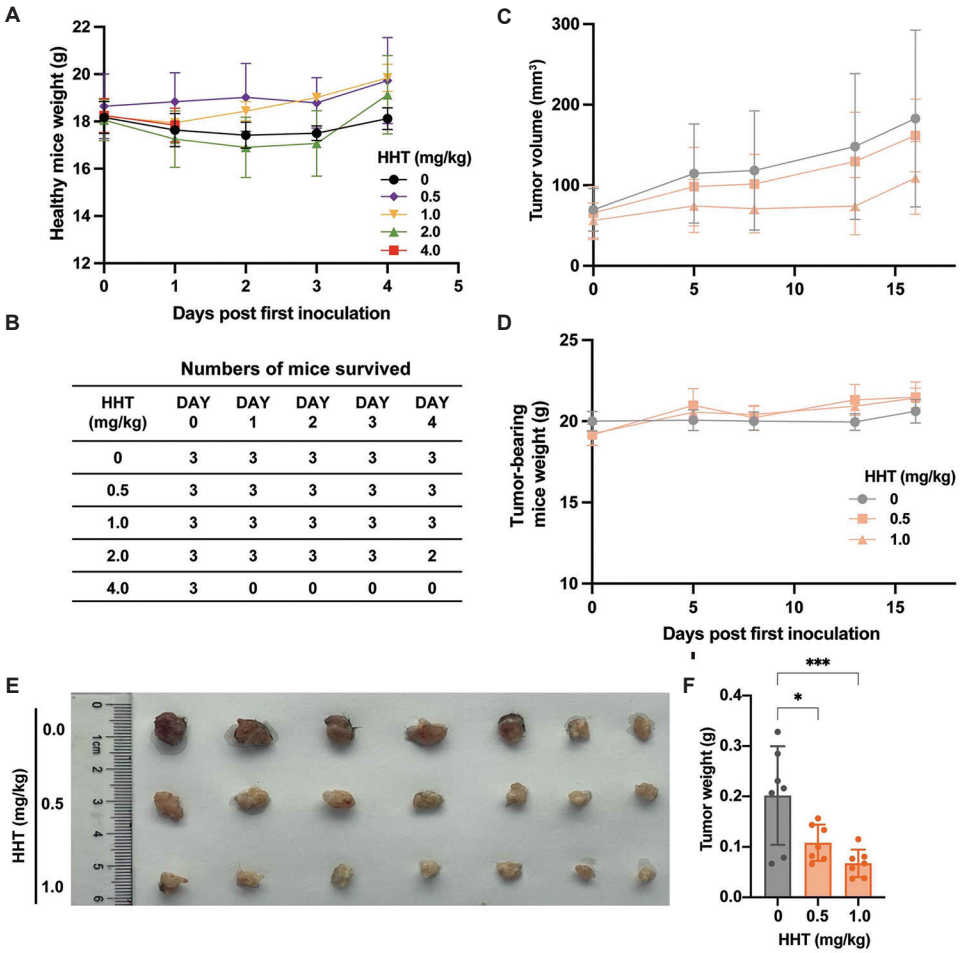

HHT (mg/kg)	DAY 0	DAY 1	DAY 2	DAY 3	DAY 4
0	3	3	3	3	3
0.5	3	3	3	3	3
1.0	3	3	3	3	3
2.0	3	3	3	3	2
4.0	3	0	0	0	0

Figure 6. Toxicity evaluation and therapeutic effects of HHT on pancreatic cancer *in vivo*. (A) Body weight of healthy mice received intravenous administration of HHT at four dosages including 0.5 mg/kg, 1.0 mg/kg, 2.0 mg/kg, and 4.0 mg/kg (once per day for 4 days) (n = 3). (B) Numbers of surviving mice after receiving the treatment described in panel A. (C) Tumor volume growth curve for each group. The tumor-loading mice were given a 2-week treatment. Each week, HHT at 0.5 mg/kg and 1.0 mg/kg were administered once per day for five consecutive days, followed by a 2-day break. (D) Body weight change curve for the three groups. (E) Representative tumor images from each group after 2 weeks of HHT treatment. On the day 16, all tumors were collected and analyzed. (F) Tumor weights of mice in each group (n = 7). Note: $^{*}P < 0.05$, $^{***}P < 0.001$.
Abbreviations: HHT: Homoharringtonine; g: Gram.

3.5. HHT alleviated immunosuppressive status within the TME

To further assess whether HHT affected the TME, the viability of RAW264.7 macrophages was examined using the CCK-8 assay. It was shown that HHT treatment led to a dose-dependent reduction in macrophage viability (Figure 8A), with an IC50 of 52.33 nM. Immunofluorescence staining indicated that the number of macrophages was reduced by the HHT treatment. In the control group, a large amount of F4/80-positive macrophages (green fluorescence) were distributed and surrounded the ductal carcinoma structures. However, treatment with 1.0 mg/kg HHT significantly decreased the number of macrophages in the tumor tissues (Figure 8B).

4. Discussion

PDAC is a highly invasive and deadly malignant tumor.[23] Although current standard-of-care treatments such as FOLFIRINOX (a combination of 5-fluorouracil, leucovorin, irinotecan, and oxaliplatin) and gemcitabine with nanoparticle albumin-bound paclitaxel (nab-paclitaxel) have achieved great progress in PDAC therapy,[4] clinical outcomes remain unsatisfactory. Therefore, it is of great significance to develop more effective chemotherapeutic drugs and understand their underlying mechanisms.

Previous studies have reported the inhibitory effects of HHT on the proliferation of certain pancreatic cancer cell lines, focusing primarily on signaling pathway activation

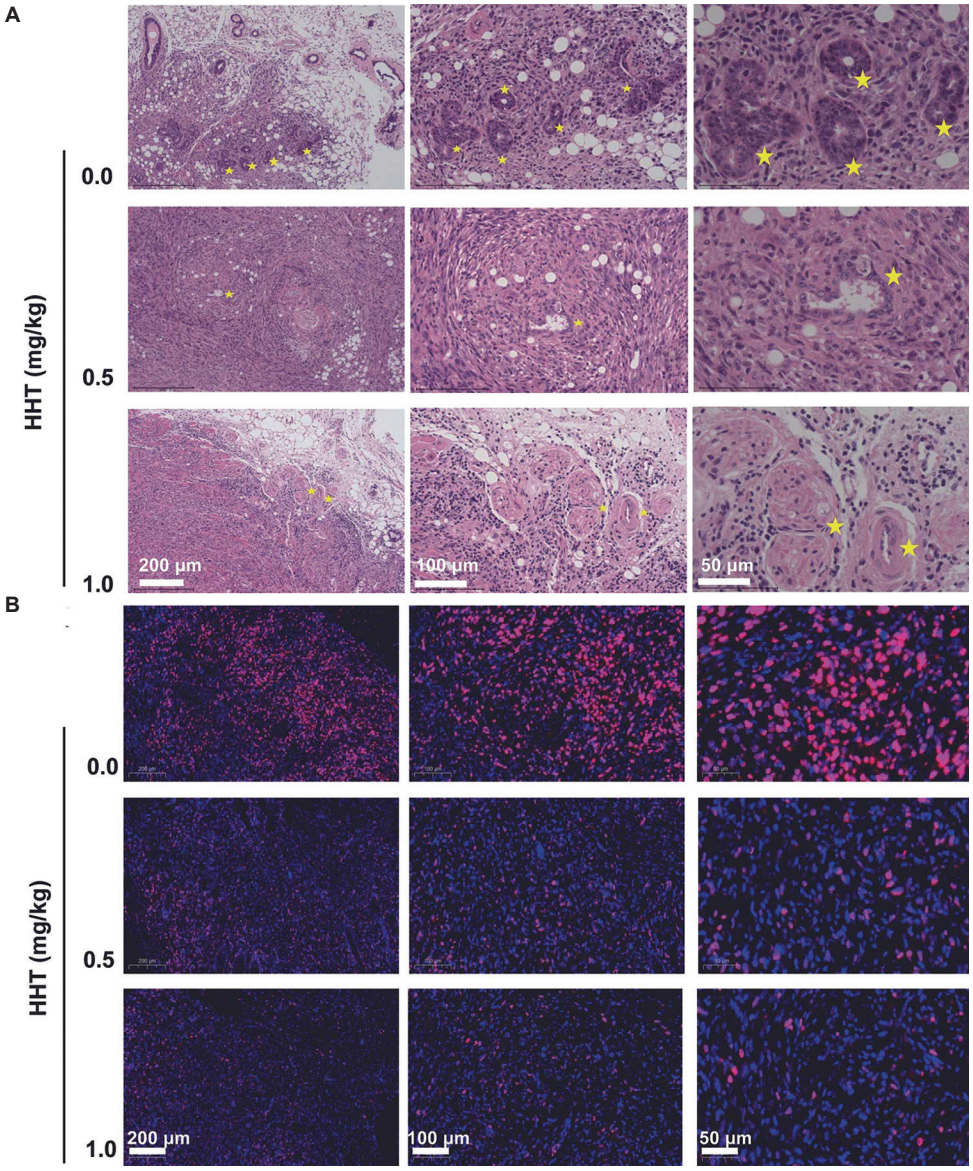

Figure 7. HHT inhibits the proliferation of pancreatic tumor cells *in vivo*. (A) Representative H&E-stained images of pancreatic tumor tissues treated with different dosages of HHT. Pancreatic cancer foci were indicated by yellow stars. Magnification: 10×, 20×, and 40×, respectively, from left to right for panel A. (B) Representative images of Ki67-stained cells in the pancreatic tumor tissues treated with different dosages of HHT. Ki67-positive cells showed red fluorescence, while nuclei were stained with DAPI in blue fluorescence. Magnification: 5×, 10×, and 20×, respectively, from left to right for panel B. Abbreviation: HHT: Homoharringtonine.

and cell cycle arrest. However, the mechanisms of HHT's action against pancreatic cancer have not been adequately investigated.

In this study, the therapeutic effect of HHT was investigated from the perspective of energy tumor cell energy metabolism to provide new insights into its underlying mechanisms. Chemotherapies have been widely recognized to increase intracellular ROS levels, disrupting cellular redox balance and damaging organelles.[24-27] Previous studies have shown that combining HHT with etoposide increased ROS-mediated cytotoxicity in AML cells,[28] whereas HHT inhibited mitochondrial complex I activity and OCR in CML cells.[16] Similarly, in 5-FU-resistant rectal cancer cells, HHT reduced OCR, mitochondrial complex I activity, and ATP production.[29] Experimental results further suggest that mitochondrial ROS could serve as a therapeutic target for pancreatic cancer cells. HHT-induced upregulation of ROS impaired mitochondrial respiration in PANC-1 cells. As mitochondria function as the "energy factories" within the cell, producing ATP essential to maintain normal physiological functions,[30]

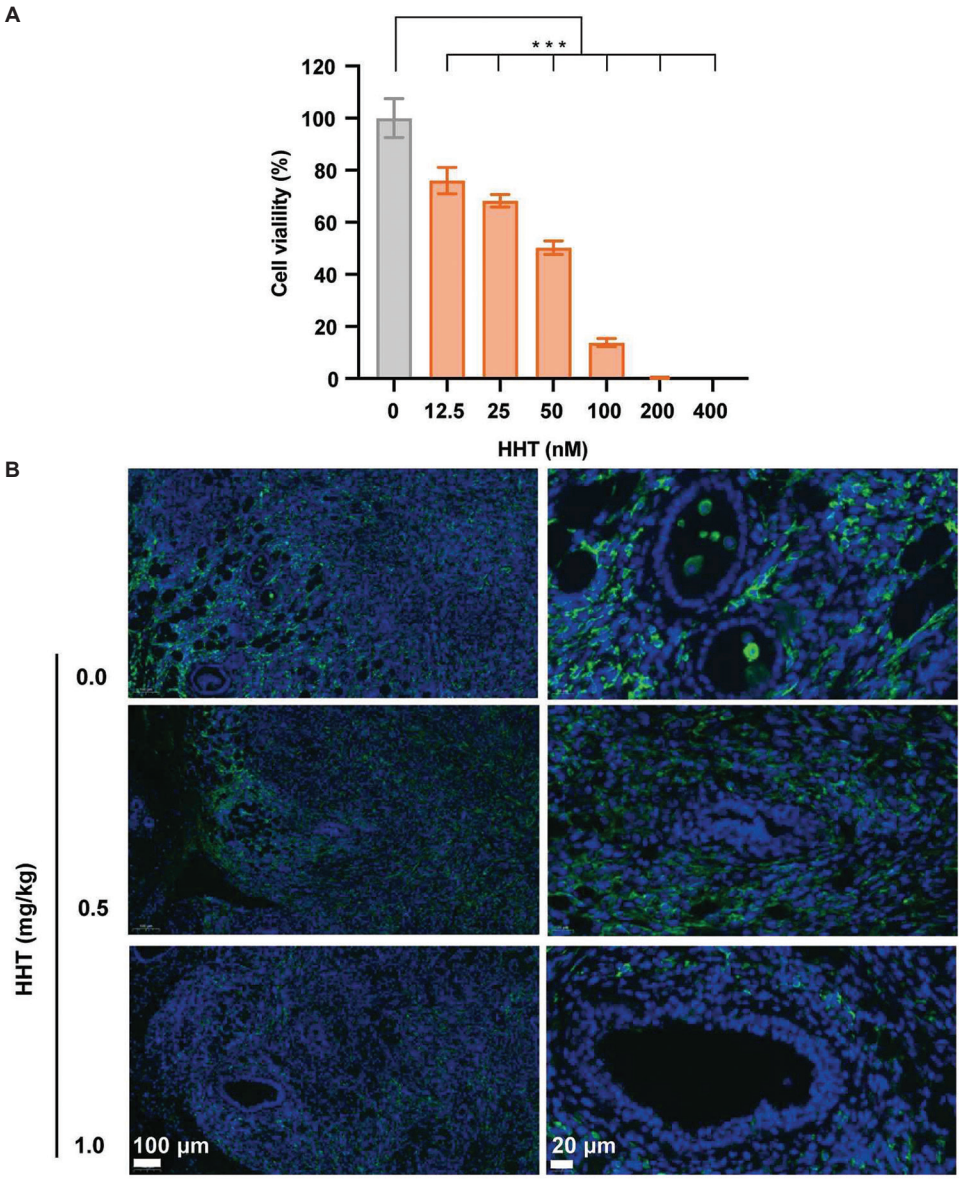

Figure 8. HHT alters the tumor microenvironment by inhibiting macrophages. (A) Viability of RAW264.7 cells incubated with HHT for 24 h, was measured by the CCK-8 assay (n = 4). (B) Representative images of tumor tissue stained with F4/80 (green fluorescence) and DAPI (blue fluorescence). Magnification: 10× and 40×, respectively, from left to right for panel B. Note: ***$P < 0.001$.
Abbreviations: HHT: Homoharringtonine; CCK-8 assay: Cell counting kit-8 assay.

the observed reduction in OCR following HHT treatment indicated inhibition of mitochondrial energy metabolism. This impairment rendered PANC-1 cells unable to adapt to mitochondrial dysfunction, thus inhibiting their proliferation. Taken together, targeting mitochondrial energy metabolism may serve as a promising therapeutic strategy for pancreatic cancer.

The present study also showed that the cell cycles of PANC-1 cells were arrested, accompanied by the dose-dependent downregulation of CDC2, CDC25c, and cyclin D2. In addition, HHT treatment reduced the expression of mutant p53 (mp53) in PANC-1 cells. Mutant p53 has been shown to have potential gain-of-function activities, such as interference with the regulation of cell survival, DNA damage repair, and drug resistance, in contrast to the tumor-suppressive roles of wild-type p53.[31,32] Previous studies have shown a positive correlation between mp53 and CDC2[33] in PANC-1 cells,[22] as well as in breast metastatic cancer cell line SKBR3, and head and neck cancer cell lines CAL27 and FADU.[34] It is known that

p53 and checkpoint protein kinases checkpoint kinase 1 (CHK1) and checkpoint kinase 2 (CHK2) regulate the phosphorylation of CDC25c, inhibiting its activity during DNA damage. This results in the breakdown of CDC25c in the cytoplasm, prevents the activation of the cyclin B1/CDK1 complex, and induces G2/M phase cell cycle arrest.[35-37] In this study, the downregulation of mp53 by HHT treatment may be associated with its impact on cell cycle proteins.

Moreover, pancreatic cancer is well-known for its characteristic immunosuppressive TME, which includes a large population of macrophages and fibroblasts. This study revealed that macrophages were more sensitive to HHT than PANC-1 cells, suggesting that HHT might alleviate the TME. Tumor-associated macrophages are widely recognized for their role in facilitating the TME,[38,39] which may contribute to the inhibitory effect of HHT on pancreatic cancer progression. In addition, this effect may promote the therapeutic efficacy of pancreatic cancer treatments when combined with other existing drugs. Although no clear mechanisms have been established, prior investigations have shown signs of HHT sensitizing other chemotherapeutic drugs in immunosuppressive cancers. For example, HHT acts synergistically with paclitaxel to combat triple-negative breast cancer cell lines[40] and sensitizes resistant human colorectal carcinoma cells to tumor necrosis factor-related apoptosis-inducing ligand-induced apoptosis.[41]

5. Conclusion

HHT showed potent antiproliferative effects on pancreatic cancer by inducing ROS elevation, impairing mitochondrial energy metabolism, and causing cell cycle arrest. In addition, it reduced macrophages in the TME to alleviate the immunosuppressive status. These findings suggest that HHT could potentially serve as a novel therapeutic agent for this devastating disease. Investigating the long-term effects of HHT on PDAC relapse and its efficacy in combination with other existing drugs is worthy of future studies.

Acknowledgments

The confocal microscopy was performed at the Core Labs, Institute of Basic Medical Sciences Chinese Academy of Medical Sciences. The optical small animal imaging was performed at the State Key Laboratory of Common Mechanism Research of Major Disease Platform. We would like to thank the lab personnel for their help in data collection.

Funding

This work was supported by CAMS Innovation Fund for Medical Science (CIFMS 2021-I2M-1-026), Haihe Laboratory of Cell Ecosystem Innovation Fund (22HHXBSS00040) and Beijing Natural Science Foundation (7244372).

Conflict of interest

The authors declare they have no competing interests.

Author contributions

Conceptualization: Haiyan Xu
Formal analysis: Xiaoxia Wang
Funding acquisition: Haiyan Xu
Methodology: Xiaoxia Wang, Tao Wang, Jie Meng, Xuelu Peng, Ke Zhu, Ming Ye
Project administration: Haiyan Xu
Resources: Haiyan Xu
Supervision: Haiyan Xu
Validation: Xiaoxia Wang, Tao Wang
Writing – original draft: Jie Meng, Xiaoxia Wang
Writing – review & editing: Haiyan Xu, Tao Wang

Ethics approval and consent to participate

All the animal experiments reported were carried out in accordance with the guidelines stipulated by the committee on the Animal Care and Use of Institute of Basic Medical Sciences, Chinese Academy of Medical Sciences and Peking Union Medical College (Ethics Approval ID: ACUC-A02-2023-015). Mice were euthanized using cervical dislocation following isoflurane anesthesia, in accordance with the 2020 AVMA Guidelines for the Euthanasia of Animals to ensure humane treatment.

Consent for publication

Not applicable.

Availability of data

The datasets used and analyzed during the current study are available from the corresponding author upon reasonable request.

References

1. Cai J, Chen H, Lu M, *et al*. Advances in the epidemiology of pancreatic cancer: Trends, risk factors, screening, and prognosis. *Cancer Lett*. 2021;520:1-11.

   doi: 10.1016/j.canlet.2021.06.027

2. Bray F, Laversanne M, Sung H, *et al*. Global cancer statistics 2022: GLOBOCAN estimates of incidence and mortality worldwide for 36 cancers in 185 countries. *CA Cancer J Clin*. 2024;74(3):229-263.

   doi: 10.3322/caac.21834

3. Connor AA, Gallinger S. Pancreatic cancer evolution and

heterogeneity: Integrating omics and clinical data. *Nat Rev Cancer*. 2022;22(3):131-142.

doi: 10.1038/s41568-021-00418-1

4. Christenson ES, Jaffee E, Azad NS. Current and emerging therapies for patients with advanced pancreatic ductal adenocarcinoma: A bright future. *Lancet Oncol*. 2020;21(3):e135-e145.

doi: 10.1016/S1470-2045(19)30795-8

5. Niu N, Shen X, Wang Z, *et al*. Tumor cell-intrinsic epigenetic dysregulation shapes cancer-associated fibroblasts heterogeneity to metabolically support pancreatic cancer. *Cancer Cell*. 2024;42(5):869-884.e9.

doi: 10.1016/j.ccell.2024.03.005

6. Raghavan S, Winter PS, Navia AW, *et al*. Microenvironment drives cell state, plasticity, and drug response in pancreatic cancer. *Cell*. 2021;184(25):6119-6137.e26.

doi: 10.1016/j.cell.2021.11.017

7. Li E, Cheung HCZ, Ma S. CTHRC1^{+} fibroblasts and SPP1^{+} macrophages synergistically contribute to pro-tumorigenic tumor microenvironment in pancreatic ductal adenocarcinoma. *Sci Rep*. 2024;14(1):17412.

doi: 10.1038/s41598-024-68109-z

8. Spratlin J, Sangha R, Glubrecht D, *et al*. The absence of human equilibrative nucleoside transporter 1 is associated with reduced survival in patients with gemcitabine-treated pancreas adenocarcinoma. *Clin Cancer Res*. 2004;10(20):6956-6961.

doi: 10.1158/1078-0432.CCR-04-0224

9. Fresno M, Jiménez A, Vázquez D. Inhibition of translation in eukaryotic systems by harringtonine. *Eur J Biochem*. 1977;72(2):323-330.

doi: 10.1111/j.1432-1033.1977.tb11256.x

10. Baaske DM, Heinstein P. Cytotoxicity and cell cycle specificity of homoharringtonine. *Antimicrob Agents Chemother*. 1977;12(2):298-300.

doi: 10.1128/AAC.12.2.298

11. Kantarjian HM, O'Brien S, Cortes J. Homoharringtonine/omacetaxine mepesuccinate: The long and winding road to food and drug administration approval. *Clin Lymphoma Myeloma Leuk*. 2013;13(5):530-533.

doi: 10.1016/j.clml.2013.03.017

12. Powell RG, Weisleder D, Smith CR, Rohwedder WK. Structures of harringtonine, isoharringtonine, and homoharringtonine. *Tetrahedron Lett*. 1970;(11):815-818.

doi: 10.1016/s0040-4039(01)97839-6

13. Wang L, Zhao L, Wei G, *et al*. Homoharringtonine could induce quick protein synthesis of PSMD11 through activating MEK1/ERK1/2 signaling pathway in pancreatic cancer cells. *J Cell Biochem*. 2018;119(8):6644-6656.

doi: 10.1002/jcb.26847

14. Fountzilas G, Lim LO, Yunis AA. The inhibitory effects of teniposide and homoharringtonine on the growth of pancreatic carcinoma cells *in vitro*. *Anticancer Res*. 1988;8(3):343-346.

15. Sarwar A, Zhu Z, Zhu M, *et al*. Homoharringtonine sensitizes pancreatic cancer to erlotinib by direct targeting and miRNA-130b-3p-mediated EphB4-JAK2-STAT3 axis. *J Pharm Pharmacol*. 2023;75(10):1294-1309.

doi: 10.1093/jpp/rgad055

16. Han H, Zhao C, Liu M, *et al*. Mitochondrial complex I inhibition by homoharringtonine: A novel strategy for suppression of chronic myeloid leukemia. *Biochem Pharmacol*. 2023;218:115875.

doi: 10.1016/j.bcp.2023.115875

17. Jeong KY, Sim JJ, Park M, Kim HM. Accumulation of poly (adenosine diphosphate-ribose) by sustained supply of calcium inducing mitochondrial stress in pancreatic cancer cells. *World J Gastroenterol*. 2022;28(27):3422-3434.

doi: 10.3748/wjg.v28.i27.3422

18. Zhu X, Zhang Y, Wang Y, *et al*. Agrimoniin sensitizes pancreatic cancer to apoptosis through ROS-mediated energy metabolism dysfunction. *Phytomedicine*. 2022;96:153807.

doi: 10.1016/j.phymed.2021.153807

19. Xia S, Miao Y, Liu S. Withaferin A induces apoptosis by ROS-dependent mitochondrial dysfunction in human colorectal cancer cells. *Biochem Biophys Res Commun*. 2018;503(4):2363-2369.

doi: 10.1016/j.bbrc.2018.06.162

20. Percie du Sert N, Ahluwalia A, Alam S, *et al*. Reporting animal research: Explanation and elaboration for the ARRIVE guidelines 2.0. *PLoS Biol*. 2020;18(7):e3000411.

doi: 10.1371/journal.pbio.3000411

21. Marchetti P, Fovez Q, Germain N, Khamari R, Kluza J. Mitochondrial spare respiratory capacity: Mechanisms, regulation, and significance in non-transformed and cancer cells. *FASEB J*. 2020;34(10):13106-13124.

doi: 10.1096/fj.202000767R

22. Fiorini C, Cordani M, Padroni C, Blandino G, Di Agostino S, Donadelli M. Mutant p53 stimulates chemoresistance of pancreatic adenocarcinoma cells to gemcitabine. *Biochim Biophys Acta*. 2015;1853(1):89-100.

doi: 10.1016/j.bbamcr.2014.10.003

23. Rahib L, Smith BD, Aizenberg R, Rosenzweig AB, Fleshman JM, Matrisian LM. Projecting cancer incidence and deaths to 2030: The unexpected burden of thyroid,

liver, and pancreas cancers in the United States. *Cancer Res*. 2014;74(11):2913-2921.

doi: 10.1158/0008-5472.CAN-14-0155

24. Liu J, He X, Deng S, *et al*. QDPR deficiency drives immune suppression in pancreatic cancer. *Cell Metab*. 2024;36(5):984-999.e8.

doi: 10.1016/j.cmet.2024.03.015

25. Tintelnot J, Xu Y, Lesker TR, *et al*. Microbiota-derived 3-IAA influences chemotherapy efficacy in pancreatic cancer. *Nature*. 2023;615(7950):168-174.

doi: 10.1038/s41586-023-05728-y

26. Zhang W, Gong M, Zhang W, *et al*. Thiostrepton induces ferroptosis in pancreatic cancer cells through STAT3/GPX4 signalling. *Cell Death Dis*. 2022;13(7):630.

doi: 10.1038/s41419-022-05082-3

27. Badgley MA, Kremer DM, Maurer HC, *et al*. Cysteine depletion induces pancreatic tumor ferroptosis in mice. *Science*. 2020;368(6486):85-89.

doi: 10.1126/science.aaw9872

28. Zhang J, Geng H, Liu L, Zhang H. Synergistic cytotoxicity of homoharringtonine and etoposide in acute myeloid leukemia cells involves disrupted antioxidant defense. *Cancer Manag Res*. 2019;11:1023-1032.

doi: 10.2147/CMAR.S187597

29. Chenghao H, Xuefeng L, Junli P, *et al*. Mitochondrial-targeting strategies with homoharringtonine: A novel approach for chemoresistant rectal cancer. *Biochem Biophys Res Commun*. 2025;743:151141.

doi: 10.1016/j.bbrc.2024.151141

30. Nunnari J, Suomalainen A. Mitochondria: In sickness and in health. *Cell*. 2012;148(6):1145-1159.

doi: 10.1016/j.cell.2012.02.035

31. Bullock AN, Fersht AR. Rescuing the function of mutant p53. *Nat Rev Cancer*. 2001;1(1):68-76.

doi: 10.1038/35094077

32. Acin S, Li Z, Mejia O, Roop DR, El-Naggar AK, Caulin C. Gain-of-function mutant p53 but not p53 deletion promotes head and neck cancer progression in response to oncogenic K-ras. *J Pathol*. 2011;225(4):479-489.

doi: 10.1002/path.2971

33. Di Agostino S, Strano S, Emiliozzi V, *et al*. Gain of function of mutant p53: The mutant p53/NF-Y protein complex reveals an aberrant transcriptional mechanism of cell cycle regulation. *Cancer Cell*. 2006;10(3):191-202.

doi: 10.1016/j.ccr.2006.08.013

34. Di Agostino S, Sorrentino G, Ingallina E, *et al*. YAP enhances the pro-proliferative transcriptional activity of mutant p53 proteins. *EMBO Rep*. 2016;17(2):188-201.

doi: 10.15252/embr.201540488

35. Winters ZE, Ongkeko WM, Harris AL, Norbury CJ. p53 regulates Cdc2 independently of inhibitory phosphorylation to reinforce radiation-induced G2 arrest in human cells. *Oncogene*. 1998;17(6):673-684.

doi: 10.1038/sj.onc.1201991

36. Le Gac G, Estève PO, Ferec C, Pradhan S. DNA damage-induced down-regulation of human Cdc25C and Cdc2 is mediated by cooperation between p53 and maintenance DNA (cytosine-5) methyltransferase 1. *J Biol Chem*. 2006;281(34):24161-24170.

doi: 10.1074/jbc.M603724200

37. Thanasoula M, Escandell JM, Suwaki N, Tarsounas M. ATM/ATR checkpoint activation downregulates CDC25C to prevent mitotic entry with uncapped telomeres. *EMBO J*. 2012;31(16):3398-3410.

doi: 10.1038/emboj.2012.191

38. Lin Y, Xu J, Lan H. Tumor-associated macrophages in tumor metastasis: Biological roles and clinical therapeutic applications. *J Hematol Oncol*. 2019;12(1):76.

doi: 10.1186/s13045-019-0760-3

39. Wang Y, Johnson KCC, Gatti-Mays ME, Li Z. Emerging strategies in targeting tumor-resident myeloid cells for cancer immunotherapy. *J Hematol Oncol*. 2022;15(1):118.

doi: 10.1186/s13045-022-01335-y

40. Plett R, Mellor P, Kendall S, *et al*. Homoharringtonine demonstrates a cytotoxic effect against triple-negative breast cancer cell lines and acts synergistically with paclitaxel. *Sci Rep*. 2022;12(1):15663.

doi: 10.1038/s41598-022-19621-7

41. Beranova L, Pombinho AR, Spegarova J, *et al*. The plant alkaloid and anti-leukemia drug homoharringtonine sensitizes resistant human colorectal carcinoma cells to TRAIL-induced apoptosis via multiple mechanisms. *Apoptosis*. 2013;18(6):739-750.

doi: 10.1007/s10495-013-0823-9

ACCSCIENCE PUBLISHING

Tumor Discovery

CASE REPORT

Efficacy of pyrotinib and capecitabine in recurrent breast cancer with a HER2-negative genetic switch following systemic therapy: A case report and literature review

Yuling Zhang[1], Bingfeng Chen[2], Jundong Wu[2,3], and Chunfa Chen[2,3]*

[1]Department of Medical Quality Management, Cancer Hospital of Shantou University Medical College, Shantou, Guangdong Province, China

[2]The Breast Center, Cancer Hospital of Shantou University Medical College, Shantou, Guangdong Province, China

[3]The Research Laboratory for Breast Cancer Diagnosis and Treatment, Cancer Hospital of Shantou University Medical College, Shantou, Guangdong Province, China

Abstract

Despite the demonstrated safety and efficacy of pyrotinib and capecitabine in treating human epidermal growth factor receptor 2 (HER2)-positive metastatic breast cancer, their efficacy in recurrent breast cancer in which the HER2 status has changed to negative remains unexplored. Here, we report a case of a 38-year-old female diagnosed with invasive ductal adenocarcinoma of the left breast, staged as mcT2N0M0. Fluorescence *in situ* hybridization (FISH) confirmed that the tumor was hormone receptor (HR) positive with low HER2 expression (2+) and a HER2/CEP17 ratio of 3.56. Following neoadjuvant targeted therapy and chemotherapy, she underwent a modified radical mastectomy. Post-surgical histopathological examination revealed a non-pathological complete response, classified as ypT1cypN1M0. The tumor remained HR positive with low HER2 expression (2+), but the FISH result was negative (HER2/CEP17 ratio of 1.65). For 1 year, she was administered dual-targeted therapy with goserelin and exemestane. Sequential therapy with neratinib was initiated; however, it was discontinued due to grade IV diarrhea. Despite ongoing endocrine therapy, she experienced tumor recurrence on the left chest wall. A biopsy of the recurrent lesion revealed it to be HR positive with low HER2 expression (2+) and a negative FISH result (HER2/CEP17 ratio of 1.33). The recurrent lesion responded to combination therapy consisting of pyrotinib and capecitabine, with tolerable adverse events. This case highlights the potential advantages of combining pyrotinib and capecitabine when the HER2 status changes to negative following systemic therapy.

Keywords: Breast cancer; Human epidermal growth factor receptor 2 change; Low human epidermal growth factor receptor 2 expression; Pyrotinib; Case report

***Corresponding author:**
Chunfa Chen
(chenchunfa@stu.edu.cn)

Citation: Zhang Y, Chen B, Wu J, Chen C. Efficacy of pyrotinib and capecitabine in recurrent breast cancer with a HER2-negative genetic switch following systemic therapy: A case report and literature review. *Tumor Discov*. 2025;4(1):113-119.
doi: 10.36922/td.4093

Received: June 30, 2024

Revised: August 3, 2024

Accepted: August 19, 2024

Published online: October 8, 2024

1. Background

Human epidermal growth factor receptor 2 (HER2) status discordance is prevalent in breast cancer, reflecting its heterogeneity. Approximately 15% – 22% of patients exhibit

HER2 status alterations post-neoadjuvant therapy.[1-3] After chemotherapy, HER2-positive patients typically become HER2 negative, whereas the reverse is less frequent. A meta-analysis reported a 21.3% conversion rate from HER2 positive to negative and a 9.5% conversion rate from negative to positive.[4] Intratumoral HER2 heterogeneity, linked to ambiguous expression and minor gene amplification,[5] is associated with increased recurrence and metastasis[6] and poor response to HER2-targeted therapy,[7] impacting prognosis in metastatic cases.[8] Despite the efficacy of combination chemotherapy in treating HER2-positive cancer, residual disease may cause loss of HER2 amplification, increasing the risk of recurrence and metastasis.[9-11]

Tyrosine kinase inhibitors (TKIs) have become pivotal in treating HER2-positive metastatic breast cancer. By inhibiting tyrosine kinases, enzymes that activate proteins through signal transduction, TKIs can limit cancer cell growth and proliferation.[12] HER2 is the target of several notable TKIs, including afatinib, lapatinib, neratinib, tucatinib, and pyrotinib.[13] In particular, pyrotinib, when paired with capecitabine, significantly increases patient survival.[14] The PERMEATE trial revealed the efficacy of pyrotinib and capecitabine against brain metastases in HER2-positive cases.[15] Pyrotinib also appears to be more potent than lapatinib in countering T-DM1 resistance.[16]

This case report presents a breast cancer patient who transitioned from a HER2-positive status to HER2-negative status following systemic anticancer therapy. Upon experiencing recurrence with a HER2-negative lesion, the patient demonstrated a favorable response to the combination therapy of pyrotinib and capecitabine, suggesting potential therapeutic benefits in such scenarios.

2. Case presentation

In November 2021, a 38-year-old female noted a mass in her left breast that persisted for 3 months. Physical examination and imaging revealed two irregular, firm, mobile, non-tender lumps in the left breast: one located 1 cm from the nipple in the inner upper quadrant (5.0 × 4.0 cm) and another 2 cm from the nipple in the outer upper quadrant (3.5 × 2.5 cm). In addition, a 2.0 × 1.0 cm firm, mobile, painless lymph node was identified in the left axilla. Breast cancer was confirmed through imaging modalities, such as mammography, magnetic resonance imaging (MRI), and ultrasonography. Head MRI; neck, chest, and abdominal computed tomography; and bone scan did not reveal any distant metastases. A core biopsy of two lesions in the left breast and axillary lymph node revealed invasive ductal adenocarcinoma of non-specific type (Figures 1A and B) with two primary tumors and a negative axillary node (Figure 1C). Immunohistochemistry (IHC) of the inner upper quadrant lesion demonstrated estrogen receptor (ER) positivity (90%, moderate to strong) (Figure 1D), progesterone receptor (PR) positivity (5%, weak to moderate), low HER2 expression (2+) (Figure 1E), and Ki67 positivity (10%). IHC of the outer upper quadrant lesion revealed low HER2 expression (2+) and positive results for ER (90%, moderate to strong), PR (90%, weak to moderate), and Ki67 (25%). HER2 amplification was verified using fluorescence *in situ* hybridization (FISH) (HER2/CEP17 ratio of 3.56) (Figure 1F). Consequently, she was diagnosed with hormone receptor (HR)- and HER2-positive breast cancer (mcT2N0M0).

The patient received six cycles of neoadjuvant therapy, which included docetaxel (75 mg/m^2), carboplatin (area under the curve 6), trastuzumab (initial dose, 8 mg; subsequent doses, 6 mg), and pertuzumab (initial dose, 840 mg; subsequent doses, 420 mg). She underwent total mastectomy of the left breast and axillary lymph node dissection in May 2022 after showing a partial response to neoadjuvant therapy, as determined by the response evaluation criteria in solid tumors.[17] Both the intraoperative frozen sections and post-operative skin margins exhibited negative results (Figure 2A). The surgical specimen revealed a moderately differentiated invasive ductal adenocarcinoma of non-specific type measuring 1.5 × 1.5 cm in the inner upper quadrant (Figure 2B), with high-grade ductal carcinoma *in situ*, comedo type, and no vascular or perineural invasion. One of the 10 dissected lymph nodes demonstrated metastases, including extranodal fibrous tissue. Of the remaining nodes, one exhibited micrometastasis (Figure 2C), and two contained isolated tumor cells (Figure 2D). The IHC results demonstrated low HER2 expression (2+) (Figure 2E), PR negativity, and positive results for ER (70%, weak to moderate) and Ki67 (3%), with a negative HER2 status on FISH (HER2/CEP17 ratio of 1.65) (Figure 2F). Financial constraints prevented the patient from receiving T-DM1 therapy. Post-operative adjuvant radiotherapy included computer tomography-guided volumetric modulated arc therapy with 6MV-X external beam radiation, targeting the left chest wall and supra/infra-clavicular areas. The planned target volume was formed by expanding the clinical target volume by 5 mm with a cumulative dose of 50 Gy in 25 fractions. The patient received goserelin and exemestane between May 2022 and February 2023. Sequential neratinib therapy was initiated but discontinued due to the onset of grade IV diarrhea. The patient persisted with goserelin and exemestane endocrine therapy. Two subsequent follow-up visits revealed no abnormalities. The patient discovered a chest wall lesion in November 2023 (Figure 3A). A biopsy of this lesion revealed invasive carcinoma (Figure 3B).

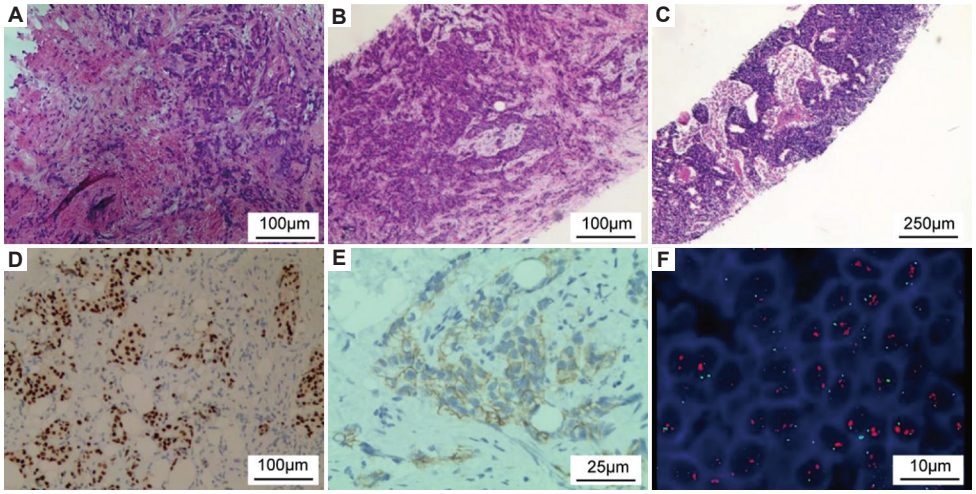

Figure 1. Initial diagnostic histopathologic findings. (A) Hematoxylin-eosin (H&E)-stained core needle biopsy specimen from the inner upper quadrant of the left breast, demonstrating invasive ductal carcinoma (×100 magnification). (B) H&E-stained core needle biopsy specimen from the outer upper quadrant of the left breast, suggesting invasive ductal carcinoma (×100 magnification). (C) H&E-stained core needle biopsy specimen of the left axillary lymph node, wherein no tumor cells were observed (×40 magnification). (D) Immunohistochemistry findings were positive for estrogen receptors in the primary tumor (×100 magnification). (E) HER2 immunohistochemistry scored 2+ in the primary tumor (×400 magnification). (F) Fluorescence *in situ* hybridization revealed HER2 gene amplification (HER2/CEP17 ratio: 3.56) in the primary tumor's core needle biopsy specimen (×1000 magnification).
Abbreviation: HER2: Human epidermal growth factor receptor 2.

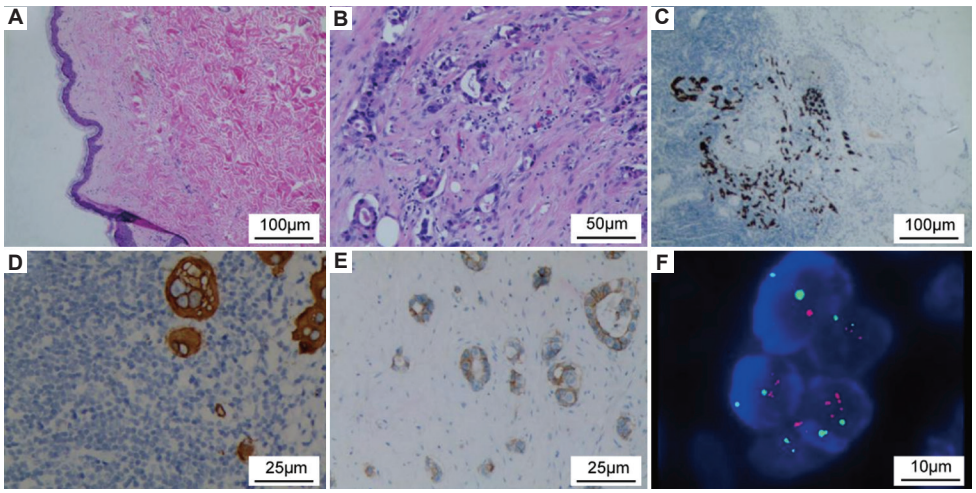

Figure 2. Surgical specimen histopathology. (A) hematoxylin–eosin (H&E) stain reveals negative skin margins (×100 magnification). (B) H&E stain of the excised primary tumor lesion (×200 magnification). (C) Immunohistochemistry-based findings of post-operative axillary lymph nodes exhibited micrometastasis (×100 magnification). (D) Immunohistochemistry-based findings of post-operative axillary lymph nodes reveal isolated tumor cells (×400 magnification). (E) Immunohistochemistry-based findings of the post-operative lesion demonstrated a HER2 score of 2+ (×400 magnification). (F) Fluorescence *in situ* hybridization revealed HER2 gene-negative (HER2/CEP17 ratio: 1.65) post-operative lesion ×1000 magnification).
Abbreviation: HER2: Human epidermal growth factor receptor 2.

IHC of the lesion revealed low HER2 expression (2+) (Figure 3D) and positive results for ER (95%, strong) (Figure 3C), PR (1% weak), and Ki67 (25%), with a negative FISH result (HER2/CEP17 ratio of 1.33) (Figure 3E). No distant metastases were detected on head, neck, chest, and abdominal computed tomography or bone scans.

A multidisciplinary team (MDT) proposed four treatment options, including T-DXd, pyrotinib and capecitabine, T-DM1, and a CDK4/6 inhibitor with fulvestrant. Due to cost constraints, the patient chose the pyrotinib and capecitabine and experienced manageable grade II diarrhea treated with loperamide. After one cycle, the tumor exhibited necrosis and reduced size (Figure 3F). At present, the patient's condition is stable on medication. Figure 4 summarizes the patient's diagnosis and treatment process.

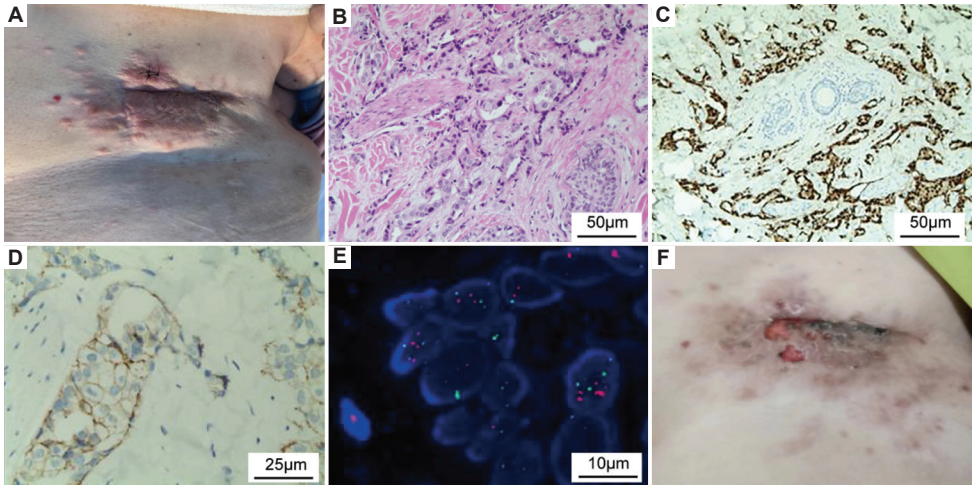

Figure 3. Recurrent lesion image and histopathology. (A) Image of the recurrent lesion on the left chest wall. (B) Hematoxylin–eosin (H&E) staining of the excised recurrent lesion revealed invasive ductal carcinoma (×200 magnification). (C) Positive estrogen receptor immunohistochemistry findings in the recurrent lesion (×200 magnification). (D) Immunohistochemistry examination of the recurrent lesion revealed a HER2 score of 2+ (×400 magnification). (E) Fluorescence *in situ* hybridization revealed HER2 gene negative (HER2/CEP17 ratio: 1.33) recurrent lesion (×1000 magnification). (F) Post-treatment image of the left chest wall lesion after one cycle of pyrotinib plus capecitabine.
Abbreviation: HER2: Human epidermal growth factor receptor 2.

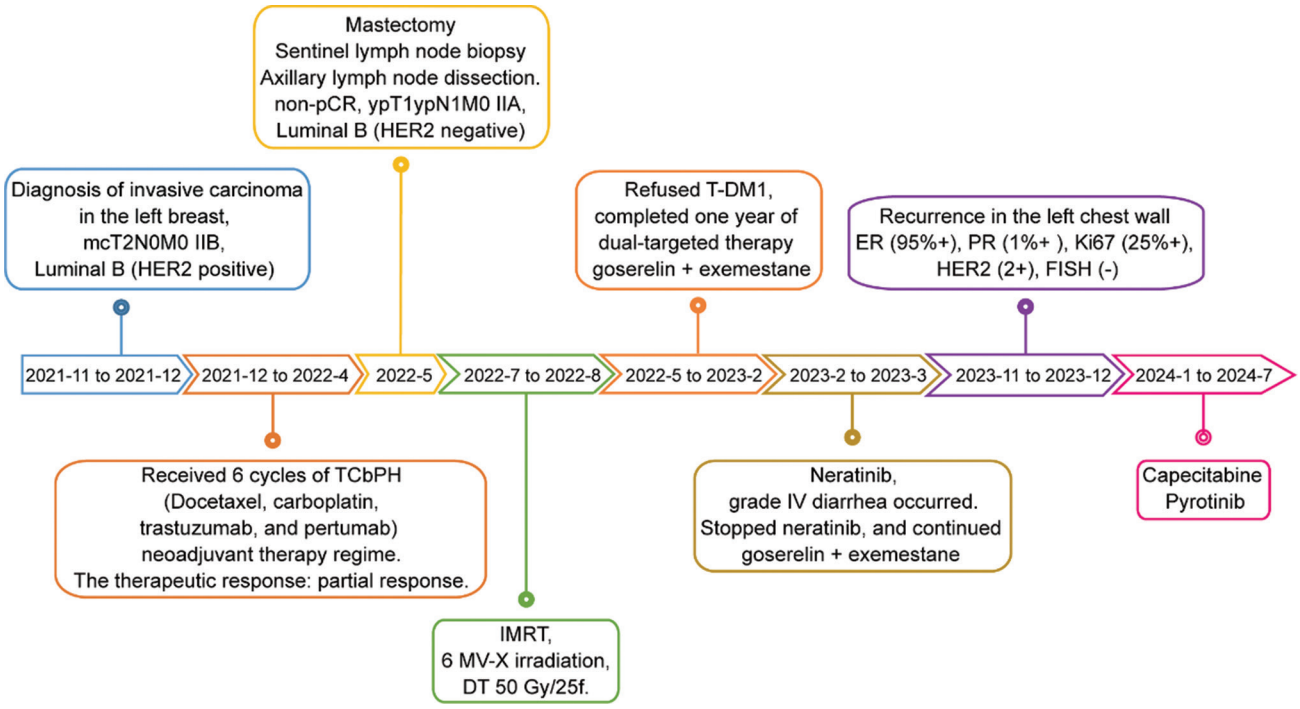

Figure 4. Diagnosis and treatment summary of the present case

3. Discussion

Tumor heterogeneity often leads to therapeutic refractoriness, posing significant challenges in cancer treatment.[18] Considering the dynamic and diverse nature of cancer, periodic evaluation of individual patients, specific lesions, and distinct sites is imperative. These assessments enable tailored disease treatments at the molecular level. The patient in the presented case was initially diagnosed with left breast cancer. The primary lesion, post-operative specimen, and recurrent lesion were all found to consistently exhibit high ER expression. PR expression declined to near absence, whereas HER2 expression remained low. FISH test results for HER2

were negative in post-operative and recurrent samples, confirming tumor heterogeneity.

MDT involves a comprehensive approach that aims to maximize therapeutic efficacy, improve survival through multimodal therapy, and ensure adherence to guidelines.[19] It is especially recommended for locoregional recurrent breast cancer management.[20] It promotes patient autonomy and collective decision-making for effectively treating locoregional recurrence. MDT was consistently employed in this patient's care, encompassing pre-neoadjuvant therapy, post-operative therapy, and post-locoregional recurrent therapy plans. Following a single salvage therapy course, the patient exhibited a partial response with notable lesion reduction. Ultimately, MDT involves a customized, synergistic strategy to enhance breast cancer outcomes.

Both positive-to-negative and negative-to-positive conversions of HER2 status were observed, with no clear predominance.[1] Typically, the transition from HER2-negative or HER2-equivocal primary to HER2-positive metastatic disease is more prevalent, especially in HR-positive patients. This may be the result of excluding patients with HER2-negative metastatic lesions and could be influenced by subclonal expansion and treatment-specific selective pressures in early breast cancer. Non-centralized testing may also contribute. These findings suggest reassessing HER2 status during disease recurrence or progression to determine therapeutic strategies. Studies have detected HER2-positive circulating tumor cells in a significant subset of patients with HER2-negative primary tumors.[21] While metastatic lesion biopsy may not always be possible or informative, circulating tumor biomarkers may be a non-invasive alternative for tissue-based HER2 status biomarkers.[22]

According to the fifth international consensus guidelines for advanced breast cancer by the European School of Oncology and the European Society for Medical Oncology, optimal treatment strategies following the loss of HER2 amplification remain undefined.[23] The current recommendations advocate continuing therapies targeting the HER2 signaling pathway.[24,25] Another strategy is to switch to alternative HER2-targeted therapies, such as ADCs (T-DM1 and T-DXd), and combine other TKIs with chemotherapy to overcome resistance to initial therapy and enhance patient outcomes.[24,26,27] The KATHERINE study detected HER2-negative residual disease in 70 out of 845 (8.3%) patients upon retesting at surgery. Among these, 11 invasive disease-free survival events occurred in the 42 trastuzumab-treated patients (26.2%), whereas none were observed in the 28 T-DM1-treated patients. This suggests that patients with HER2 status conversion may continue to benefit from HER2-targeted therapy.[28] The DESTINY-Breast04 study found that T-DXd significantly improved progression-free survival and overall survival with manageable safety compared to the physician's choice of treatment in low-HER2 metastatic breast cancer patients who had received 1 – 2 prior lines of chemotherapy.[29] Subgroup analysis revealed that the median treatment duration was 8.4 months with T-DXd and 3.5 months with the physician's choice in 213 Asian patients.[30] Further clinical trials are needed to find the best treatments and understand their long-term effects on patients with a HER2-negative switch.

Pyrotinib efficacy in treating HER2-positive metastatic breast cancer is well established.[31,32] A Chinese phase II trial involving patients previously treated with taxanes, anthracyclines, and/or trastuzumab demonstrated that pyrotinib with capecitabine exhibited a higher response rate (78.5%) and longer median progression-free survival (18.1 months) than lapatinib.[33] The phase III PHOEBE trial corroborated these benefits, with pyrotinib demonstrating improved overall survival and progression-free survival across various subgroups, regardless of trastuzumab resistance or prior chemotherapy.[14] Xu *et al.* advocate pyrotinib as a viable second-line treatment for trastuzumab-resistant cases, especially where access to newer therapies is limited.[32] Pyrotinib and capecitabine significantly decreased lesion size in the current patient.

4. Conclusions

Our case emphasizes that the pyrotinib and capecitabine combination may be beneficial in patients experiencing a HER2-negative switch following systemic therapy. This finding may lead to promising breast cancer research and the development of therapeutic strategies.

Acknowledgments

None.

Funding

This work was supported by the Foundation of Basic and Applied Basic Research of Guangdong Province, China (No. 2022A1515220202) and funds from the 2023 Science and Technology Innovation Strategy Project of Guangdong Province (Big Project + Task list), China (No. STKJ2023009, 20230403).

Conflict of interest

The authors declare that they have no competing interests.

Author contributions

Conceptualization: Chunfa Chen, Jundong Wu
Formal analysis: Bingfeng Chen, Yuling Zhang

Investigation: Yuling Zhang, Bingfeng Chen
Methodology: Chunfa Chen
Writing–original draft: Yuling Zhang
Writing–review & editing: Chunfa Chen, Jundong Wu

Ethics approval and consent to participate

The study was approved by the Ethics Committee of the Cancer Hospital of Shantou University Medical College (approval no.: 2022139).

Consent for publication

Written informed consent was obtained from the patient for publication of the details of her medical case and any accompanying images. A copy of the written consent is available for review by the Editor-in-Chief of this journal upon request.

Availability of data

Not applicable.

References

1. Ahn S, Woo JW, Lee K, Park SY. HER2 status in breast cancer: changes in guidelines and complicating factors for interpretation. *J Pathol Transl Med*. 2020;54(1):34-44.

   doi: 10.4132/jptm.2019.11.03

2. Niikura N, Tomotaki A, Miyata H, *et al*. Changes in tumor expression of HER2 and hormone receptors status after neoadjuvant chemotherapy in 21,755 patients from the Japanese breast cancer registry. *Ann Oncol*. 2016;27(3):480-487.

   doi: 10.1093/annonc/mdv611

3. Katayama A, Miligy IM, Shiino S, *et al*. Predictors of pathological complete response to neoadjuvant treatment and changes to post-neoadjuvant HER2 status in HER2-positive invasive breast cancer. *Mod Pathol*. 2021;34(7):1271-1281.

   doi: 10.1038/s41379-021-00738-5

4. Schrijver W, Suijkerbuijk KPM, van Gils CH, van der Wall E, Moelans CB, van Diest PJ. Receptor conversion in distant breast cancer metastases: A systematic review and meta-analysis. *J Natl Cancer Inst*. 2018;110(6):568-580.

   doi: 10.1093/jnci/djx273

5. Merola R, Mottolese M, Orlandi G, *et al*. Analysis of aneusomy level and HER-2 gene copy number and their effect on amplification rate in breast cancer specimens read as 2+ in immunohistochemical analysis. *Eur J Cancer*. 2006;42(10):1501-1506.

   doi: 10.1016/j.ejca.2006.03.011

6. Seol H, Lee HJ, Choi Y, *et al*. Intratumoral heterogeneity of HER2 gene amplification in breast cancer: Its clinicopathological significance. *Mod Pathol*. 2012;25(7):938-948.

   doi: 10.1038/modpathol.2012.36

7. Hou Y, Nitta H, Wei L, *et al*. HER2 intratumoral heterogeneity is independently associated with incomplete response to anti-HER2 neoadjuvant chemotherapy in HER2-positive breast carcinoma. *Breast Cancer Res Treat*. 2017;166(2):447-457.

   doi: 10.1007/s10549-017-4453-8

8. Lee HJ, Seo AN, Kim EJ, *et al*. HER2 heterogeneity affects trastuzumab responses and survival in patients with HER2-positive metastatic breast cancer. *Am J Clin Pathol*. 2014;142(6):755-766.

   doi: 10.1309/AJCPIRL4GUVGK3YX

9. Guarneri V, Dieci MV, Barbieri E, *et al*. Loss of HER2 positivity and prognosis after neoadjuvant therapy in HER2-positive breast cancer patients. *Ann Oncol*. 2013;24(12):2990-2994.

   doi: 10.1093/annonc/mdt364

10. Mittendorf EA, Wu Y, Scaltriti M, *et al*. Loss of HER2 amplification following trastuzumab-based neoadjuvant systemic therapy and survival outcomes. *Clin Cancer Res*. 2009;15(23):7381-7388.

    doi: 10.1158/1078-0432.CCR-09-1735

11. Larionov AA. Current therapies for human epidermal growth factor receptor 2-positive metastatic breast cancer patients. *Front Oncol*. 2018;8:89.

    doi: 10.3389/fonc.2018.00089

12. Suzuki T, Matsushima C, Nishimura S, Higashiyama T, Sasabe M, Machida Y. Identification of phosphoinositide-binding protein PATELLIN2 as a substrate of *Arabidopsis* MPK4 MAP kinase during septum formation in cytokinesis. *Plant Cell Physiol*. 2016;57(8):1744-1755.

    doi: 10.1093/pcp/pcw098

13. Singh DD, Lee HJ, Yadav DK. Clinical updates on tyrosine kinase inhibitors in HER2-positive breast cancer. *Front Pharmacol*. 2022;13:1089066.

    doi: 10.3389/fphar.2022.1089066

14. Xu B, Yan M, Ma F, *et al*. Pyrotinib plus capecitabine versus lapatinib plus capecitabine for the treatment of HER2-positive metastatic breast cancer (PHOEBE): A multicentre, open-label, randomised, controlled, phase 3 trial. *Lancet Oncol*. 2021;22(3):351-360.

    doi: 10.1016/S1470-2045(20)30702-6.

15. Yan M, Ouyang Q, Sun T, *et al*. Pyrotinib plus capecitabine for patients with human epidermal growth factor receptor 2-positive breast cancer and brain metastases (PERMEATE): A multicentre, single-arm, two-cohort, phase 2 trial. *Lancet Oncol*. 2022;23(3):353-361.

doi: 10.1016/S1470-2045(21)00716-6

16. Yin Y, Li W, Huang X, *et al*. Abstract P1-11-16: Treatment with tyrosine kinase inhibitors (TKIs) in HER2-positive metastatic breast cancer after trastuzumab emtansine (T-DM1) failure: A real-world study. *Cancer Res*. 2023;83:P1-11-16.

17. Schwartz LH, Litiere S, de Vries E, *et al*. RECIST 1.1-Update and clarification: From the RECIST committee. *Eur J Cancer*. 2016;62:132-137.

doi: 10.1016/j.ejca.2016.03.081

18. Baliu-Pique M, Pandiella A, Ocana A. Breast cancer heterogeneity and response to novel therapeutics. *Cancers* (*Basel*). 2020;12(11):3271.

doi: 10.3390/cancers12113271

19. Curigliano G, Burstein HJ, Gnant M, *et al*. Understanding breast cancer complexity to improve patient outcomes: The St Gallen International Consensus Conference for the Primary Therapy of Individuals with Early Breast Cancer 2023. *Ann Oncol*. 2023;34(11):970-986.

doi: 10.1016/j.annonc.2023.08.017

20. Buchholz TA, Ali S, Hunt KK. Multidisciplinary management of locoregional recurrent breast cancer. *J Clin Oncol* 2020;38(20):2321-2328.

doi: 10.1200/JCO.19.02806

21. Fehm T, Muller V, Aktas B, *et al*. HER2 status of circulating tumor cells in patients with metastatic breast cancer: A prospective, multicenter trial. *Breast Cancer Res Treat*. 2010;124(2):403-412.

doi: 10.1007/s10549-010-1163-x

22. Jacot W, Cottu P, Berger F, *et al*. Actionability of HER2-amplified circulating tumor cells in HER2-negative metastatic breast cancer: The CirCe T-DM1 trial. *Breast Cancer Res*. 2019;21(1):121.

doi: 10.1186/s13058-019-1215-z

23. Cardoso F, Paluch-Shimon S, Senkus E, *et al*. 5th ESO-ESMO international consensus guidelines for advanced breast cancer (ABC 5). *Ann Oncol*. 2020;31(12):1623-1649.

doi: 10.1016/j.annonc.2020.09.010

24. Li J, Wang X, Wang S, *et al*. Expert consensus on the clinical diagnosis and targeted therapy of HER2 breast cancer (2023 edition). *Transl Breast Cancer Res*. 2022;3:30.

doi: 10.21037/tbcr-22-48

25. Wang RX, Chen S, Jin X, Chen CM, Shao ZM. Weekly paclitaxel plus carboplatin with or without trastuzumab as neoadjuvant chemotherapy for HER2-positive breast cancer: Loss of HER2 amplification and its impact on response and prognosis. *Breast Cancer Res Treat*. 2017;161(2):259-267.

doi: 10.1007/s10549-016-4064-9

26. Zhu K, Yang X, Tai H, Zhong X, Luo T, Zheng H. HER2-targeted therapies in cancer: A systematic review. *Biomark Res*. 2024;12(1):16.

doi: 10.1186/s40364-024-00565-1

27. Graeser M, Gluz O. HER2+ early breast cancer: From escalation via targeted and post-neoadjuvant treatment to de-escalation. *Breast Care* (*Basel*). 2023;18(6):455-463.

doi: 10.1159/000534670

28. Loibl S, Huang CS, Mano MS, *et al*. Adjuvant trastuzumab emtansine in HER2-positive breast cancer patients with HER2-negative residual invasive disease in KATHERINE. *NPJ Breast Cancer*. 2022;8(1):106.

doi: 10.1038/s41523-022-00477-z

29. Modi S, Jacot W, Yamashita T, *et al*. Trastuzumab deruxtecan in previously treated HER2-low advanced breast cancer. *N Engl J Med*. 2022;387(1):9-20.

doi: 10.1056/NEJMoa2203690

30. Yamashita T, Sohn JH, Tokunaga E, *et al*. Trastuzumab deruxtecan versus treatment of physician's choice in previously treated Asian patients with HER2-low unresectable/metastatic breast cancer: Subgroup analysis of the DESTINY-Breast04 study. *Breast Cancer*. 2024;31:858-868.

doi: 10.1007/s12282-024-01600-7

31. Gourd E. Pyrotinib shows activity in metastatic breast cancer. *Lancet Oncol*. 2017;18(11):e643.

doi: 10.1016/S1470-2045(17)30755-6

32. Jacobson A. Pyrotinib improves survival in previously treated HER2-positive metastatic breast cancer. *Oncologist*. 2022;27(Suppl 1):S5-S6.

doi: 10.1093/oncolo/oyac013

33. Ma F, Ouyang Q, Li W, *et al*. Pyrotinib or lapatinib combined with capecitabine in HER2-positive metastatic breast cancer with prior Taxanes, anthracyclines, and/or trastuzumab: A randomized, phase II study. *J Clin Oncol*. 2019;37(29):2610-2619.

doi: 10.1200/JCO.19.00108

ACCSCIENCE PUBLISHING

Tumor Discovery

CASE REPORT

Biallelic *MUTYH* gene mutation resulting in fluoropyrimidine-resistant advanced rectal cancer: A case report

Tawasapon Thambamroong[1]* and Chawanya Rabiltossaporn[2]

[1]Division of Medical Oncology, Department of Medicine, Phramongkutklao Hospital and College of Medicine, Bangkok, Thailand

[2]Medical Oncology Unit, Department of Medicine, Nakhon Pathom Hospital, Nakhon Pathom, Thailand

(This article belongs to the *Special Issue: Colorectal Cancer: Best Tools for Diagnosis to Management Strategies*)

Abstract

Colorectal cancer (CRC) is a leading cause of cancer-related mortality worldwide and the third most common cancer in Thailand. Approximately 2% – 5% of CRC cases are associated with inherited cancer syndromes, whereas the majority is sporadic. Herein, we have reported the case of a 32-year-old male with poorly differentiated middle rectal adenocarcinoma (T4bN1M1, Stage IV) that was refractory to fluoropyrimidine-based chemotherapy. Genetic profiling revealed a homozygous c.934-2A>G mutation in the *MUTYH* gene, which disrupted the DNA repair. Despite palliative radiation (30 Gy in 10 fractions) and systemic therapies (capecitabine plus oxaliplatin + panitumumab and fluorouracil, leucovorin, and irinotecan + bevacizumab), the disease progressed rapidly. Third-line therapy with Irinotecan plus oxaliplatin demonstrated initial success (partial response). Eventually, disease progression ensued. This report highlights the challenges of managing CRC caused by biallelic *MUTYH* mutations and emphasizes the importance of comprehensive genomic profiling for guiding therapeutic decisions. A review of similar cases in the literature is also presented.

Keywords: Colorectal neoplasms; Colonic neoplasms; Rectal neoplasms; Colorectal neoplasms; Hereditary non-polyposis; Antineoplastic agents; *MUTYH*

***Corresponding author:**
Tawasapon Thambamroong
(t.thambamroong@pmk.ac.th)

Citation: Thambamroong T, Rabiltossaporn C. Biallelic *MUTYH* gene mutation resulting in fluoropyrimidine-resistant advanced rectal cancer: A case report. *Tumor Discov*. 2025;4(1):120-124. doi: 10.36922/td.5164

Received: October 15, 2024

1st revised: November 30, 2024

2nd revised: December 5, 2024

Accepted: December 11, 2024

Published online: December 27, 2024

1. Background

Colorectal cancer (CRC) is a primary global health concern, accounting for > 9% of cancer-related deaths annually.[1] In Thailand, CRC is the third most common malignancy. Although most CRC cases are sporadic, 2% – 5% are hereditary and linked to genetic syndromes, such as Lynch syndrome (LS) and familial adenomatous polyposis (FAP).[2]

LS, which is caused by mutations in mismatch repair (MMR) genes such as *MLH1*, *MSH2*, *MSH6*, and *PMS2*, is associated with microsatellite instability (MSI) and early-onset CRC.[2-5] FAP, an autosomal dominant syndrome is caused by mutations in *APC*. FAP is associated with the development of numerous polyps and a high risk of CRC.[2,6] In contrast, MUTYH-associated polyposis (MAP) is an autosomal recessive syndrome

caused by biallelic mutations in the *MUTYH* gene, which encodes a DNA glycosylase that is essential for oxidative damage repair.[7,8]

MUTYH mutations are associated with an increased risk of CRC.[9] However, their clinical significance remains uncertain.[10,11] Variants such as c.934-2A>G, which have been identified predominantly in Asian populations, may disrupt splicing and impair the DNA repair function of the *MUTYH* gene.[12,13]

Herein, we report the case of a young Thai male with advanced rectal cancer who harbored a homozygous c.934-2A>G mutation, while emphasizing the mutation's clinical relevance and implications for treatment.

2. Case presentation

A 32-year-old Thai male presented with recurrent urinary tract infections and sepsis caused by *Escherichia coli*. Computed tomography (CT) imaging revealed a 10-cm ulcerated rectal mass invading the urinary bladder. Colonoscopy confirmed the presence of poorly differentiated adenocarcinoma, which exhibited positive immunohistochemical staining for CK20 and CDX2 and negative staining for CK7. Molecular testing revealed wild-type *BRAF*, *KRAS*, and *NRAS* genes and a proficient MMR status, excluding LS. The patient was diagnosed with rectal cancer and the TNM stage of the tumor was T4bN1M1 (Stage IV).

Given the advanced stage of the tumor, the multidisciplinary tumor board advised palliative colostomy and administration of radiation therapy (30 Gy in 10 fractions) to alleviate the symptoms. First-line treatment with capecitabine plus oxaliplatin (CAPOX)[14,15] and panitumumab[16,17] was initiated. Despite the administration of four chemotherapy cycles (each lasting 3 weeks; Figure 1), the carcinoembryonic antigen (CEA) levels increased tenfold, from 2.93 to 102.54 ng/dL. Furthermore, CT imaging revealed multiple liver metastases (Figure 2).

Second-line therapy with fluorouracil, leucovorin, and irinotecan (FOLFIRI) was administered in addition to bevacizumab.[18-20] Disease progression, in the form of new lung metastases, was observed after 2 months. The CEA level increased to 860.32 ng/dL. Comprehensive genomic profiling revealed a homozygous c.934-2A>G *MUTYH* mutation.[21] This variant, which is linked to altered splicing, is associated with disrupted DNA repair. There were no mutations of the *MLH1*, *MSH2*, *MSH3*, *MSH6*, *PMS2*, *APC*, *PTEN*, *ATM*, *AXIN2*, *STK11*, *SMAD4*, *TP53*, *CDH1*, *CHEK2*, and *EPCAM* genes.

Third-line treatment with irinotecan and oxaliplatin (IROX)[22] led to a partial response, with CEA levels decreasing to 27.71 ng/mL after the fourth cycle and improved performance status. However, oxaliplatin hypersensitivity limited the treatment to eight cycles. After 16 months of stable disease, progression was observed in the form of new metastatic lesions. The patient declined further systemic therapy and transitioned to end-of-life care. He passed away peacefully just 1 month period after the disease progression. He cannot fit for the 4th-line treatment of regorafenib.

3. Discussion

MUTYH was first described in 2002 and is on the chromosome 1p34.3-1p32.1. The gene encodes a DNA glycosylase that is crucial for repairing oxidative damage.[23,24] Biallelic mutations in *MUTYH* lead to MAP, which is characterized by multiple adenomas and an elevated risk of CRC. In Asian populations, variants such

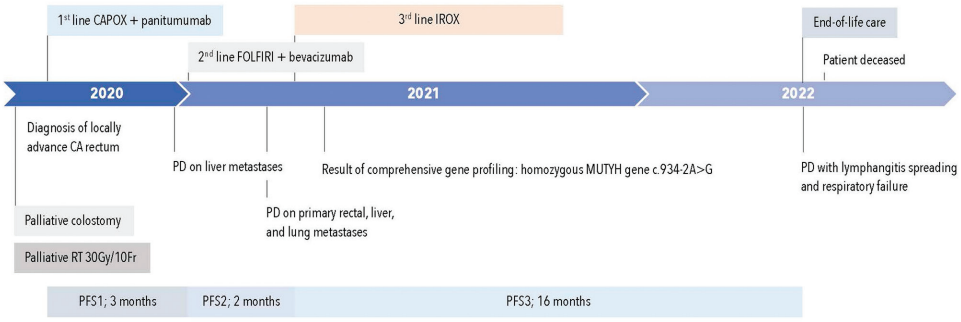

Figure 1. The patient's treatment timeline. In late 2020, the patient was diagnosed with advanced rectal cancer, and he underwent a palliative colostomy to prevent obstruction and radiation. The first-line treatment included CAPOX and panitumumab. The second-line therapy included FOLFIRI and bevacizumab. Both lines of treatment were ineffective within the first 2 months. The third line of treatment, which included IROX, was highly effective. In addition, a homozygous *MUTYH* gene mutation was detected. The patient responded well to this treatment for 16 months. Subsequently, the disease progressed. End-of-life care was initiated as the patient refused further treatment. The patient eventually passed away 1 month after the cessation of chemotherapy.
Abbreviations: CA: Cancer; CAPOX: Capecitabine plus oxaliplatin; Fr: Fractions; FOLFIRI: Fluorouracil, leucovorin, and irinotecan; Gy; Gray; IROX: Irinotecan plus oxaliplatin; PD: Progression of disease; PFS: Progression-free survival; RT: Radiation therapy.

Table 1. Summary of the previously reported cases of CRC with MUTYH mutations

Study	Mutation	Clinical presentation	Treatment regimens	Outcome
Current Case (2024)	Homozygous c.934-2A>G	Middle rectal adenocarcinoma (Stage IV) with bladder invasion	CAPOX+panitumumab; FOLFIRI+bevacizumab; IROX	Stable disease for 16 months with IROX before disease progression
Miyaki *et al.*[28]	c.934-2A>G	Multiple adenomas CRC diagnosed at 40 years of age	Surgery+5-FU-based chemotherapy	Disease-free survival for 18 months
Nielsen *et al.*[13]	Y179C, G396D	Advanced CRC with polyposis	FOLFIRI+bevacizumab	Stable disease for 12 months
Taki *et al.*[25]	c.934-2A>G	Rectal adenocarcinoma with local invasion	Surgery+XELOX+bevacizumab	Progression-free survival of 10 months
Tao *et al.*[27]	c.312C>A (Y104X)	Advanced rectal cancer and recurrent polyps	5-FU+leucovorin	Rapid progression despite standard chemotherapy
Cleary *et al.*[23]	Y179C, G396D	Early-onset CRC and polyposis	Surgery, observation	Long-term survival after surgical resection
Sampson *et al.*[29]	G382D	Advanced CRC with few polyps	FOLFIRI	Partial response followed by disease progression

Abbreviations: CAPOX, XELOX: Capecitabine plus oxaliplatin; CRC: Colorectal cancer; IROX: Irinotecan plus oxaliplatin; FOLFIRI: Fluoropyrimidine, leucovorin, irinotecan; 5-FU: fluoropyrimidine.

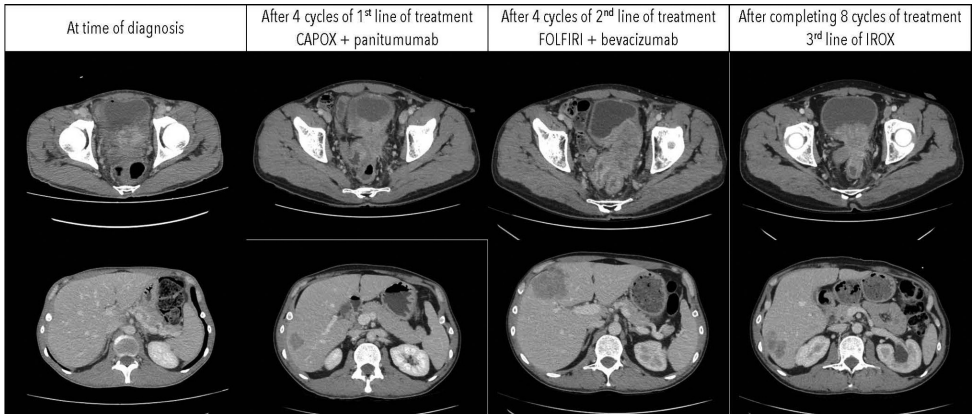

Figure 2. The patient's CT scans at different stages of treatment. The first CT was obtained at the time of diagnosis. The subsequent CTs were obtained after the first line of treatment (CAPOX with panitumumab), the second line of treatment (FOLFIRI with bevacizumab), and the third line of treatment (IROX) were completed.
Abbreviations: CT: Computed tomography; CAPOX: Capecitabine plus oxaliplatin. FOLFIRI: Fluorouracil, Leucovorin, and Irinotecan; IROX: Irinotecan and Oxaliplatin.

as c.934-2A>G21 are linked to CRC, disrupting splicing and impairing DNA repair mechanisms.[25-27]

The refractory response to fluoropyrimidine-based therapies in pur patient highlights the challenges of managing CRC associated with *MUTYH* mutations. Fluoropyrimidine resistance may result from impaired DNA repair, as observed in other MUTYH-associated CRCs (Table 1). The effectiveness of IROX in our patient demonstrates the potential of non-fluoropyrimidine regimens in similar cases.

Although targeted therapies for MUTYH-associated CRC are limited, comprehensive genomic profiling can guide personalized treatment. In our patient, genomic insights informed the use of IROX, which provided temporary disease control. Further studies are required to elucidate the clinical significance of *MUTYH* mutations and optimize therapeutic strategies.

4. Conclusion

This case report highlights the aggressive nature of CRC with a homozygous c.934-2A>G *MUTYH* mutation and the challenges associated with treatment resistance. Comprehensive genomic profiling was pivotal in guiding therapy, emphasizing its importance in young patients with CRC.

Acknowledgments

We acknowledge our patient and family for permitting us to publish this case report for mankind's benefit. We

also compliment the multidisciplinary teams for the good clinical decisions made for this patient.

Funding

None.

Conflict of interest

The authors declare they have no competing interests.

Author contributions

Conceptualization: Tawasapon Thambamroong
Formal analysis: Tawasapon Thambamroong
Investigation: All authors
Methodology: All authors
Writing – original draft: Tawasapon Thambamroong
Writing – review & editing: Tawasapon Thambamroong

Ethics approval and consent to participate

Not applicable.

Consent for publication

The patient's next of kin provided consent for the publication of this case report.

Availability of data

Not applicable.

Reference

1. Sung H, Ferlay J, Siegel RL, *et al*. Global cancer statistics 2020: GLOBOCAN estimates of incidence and mortality worldwide for 36 cancers in 185 countries. *CA Cancer J Clin*. 2021;71:209-249.

   doi: 10.3322/caac.21660

2. Jasperson KW, Tuohy TM, Neklason DW, Burt RW. Hereditary and familial colon cancer. *Gastroenterology*. 2010;138:2044-2058.

   doi: 10.1053/j.gastro.2010.01.054

3. Lynch HT, Lynch PM, Lanspa SJ, Snyder CL, Lynch JF, Boland CR. Review of the Lynch syndrome: History, molecular genetics, screening, differential diagnosis, and medicolegal ramifications. *Clin Genet*. 2009;76:1-18.

   doi: 10.1111/j.1399-0004.2009.01230.x

4. Vasen HF, Watson P, Mecklin JP, Lynch HT. New clinical criteria for hereditary nonpolyposis colorectal cancer (HNPCC, Lynch syndrome) proposed by the International Collaborative group on HNPCC. *Gastroenterology*. 1999;116:1453-1456.

   doi: 10.1016/s0016-5085(99)70510-x

5. Umar A, Boland CR, Terdiman JP, *et al.* Revised Bethesda Guidelines for hereditary nonpolyposis colorectal cancer (Lynch syndrome) and microsatellite instability. *J Natl Cancer Inst*. 2004;96:261-268.

   doi: 10.1093/jnci/djh034

6. Nagy R, Sweet K, Eng C. Highly penetrant hereditary cancer syndromes. *Oncogene*. 2004;23:6445-6470.

   doi: 10.1038/sj.onc.1207714

7. Takao M, Zhang QM, Yonei S, Yasui A. Differential subcellular localization of human MutY homolog (hMYH) and the functional activity of adenine:8-oxoguanine DNA glycosylase. *Nucleic Acids Res*. 1999;27:3638-3644.

   doi: 10.1093/nar/27.18.3638

8. Shinmura K, Yamaguchi S, Saitoh T, *et al.* Adenine excisional repair function of MYH protein on the adenine:8-hydroxyguanine base pair in double-stranded DNA. *Nucleic Acids Res*. 2000;28:4912-4918.

   doi: 10.1093/nar/28.24.4912

9. Lubbe SJ, Di Bernardo MC, Chandler IP, Houlston RS. Clinical implications of the colorectal cancer risk associated with MUTYH mutation. *J Clin Oncol*. 2009;27:3975-3980.

   doi: 10.1200/JCO.2008.21.6853

10. Slupska MM, Baikalov C, Luther WM, Chiang JH, Wei YF, Miller JH. Cloning and sequencing a human homolog (hMYH) of the *Escherichia coli* mutY gene whose function is required for the repair of oxidative DNA damage. *J Bacteriol*. 1996;178:3885-3892.

    doi: 10.1128/jb.178.13.3885-3892.1996

11. Ohtsubo T, Nishioka K, Imaiso Y, *et al*. Identification of human MutY homolog (hMYH) as a repair enzyme for 2-hydroxyadenine in DNA and detection of multiple forms of hMYH located in nuclei and mitochondria. *Nucleic Acids Res*. 2000;28:1355-1364.

    doi: 10.1093/nar/28.6.1355

12. Jones S, Lambert S, Williams GT, Best JM, Sampson JR, Cheadle JP. Increased frequency of the k-ras G12C mutation in MYH polyposis colorectal adenomas. *Br J Cancer*. 2004;90:1591-1593.

    doi: 10.1038/sj.bjc.6601747

13. Nielsen M, de Miranda NF, van Puijenbroek M, *et al.* Colorectal carcinomas in MUTYH-associated polyposis display histopathological similarities to microsatellite unstable carcinomas. *BMC Cancer*. 2009;9:184.

    doi: 10.1186/1471-2407-9-184

14. Cassidy J, Clarke S, Diaz-Rubio E, *et al.* Randomized phase III study of capecitabine plus oxaliplatin compared with fluorouracil/folinic acid plus oxaliplatin as first-line therapy for metastatic colorectal cancer. *J Clin Oncol*. 2008;26: 2006-2012.

doi: 10.1200/JCO.2007.14.9898

15. Ducreux M, Bennouna J, Hebbar M, *et al*. Capecitabine plus oxaliplatin (XELOX) versus 5-fluorouracil/leucovorin plus oxaliplatin (FOLFOX-6) as first-line treatment for metastatic colorectal cancer. *Int J Cancer*. 2011;128:682-690.

doi: 10.1002/ijc.25369

16. Douillard JY, Siena S, Cassidy J, *et al*. Final results from PRIME: Randomized phase III study of panitumumab with FOLFOX4 for first-line treatment of metastatic colorectal cancer. *Ann Oncol*. 2014;25:1346-1355.

doi: 10.1093/annonc/mdu141

17. Douillard JY, Siena S, Cassidy J, *et al*. Randomized, phase III trial of panitumumab with infusional fluorouracil, leucovorin, and oxaliplatin (FOLFOX4) versus FOLFOX4 alone as first-line treatment in patients with previously untreated metastatic colorectal cancer: The PRIME study. *J Clin Oncol*. 2010;28:4697-4705.

doi: 10.1200/JCO.2009.27.4860

18. Beretta GD, Petrelli F, Stinco S, *et al*. FOLFIRI+bevacizumab as second-line therapy for metastatic colorectal cancer pretreated with oxaliplatin: A pooled analysis of published trials. *Med Oncol*. 2013;30:486.

doi: 10.1007/s12032-013-0486-y

19. Jo H, Lee MS, Lee YP, *et al*. A comparison of folinic acid, fluorouracil and irinotecan (FOLFIRI) plus bevacizumab and FOLFIRI plus aflibercept as second-line treatment for metastatic colorectal cancer. *Clin Oncol* (*R Coll Radiol*). 2022;34:e323-e328.

doi: 10.1016/j.clon.2022.02.011

20. Iwamoto S, Takahashi T, Tamagawa H, *et al*. FOLFIRI plus bevacizumab as second-line therapy in patients with metastatic colorectal cancer after first-line bevacizumab plus oxaliplatin-based therapy: The randomized phase III EAGLE study. *Ann Oncol*. 2015;26:1427-1433.

doi: 10.1093/annonc/mdv197

21. *Information NCfB. ClinVar; [VCV000041766.57]*. Available from: https://www.ncbi.nlm.nih.gov/clinvar/variation/VCV000041766.57 [Last accessed on 2023 Jun 02].

22. Haller DG, Rothenberg ML, Wong AO, *et al*. Oxaliplatin plus irinotecan compared with irinotecan alone as second-line treatment after single-agent fluoropyrimidine therapy for metastatic colorectal carcinoma. *J Clin Oncol*. 2008;26:4544-4550.

doi: 10.1200/JCO.2008.17.1249

23. Cleary SP, Cotterchio M, Jenkins MA, *et al*. Germline MutY human homologue mutations and colorectal cancer: A multisite case-control study. *Gastroenterology*. 2009;136:1251-1260.

doi: 10.1053/j.gastro.2008.12.050

24. Ali M, Kim H, Cleary S, Cupples C, Gallinger S, Bristow R. Characterization of mutant MUTYH proteins associated with familial colorectal cancer. *Gastroenterology*. 2008;135:499-507.

doi: 10.1053/j.gastro.2008.04.035

25. Taki K, Sato Y, Nomura S, *et al*. Mutation analysis of *MUTYH* in Japanese colorectal adenomatous polyposis patients. *Fam Cancer*. 2016;15:261-265.

doi: 10.1007/s10689-015-9857-1

26. Thibodeau ML, Zhao EY, Reisle C, *et al*. Base excision repair deficiency signatures implicate germline and somatic MUTYH aberrations in pancreatic ductal adenocarcinoma and breast cancer oncogenesis. *Cold Spring Harb Mol Case Stud*. 2019;5:a003681.

doi: 10.1101/mcs.a003681

27. Tao H, Shinmura K, Hanaoka T, *et al*. A novel splice-site variant of the base excision repair gene MYH is associated with production of an aberrant mRNA transcript encoding a truncated MYH protein not localized in the nucleus. *Carcinogenesis*. 2004;25:1859-1866.

doi: 10.1093/carcin/bgh206

28. Miyaki M, Iijima T, Yamaguchi T, *et al*. Germline mutations of the MYH gene in Japanese patients with multiple colorectal adenomas. *Mutat Res*. 2005;578:430-433.

doi: 10.1016/j.mrfmmm.2005.01.017

29. Sampson JR, Dolwani S, Jones S, *et al*. Autosomal recessive colorectal adenomatous polyposis due to inherited mutations of MYH. *Lancet*. 2003;362:39-41.

doi: 10.1016/S0140-6736(03)13805-6

ACCSCIENCE PUBLISHING

Tumor Discovery

CASE REPORT

Clinical presentation and demographic characteristics of polypoid melanoma on the back: A case study

Emmanuel Angel Zappettini* and **Sergio Fernández Vértiz**

Department of Surgery, Rural Hospital of Santa María Magdalena, Magdalena, Buenos Aires, Argentina

Abstract

Polypoid melanoma (PM) is a variant of nodular melanoma characterized by exophytic growth, an irregular surface, and a cauliflower-like appearance. Its reported incidence varies widely, ranging from 2% to 43%, and it is associated with a poor prognosis. This study presents a case of this rare melanoma subtype, along with its demographic characteristics, as reported in the international literature. PM is recognized as an independent risk factor in the evolving landscape of melanoma and requires tailored management strategies. Dermatologists and surgical oncologists should maintain a high level of suspicion to improve patient outcomes.

Keywords: Polypoid melanoma; Nodular melanoma; Demographic; Surgical treatment; Overall survival

***Corresponding author:**
Emmanuel Angel Zappettini
(eazappettini@med.unlp.edu.ar)

Citation: Zappettini EA, Vértiz SF. Clinical presentation and demographic characteristics of polypoid melanoma on the back: A case study. *Tumor Discov*. 2025;4(1):125-128.
doi: 10.36922/td.5105

Received: October 10, 2024

1st revised: January 14, 2025

2nd revised: January 24, 2025

Accepted: January 24, 2025

Published online: February 17, 2025

1. Background

Polypoid melanoma (PM) is a rare and aggressive subtype of nodular melanoma (NM), associated with one of the worst prognoses among all melanoma types.[1] The biological behavior of this tumor remains poorly understood due to the scarcity of available evidence, which is largely limited to case reports. In addition, the definition of PM has evolved over the years, complicating the interpretation of available scientific evidence. PM often shares characteristics with other conditions that may appear benign but conceal a malignant diagnosis, making its detection particularly challenging.

This case report describes a case of PM from an epidemiological, clinical, and therapeutic perspective. By providing a detailed analysis, this report seeks to raise awareness of this rare disease and highlight the importance of differential diagnoses to optimize accurate identification and treatment.

2. Case presentation

An 82-year-old male patient, living alone in a rural area, presented to the Surgery Department with a 1-year history of a polypoid tumor on his back (Figure 1). The lesion was associated with itching, burning pain, and occasional bleeding. His medical records revealed only dyslipidemia, for which he was treated with micronized fenofibrate (200 mg daily). Physical examination revealed a brown polypoid tumor with a cauliflower-like appearance (Table 1). The lesion had a small stalk, was ulcerated, and

exhibited discoloration of the adjacent skin (Figure 2). After obtaining informed consent, an incisional biopsy confirmed the diagnosis of melanoma. In accordance with the melanoma protocol at our hospital, the patient underwent a triple assessment, including chest X-ray, abdominal ultrasound, and a thorough evaluation of the lymph nodes and central nervous system, all of which showed no evidence of distant metastasis. In addition, a brain magnetic resonance imaging (MRI) scan performed in Buenos Aires revealed no signs of oncological disease. However, a skin assessment identified an indurated area with edema and erythema, raising concerns about potential in-transit metastases.

Table 1. Clinical and epidemiological features of PM

Epidemiology	Signs and symptoms	PM Clinical presentation
• Age: 82	• Burning pain	• Location: Back
• Gender: Male	• Itching	• Shape: Cauliflower
• Comorbidities: Dyslipidemia	• Bleeding	• Consistency: Stony
-	• Evolution: One year	• Mobility: Not mobile
-	-	• Margins: Adjacent skin coloration

Abbreviation: PM: Polypoid melanoma.

Figure 1. Polypoid melanoma on the back

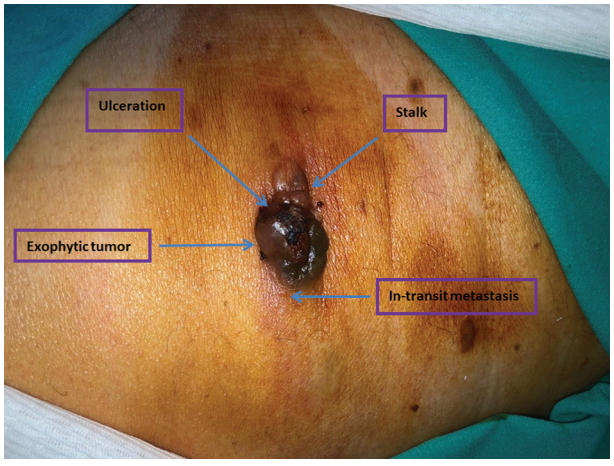

Figure 2. Polyploid melanoma characterized by the exophytic tumor, ulceration, stalk, and in-transit metastasis

Following a multidisciplinary team discussion, and considering the patient's isolated living situation and potential low adherence to further adjuvant treatments, a wide resection surgery was performed with a 2 cm margin of surrounding healthy tissue. The deep margin extended to the fascia of the latissimus dorsi muscle (Figure 3), and the tumor was removed *en bloc*. Sentinel lymph node biopsy results were negative. Histopathological analysis confirmed a diagnosis of NM (PM subtype), with Clark level V invasion, a Breslow thickness of 15 mm, ulceration, a mitotic rate of 4 mitoses/mm^2, and no evidence of lymphovascular invasion.

Post-operatively, the patient underwent adjuvant chemotherapy with pembrolizumab for 4 months, with an initial good response. However, disease progression ensued, with the development of distant metastases in the lungs, inguinal lymph nodes, and subcutaneous tissue. The patient ultimately succumbed to complications related to a concurrent coronavirus disease 2019 infection.

3. Discussion

PM is a variant of NM, characterized by an exophytic growth, an irregular surface, and a cauliflower-like appearance.[2] Its incidence varies from 2% to 43%, making it a very rare disease with a poor prognosis.[3] The poor prognosis[4] of PM is primarily associated with early, often hidden metastasis,[5,6]

Figure 3. The surgical site showing the removal of the latissimus dorsi fascia

through vascular and lymphatic invasion, making it one of the most lethal forms of melanomas.[5] While PM can affect younger patients[4] and mucosal areas such as the vagina, rectum, esophagus, and airway,[6] skin involvement occurs in less than a third of patients,[1] mostly commonly on the back.[2,4,6] Many definitions have been used to describe PM, but they generally converge on a set of common characteristics. Essentially, PM is characterized by an exophytic[3] growth caused by an aggregation of melanoma cells[6] above the skin surface. More than 50% of the tumor[3,5] is typically located on the cutaneous surface and is often accompanied by ulceration.[2,6] If an endophytic component is present, it accounts for <50% of the total tumor depth.[4] Notably, PM can be either pedunculated or sessile,[3] with or without pigmentation,[3] and it usually lacks radial growth.[2,4] Instead, it typically demonstrates rapid vertical growth, which is responsible for vascular embolism.[2]

The diagnosis of PM is challenging due to its atypical presentation, which often does not follow the asymmetry, border, color, diameter, and evolving[5] rule but aligns more with elevated, firm, and progressive growth (EFG[6]). Its ability to mimic benign conditions such as pyogenic granuloma,[3,5] intradermal nevus,[3,5] fibroepithelial polyp,[3] cutaneous metastasis,[5] infectious disorders,[5] other benign lesions,[5] skin cancers,[5] and skin sarcomas[7] makes its detection particularly difficult.[5] Moreover, PM may appear either pigmented or non-pigmented, sessile or pedunculated, and its tendency to ulcerate further complicates diagnosis.[8] These overlapping characteristics with benign or malignant conditions emphasize the need for heightened diagnostic suspicion to ensure timely identification.

Histopathological analysis is essential for diagnosing PM, revealing a higher degree of cellular atypia, cellular and nuclear pleomorphism, a high mitotic index, and significant Breslow depth. These factors, along with the rate of ulceration and presence of lymphovascular invasion,[4] contribute to the poor prognosis of PM[2,5,6] compared to other melanoma subtypes, as they are linked to the development of hidden metastases.[6]

Imaging, including positron emission tomography (PET) scans, computed tomography (CT) scans, and MRI of the head, chest, abdomen, and pelvis, is crucial for staging and detecting distant metastases[8] in soft tissues, the brain, lungs, liver, and skin.

The cornerstone of treatment for PM is wide local resection,[9] with a recommended 2 cm margin for lesions with a Breslow thickness[6] of 2 mm or greater. This procedure is typically combined with sentinel lymph node assessment[9] to improve staging accuracy. Adjuvant chemotherapy is also part of the standard treatment[9] protocol. Targeted therapies, such as *BRAF* and mitogen-activated protein kinase inhibitors, may become relevant in certain stages of the disease.[8] In addition, systemic therapy using programmed cell death protein 1 inhibitors like pembrolizumab has shown promise for surgically resected stage IIB or IIC melanoma, irrespective of histopathological features such as subtype, ulceration, or tumor thickness.[10]

Follow-up is mandatory for PM due to the tumor's ability to develop early local recurrence within 5 cm of the surgical scar.[6] Although specific follow-up protocols for PM are lacking,[11] active surveillance criteria used for other melanoma types are often applied. This surveillance includes follow-up visits every 3 months during the first 3 years and every 6 months thereafter.[11] Early detection of metastases or local recurrence is facilitated through lymph node ultrasonography, CT scans, and PET scans.[11]

The 5-year survival rate for PM ranges from 32% to 42%, significantly lower than the 57% observed in non-PM[8] cases. Given this poor prognosis, prevention and early detection are paramount. A high index of suspicion is necessary when evaluating atypical presentations, such as polypoid and amelanotic lesions, to ensure timely diagnosis and treatment. Raising awareness among dermatologists and surgical oncologists is equally important. Moreover, educating patients[12] about their diagnosis and risk factors enables practitioners to identify and address small, non-life-threatening lesions before they progress. Preventive strategies, such as the use of regular sunscreen and appropriate clothing for physical protection, are strongly recommended to prevent deoxyribonucleic acid (DNA) damage associated with ultraviolet radiation.[11] These measures contribute significantly to reducing melanoma risk and improving patient outcomes.

Several challenges[9] to PM diagnosis have been identified, including the lack of pigmentation in some lesions, the tumor's similarity to benign and malignant entities, limited awareness of this condition, and its atypical clinical presentation, which often fails to meet the ABCD or EFG criteria. These factors delay diagnosis and treatment, resulting in missed opportunities for timely intervention.

4. Conclusion

PM represents a distinct risk factor in the evolving landscape of melanoma management.[4] A high level of clinical suspicion and a comprehensive diagnostic approach are essential for timely and effective treatment. Educating both practitioners and patients about atypical melanoma presentations is vital for improving outcomes and minimizing diagnostic delays. Preventive measures,

such as the use of sunscreen and protective clothing, remain critical in reducing ultraviolet radiation-induced DNA damage.

Acknowledgments

None

Funding

None.

Conflict of interest

The authors declare that they have no competing interests.

Author contributions

Conceptualization: Emmanuel Zappettini
Investigation: Emmanuel Zappettini
Writing-original draft: Sergio Fernández Vértiz
Writing-review & editing: Sergio Fernández Vértiz

Ethics approval and consent to participate

The study was approved by the Ethical Committee of our institution. The authors certify that appropriate consent was obtained from the patient. The patient gave his consent and understands that his name and initials will not be published. Efforts are made to conceal his identity, although anonymity cannot be guaranteed.

Consent for publication

The patient gave his consent for his images and other clinical information to be reported in the manuscript.

Availability of data

Data used in this work are available from the corresponding author upon reasonable request.

References

1. Valdebran M, Wu K, Wu A, Junkins-Hopkins J. Polypoid melanoma: A rare clinical subtype frequently confused with benign entities. *Our Dermatol Online*. 2016;7(2):179-180.

2. Di Altobrando A, Patrizi A, Dika E, Savoia F. Cauliflower-like exophytic mass on the skin: Polypoid melanoma. Clinical, dermoscopic, and histologic features. *An Bras Dermatol*. 2020;95(6):748-750.

   doi: 10.1016/j.abd.2020.04.010

3. Hikawa RS, Kanehisa ES, Enokihara MM, Enokihara MY, Hirata SH. Polypoid melanoma and superficial spreading melanoma different subtypes in the same lesion. *An Bras Dermatol*. 2014;89(4):666-668.

   doi: 10.1590/abd1806-4841.20142802

4. Pedersen EA, Harms PW, Zhao L, *et al*. Polypoid melanoma is associated with aggressive histopathological characteristics and poor clinical prognosis: A retrospective cohort study. *J Am Acad Dermatol*. 2023;88(5):1169-1170.

   doi: 10.1016/j.jaad.2022.11.055

5. Maury ME, Jukic DM. A case presentation of three polypoid melanomas with divergent features. *Cureus*. 2023;15(10):e46951.

   doi: 10.7759/cureus.46951

6. Navarro-Nuño DE, Villarreal-Salgado JL, Grano-González VH, García-Marín G, Nuño-Rodríguez VH, Torres-Salazar QL. Surgical technique for margin widening in the treatment of polypoid nodular malignant back melanoma. *Int J Surg Case Rep.* 2023;110:108659.

   doi: 10.1016/j.ijscr.2023.108659

7. Kalmykova A, Mosaieby E, Kacerovská D, *et al*. MITF::CREM-rearranged tumor: a novel group of cutaneous tumors with melanocytic differentiation. *Virchows Arch*. 2023;483(4):569-575.

   doi: 10.1007/s00428-023-03621-7

8. Tan A, Gutierrez D, Brinster NK, Stein JA. Polypoid melanoma mistaken for verruca vulgaris. *Cleve Clin J Med*. 2020;87(9):534-536.

   doi: 10.3949/ccjm.87a.19079

9. Boccardi A, Trigg J, Reite, P, Papadopoulos D, Sirota Rozenberg S. Polypoid melanoma: Diagnostic hardships concerning a rare melanoma variant. *SKIN J Cutan Med*. 2022;6(3):250-253.

   doi: 10.25251/skin.6.3.13

10. Schadendorf D, Luke JJ, Ascierto PA, *et al.* Pembrolizumab versus placebo as adjuvant therapy in resected stage IIB or IIC melanoma: Outcomes in histopathologic subgroups from the randomized, double-blind, phase 3 KEYNOTE-716 trial. *J Immunother Cancer*. 2024;12(3):e007501.

    doi: 10.1136/jitc-2023-007501

11. Michielin O, van Akkooi ACJ, Ascierto PA, Dummer R, Keilholz U; ESMO Guidelines Committee. Electronic address: clinicalguidelines@esmo.org. Cutaneous melanoma: ESMO Clinical Practice Guidelines for diagnosis, treatment and follow-up. *Ann Oncol*. 2019;30(12):1884-1901.

    doi: 10.1093/annonc/mdz411

12. Pérez-Wilson J, Arellano J, Castro A. Polypoid melanoma: an aggressive variant of nodular melanoma. *Cutis*. 2018;101(6):E6-E7.

ACCSCIENCE PUBLISHING

Tumor Discovery

LETTER TO EDITOR

Dosiomics in lung cancer

Melek Yakar*

Department of Radiation Oncology, Faculty of Medicine, Osmangazi University, Eskişehir, Turkey

Dear Editor,

I am writing to express my opinion on dosiomics as a very current and developing topic in lung cancer treatment.

Dosiomics has emerged as a promising tool in oncology that uses advanced radiotherapy dose distribution features to predict clinical outcomes. In lung cancer, where individualized treatment strategies are critical, dosiomics offers a unique approach to integrating radiotherapy planning with predictive analysis. The focus of dosiomic research has been to predict toxicity such as radiation pneumonitis or fibrosis. However, recent studies have begun to explore its potential in predicting oncological outcomes such as tumor control and survival. Despite these developments, literature pertaining to this new topic remains quite limited.[1] This letter aims to highlight the dual applications of dosiomics in lung cancer, discuss current limitations, and suggest future directions for research.

Inspired by radiomics, dosiomics is being developed to parameterize the dose distribution of regions of interest using textural features and to allow the spatial description of the dose distribution. The first studies on the use of dosiomics in lung cancer were set to predict treatment-related toxicity.[2-7] Radiation-induced toxicity remains a major challenge in radiotherapy, especially in the treatment of lung cancer, where critical body structures such as the lung, heart, and esophagus are in close proximity to the tumor. Studies have shown that dosiomics can extract meaningful features from dose distribution maps, such as texture, shape, and density, which are associated with the likelihood of developing radiation pneumonitis or esophageal toxicity.[2,3] Dosiomic features can be extracted using a handcrafted method. Handcrafted features have been used to predict toxicity such as radiation esophagitis, pneumonia, and lymphopenia.[2-7] Handcrafted features contain 3D dose distribution information but do not fully reflect it. If well trained, the convolutional neural network method can reveal more detailed features hidden in the original data,[2] for example, upon testing radiomics, dosiomics, clinical features, and dose-volume histogram, both in isolation and combination, Zhang *et al.*[7] revealed that the hybrid model achieved high prediction accuracy rates. These findings highlight the potential of dosiomics to improve patient selection and treatment planning, thereby reducing the incidence of severe toxicity. Furthermore, integrating dosiomics with clinical and radiomics data increases the predictive power, allowing for a more comprehensive risk assessment.[7]

Tumor control probability and progression-free survival are critical measures for evaluating the efficacy of lung cancer treatments. Recent studies have shown that dosiomics can provide insights into these outcomes by analyzing the spatial and volumetric distribution of radiation dose within the tumor and surrounding tissues. For example, Bhandari *et al.*[8] conducted a study on lung cancer patients undergoing stereotactic body radiotherapy (SBRT) and effectively predicted treatment failure in the lung SBRT treatment with a dosiomic model that integrated the interaction between computed

***Corresponding author:**
Melek Yakar
(myakar@ogu.edu.tr)

Citation: Yakar M. Dosiomics in lung cancer. *Tumor Discov*. 2025;4(1):129-131. doi: 10.36922/td.8465

Received: January 9, 2025

Accepted: January 14, 2025

Published online: January 31, 2025

tomography and dose. Similarly, dosiomic-based models have been used to predict distant metastasis by analyzing the dose delivered to peritumoral regions.[1] These findings suggest that dosiomics may serve as a valuable tool for tailoring radiotherapy protocols to maximize therapeutic efficacy while minimizing unnecessary exposure to healthy tissues.

Despite these promising developments, there are still challenges in integrating dosiomics into routine clinical practice. First, the lack of standardization in feature extraction and analysis methods limits the reproducibility of findings across studies. Notwithstanding the existence of commercial software for extracting dosiomic features, much more informative feature extraction methods powered by artificial intelligence (AI) are also available. The creation of prediction models requires the usage of very different algorithms, with certain pilot studies diving into the incorporation of big data to enhance their predictability[1-8] There is no standardization in the studies yet, but these studies are very valuable and shed light on the studies that will be created with big data. Different algorithms and software platforms often produce inconsistent results, making it difficult to establish universal guidelines. Second, most dosiomic studies are retrospective, relying on a small number of pre-existing datasets with limited diversity. Prospective, multicenter, and international studies are needed to validate the clinical utility of dosiomics and ensure its generalizability across different patient populations and treatment settings, considering that demographic characteristics also affect prognosis. Future studies should take a holistic approach by integrating dosiomics with other forms of data, such as genomics and immunomics, to capture the complexity of treatment responses. To achieve personalized and successful treatments, decisions must be made based on more comprehensive data.

For clinically adopting dosiomics in the context of lung cancer, standardization with heterogeneous big data is necessary. First, efforts should be made to standardize methods for dosiomic feature extraction and identification of significant variables, which can be achieved through cross-study comparisons and meta-analyses. Second, AI techniques need to be integrated with dosiomics. AI-driven models can process high-dimensional dosiomic data to reveal complex patterns and relationships that may be overlooked by traditional statistical methods. In addition, incorporating AI into dosiomic workflows can also facilitate clinical decision-making by evaluating large amounts of data and providing real-time prediction. Third, collaborative efforts among researchers, clinicians, and industry stakeholders are essential to advance dosiomic research. Multicenter and international clinical studies should be designed to evaluate the predictive accuracy of dosiomics in both toxicity and oncologic outcomes. These studies should include diverse patient populations and treatment modalities to ensure that the findings are broadly applicable. Finally, expanding the scope of dosiomics beyond radiotherapy to include other treatment modalities such as concurrent chemotherapy, immunotherapy, and targeted therapies may provide a more comprehensive understanding of treatment responses. For example, analyzing the interaction between radiation dose distribution and immune activation may open new avenues to optimize combination therapies in lung cancer. In addition, consensus guidelines and guidelines for predictive models in dosiomics need to be established.

In conclusion, dosiomics is a powerful tool for achieving personalized treatments in lung cancer patients. Addressing standardization challenges will be crucial for integrating dosiomics into routine clinical practice. Dosiomics has the potential to improve both treatment efficacy and quality of life of patients undergoing lung cancer treatment by leveraging technologies. Further research with international collaboration is needed in this exciting area to realize its full potential.

Conflict of interest

The author declares that she has no conflict of interest and has no competing interests.

References

1. Dudas D, Dilling TJ, Naqa IE. A deep learning-informed interpretation of why and when dose metrics outside the PTV can affect the risk of distant metastasis in SBRT NSCLC patients. *Radiat Oncol*. 2024;19(1):127.

   doi: 10.1186/s13014-024-02519-1

2. Ma Z, Liang B, Wei R, *et al*. Enhanced prediction of postoperative radiotherapy-induced esophagitis in non-small cell lung cancer: Dosiomic model development in a real-world cohort and validation in the PORT-C randomized controlled trial. *Thorac Cancer*. 2023;14(28):2839-2845.

   doi: 10.1111/1759-7714.15068

3. Zhou L, Wen Y, Zhang G, Wang L, Wu S, Zhang S. machine learning-based multiomics prediction model for radiation pneumonitis. *J Oncol*. 2023;2023:5328927.

   doi: 10.1155/2023/5328927

4. Adachi T, Nakamura M, Shintani T, *et al*. Multi-institutional dose-segmented dosiomic analysis for predicting radiation pneumonitis after lung stereotactic body radiation therapy. *Med Phys*. 2021;48(4):1781-1791.

doi: 10.1002/mp.14769

5. Monti S, Xu T, Liao Z, Mohan R, Cella L, Palma G. On the interplay between dosiomics and genomics in radiation-induced lymphopenia of lung cancer patients. *Radiother Oncol*. 2022;167:219-225.

   doi: 10.1016/j.radonc.2021.12.038

6. Puttanawarut C, Sirirutbunkajorn N, Tawong N, *et al*. Radiomic and dosiomic features for the prediction of radiation pneumonitis across esophageal cancer and lung cancer. *Front Oncol*. 2022;12:768152.

   doi: 10.3389/fonc.2022.768152

7. Zhang Z, Wang Z, Yan M, *et al*. Radiomics and dosiomics signature from whole lung predicts radiation pneumonitis: A model development study with prospective external validation and decision-curve analysis. *Int J Radiat Oncol Biol Phys*. 2023;115(3):746-758.

   doi: 10.1016/j.ijrobp.2022.08.047

8. Bhandari A, Johnson K, Oh K, *et al*. Developing a novel dosiomics model to predict treatment failures following lung stereotactic body radiation therapy. *Front Oncol*. 2024;14:1438861.

   doi: 10.3389/fonc.2024.1438861

Our Journals

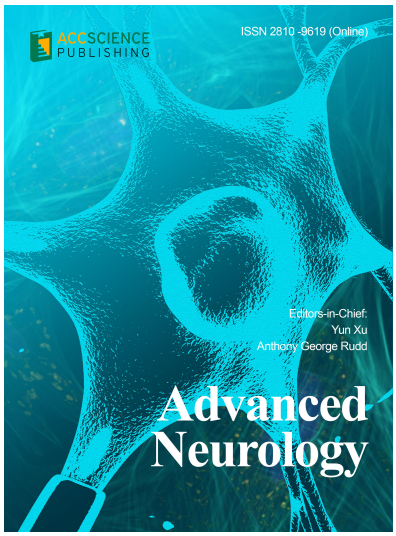

Advanced Neurology is a peer-reviewed and open-access journal that aims to publish and disseminate novel research in the breadth of neurology and neuroscience. The journal aims to advance our understanding in the nervous system and provide a platform to neuroscientists and physicians to showcase their findings in original fundamental and clinical research as well as to present new ideas that highlight the changes in the neurological clinical practice.

Advanced Neurology covers subject areas, including but not limited to the following:

- Neurological disorders
- Neurodegenerative disease
- Cerebrovascular disease
- Epilepsy and movement disorders
- Neuroimmune disease
- Neurological infections
- Muscle disease
- Molecular and cellular neuroscience
- Systems neuroscience
- Cognitive neuroscience
- Computational modeling of nervous system

Global Translational Medicine is a quarterly journal that focuses on medicine, biological sciences, and biomaterials engineering. The goal of *Global Translational Medicine* is to provide a platform to researchers for showcasing their latest research works in translational medicine so as to advance the field towards the betterment of human health. Despite the advancement of omics and new technologies, the process of transforming these technologies and scientific research results into effective therapies and putting them into clinical use still has a long way to go. *Global Translational Medicine* provides a platform to fill the gaps in preclinical and inter-disciplinary research, to promote clinical translation of scientific research results, and to contribute to the conception of new and improved preventive measures as well as diagnostic and therapeutic techniques of diseases.

Global Translational Medicine covers the following themes: cardiovascular disease, metabolism/diabetes/obesity, neuroscience/neurology, cancer, biomaterials and their applications in medicine, proteomics/metabolomics, pharmacogenomics, biomarkers, bioinformatics and data mining, animal and clinical research, and medical methods arising from interdisciplinary crossover.

Start a new journal

Write to us via email if you are interested to start a new journal with AccScience Publishing. Please attach your CV, professional profile page and a brief pitch proposal in your email. We shall inform you of our decision whether we are interested to collaborate in starting a new journal.

Contact: info@accscience.com

https://accscience.com/journal/TD

Contact

www.accscience.com

8 Burn Road, #15-03 Trivex, Singapore 369977

Email: editorial@accscience.com

Phone: +65 8182 1586